COMPILATION OF SANDIA COAL DEVOLATILIZATION DATA

MILESTONE REPORT

May 1992

Submitted By: Thomas H. Fletcher and Donald R. Hardesty
Combustion Research Facility
Sandia National Laboratories, Livermore

Submitted To: Philip Goldberg
Pittsburgh Energy Technology Center

Research supported by the United States Department of Energy,
Office of Fossil Energy, Pittsburgh Energy Technology Center

TABLE OF CONTENTS

TABLE OF CONTENTS (CONTINUED)

TABLE OF CONTENTS (CONTINUED)

LIST OF ILLUSTRATIONS (Continued)

LIST OF ILLUSTRATIONS (Continued)

LIST OF ILLUSTRATIONS (Continued)

LIST OF ILLUSTRATIONS (Continued)

LIST OF ILLUSTRATIONS

LIST OF ILLUSTRATIONS (Continued)

LIST OF ILLUSTRATIONS (Continued)

LIST OF TABLES

LIST OF TABLES (Continued)

EXECUTIVE SUMMARY

This is a comprehensive document containing the results of coal devolatilization experiments performed at Sandia National Laboratories during the period 1985 to 1991. This document was prepared at the request of the Department of Energy's Pittsburgh Energy Technology Center (PETC), and is meant to include *all* of the data in tabular form as well as a discussion of results. This executive summary provides background information, a description of the apparatus, and a summary of the results.

Background

Coal pyrolysis has been a subject of intensive study for many years because of the impact it has on most other aspects of coal combustion. The overall yield and composition of volatile products determines near-burner combustion temperatures and is often a governing factor for flame stability. The rate of coal devolatilization is important in determining the ignition characteristics of a coal flame, which in turn can influence the near-burner flow field and chemistry [Fletcher, 1985]. The near-burner flow field and stoichiometry significantly affects the amount of nitrogen pollutant formation; low-NO_x burners work on the principle that the volatile nitrogen reacts in fuel rich regions near the burner. Recent comprehensive coal combustor modeling efforts [Lockwood, et al., 1984] demonstrate the need to accurately describe the devolatilization rate, especially when trying to model other concurrent combustion processes.

Despite the many years of research, even the most recent investigations of coal pyrolysis rates disagree by many orders of magnitude. The difficulty of measuring the rate during rapid heating conditions results from the small time scales involved, coupled with the fact that most of the chemical processes occur during particle heating rather than at isothermal conditions. Representative comparisons of different devolatilization rates, based on 1-step Arrhenius kinetics for similar coals, are reported elsewhere [Solomon and Hamblen, 1985, Howard, et al., 1981]. Such comparisons are limited because the effect of heating rate is often misrepresented, but large differences in reported rates exist for experiments conducted at similar heating rates. The differences in the reported rates of devolatilization are often attributed to errors in the determination of particle temperatures as a function of residence time. Other sources for such large differences in the reported rates, such as errors in the determination of weight loss and/or residence time, would only change the rate by a factor of 2 or 3. The particle heating rates encountered in common devolatilization experiments range from 10^3 to 10^4 K/s, which is not a broad enough range to account for the differences in reported rates. The devolatilization rate obtained using the correlation of Kobayashi, et al. [1976] at 1800 K matches the rate from the correlation reported by Solomon, et al. [1986] at 1000 K; an 800 K difference in the temperature of reaction. The large differences in reported devolatilization rates therefore indicate the need for careful measurements of particle temperature during the initial particle heating zone.

This is the first study in which single particle temperatures were measured during devolatilization in an entrained flow reactor. Very few other investigators have attempted measurements of coal particle temperatures during devolatilization. Most pulverized coal pyrolysis experiments have not involved direct particle temperature measurements, but have inferred particle temperature from gas temperatures and the radiative field [Kobayashi, et al., 1976; Tsai and Scaroni, 1984; Maloney and Jenkins, 1984] or from screen temperatures [Anthony, et al., 1974; Niksa, et al., 1984; Suuberg, et al., 1978; Gibbins-Matham and Kandiyoti, 1988; Freihaut, et al., 1989].

Gat et al. [1983] measured temperatures of individual, laser-heated lignite particles at 1500-2700 K using a 3-color pyrometer at wavelengths of 0.92, 1.1, and 1.2 μm. Ballantyne, et al. [1983] measured particle cloud temperatures in a laser-heated cavity at temperatures between 1400 and 1800 K using a two-color pyrometer operating at 0.76 and 0.84 μm. Very little weight loss was observed in this experiment, evidently due either to the rapid surface heating of the particle with large internal temperature gradients or due to the condensation of tar onto the char. The minimum particle temperatures measured in these two experiments are quite high; significant weight loss can occur at lower temperatures.

Best, et al. [1986] measured particle cloud temperatures in two different reactors using an FTIR emission/transmission technique, which uses the normalized emission in the region from 6-10 μm to determine particle temperatures as low as 700 K. Agreement between measured and calculated particle temperatures was obtained by assuming that particles spread over the central 3 cm of the 5 cm diameter duct. Particle temperature was found to be sensitive to particle loading as well as to particle heat capacity, absorptivity, and flow instabilities resulting in non-laminar mixing behavior.

Recent particle temperature measurements during the devolatilization of a single particle have been performed by Maloney, et al. [1990, 1991] in an electrodynamic balance. A single particle is suspended in the balance and heated with a CO_2 laser. It is not possible to accurately measure the particle mass in this electrodynamic balance, and therefore visible features of the coal particles are used to determine the beginning and end of the mass release period. These features are monitored with a high-speed video camera system. The onset of particle spinning is used to determine the onset of gas release, while the appearance of the tar/soot cloud is used to determine the onset of tar release. The completion of devolatilization is monitored by the disappearance of the tar/soot cloud. Results indicate that the time scales for initiation of the pyrolysis reactions are comparable to those measured by Solomon, et al. [1986] and by Fletcher [1989a and 1989b], but Maloney's data imply that the time required to complete pyrolysis may be greater than reported by Fletcher and by Solomon. However, the data from the electrodynamic balance are inconclusive since mass release is not measured quantitatively.

After publication of pyrolysis rates from the first set of experiments from the Sandia coal devolatilization laboratory, attention shifted to characterization of the chemical

and physical properties of tar and char produced from different coals. Sizing-pyrometer measurements of particle size, temperature and velocity were performed in all of the experiments in order to provide well-characterized particle temperature histories. The physical nature of the coal char significantly influences the subsequent char reactivity, while the chemical structure of the coal and char determines the types of products released as light gas and tar. Measurements of the chemical structure of coal char and tar provide a strong basis for the development of the chemical percolation devolatilization (CPD) model [Grant, et al. 1989; Fletcher, et al. 1990; Fletcher, et al. 1991]. This is the first set of detailed measurements of the chemical structure of coal char and tar formed during devolatilization at rapid heating conditions. These data provide a unique test of current devolatilization models, in that the correct volatiles yields must be obtained in addition to the correct chemical structure (and hence reaction mechanism).

Experimental Apparatus

The Sandia coal devolatilization laboratory (CDL) consists of a transparent-wall flow reactor, an infrared sizing-pyrometer system, and a solids sampling system. Heating rates in the CDL flow reactor are approximately 10^4 K/s, and most experiments were performed in 100% N_2. The maximum gas temperature in the laminar flow reactor is 1250 K, with gas velocities on the order of 1 m/s. The sizing-pyrometer system has a lower temperature threshold of 850 K for a 100 μm diameter particle, which is adequate for determination of coal devolatilization rates under these conditions.

A few additional coal devolatilization experiments were conducted in the Sandia char combustion laboratory (CCL), which is also described in this report (see Section 2). Hurt, et al. [1992] have recently provided a comprehensive description of the CCL, along with a compilation of the Sandia coal char combustion data from the CCL. The flow reactor in the CCL consists of a laminar diffusion flame with a transparent-wall tower. The flame zone begins at a distance of approximately 5 mm above the burner and is about 3 mm thick. Entrained coal particles enter the flow reactor through a small tube located in the center of the burner. Particle heating rates in the CCL are approximately 5 x 10^4 K/s, with maximum gas temperatures of about 1500 K. The coal devolatilization experiments performed in the CCL consisted of operating the flame with 0% post-flame oxygen.

Sample Analysis

Collected char samples were analyzed by Adolph Coors Analytical Laboratories Division (in Golden, Colorado). The total ash content and the moisture content were measured using ASTM procedures, modified for small sample sizes. The organic portion of the samples were analyzed for elemental composition (C, H, O, N, S) on four independent Leco instruments. The sum of compositions of the five organic elements generally adds to 100 $\pm$5%.

A tracer technique was used to determine mass loss due to devolatilization, since occasional probe deposits consisting of tar and char agglomerates prevented complete mass closure during sampling. The inorganic elements were analyzed by Inductively Coupled Plasma (ICP) spectroscopy. The concentrations of the following elements were measured: Si, K, Ti, Fe, Al, Ca, Na, and Mg. Only the Si, Al, and Ti were used as tracers in this study; the concentrations of other elements were measured in connection with an associated mineral matter study at Sandia. The total ash content is also used as a tracer.

The apparent density is defined as the particle mass divided by its apparent volume (i.e., the volume based on the particle diameter). In softening coals, the apparent density changes significantly due to the formation of large internal voids. The true density of the solid material, which does not include the void volume, may also change due to preferential release of functional groups during pyrolysis. In this discussion, the term bulk density refers to the mass of particles occupying a known container volume, and is related to the apparent density through a packing factor. Bulk densities of coal samples were determined using mercury intrusion porosimetry at the Particle Characterization Facility at Lawrence Livermore National Laboratory.

A second method was also used for determination of apparent density ratios. A graduated cylinder is filled with particles and tapped gently to allow uniform packing. The bulk density is measured, and the packing factor is assumed to be constant for the both the parent coal and char particles. The bulk density ratio of char to parent coal is therefore equivalent to the apparent density ratio.

Internal surface areas of char samples were measured at the Particle Characterization Facility at Lawrence Livermore National Laboratory using nitrogen BET analysis. The physical features of the surface of coal and particles were examined using a scanning electron microscope (SEM). The internal structure of coal particles was examined by sectioning the particles.

The ^{13}C NMR data on the coal and char particles were obtained at the University of Utah, under the direction of Professor Ronald Pugmire, using a variation of the method described by Solum, et al. [1989]. Cross-polarization magic-angle spinning (CP/MAS) was used to quantitatively determine the chemical structures in coal and char samples. Dipolar dephasing data were employed to separate the aromatic Gaussian (C-H) component from the Lorentzian (non-protonated) component of the carbon magnetization. Using parameters from the above ^{13}C NMR analyses, twelve structural parameters relating to the carbon skeletal structure can be obtained. The average aromatic cluster size and the number of attachments on an aromatic cluster can also be estimated.

The ^{1}H and ^{13}C NMR data for each tar sample were obtained with a Varian VXR-500 spectrometer. Tars were removed from the tar filter and dissolved in 1 ml samples of deuterated (98%) dimethyl sulfoxide (DMSO). Small amounts of particulate matter

were observed in the tar/DMSO solutions, but no serious degradation of spectral resolution was observed due to the presence of colloidal material.

Analyses of the tar samples by combined gas chromatography and mass spectrometry (GC/MS) were performed at the University of Utah's Center for Micro Analysis and Reaction Chemistry under the direction of Professor Henk Meuzelaar. Low-voltage mass spectrometry (LV/MS) experiments were carried out using an extranuclear Model 5000-1 Curie-point pyrolysis MS system. The LV/MS system allows for a relatively quick, first-order analysis of the types of species that occur in tar samples, whereas the GC/MS system is used to confirm results from the LV/MS system and to provide further detail on specific species.

Coals Examined

The main body of experiments were performed on five coals from the PETC standardized suite of coals, ranging from a lignite to a low-volatile bituminous coal. The names of the coals examined in the CDL, along with the respective designation number from the Penn State Coal Bank, are as follows:

PSOC-1507D	North Dakota Beulah Zap lignite
PSOC-1445D	New Mexico Blue Subbituminous coal
PSOC-1493D	Illinois #6 hvb bituminous coal
PSOC-1451D	Pittsburgh #8 hva bituminous coal
PSOC-1508D	West Virginia Pocahontas #3 lv bituminous coal

The "D" designation refers to the PETC coals that were sieved and aerodynamically classified under a nitrogen atmosphere under the direction of PETC. These five coals are part of the ten coals distributed to several institutions and examined for fundamental coal devolatilization, char oxidation, and mineral matter properties. All ten of these coals were examined in a companion study at Sandia addressing char combustion.

Results and Conclusions

The motivation for the development of the Sandia Coal Devolatilization Laboratory was to provide a means for determining devolatilization rates based on direct measurements of the size, temperature, and velocity of individual particles during devolatilization. After that task was accomplished, attention was focused on studying the chemical and physical processes that occur to coal particles during devolatilization in experiments where the particle temperature was well characterized. This comprehensive document presents all of the coal devolatilization data obtained at Sandia, and discusses the results. The quantitative information contained in the appendix represents a significant contribution, since these data may now be used to refine modern devolatilization models. The data for different coals are discussed in the main body of the report with regard to a number of subtopics (e.g., elemental mass release, chemical structure, etc.) relevant to coal devolatilization. The presentation of

the data and discussion of the results are included in the main body of the document by topic. Conclusions from the different areas of research are summarized below.

A. Experiments in 100% N_2

Particle Temperature Histories

The large differences in reported devolatilization rates are attributed to the difficulty in determining accurate particle time-temperature profiles during devolatilization under rapid heating conditions. This difficulty arises because a major portion of volatiles are released during particle heating. Particle temperature histories are acutely sensitive to the local gas temperature and to the diameter, heat capacity, and apparent density of the particles.

In order to avoid the difficulties associated with inferred particle temperatures, an optically accessible entrained flow reactor and infrared sizing-pyrometer system was developed and used to measure simultaneously the size, temperature, and velocity of individual particles in the flow reactor at different residence times. This is the first time that individual coal particle temperatures have been measured during devolatilization. Comparison of measured sizes and temperatures of pure carbon spheres with those of pyrolizing coal particles shows that the temperature measurement is not influenced significantly by the tar cloud surrounding each particle. Results indicate that gas and particle temperatures and velocities in the flow reactor are significantly influenced by local cooling near the point of coal injection, which may be a cause for the large discrepancy in reported devolatilization rates measured in conventional drop tube reactors.

Temperatures as low as 850 K were measured for 100 μm diameter particles, which is low enough for particle temperature measurements during the middle to late stages of devolatilization at rapid heating rates. Spherocarb and coal particle temperatures, measured as a function of particle size, were compared with calculated temperatures as a function of residence time. Measured particle temperatures were found to be higher than calculated based on the centerline gas temperatures, emphasizing the need for the particle temperature measurements. Measured coal particle temperatures and velocities are fit using the general form of the particle energy equation in order to extrapolate to particle temperatures lower than 850 K.

Extent of Mass Release

Extents of mass release were determined from char samples using Si, Al, Ti, and total ash content as tracers. Tracers were chosen for each coal to minimize scatter in the mass release data, since the ICP and ashing procedures did not seem to give uniform results as a function of coal type. The total volatiles yields for four of the coals in the 1250 K gas condition (lignite, subbituminous, hvb and hva bituminous) were ~ 53% on a daf basis, while the total yield for the low volatile bituminous coals in this gas condition was 16% daf. The measured yields were in excess of the ASTM volatiles

yields by factors ranging from 1.08 for the lignite to 1.37 for the hva bituminous coal, while the ASTM volatiles yield for the low volatile bituminous coal was similar to the measured yield.

Coal Devolatilization Rates

Char particles were collected from the flow reactor using a helium quench probe with an on-line aerodynamic separation of char particles from the devolatilized tars and gases. Char samples were analyzed for elemental inorganic composition, and several elements were used as tracers to determine the extent of mass release during devolatilization. The statistical uncertainty in the mass release data is reduced by using the average of four independent tracers. The measured mass of volatiles released in the flow reactor has been compared with several commonly used rate models.

The data show evidence that the volatiles release is very rapid, and agrees quite well with the 1-step Arrhenius expression for tar release reported by Solomon, et al. [1986] for coals experiencing similar heating rates. Three simple rate models, with constants taken from other experiments, have also been compared with these temperature-resolved experimental data. Only the 2-step model with coefficients recommended by Ubhayakar et al. [1976] gives pyrolysis time scales comparable with this set of data. A more sophisticated model based on the chemical structure of the coal (the CPD model) used these data as a basis to determine rate coefficients. Evidence for rank-dependent kinetics is observed when the CPD model is compared with the time-dependent mass release data from five different coals at two temperature conditions.

The particle temperature measurements are viewed as critical to the determination of pulverized coal pyrolysis rates under rapid heating conditions. Kinetic coefficients derived from this experiment should be more universally applicable than previous data where particle temperature measurements were not performed. The facts that the minimum particle temperature measurement threshold is 850 K, and that devolatilization commences at lower temperatures than 850 K, do not impede the use of these data. On the contrary, if the kinetic rates were slower, as proposed by other investigators, 850 K would be the temperature at which devolatilization begins. The data presented here, however, indicate that approximately 50% of the mass release during devolatilization occurs by the time a particle temperature of 850 K is achieved, and hence kinetic rates obtained from these data are higher than initially expected. These data therefore serve as an excellent basis for determining the kinetics of devolatilization, even though temperature measurements over the entire extent of mass release are not available. *When this project started, the range of devolatilization rates at any temperature was five orders of magnitude. As a result of these experiments, the current uncertainty in devolatilization rates at rapid heating rates is thought to be less than a factor of five.*

Physical Structure of Char Particles

Char samples collected in the CDL and in the CCL were analyzed for apparent density, and an effective diameter was calculated from the apparent density and the extent of mass release. Maximum particle swelling occurred in the chars from Pittsburgh #8 coal collected in the CDL, with a 50% diameter increase observed. The low rank coals did not swell significantly. The low rank coal chars exhibited a great increase in internal surface area compared with the high rank coals chars. Chars from a softening coal (Pittsburgh #8) were examined with SEM in order to show the different stages of swelling, including the opening of fissures, the generation of internal voids, and the rounding of surface features due to softening.

Elemental Mass Release

Elemental release rates from five different coals during devolatilization were measured. Low rank coals release oxygen earlier than high rank coals. In general, oxygen and hydrogen release occur at similar rates, while carbon and nitrogen release rates seem to be correlated for all coals. The carbon release rate is proportional to the total mass release rate in the high rank coals, but is slower than the total mass release for low rank coals due to the large quantity of oxygen that is released early in the devolatilization process.

When coals devolatilize, the elemental release profiles do not follow the coalification band. Oxygen and hydrogen are released during devolatilization at similar rates, and hence the low rank coal char profiles bypass the bend in the coalification band. The fully-devolatilized coal chars all lie in a small region of the coalification chart compared to the diversity of the parent coals. However, the fully-devolatilized chars collected do exhibit slight differences, especially with respect to oxygen content, and none approach the composition of graphite.

Char Structure from NMR Analyses

Based on the NMR analyses of the chars formed during devolatilization of five coals of different rank at the 1250 K gas condition, the following conclusions are reached:

1) NMR data can be used to track lattice parameters associated with average cluster size and cross linking reactions. Under rapid heating conditions the NMR data demonstrate that the Zap lignite undergoes early cross linking behavior, while higher rank coals exhibit a slower overall rate of crosslinking.

2) Under rapid heating conditions (10^4 K/sec), the data exhibit: a) little evidence of cluster size growth in the macromolecular structure; b) crosslinking at the same time that aliphatic carbons are released; c) little evidence for graphitization under the temperature and residence time conditions of these experiments.

3) In the Illinois No. 6 coal, most of the mass release has occurred before significant changes in carbon aromaticity has occurred. In chars from Zap lignite, the changes in carbon aromaticity occur much earlier than for the bituminous coal.

4) The carbon skeletal structure of the final chars from coals of all ranks are quite similar, even though the structures of the initial coals are quite different.

Tar Structure from NMR Analyses

Based on the ^{1}H and ^{13}C NMR analysis of the tars collected from four coals of different rank in the 1250 K and 1050 K gas conditions, the following conclusions are reached:

1) The pyrolysis temperature has a major effect on the tar structure. The proton and carbon aromaticities of the tars from a given coal in the 1250 K gas condition are higher than for samples collected at comparable extents of mass release in the 1050 K gas condition.

2) The carbon aromaticities of the bituminous and subbituminous coal tars at 1250 K are higher than the values for the corresponding chars collected at the same residence time. On the other hand, the carbon aromaticities found in the Zap lignite tars are comparable to those observed in the chars.

3) The proton NMR data suggest that in the 1250 K gas condition, hydrogens associated with 2- and 3-ring aromatic compounds increase, while that of 1-ring compounds decrease for the Illinois No. 6 tars. Similar but less compelling evidence is noted for the lignite and subbituminous coal tars. These data may suggest the conversion of hydroaromatic species to condensed polynuclear aromatic species and/or ring polymerization.

4) The α-hydrogen content in the initial tars evolved increases as a function of coal rank. The α-hydrogen in the tars from the three non-lignitic coals decreases with residence time at the 1250 K condition but not at the 1050 K condition. This observation suggests that relatively stable CH and/or CH_2 bridges exist at the 1050 K gas condition in the higher rank coals. However, at 1250 K substantial bond rupture may be occurring.

5) The α-methyl groups are released early in tars from all four coals at 1250 K, but do not decrease significantly at 1050 K.

6) The γ-methyl groups in both tars are the most susceptible to cracking reactions in the gas phase, but the extent of release of the β- and γ-hydrogens is based on gas temperature conditions and residence time. The percentage of γ-methyl groups in the initial tar evolved decreases as coal rank increases.

The NMR data presented here for char and tar samples from the CDL have led to greater understanding of the pyrolysis process. These data are unique, not only because they are the first to be taken as a function of residence time at rapid heating rates, but because the temperature and reaction history is so well-characterized. The chemical percolation devolatilization (CPD) model [Grant, et al., 1989; Fletcher, et al, 1990; Fletcher, et al., 1991] directly uses these data on the chemical structure of parent coals as input parameters, and the data at later residence times are used to evaluate the model.

Tar Structure from Mass Spectrometry

Based on the Curie-point GC/MS and low-voltage MS analyses of the tar formed during devolatilization of Beulah Zap, New Mexico Blue, Illinois #6, Pittsburgh #8, and Pocahontas #3 coals, the following conclusions are reached:

1. The degree of aromaticity increases rapidly in tars from all five coals as a function of residence time at the 1250 K gas temperature. However, little increase in aromaticity in the tars is detected at the 1050 K gas temperature.

2. At a gas temperature of 1250 K, devolatilization is complete within 70 msec and secondary gas-phase reactions of tar vapors can be observed within 100 msec. At 1050 K, the devolatilization process appears to be more or less complete after 250 msec.

3. In order to study the complete devolatilization process and the possible onset of secondary reactions, further experiments should be conducted at an intermediate temperature, e.g., 1150 K.

These conclusions are consistent with the ^{1}H and ^{13}C NMR analyses performed previously on these same tars.

B. Results of Additional Experiments

Two types of experiments were conducted in the Sandia Coal Devolatilization Laboratory (CDL) where up to 10 mole-% oxygen was added to the nitrogen in the flow reactor. The first set of experiments was performed at the request of PETC personnel as a complementary check on some char combustion experiments performed at the University of North Dakota Energy and Environmental Research Center (UNDEERC). In this set of experiments, particle temperatures for two coal types were examined at a gas temperature of ~ 1000 K and an oxygen concentration of ~ 10 mole-%. This work involved only sizing-pyrometer experiments without solids sampling experiments.

A second set of experiments was performed in the CDL in 0 to 10 mole-% O_2 to determine the effect of oxygen on particle swelling characteristics. This purpose of these experiments was to investigate possible reasons for notable differences in

particle swelling behavior between samples collected in 100% N_2 in the CDL and samples collected in post-flame combustion environments of 3 to 12% O_2 in the Char Combustion Laboratory (CCL). The experiments in the CDL were conducted mainly with the solids sampling apparatus, and did not involve the sizing-pyrometer. Conclusions from these two sets of experiments are summarized below.

Temperature Measurements of Burning Char Particles

The size and temperatures of burning char particles were measured in the CDL in N_2-O_2 atmospheres at 1000 K containing up to 12% O_2. Temperatures of burning bituminous char particles were estimated to exceed 1500 K (compared to 1686 K measured at UNDEERC), but less than 5% of the particles ignited under these conditions, and detailed statistical measurements were not possible. It is difficult to compare the temperatures measured in this experiment with those measured at UNDEERC, since it not clear how to conditionally average the data from ignited and non-reacting particles. Lignite char particle temperatures measured in the CDL in 10% O_2 were approximately 1600 K, which is the in the same range as measured at UNDEERC (1586 K). However, data from the lignite char experiments in the CDL also indicate the presence of significant numbers of non-burning particles (25 to 75%). Extents of burnout in solid samples taken from experiments where significant numbers of char particles have not ignited are impossible to interpret unless the precise percentage of non-burning particles is known.

Transition from Coal Devolatilization to Char Oxidation

Based on the results of the experiments conducted in the CDL and the CCL as a function of gas phase oxygen concentration, the following conclusions are reached:

1. The degree of swelling during coal pyrolysis at rapid heating conditions ($> 10^4$ K/s) is not affected by the gas phase oxygen concentration. Changes in particle swelling caused by the presence of oxygen reported in other experiments may be due to partial oxidation of char samples subsequent to pyrolysis.

2. Pittsburgh #8 coal particles increased in diameter by 50% in the CDL experiments and by less than 10% in the CCL experiments. Differences in swelling behavior were caused by differences in particle heating rate and/or the presence of post-flame combustion gases (e.g., CO_2, H_2O, or trace radical species).

3. An examination of samples obtained in the char combustion experiments in the CCL revealed the absence of any transparent cenospheres; these types of particles were either not formed or were consumed upstream of the sampling location.

4. Calculations of particle heating rates indicate that maximum particle heating rate in the CCL for the size fractions typically used (106-125 μm) is 4.5 x 10^4 K/s, which is a factor of two to three higher than the maximum heating rate experienced in the CDL experiments. The calculated difference between the particle heating rates at 0% O_2 in the two different laboratories may be responsible for the differences in the physical properties of the char particles. Because the heating rates were within a factor of two to three, however, other possible causes for the observed differences in swelling behavior should also be investigated.

References for Executive Summary

Anthony, D. B., J. B. Howard, H. C. Hottel, and M. P. Meissner, *Fifteenth Symp. (Int.) on Comb.*, The Combustion Institute, p. 1303 (1974).

Ballantyne, A., H. P. Chou, A. Flusberg, R. Neoh, N. Orozco, and D. Stickler, "Volatile Prodution During Preignition Heating," DOE Final Report, PETC Contract No. DE-AC22-80PC30291 (1983).

Best, P. E., R. M. Carangelo, J. R. Markham, and P. R. Solomon, *Comb. Flame*, **66**, 47 (1986).

Fletcher, T. H., "Sensitivity of Combustion Calculations to Devolatilization Rate Expressions," presented at the Fall AFRC Meeting, Livermore, California (1985).

Fletcher, T. H., *Comb. Sci. Tech.*, **63**, 89 (1989a).

Fletcher, T. H., *Comb. Flame*, **78**, 223 (1989b).

Fletcher, T. H., A. R. Kerstein, R. J. Pugmire, and D. M. Grant, *Energy & Fuels*, **4**, 54 (1990).

Fletcher, T. H., A. R. Kerstein, R. J. Pugmire, and D. M. Grant, "A Chemical Percolation Model for Devolatilization: 3. Chemical Structure as a Function of Coal Type," in press (1991). See also Fletcher, T. H. and D. R. Hardesty, "Coal Combustion Science: Task 1, Coal Devolatilization," DOE/PETC Quarterly Progress Report for October to December, 1990, edited by D. R. Hardesty, Sandia Report No. SAND91-8210, available NTIS (1991).

Freihaut, J. D., W. M. Proscia, and D. J. Seery, *Energy & Fuels*, **3**, 692 (1989).

Gat, N., L. M. Cohen, and A. B. Witte, "Three-Color Pyrometer for Burning Particle Temperature Measurement," presented at the JANNAF Combustion Meeting, Monterey, California (1983).

Gibbins-Matham, J. and R. Kandiyoti, *Energy and Fuels*, **2**, 505, (1988).

Grant, D. M., R. J. Pugmire, T. H. Fletcher, and A. R. Kerstein, *Energy & Fuels*, **3**, 175 (1989).

Howard, J. B., "Fundamentals of Coal Pyrolysis and Hydropyrolysis," in *Chemistry of Coal Utilization*, ed. by M. A. Elliott, Wiley and Sons, New York, p. 689 (1981).

Hurt, R. H., R. E. Mitchell, and D. R. Hardesty, "Compilation of Sandia Coal Char Combustion Data and Kinetic Analyses," Milestone Report for DOE/PETC Contract FWP 0709 (in press, 1992).

Kobayashi, H., J. B. Howard, and A. F. Sarofim, *Sixteenth Symp. (Int.) on Comb.*, The Combustion Institute, 411 (1976).

Lockwood, F. C., S. M. A. Rizvi, G. K. Lee, and H. Whaley, *Twentieth Symp. (Int.) on Comb.*, The Combustion Institute, p. 513 (1984).

Maloney, D. J. and R. G. Jenkins, *Twentieth Symp. (Int.) on Comb.*, The Combustion Institute, p. 1435 (1984).

Maloney, D. J., S. D. Woodruff, E. R. Monazam, and S. Ramanathan, "Single Particle Combustion Studies," proceedings of the DOE PETC/METC AR&TD, Direct Utilization, and Instrument and Diagnostics Contractors' Review Meeting, Pittsburgh, PA, CONF-900981--(De91006344), p. 177 (September, 1990).

Maloney, D. J., E. R. Monazam, S. D. Woodruff, and L. O. Lawson, *Comb. Flame*, **84**, 210 (1991).

Niksa, S., L. E. Heyd, W. B. Russel, and D. A. Saville, *Twentieth Symp. (Int.) on Comb.*, The Combustion Institute, p. 1445 (1984).

Solomon, P. R. and D. G. Hamblen, "Pyrolysis," in *Chemistry of Coal Conversion*, ed. Schlosberg, R. H., Plenum Press, New York, 121 (1985).

Solomon, P. R., M. A. Serio, R. M. Carangelo, and J. R. Markham, *Fuel*, **65**, 182 (1986).

Suuberg, E. M., W. A. Peters, and J. B. Howard, *Seventeenth Symp. (Int.) on Comb.*, The Combustion Institute, Pittsburgh, Pennsylvania, p. 117 (1978).

Tsai, C. and Scaroni, A. W., *Twentieth Symp. (Int.) on Comb.*, The Combustion Institute, p. 1455 (1984).

Ubhayakar, S. K., D. N. Stickler, C. W. von Rosenberg, and R. E. Gannon, *16th Symp. (Int.) on Comb.*, The Combustion Institute, Pittsburgh, PA, 427 (1976).

1. INTRODUCTION

Coal pyrolysis has been a subject of intensive study for many years because of the impact it has on most other aspects of coal combustion. The overall yield and composition of volatile products determines near-burner combustion temperatures and is often a governing factor for flame stability. The rate of coal devolatilization is important in determining the ignition characteristics of a coal flame, which in turn can influence the near-burner flow field and chemistry [Fletcher, 1985]. Recent comprehensive coal combustor modeling efforts [Lockwood, et al., 1984] demonstrate the need to accurately describe the devolatilization rate, especially when trying to model other concurrent combustion processes.

Despite the many years of research, even the most recent investigations of coal pyrolysis rates disagree by many orders of magnitude. The difficulty of measuring the rate during rapid heating conditions results from the small time scales involved, coupled with the fact that most of the chemical processes occur during particle heating rather than at isothermal conditions. Representative comparisons of different devolatilization rates, based on 1-step Arrhenius kinetics for similar coals, are reported elsewhere [Solomon and Hamblen, 1985, Howard, et al., 1981]. Such comparisons are limited because the effect of heating rate is often misrepresented, but large differences in reported rates exist for experiments conducted at similar heating rates. The differences in the reported rates of devolatilization are often attributed to errors in the determination of particle temperatures as a function of residence time. Other sources for such large differences in the reported rates, such as errors in the determination of weight loss and/or residence time, would only change the rate by a factor of 2 or 3. The particle heating rates encountered in common devolatilization experiments range from 10^3 to 10^4 K/s, which is not a broad enough range to account for the differences in reported rates. The devolatilization rate obtained using the correlation of Kobayashi, et al. [1976] at 1800 K matches the rate from the correlation reported by Solomon , et al. [1986] at 1000 K; an 800 K difference in the temperature of reaction. The large differences in reported devolatilization rates therefore indicate the need for careful measurements of particle temperature during the initial particle heating zone.

This is the first study in which single particle temperatures were measured during devolatilization in an entrained flow reactor. Very few other investigators have attempted measurements of coal particle temperatures during devolatilization. Most pulverized coal pyrolysis experiments have not involved direct particle temperature measurements, but have inferred particle temperature from gas temperatures and the radiative field [Kobayashi, et al., 1976; Tsai and Scaroni, 1984; Maloney and Jenkins, 1984] or from screen temperatures [Anthony, et al., 1974; Niksa, et al., 1984; Suuberg, et al., 1978; Gibbins-Matham and Kandiyoti, 1988; Freihaut, et al., 1989]. Gat et al. [1983] measured temperatures of individual, laser-heated lignite particles at 1500-2700 K using a 3-color pyrometer at wavelengths of 0.92, 1.1, and 1.2 μm. Ballantyne, et al. [1983] measured particle cloud temperatures in a laser-heated cavity at temperatures between 1400 and 1800 K using a two-color pyrometer operating at 0.76

and 0.84 μm. Very little weight loss was observed in this experiment, evidently due either to the rapid surface heating of the particle with large internal temperature gradients or due to the condensation of tar onto the char. The minimum particle temperatures measured in these two experiments are quite high; significant weight loss can occur at lower temperatures.

Best, et al. [1986] measured particle cloud temperatures in two different reactors using an FTIR emission/transmission technique, which uses the normalized emission in the region from 6-10 μm to determine particle temperatures as low as 700 K. Agreement between measured and calculated particle temperatures was obtained by assuming that particles spread over the central 3 cm of the 5 cm diameter duct. Particle temperature was found to be sensitive to particle loading as well as to particle heat capacity, absorptivity, and flow instabilities resulting in non-laminar mixing behavior.

Recent particle temperature measurements during the devolatilization of a single particle have been performed by Maloney, et al. [1990, 1991] in an electrodynamic balance. A single particle is suspended in the balance and heated with a CO_2 laser. It is not possible to accurately measure the particle mass in this electrodynamic balance, and therefore visible features of the coal particles are used to determine the beginning and end of the mass release period. These features are monitored with a high-speed video camera system. The onset of particle spinning is used to determine the onset of gas release, while the appearance of the tar/soot cloud is used to determine the onset of tar release. The completion of devolatilization is monitored by the disappearance of the tar/soot cloud. Results indicate that the time scales for initiation of the pyrolysis reactions are comparable to those measured by Solomon, et al. [1986] and by Fletcher [1989a and 1989b], but Maloney's data imply that the time required to complete pyrolysis may be greater than reported by Fletcher and by Solomon. However, the data from the electrodynamic balance are inconclusive since mass release is not measured quantitatively.

After publication of pyrolysis rates from the first set of experiments from the Sandia coal devolatilization laboratory, attention shifted to characterization of the chemical and physical properties of tar and char produced from different coals. Sizing-pyrometer measurements of particle size, temperature and velocity were performed in all of the experiments in order to provide well-characterized particle temperature histories. The physical nature of the coal char significantly influences the subsequent char reactivity, while the chemical structure of the coal and char determines the types of products released as light gas and tar. Measurements of the chemical structure of coal char and tar provide a strong basis for the development of the chemical percolation devolatilization (CPD) model [Grant, et al. 1989; Fletcher, et al. 1990; Fletcher, et al. 1991]. This is the first set of detailed measurements of the chemical structure of coal char and tar formed during devolatilization at rapid heating conditions. These data provide a unique test of current devolatilization models, in that the correct volatiles yields must be obtained in addition to the correct chemical structure (and hence reaction mechanism).

This is a comprehensive document containing the results of coal devolatilization experiments performed at Sandia National Laboratories during the period 1985 to 1991. This document was prepared at the request of the Department of Energy's Pittsburgh Energy Technology Center (PETC), and is meant to include *all* of the data in tabular form as well as a discussion of results.

References for Chapter 1

Anthony, D. B., J. B. Howard, H. C. Hottel, and M. P. Meissner, *Fifteenth Symp. (Int.) on Comb.*, The Combustion Institute, p. 1303 (1974).

Ballantyne, A., H. P. Chou, A. Flusberg, R. Neoh, N. Orozco, and D. Stickler, "Volatile Prodution During Preignition Heating," DOE Final Report, PETC Contract No. DE-AC22-80PC30291 (1983).

Best, P. E., R. M. Carangelo, J. R. Markham, and P. R. Solomon, *Comb. Flame*, **66**, 47 (1986).

Fletcher, T. H., "Sensitivity of Combustion Calculations to Devolatilization Rate Expressions," presented at the Fall AFRC Meeting, Livermore, California (1985).

Fletcher, T. H., *Comb. Sci. Tech.*, **63**, 89 (1989a).

Fletcher, T. H., *Comb. Flame*, **78**, 223 (1989b).

Fletcher, T. H., A. R. Kerstein, R. J. Pugmire, and D. M. Grant, *Energy & Fuels*, **4**, 54 (1990).

Fletcher, T. H., A. R. Kerstein, R. J. Pugmire, and D. M. Grant, "A Chemical Percolation Model for Devolatilization: 3. Chemical Structure as a Function of Coal Type," in press (1991). See also Fletcher, T. H. and D. R. Hardesty, "Coal Combustion Science: Task 1, Coal Devolatilization," DOE/PETC Quarterly Progress Report for October to December, 1990, edited by D. R. Hardesty, Sandia Report No. SAND91-8210, available NTIS (1991).

Freihaut, J. D., W. M. Proscia, and D. J. Seery, *Energy & Fuels*, **3**, 692 (1989).

Gat, N., L. M. Cohen, and A. B. Witte, "Three-Color Pyrometer for Burning Particle Temperature Measurement," presented at the JANNAF Combustion Meeting, Monterey, California (1983).

Gibbins-Matham, J. and R. Kandiyoti, *Energy and Fuels*, **2**, 505, (1988).

Grant, D. M., R. J. Pugmire, T. H. Fletcher, and A. R. Kerstein, *Energy & Fuels*, **3**, 175 (1989).

Howard, J. B., "Fundamentals of Coal Pyrolysis and Hydropyrolysis," in *Chemistry of Coal Utilization*, ed. by M. A. Elliott, Wiley and Sons, New York, p. 689 (1981).

Kobayashi, H., J. B. Howard, and A. F. Sarofim, *Sixteenth Symp. (Int.) on Comb.*, The Combustion Institute, 411 (1976).

Lockwood, F. C., S. M. A. Rizvi, G. K. Lee, and H. Whaley, *Twentieth Symp. (Int.) on Comb.*, The Combustion Institute, p. 513 (1984).

Maloney, D. J. and R. G. Jenkins, *Twentieth Symp. (Int.) on Comb.*, The Combustion Institute, p. 1435 (1984).

Maloney, D. J., S. D. Woodruff, E. R. Monazam, and S. Ramanathan, "Single Particle Combustion Studies," proceedings of the DOE PETC/METC AR&TD, Direct Utilization, and Instrument and Diagnostics Contractors' Review Meeting, Pittsburgh, PA, CONF-900981--(De91006344), p. 177 (September, 1990).

Maloney, D. J., E. R. Monazam, S. D. Woodruff, and L. O. Lawson, *Comb. Flame*, **84**, 210 (1991).

Niksa, S., L. E. Heyd, W. B. Russel, and D. A. Saville, *Twentieth Symp. (Int.) on Comb.*, The Combustion Institute, p. 1445 (1984).

Solomon, P. R. and D. G. Hamblen, "Pyrolysis," in *Chemistry of Coal Conversion*, ed. Schlosberg, R. H., Plenum Press, New York, 121 (1985).

Solomon, P. R., M. A. Serio, R. M. Carangelo, and J. R. Markham, *Fuel*, **65**, 182 (1986).

Suuberg, E. M., W. A. Peters, and J. B. Howard, *Seventeenth Symp. (Int.) on Comb.*, The Combustion Institute, Pittsburgh, Pennsylvania, p. 117 (1978).

Tsai, C. and Scaroni, A. W., *Twentieth Symp. (Int.) on Comb.*, The Combustion Institute, p. 1455 (1984).

2. EXPERIMENTAL APPARATUS

The Sandia coal devolatilization laboratory (CDL) consists of a transparent-wall flow reactor, an infrared sizing-pyrometer system, and a solids sampling system, as discussed below. The majority of experiments reported here were conducted in the CDL. A few additional experiments were conducted in the Sandia char combustion laboratory (CCL), which is also described in this chapter.

CDL Flow Reactor

In conventional drop-tube reactor studies the reactor walls are generally heated to match the gas temperature; particle temperatures and velocities near the injection point are then calculated. This type of reactor is well-suited to examining reactions occurring in the isothermal region rather than transient pyrolysis reactions (where major weight loss occurs during particle heating). Optical access in these reactors is often limited, making it difficult to measure particle temperature histories near the water-cooled coal injector where gas temperatures and velocities are two-dimensional. Some studies move the coal feed tube to provide different residence times, and must account for changes in the flow conditions at each axial position.

In CDL experiments, particles are injected from a water-cooled tube into a transparent flow reactor. The main process nitrogen flow is heated by a series of electric heaters, as shown schematically in Fig. 2.1. The first heater consists of an Inconnel tube filled with ceramic beads and surrounded by Thermcraft clamshell heaters made from nichrome resistance heating elements. This heater is surrounded by insulation, and is connected to the final heater stage with a 1/4 inch inconnel tube. The final heater consists of Kanthal 33 heating elements surrounding an alumina cylinder. The temperatures of the heaters are controlled by Omegaa ramping temperature controllers; startup and shutdown heating and cooling rates are limited to 200 K/hr to avoid shattering ceramic parts in the heaters. Mullite honeycomb flow straighteners are used to provide laminar flow.

The flow reactor has a square cross-section (5 cm x 5 cm) to facilitate optical imaging of the particles. The final heater therefore has shaped ceramic inserts to smooth the transition from annular flow in the alumina cylinder to the flow in the square cross-section of the flow reactor. The main body of experiments ere conducted in a 12 inch long tower, although a few preliminary experiments were conducted in a 24 inch long tower. The entire flow reactor system is mounted on a three-way traversing system, so that the optical system and sample collection system can remain fixed to an optical bench. The reactor is moved in the horizontal plane to maximize the data collection rate, which yields data from the location with the maximum particle number density. The reactor is moved in the vertical plane to change residence time, since the pyrometer system and probe sampling system remain at fixed locations. Axial distance in the flow reactor is measured from the tip of the coal injection probe using a

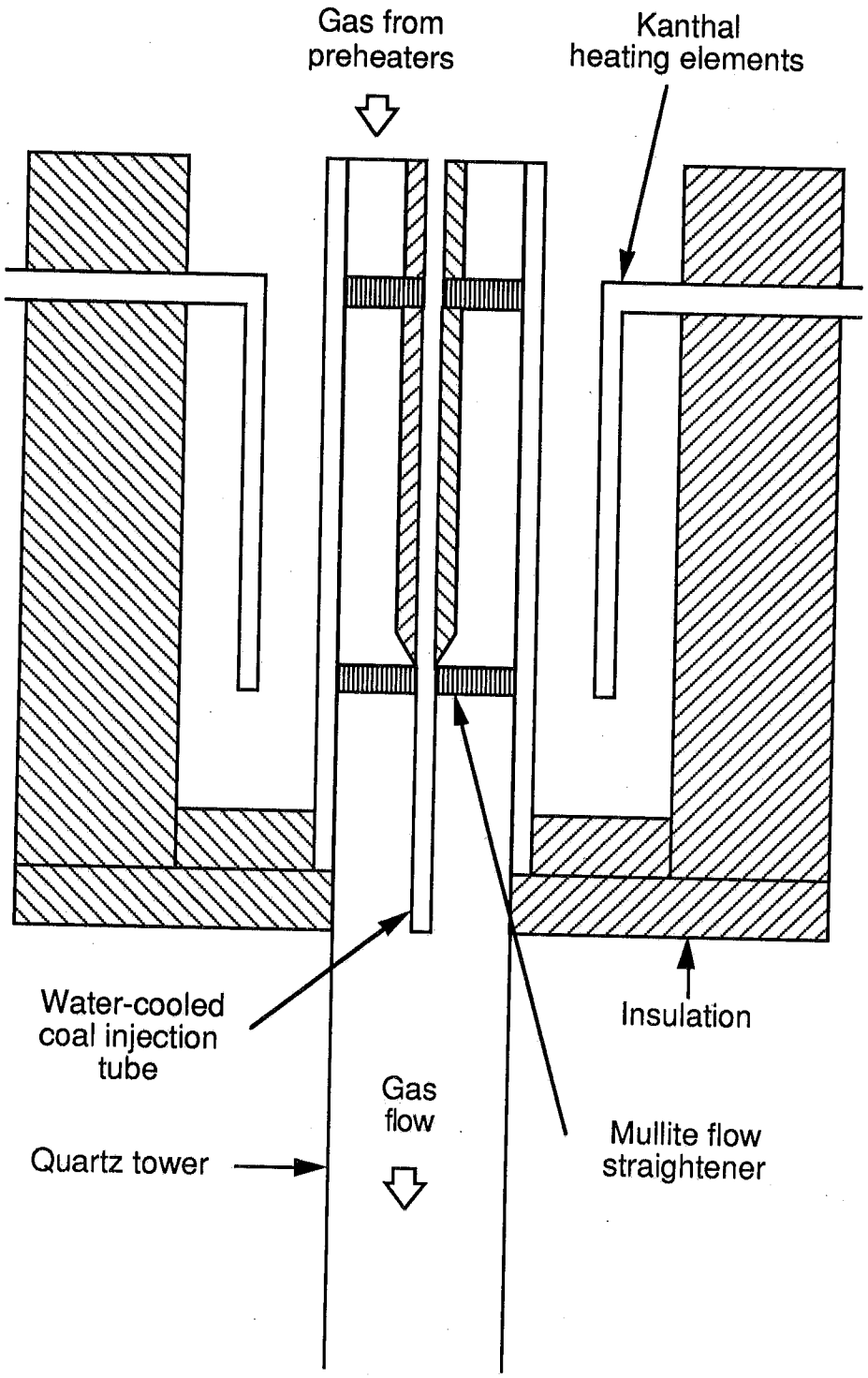

Figure 2.1 Schematic of the heater and flow system for the inert-gas flow reactor in the Coal Devolatilization Laboratory.

Bausch and Lomb Acu-Rite III digital scale, similar to that used in a milling machine. The reference scale is mounted to the superstructure supporting the moveable heater assembly. The scale is zeroed at the tip of the injection probe using the HeNe laser from the pyrometer system, and the scale changes automatically as the reactor is raised and lowered. Flow rates of different gases into the reactor are controlled by Brooks model 5850 flow controllers with digital readouts. The flow rate controllers are calibrated with wet test meters. The standard operating conditions for these tests were nitrogen flow rates of 30 standard liters per minute (slpm) at atmospheric pressure. Higher flow rates were found to cause flow instabilities (lazy turbulence), which greatly hindered detection of particles in the small optical focal volume of the sizing-pyrometer system.

Maximum gas temperatures in the flow reactor are 1250 K, as measured by a 100 μm diameter Pt/Pt-13%Rh thermocouple. The thermocouple bead diameter is measured using a microscope and polaroid camera. Fine-wire thermocouple beads were purchased and spot-welded to large-diameter (1 mm) Pt or Pt-13%Rh wires threaded through a 3 foot long, 1/4 inch diameter two-holed alumina tube. The three-foot alumina tube is held in place, with the bead at the location of the laser from the sizing-pyrometer system, and the flow reactor and heater assembly is raised and lowered to obtain gas temperatures as a function of distance from the coal injection tube. The centerline gas temperature is found by positioning the gas temperature thermocouple within 5 mm of the tip of the coal injection tube, and then moving the flow reactor assembly in the horizontal directions until the minimum gas temperature is found. The flow reactor is then raised and lowered without further changes to horizontal position in order to obtain gas temperatures as a function of distance from the tip of the coal injection tube. Thermocouple temperatures are displayed digitally (Fluke thermocouple readout) after automatic correction to the ice point reference temperature. Using the bead diameter, the thermal conductivity of the gas in the flow reactor, and the bead emissivity, the thermocouple reading is corrected for radiative losses to the reactor walls in order to obtain the gas temperature. Because of the small thermocouple beads and the moderate temperatures employed in these experiments, the maximum thermocouple correction for radiation was only 25 to 50 K.

The maximum gas temperature is limited because of the transparent reactor walls due to radiant heat loss from upstream heater components. Centerline gas temperature profiles in the reactor at this flow condition are shown in Fig. 2.2, showing the local cooling near the coal injection tube. Gas temperatures as high as 1300 K occur between the coal injector and the reactor walls, causing a complex gas velocity profile near the point of coal injection.

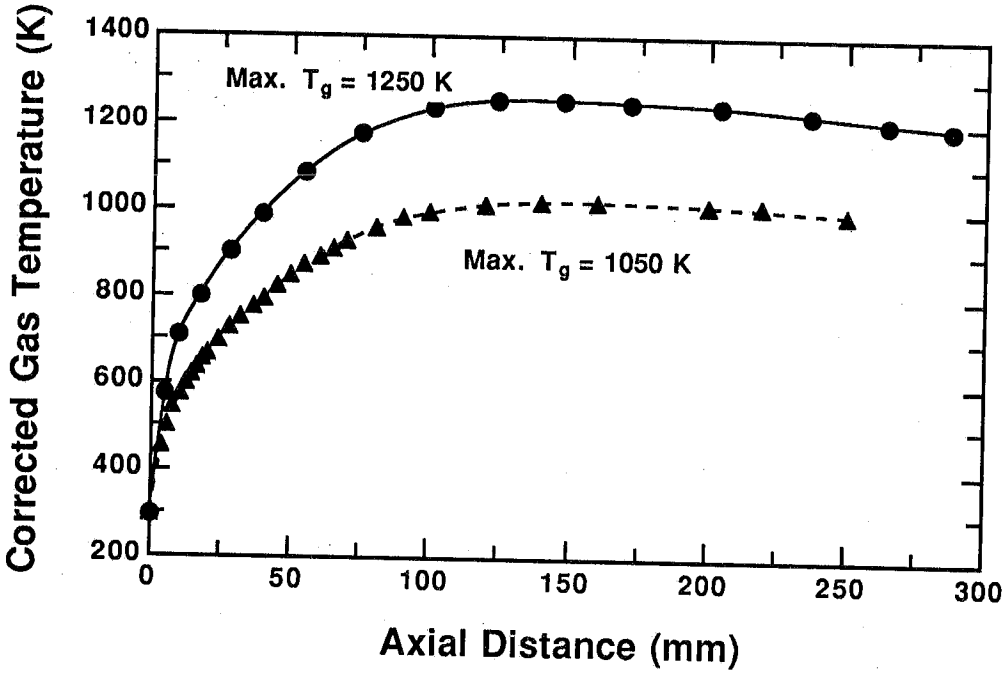

Figure 2.2 Typical gas temperature measurements for two different environments in the CDL flow reactor (100% N_2). These two reactor environments are referred to as the 1250 K and the 1050 K gas conditions.

The particle feeder consists of a gas-tight syringe loaded with particles, and the plunger is advanced with a stepping motor, as shown in Fig. 2.3. As particles fall off the end of the syringe, they are entrained by the carrier gas and fed to the flow reactor. The feeder is attached to a vibrator to aid uniform feeding. A rotating brush assembly was also attached to the feeder, so that the brush would gently break apart any agglomerated coal particles at the end of the syringe. This was particularly important for low rank coals. If the brush were located in Fig. 2.3, it would stick up out of the page at the tip of the syringe. The brush was rotated at slow speeds of 1 to 2 revolutions per second to avoid smearing the coal over the interior of the containment vessel. Particle feed rates can be adjusted independently of the flow rate of the entrainment gas. Typical flow rates used in these experiments are approximately 10 mg/min, compared to feed rates of 0.5-1 g/min used in typical drop tube studies. The low particle flow rates used here ensure single particle behavior, which is necessary for the sizing-pyrometer system. Visual observations of particle and tar cloud trajectories indicated that flow instabilities are minimal; the diameter of the particle stream is approximately 0.75 cm at an axial distance of 150 mm. Particle velocities in the flow reactor under typical operating conditions are approximately 1 m/s, as measured by the sizing-pyrometer system described in the next section.

CDL Infrared Sizing Pyrometer

Simultaneous measurements of particle size, temperature, and velocity are performed using a coded-aperture technique similar to that used by Tichenor, et al. [1984]. A schematic of the optical system is shown in Fig. 2.4, and the coded aperture is shown in Fig. 2.5. The coded apertures were photoetched from silvered glass rather than film to prevent partial transmission of emission signals. The particle emission signal that passes through the large central slit is proportional to the emissivity, the blackbody emission (which is a function of wavelength and temperature), and the projected particle area. The particle emission signal passing through the narrow slit is proportional to the emissivity, the blackbody emission, and the viewed area (diameter times the slit width). Hence, the ratio of the signal from the large slit to the signal from the small slit is proportional to particle diameter. Infrared emission from individual particles is collected by a matched pair of spherical mirrors, rather than lenses, to minimize chromatic aberrations in the infrared. A HeNe laser is used as a triggering system to determine when particles are in the optical focal volume.

The image of the particle passes through the large and small sizing slits in the aperture, through a dichroic beamsplitter and bandpass filters, and is focused onto liquid-nitrogen-cooled Judson Infrared J-12D Indium Arsenide (InAs) detectors. The detector size was only 10 mm, making alignment and calibration tedious. The dichroic beamsplitter employed transmits light at wavelengths from 2.1-2.7 μm, while the two bandpass filters transmit light at wavelengths from 1.1-1.6 μm and 1.9-2.5 μm, respectively. Care was taken to obtain a beamsplitter and bandpass filters that did not have secondary transmission bands; spectral transmission characteristics were measured with a spectrophotometer to verify manufacturer specifications. Sapphire windows are used for the flow reactor tower during optical measurements since heated quartz is semi-opaque at near-infrared wavelengths at moderate temperatures.

A typical coal particle emission signal from the sizing-pyrometer system is shown in Fig. 2.6 at two different wavelengths. The peak heights at wavelength λ_1 are labeled $E_{1,\lambda 1}$ for the large slit and $E_{2,\lambda 1}$ for the small slit, with corresponding nomenclature for the peaks at wavelength λ_2. The particle temperature is therefore calculated from the ratio of the peak heights for the large slit ($E_{1,\lambda 1}/E_{1,\lambda 2}$), assuming thermal emission follows Planck's law of radiation with spectral emissivity $\varepsilon_{\lambda,T}$:

$$E_{\lambda,T} = \frac{\varepsilon_{\lambda,T}\, C_1}{\lambda^5 \left[\exp\left(\frac{C_2}{\lambda T} - 1\right)\right]} \qquad (2.1)$$

where $C_1 = 3.742 \times 10^8$ W μm^4/m^2 and $C_2 = 1.439 \times 10^4$ μm K. It is assumed that the emissivities of the particle at the two wavelengths of interest do not change during devolatilization (i.e., $\varepsilon_{\lambda 1}/\varepsilon_{\lambda 2}$ = constant), and therefore $E_{1,\lambda 1}/E_{1,\lambda 2}$ is only a function of λ_1, λ_2, and the particle temperature. This is a less restrictive assumption than the graybody assumption, where ε_λ is a constant value for all wavelengths.

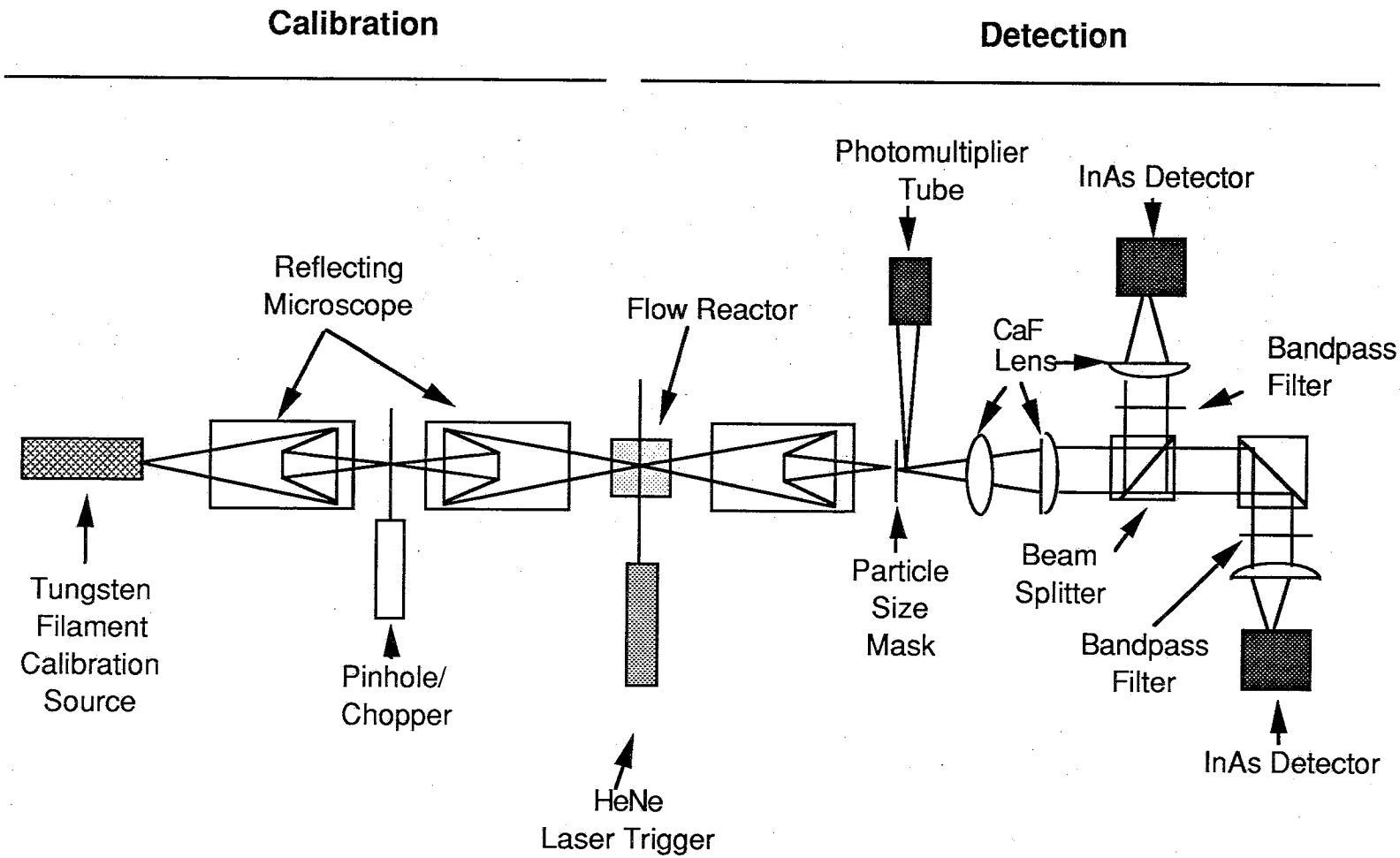

Figure 2.4 Schematic of the infrared sizing-pyrometry system in the CDL.

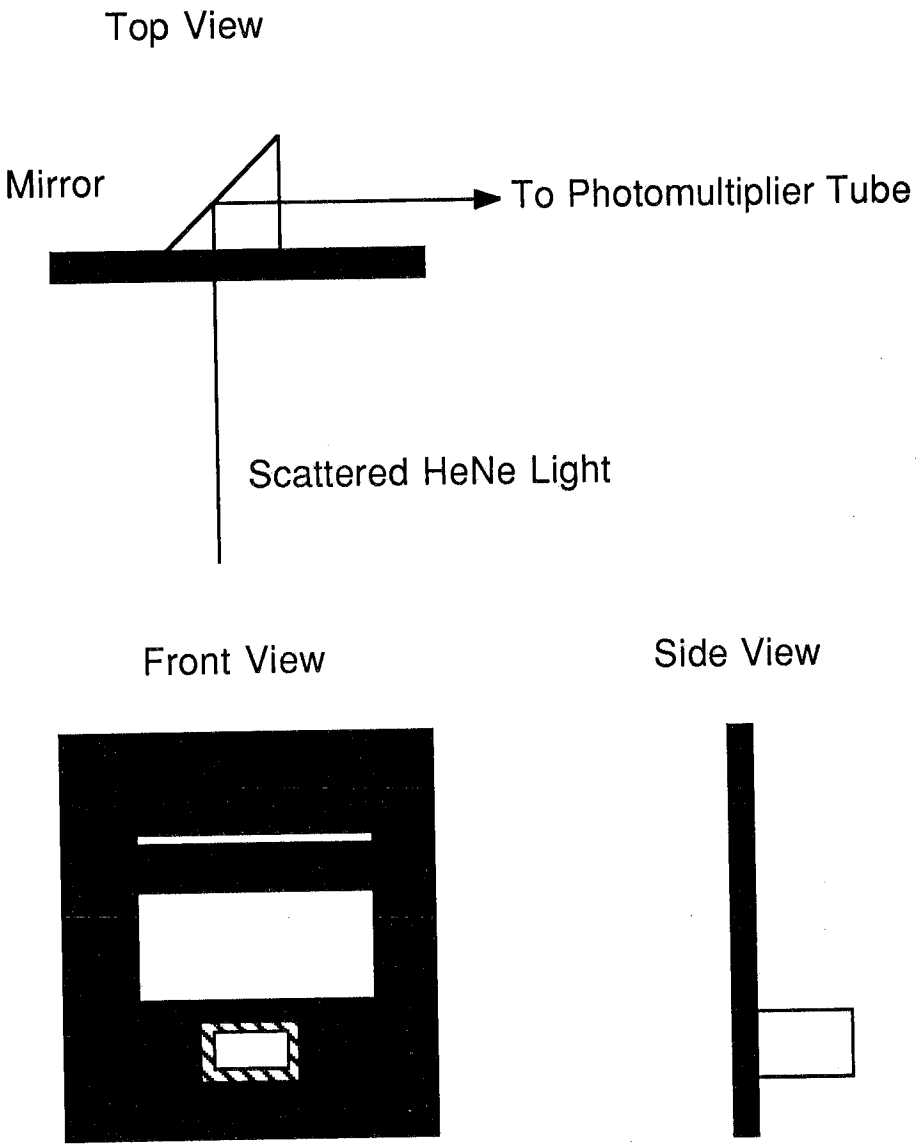

Figure 2.5 Schematic of the coded aperture used in the infrared sizing-pyrometer system in the CDL.

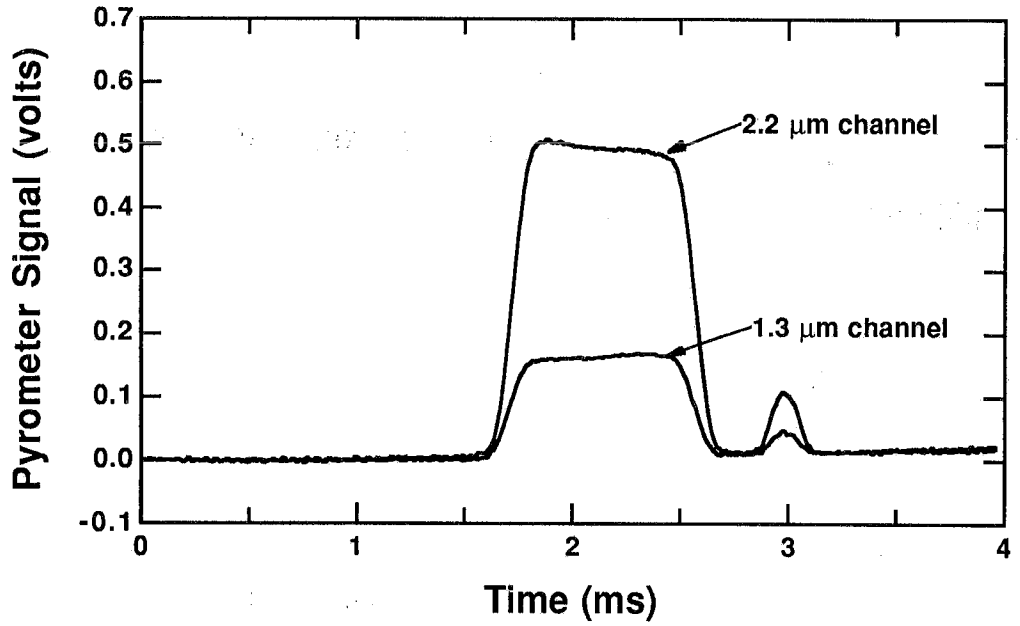

Figure 2.6 Typical emission signals from a coal particle in the CDL flow reactor, as imaged by the coded aperture and infrared sizing-pyrometer.

The particle diameter is calculated from the ratio of signals from the large and small slits at one wavelength, or $E_{1,\lambda 1}/E_{2,\lambda 2}$. The particle velocity is calculated from the traverse time of the particle image from one edge of the large slit to the other. In order to obtain accurate particle diameters and velocities, the particle must be in the focal volume of the sizing-pyrometer system. The 0.95 milliwatt HeNe laser is situated perpendicular to the optical path of the collection mirrors at the optimal focal volume where all calibrations have been performed. The laser power was held under 1 mW to allow laser safety precautions for Class II lasers instead of Class III lasers. The laser was not focused further, providing a focal volume of approximately 1 mm in the plane pependicular to the optical path of the sizing-pyrometer system. The Nicolet 4094 digital oscilloscope is set in a mode to trigger and store particle emission signals only when the scattering from a particle in the focal volume is detected. The oscilloscope stores eight particle emission signals (two wavelengths for each signal), and then transfers the data to a PDP 11/34 computer for subsequent analysis. Electronic signals from the InAs detectors are amplified with low-noise amplifiers and then electronically filtered at 25 kHz using a Wavetek low-pass filter before being sent to the digitizing oscilloscope.

The effective wavelengths of the infrared sizing pyrometer system, including the effects of the bandpass filters and the detector responses, were determined using a calibrated tungsten strip lamp. The lamp was calibrated using a one-color pyrometer, traceable to a National Institute of Standards and Technology (NIST) source. Lamp temperatures were calculated by correcting the one-color temperature for the emissivity of tungsten, as tabulated by Latyev, et al. [1970]. The lamp was operate in

a current-limited mode, with the current measured with a 0.01 ohm shunt resistor and HP voltmeter. A typical calibration curve for the lamp is shown in Table 2.1. Once the lamp temperatures were known as a function of current, the sizing-pyrometer system was calibrated. An image of the lamp was passed through a pinhole on a rotating chopper, and the pinhole image was monitored by the coded aperture and pyrometer system. Lamp temperatures from 1200-2000 K were monitored with the sizing-pyrometer system and then curve-fit using Planck's law and tabulated spectral emissivities of tungsten [Latyev, et al., 1970] in order to determine effective wavelengths for each pyrometer channel. Sample pyrometer calibrations from the tungsten lamp are shown in Table 2.2. Calibrations were repeated several times as optical adjustments were made to the system; the data shown in Table 2.2 are from early calibration experiments. For the main body of experiments discussed in this report, effective wavelengths of 1.36 and 2.20 μm were found to reproduce the lamp temperature data within 10 K.

Table 2.1
Sample Tungsten Strip Lamp Calibration

Voltmeter reading* (mv)	Lamp Temperature (K)
60.2	1167
65.1	1318
70.0	1442
75.0	1550
80.0	1641
85.0	1723
90.1	1825
95.0	1890
100.0	1957
110.0	2078

*Reading on HP voltmeter from 0.01 ohm shunt resistor to determine current to tungsten strip lamp.

Table 2.2
Determination of Effective Wavelengths for the Sizing-Pyrometer System

Pyrometer Channel 1

Peak Height (volts)	True Lamp Temperature (K)	Predicted Lamp Temperature (K)
23	1167	1167
139	1442	1439
374	1641	1650
698	1825	1820

Effective wavelength (λ_1) = 1.30 μm

Pyrometer Channel 2

Peak Height (volts)	True Lamp Temperature (K)	Predicted Lamp Temperature (K)
90	1167	1163
319	1442	1451
605	1641	1650
925	1825	1810

Effective wavelength (λ_2) = 2.06 μm

The chopper was moved to the focal point of the collection optics (with the flow reactor tower removed) in order to measure the magnification of the system, which is a critical parameter for determination of particle size and velocity. The velocity is calculated from the transit time of the magnified image across the large slit. The true chopper velocity can be calculated from the radial location of the pinhole and the rotational speed of the chopper (obtained from the oscilloscope between successive peaks). The magnification of the detection optics was thus determined to be 6.6. The calibration was further tested by measuring the size of Spherocarb particles in the flow reactor, since the Spherocarb particles do no react under pyrolysis conditions and are tightly size classified by the manufacturer to 100/120 mesh (125 to 145 μm diameter particles). Sizes of the Spherocarb particles were independently verified using photomicrographs.

One of the difficulties in measuring coal particle temperatures during devolatilization is the presence of the tar and/or soot cloud surrounding the particle (shown visually by McLean, et al., [1980]). Grosshandler [1984] presented a theoretical study on the effect of soot on pyrometric measurements of coal particle temperature, showing measurement errors associated with different wavelength regions. Infrared wavelengths were chosen for this pyrometer system in order (a) to penetrate the tar cloud and (b) to maximize the emission signal at low temperatures.

Particle emission signals are similar to those reported by Tichenor, et al. [1984]. Peak ratios, rather than absolute intensities, are used to calculate particle diameters and temperatures. After digital smoothing of baseline noise and the sizing peaks is performed, statistical information regarding variations of particle temperatures and velocities is computed for each size bin [Mitchell, 1987; Niksa, et al., 1984]. Even though particle flow rates were low, occasional emission signals from particles in the focal volume are partially contaminated with emission signals from particles in the optical path but not in the focal volume. If multiple peaks are present in the emission signal, signifying emission from more than one particle in the optical path, that particular emission signal is discarded.

A careful study was performed to determine the errors in the particle size and temperature measurements induced by the tar cloud surrounding each coal particle. The particle sizes determined from the emission signal are close to the sizes expected for coal particles and not representative of the particle cloud (observed visually to be at least 10 times the particle diameter). This is strong evidence that the tar cloud does not interfere with the particle emission signal. Also, the emission intensities per unit surface area (i.e. detector signal) for Spherocarb and bituminous coal are very similar in magnitude, indicating that the emissivities are similar. The calculated emissivity is generally used as a self-consistency check, as mentioned above. However, the fact that the calculated emissivities are similar for the Spherocarb and bituminous coal is additional evidence that the tar cloud does not influence particle temperature measurements. Measurements reported by Fletcher et al. [1987] show that Spherocarb and partially reacted char particles have similar emissivities (0.9 and 0.7, respectively). Finally, flat baseline detector signals were measured before and after the particle emission signal (as shown in Fig. 2.6); if the tar cloud interfered with the signal, a broad change in the baseline would be observed before and after the particle emission signal.

CDL Solid Sampling System

A water-cooled, helium-quench probe (3 cm o.d., 1.4 cm i.d) is used to collect solid samples iso-kinetically (see Fig. 2.7). Twelve small quench jets (~ 0.7 mm i.d.) with a 10 degree downward angle from horizontal are located in the tip of the probe. The inner wall of the probe is made from porous tubing, allowing helium to transpire through the wall to reduce tar deposition. Both the helium quench jets in the tip of the probe and the porous probe liner are served by the same plenum for helium flow. The ratio of helium reaching the quench jets to that transpiring through the porous liner is governed by the pressure drop through the porous liner vs. the pressure drop through the quench jets. This ratio was measured by placing a rubber plug in the probe interior just downstream of the quench jets, and then measuring the flow rate of helium from each end of the probe. Of the 60 standard liters per minute (slpm) of helium fed to the quench probe, 20 slpm transpired through the porous wall, leaving 40 slpm to flow through the quench jets in the probe tip.

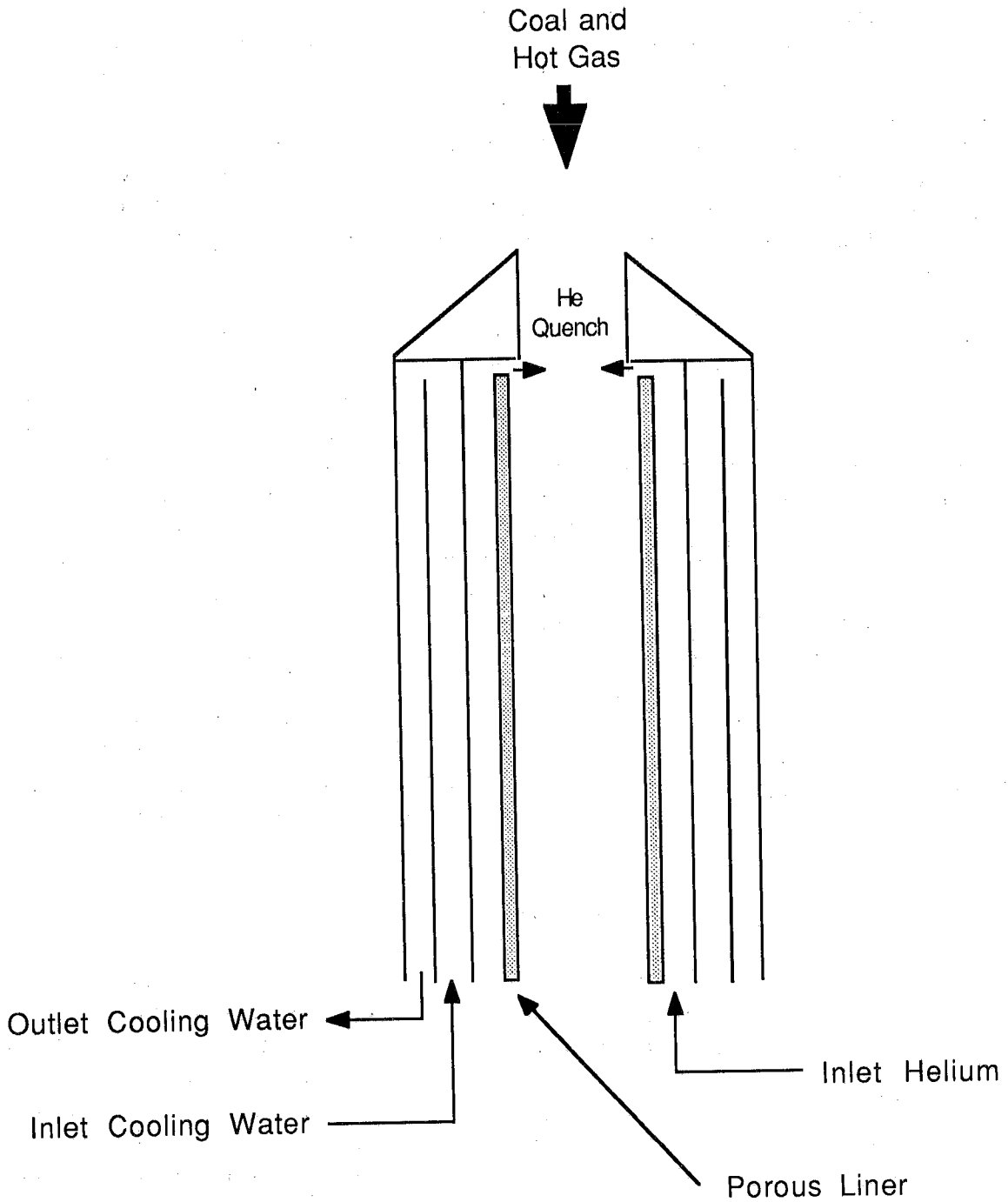

Figure 2.7 Schematic of the helium-quench solids sampling probe used in the CDL.

The effective gas quenching rate was examined by measuring the gas temperature as a function of distance using a sheathed chromel-alumel thermocouple inserted into the inner chamber of the probe. Small wires were attached to the sheath in order to

position the thermocouple in the center of the probe. The diameter of the thermocouple bead was approximately 1 mm, and radiation corrections to the thermocouple were small due to the low temperatures. A plot of gas temperature in the probe as a function of distance from the probe tip is shown in Fig. 2.8. This profile was obtained with the flow reactor conditions of 30 slpm N_2 and a gas temperature of 1023 K. The gas is quenched from 1023 K to 461 K in 4 mm (0.6 ms), corresponding to a gas quenching rate of approximately 10^6 K/s. Particle quenching times are slightly longer due to thermal inertia effects.

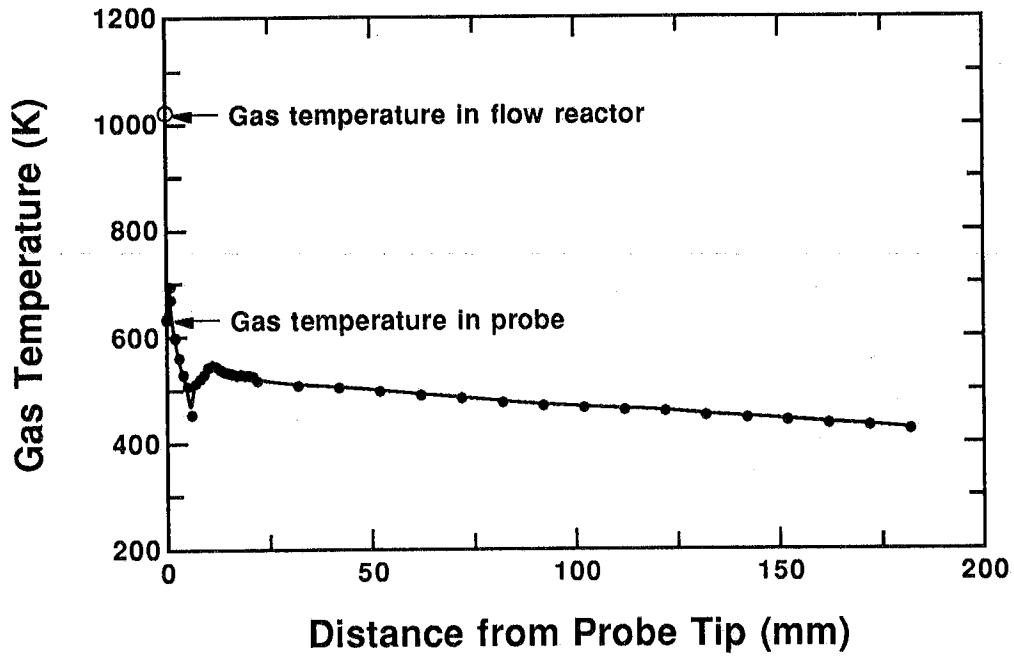

Figure 2.8 Measured gas temperatures in the helium quench probe under sampling conditions at a gas temperature of 1050 K.

A virtual impactor is used to reduce the flow rate of gas through the char filter, as shown schematically in Fig. 2.9. The impactor design is similar to that developed by Neninger et al. [1983]. The impactor utilizes the principle that the small tar particles are are more responsive to changes in flow direction than the large char particles. Velocities in the impactor are designed such that particles larger than 5 μm in diameter flow straight down through the impactor and into the cyclone separator. Approximately 70% of the gas changes direction and flows through the gap in the virtual impactor. Most of the tars and aerosols follow this gas stream and are collected on the primary tar filter (see Fig. 2.10). The remaining 30% of the gas stream, containing the char particles and any remaining tars and aerosols, passes through a three-stage Andersen cascade cyclone sampler (two cyclones and a filter). The primary cyclone is designed to collect particles above 10 μm in diameter; over 97% of the char particles are collected in this cyclone, with the remaining char particles depositing in the secondary cyclone. The tars and aerosols in the char leg of the sampling system are collected on the secondary tar filter. Nuclepore polycarbonate

filters were used, with average pore diameters in the filters of 1.0 μm for the primary tar filter and 5.0 μm for the secondary tar filter.

As tars accumulate on the filters, the pressure drop across the filters increases, and the suction pressure must be adjusted to maintain a constant sampling flow rate. An automated feedback control system adjusts the vacuum pump control valves in order to maintain a set flow rate on each sampling leg. The vacuum pumps are allowed to maintain a constant suction rate, and make-up air is bled into the vacuum line through a control valve. These valves are automatically opened or closed in order to maintain set flow rates, as measured by Hastings flow meters (as shown in Figure 2.10). Visual observations indicate that the flow of particles is undisturbed be the presence of the probe, and hence corresponds to the same conditions studied in the pyrometry experiments.

For the main series of devolatilization experiments, care was taken to reduce the exposure of char and tar samples to ambient temperature. The parent coal was generally stored in desiccators, although select samples were stored in a freezer at 0°C during the final series of experiments. The freezer storage was used to reduce polymerization reactions in both the tar and char samples, based on the recommendations of Professors Henk Meuzelaar and Ronald Pugmire from the University of Utah. The syringe in the particle feeder was weighed before and after charging with coal to determine the coal fed to the reactor. The syringe loading was typically ~500 mg of coal. The collected char samples in the cyclone were also weighed, and then placed in capped bottles in the freezer until analysis or shipment to Coors Analytical Laboratories or the University of Utah for analysis. The tar filters were also weighed carefully before and after tar collection, and then stored in sealed polyethylene bags in the freezer until analysis. Char and tar samples were shipped to the University of Utah in styrofoam dry ice chests (usually by personal automobile, since airlines object to dry ice containers). Char samples sent to Coors were sealed in additional polyethylene bags, but were not kept cold during shipment. Samples sent to Coors were generally analyzed within two weeks.

CCL Flow Reactor

The flow reactor in the CCL is described in several publications [Mitchell and McLean, 1982; Niksa, et al., 1984; Tichenor, et al., 1984; Hurt, et al., 1992], and is illustrated in Fig. 2.11. Room temperature fuel and oxidizer gases enter the flow reactor through small concentric tubes, creating a flat diffusion flame about 3 mm thick, starting at a distance of approximately 5 mm above the burner. The flow rates of N_2, O_2, CH_4, and H_2 are adjusted independently to create a flame with the desired temperature, velocity, and post-flame oxygen concentration. Typical char combustion experiments in the CCL are conducted in post-flame environments containing 3, 6, and 12 mole-% O_2. Flame temperatures for typical operating conditions range from 1500 to 2000 K. Heat loss to the transparent quartz reactor walls decreases the temperature by 200 to 300 K in the first 40 cm above the burner. .

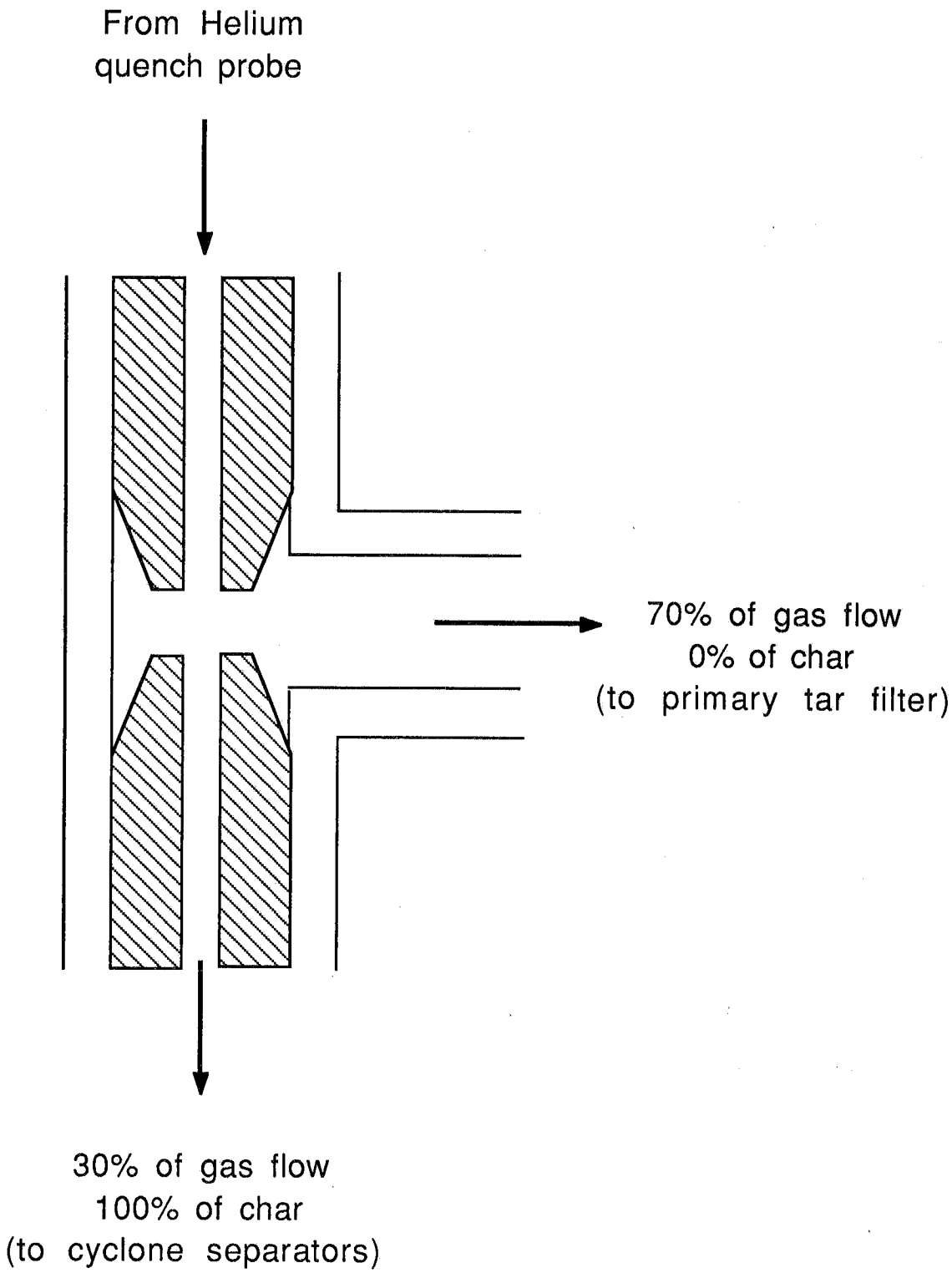

Figure 2.9 Schematic of the virtual impactor used as the initial aerodynamic separator of coal tar from char particles.

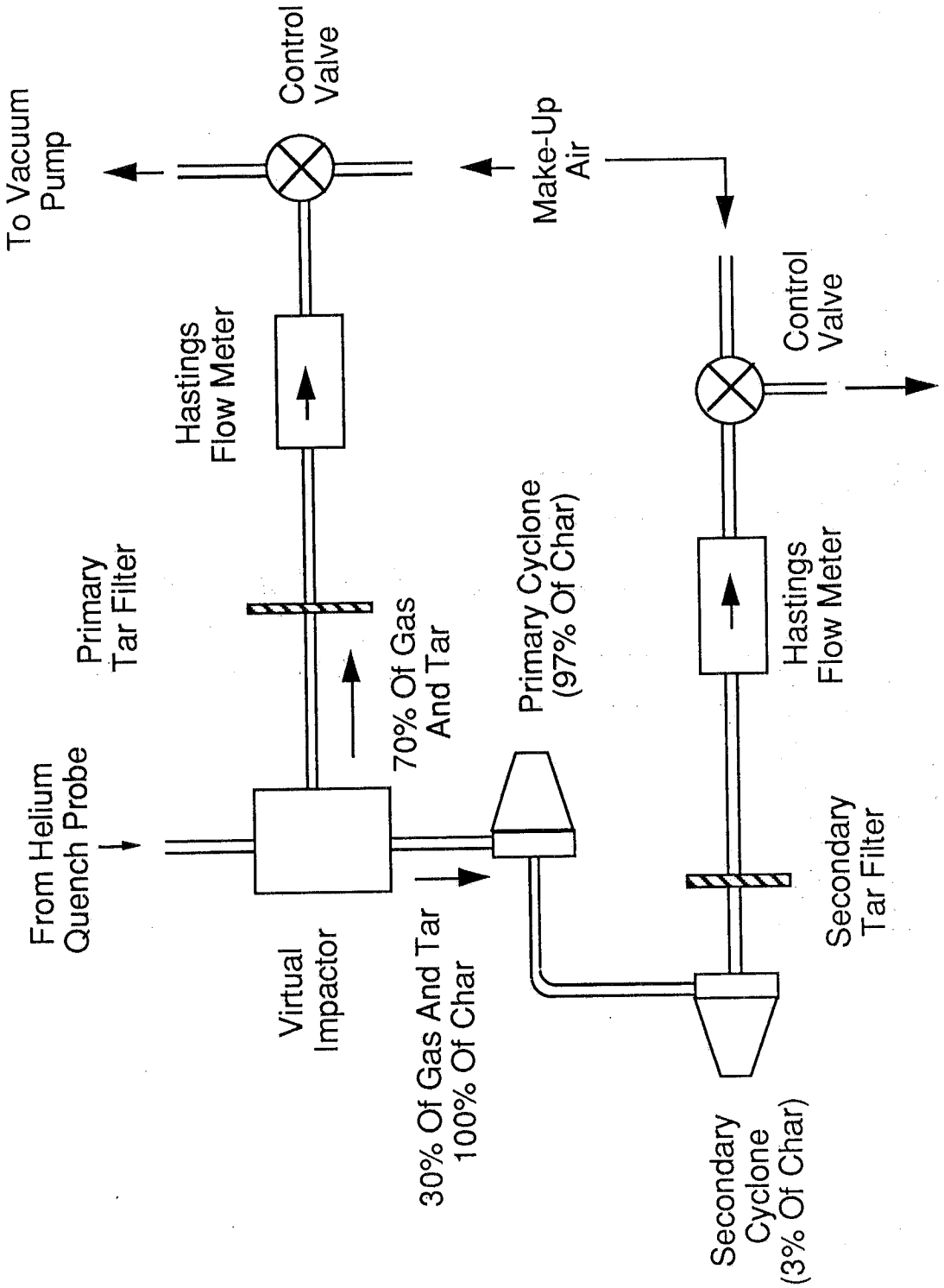

Figure 2.10 Schematic of the virtual impactor and cyclone system used in the CDL to aerodynamically separate coal tar from char particles.

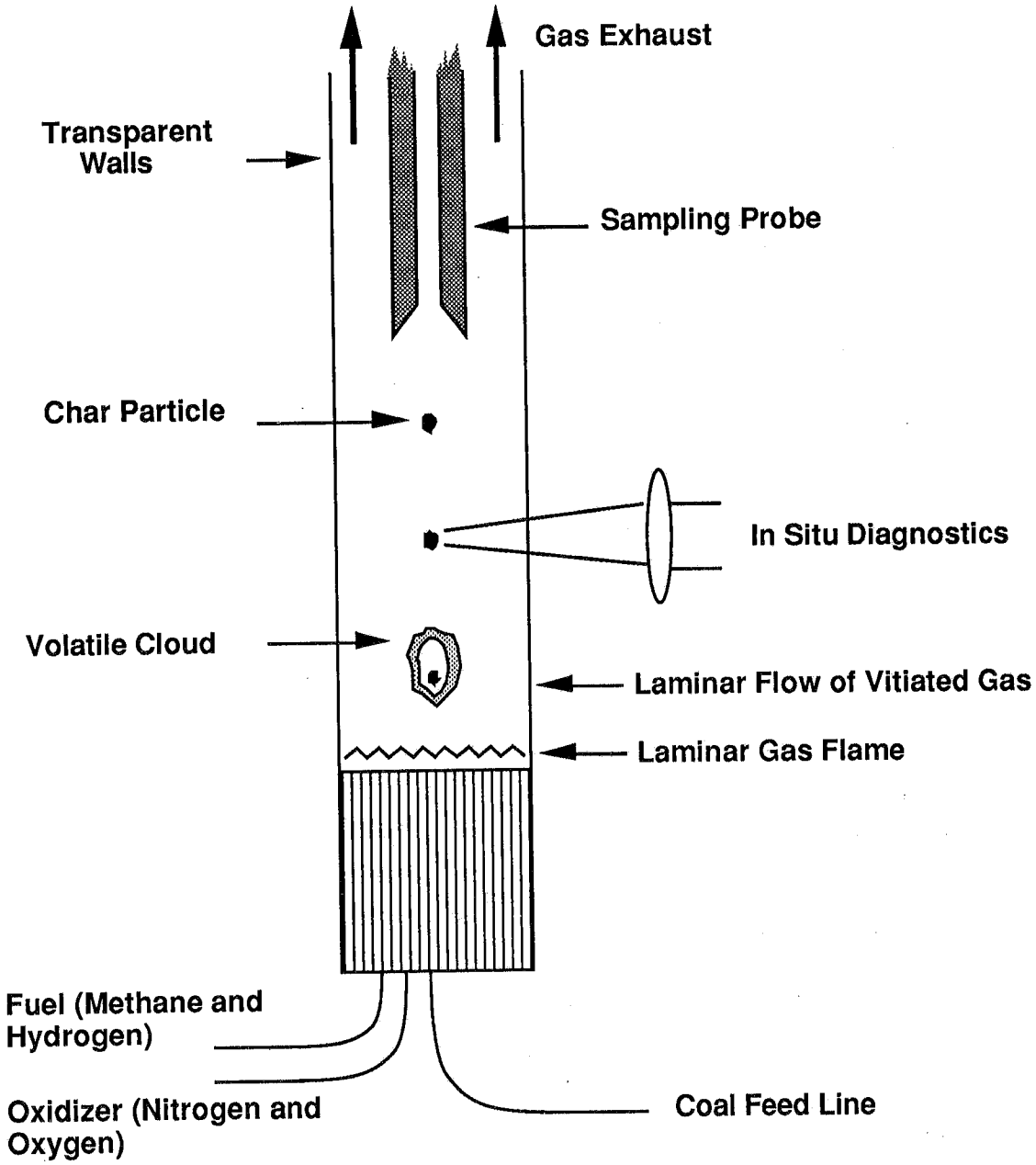

Figure 2.11 Schematic of the laminar flow reactor in the Char Combustion Laboratory, showing location of the diffusion flame and coal particle devolatilization and char oxidation.

Gas temperatures in the CCL are measured with a Pt/Pt-13% Rh thermocouple with a bead size of ~ 100 μm diameter. The measured thermocouple bead temperatures are corrected for radiation heat losses to the surrounding walls in order to obtain gas temperatures. Thermocouple beads are coated with aluminum oxide to reduce the catalytic properties of the precious metals near the flame.

Entrained coal particles enter the flow reactor through a small tube located in the center of the burner. Particles are entrained by the flow reactor gases, and travel upwards through the flame and post-flame environment in a narrow stream. Coal particles typically exhibit a bright luminous emission at a height of ~ 3 cm above the burner, which persists for about 1 cm for any given particle. The bright initial emission from the coal particle is due to soot particles generated from the cracking and combustion of devolatilized tar species. The actual brightness and length of the soot cloud emission surrounding any given particle are dependent on coal type and particle size. Following the devolatilization region, the char particle continues to emit thermal radiation in a duller orange color, depending on the post-flame oxygen concentration.

Sizes, temperatures, and velocities of individual particles are measured using a sizing pyrometer, as described by Tichenor, et al. [1984]. A schematic of the sizing-pyrometer system used in the CCL is shown in Fig. 2.12. The *in situ* calibration system in the CCL, consisting of the tungsten strip lamp and the pinholes mounted on the chopper wheel, are not shown in this figure, but operate in a manner similar to that used in the CDL. This sizing-pyrometer system in the CCL is similar to that used in the CDL, except that this system operates in the visible spectrum at 500 and 800 nm, and therefore uses standard lenses and achromats (instead of mirrors) for collection of particle emission signals. This system also uses 1:1 optics (no magnification), and electrically-cooled photomultiplier tubes are capable of monitoring the emission signals at these wavelength. The minimum particle temperature measurement threshold for the CCL sizing-pyrometer is 1200 K for a 100 μm particle, compared to 850 K for the CDL infrared sizing-pyrometer system. The sizing-pyrometer system was not used in the devolatilization experiments described in these reports, since the lowest measurable particle temperatures (1200 K) are above typical devolatilization temperatures and since the soot cloud obscures the particle (especially at visible wavelengths).

Gas velocities in the CCL flow reactor are inferred from measurements of the sizes and velocities of pure carbon particles (Spherocarb) at low oxygen concentrations in the post-flame gases [Niksa, et al., 1984]. Based on boundary layer growth correlations and conservation of mass, a correlation was developed to describe the gas velocity v_g in the CCL flow reactor as a function of gas temperature T_g and distance from the burner z [Niksa, et al., 1984]:

$$\sqrt{\frac{v_g}{T_o}} = c_1 + \frac{1}{2}\sqrt{c_2\, w} + \frac{c_2\, w}{8\sqrt{c_1}} \tag{2.2}$$

where units are in cm, sec, and K, and

$$w = z\, T_g^{\,0.68} \tag{2.3}$$

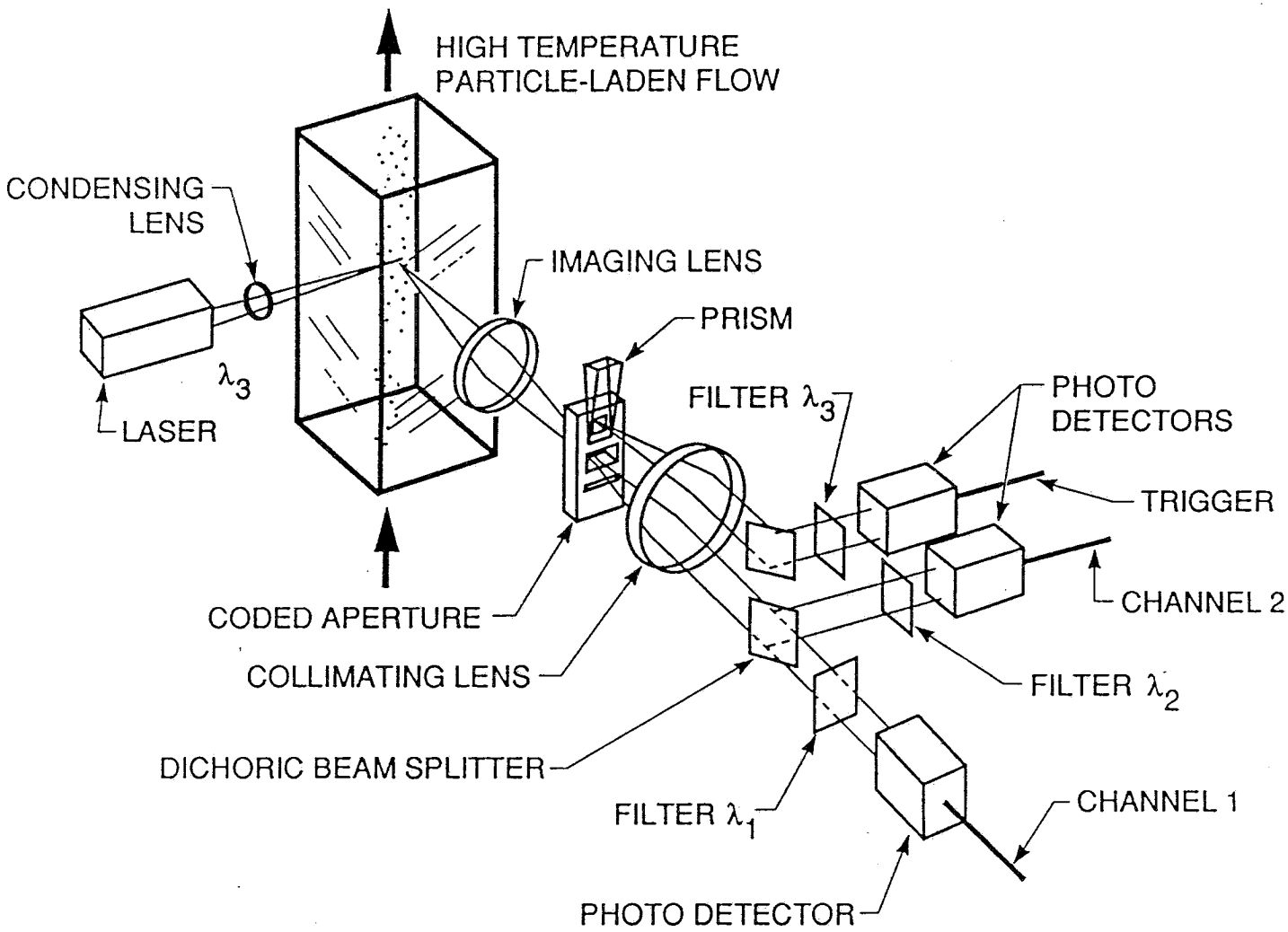

Figure 2.12 Schematic of the particle sizing-pyrometer used in the Sandia Coal Combustion Laboratory (CCL).

In Eq. 2.2, the first term represents the superficial velocity based on the cross-section (2 in. x 2 in.) of the flow reactor; the second term represents the rise in average velocity due to boundary layer growth (and hence flow restriction in the bulk stream) along the walls; and the third term represents corner effects on boundary layer growth in the flow reactor. The constants c_1 and c_2 are determined from extrapolations of measured particle velocities as a function of size at different heights above the burner. Particle size, temperature, and velocity measurements for Spherocarb particles are made at heights as low as 6.35 cm above the burner, while gas temperature measurements are made at heights as low as 1.3 cm above the burner.

The particle feeder and water-cooled helium quench probe in the CCL are similar to those used in the CDL (see Figs. 2.3 and 2.7; Hurt, et al., 1992). The solids sampling system in the CCL was modified in order to perform devolatilization experiments. A cyclone system similar to that used in the CDL is attached to the end of the helium-quench probe to aerodynamically separate tar from char; however, the sampling system in the CCL does not include the virtual impactor or the porous liner in the probe. Tars in the CCL undergo secondary gas-phase reactions, and hence do not stick to the sides of the probe as much as in the CDL experiments. The suction rate from the probe in the CCL is manually adjusted to achieve iso-kinetic sampling. Char samples from the devolatilization experiments in the CCL were weighed, transferred to sample vials, and then stored in the freezer in the CDL until analysis.

Nomenclature for Chapter 2

c_1, c_2	constants in gas velocity expression
T_g	gas temperature
v_g	gas velocity
w	similarity parameter in gas velocity equation ($w = z\,T_g^{0.68}$)
z	height above burner

References for Chapter 2

Fletcher, T. H., L. L. Baxter, and D. K. Ottesen, *1987 International Conference on Coal Science* ,J. A. Moulijn, Eds., Elsevier Science Publishers B. V., Amsterdam, p. 945, 1987.

Grosshandler, W. L., *Comb. Flame*, **55**, 59 (1984).

Hurt, R. H., R. E. Mitchell, and D. R. Hardesty, "Compilation of Sandia Coal Char Combustion Data and Kinetic Analyses," Milestone Report for DOE/PETC Contract FWP 0709 (in press, 1992).

Latyev, L. N., V. Y. Chekhovskoi, and E. N. Shestakov, *High Temperatures-High Pressures*, **2**, 175 (1970).

McLean, W. M., D. R. Hardesty, and J. H. Pohl, *Eighteenth Symp. (Int.) on Comb.*, The Combustion Institute, Pittsburgh, PA, p. 1239 (1980).

Mitchell, R. E., *Comb. Sci. Tech.*, **53**, 165 (1987).

Mitchell, R. E., and W. M. McLean, *Nineteenth Symp. (Int.) on Comb.*, The Combustion Institute, Pittsburgh, PA, p. 1113 (1982).

Neninger, R. D., J. B. Howard, and A. F. Sarofim, *International Conference on Coal Science,* Pittsburgh, PA, p. 521 (1983).

Niksa, S., R. E. Mitchell, K. R. Hencken, and D. A. Tichenor, *Comb. Flame*, **60**, 111 (1984).

Tichenor, D. A., R. E. Mitchell, K. R. Hencken, and S. Niksa, in *Twentieth Symp. (Int.) on Comb.*, The Combustion Institute, Pittsburgh, PA, p. 1213 (1984).

3. SAMPLE ANALYSIS

Elemental Analysis of Organic Material

Collected char samples were analyzed by Adolph Coors Analytical Laboratories Division in Golden, Colorado. A total of approximately 500 mg of of each sample was used in the analysis, divided as follows: ~100 mg was used for analysis of moisture and total ash content; ~250 mg was used for ICP analysis; ~5 mg was used for C,H,N, and O analysis; and ~150 mg was used for sulfur analysis. Some of the data scatter in the ICP and total ash analyses is due to the small sample size. The total ash content and the moisture content were measured using ASTM procedures, modified for small sample sizes.

The organic portion of the samples were analyzed as follows:

1. Fisher Sulfur analyzer for sulfur determination
2. Colorometric combustion technique by Champion and Houde for carbon and hydrogen determination
3. Carlo/Erba nitrogen analyzer for nitrogen determination
4. Modified Unterzaucher pyrolysis technique for oxygen.

These four analyses were performed on four independent Leco instruments. The sum of compositions of the five organic elements generally added to 100 ±5%. All five compositions were therefore renormalized by the sum for each sample.

Elemental Analysis of Inorganic Material

A tracer technique was used to determine mass loss due to devolatilization, since occasional probe deposits consisting of tar and char agglomerates prevented complete mass closure during sampling. Titanium, silicon, aluminum,and total ash were all used as tracers in this study. The fraction of mass remaining in the char m_p/m_p^o was determined from the concentration of the tracer elements x_i in each sample (on a moisture-free basis) from the following equation:

$$\frac{m_p}{m_p^o} = \frac{x_i^o}{x_i} \tag{3.1}$$

In this work, char is referred to as partially-reacted coal, and consists of unreleased volatiles (if any), fixed carbon, and ash (unless referred to on an ash-free basis). The mass of volatiles released (gas plus tar) is $1 - m_p/m_p^o$.

The inorganic elements were analyzed by Inductively Coupled Plasma (ICP) using ASTM Procedure D 3862 with the following revision: a lithium metaborate and lithium tetraborate flux was used for the fusion. The coal samples were ashed at 750°C prior

to fusion with the flux. The concentrations of the following elements were measured: Si, K, Ti, Fe, Al, Ca, Na, and Mg. Analysis of NBS standard coals and flyash have shown that each of these constituents of the ash can be measured within 5%. A 5% error in the tracer concentration would cause as much as a 10% error in the mass loss determination. Only the Si, Al, and Ti were used as tracers in this study; the concentrations of other elements were measured in connection with an associated mineral matter study. The total ash content was also used as a tracer. The use of four independent analyses for tracers lowers the statistical uncertainty in the mass loss determination, based on the 90% confidence limit, to less than 5% for most samples.

Apparent Densities

The mean diameter and apparent density of the parent coal particles must be known in order to calculate the initial particle mass m_p^o. As discussed later, m_p^o and d_p^o are used to calculate the particle temperature and reaction history when determining kinetic coefficients. Changes in the mean diameter were determined from experimental measurements of mass loss and apparent density, as discussed later. The apparent density is defined as the particle mass divided by its apparent volume (i.e., the volume based on the particle diameter). In softening coals, the apparent density changes significantly due to the formation of large internal voids. The true density of the solid material, which does not include the void volume, may also change due to preferential release of functional groups during pyrolysis. In this discussion, the term bulk density refers to the mass of particles occupying a known container volume, and is related to the apparent density through a packing factor.

Bulk densities of coal samples were determined using mercury intrusion porosimetry at the Particle Characterization Facility at Lawrence Livermore National Laboratory. Pressures as high as 60,000 psi were employed using an Autopore 9200 instrument; pore sizes as low as 30 Å were penetrated at this pressure. The apparent density of the unreacted coal particles was obtained from the mercury intrusion data for raw coals by associating all voids larger than 3 μm with interparticle spacing, as suggested by Gan et al. [1972]. For char particles from softening coals, surface voids are often larger than 3 μm in diameter, and hence the interpretation of apparent density from porosimetry measurements is difficult. However, if both the raw coal and associated char particles exhibit similar packing factors (interparticle void fractions), the apparent density ratio of the char to the parent coal can be approximated by the ratio of the bulk densities obtained from the porosimeter when interparticle spacing is not taken into account.

A second method was also used for determination of apparent density ratios, similar to that used by Tsai and Scaroni [1987]. A graduated cylinder is filled with particles and tapped gently to allow uniform packing. The bulk density is measured, and the packing factor is assumed to be constant for the both the parent coal and char particles. The bulk density ratio of char to parent coal is therefore equivalent to the

apparent density ratio. The apparent density ratios determined from these two methods agree within 5%, while the error in the experimental method has been estimated at 10% [Tsai and Scaroni, 1987].

Internal Surface Areas

Internal surface areas of char samples were measured at the Particle Characterization Facility at Lawrence Livermore National Laboratory using nitrogen BET analysis. Prior to the nitrogen adsorption analysis, each sample was baked under vacuum (10^{-5} torr) at 200°C for 10 hours to remove gaseous and liquid contaminants from the surface. A vapor deposit on the walls of the analysis tube above the heat zone was observed for each sample after the degas procedure. The analyses on the Digisorb 2600 consisted of a 5-point BET calculation for specific surface area.

Scanning Electron and Optical Microscopy

The physical features of the surface of coal and particles were examined using a scanning electron microscope (SEM). The SEM micrographs were obtained in the SEM laboratory at Sandia (Division 8314) in the secondary electron image (SEI) mode. The internal structure of coal particles was examined by sectioning the particles. Particles were mixed with EPON-828 resin, pressurized to 10,000 psig, and cured overnight. The samples were post-cured at 70°C for three hours, and then polished using a series of polishing powders to 0.5 μm resolution. The cross section photographs were obtained using a standard optical microscope with a light source.

NMR Analyses

The ^{13}C NMR data on the coal and char particles were obtained at the University of Utah, under the direction of Professor Ronald Pugmire, using a variation of the method described by Solum, et al. [1989]. Cross-polarization magic-angle spinning (CP/MAS) spectra for coals and chars were obtained on a Bruker CXP-100 spectrometer with a ^{13}C frequency of 25.15 MHz and a spectral width of 12 kHz. The radio frequency fields were $\gamma_C B_{1C} = \gamma_H B_{1H} \approx 48$ kHz. Spinning speeds were approximately 4.0 kHz. Delay times between acquisitions were 0.5 to 1.0 s. Contact times in dipolar dephasing measurements were between 0.8 to 2.5 ms depending on the maximum aromatic signal from the variable contact (VC) measurement, using 2.0 ms when signal to noise level permitted. The coal and char samples were run as received with no degassing.

The total magnetization was obtained by a variable contact time experiment in which the data were fit to a model employing a Gaussian (T_{GCH}) and a Lorentzian (T_{LCH}) time constant and a single value for the spin relaxation time ($T_{1\rho}^{H}$). The time constants, T_{GCH} and T_{LCH} and $T_{1\rho}^{H}$, along with magnetization values M_{GCH} and

M_{LCH}, were measured using a standard CP sequence while varying the contact time, τ_{cp}. The carbon magnetization was fit to the following five parameter equation:

$$M(\tau) = (M_{GCH} + M_{LCH})\, e^{-\tau / T_{1\rho}^{H}} - M_{GCH}\, e^{-0.5\,(\tau / T_{GCH})^2} - M_{LCH}\, e^{-\tau / T_{LCH}} \quad (3.2)$$

where $(M_{GCH} + M_{LCH})$ represents the total magnetization in the sample independent of relaxation effects. The above equation was used separately for the aromatic and aliphatic regions of the spectra, and the carbon aromaticity f_a was calculated from these values after including sideband intensity for the aromatic region. The second cross-polarization time constant, T_{GCH}, is included to take into account the first stage of the two stage cross-polarization from carbons with directly bonded protons [Müller, et al., 1974; Wu, et al., 1988]. The second time constant T_{LCH} is then an average of the time constants for nonprotonated carbons and the second stage for carbons with directly bonded protons. Curve fits of variable contact time data from PSOC-1507D aromatic region are shown in Fig. 3.1 for both the simple model [Solum et al., 1989] representing a single stage cross-polarization model and the two stage cross polarization model given by Eq. 3.2. Between 17 and 25 different contact times from 5 μs to 25 ms were used in variable contact time measurements.

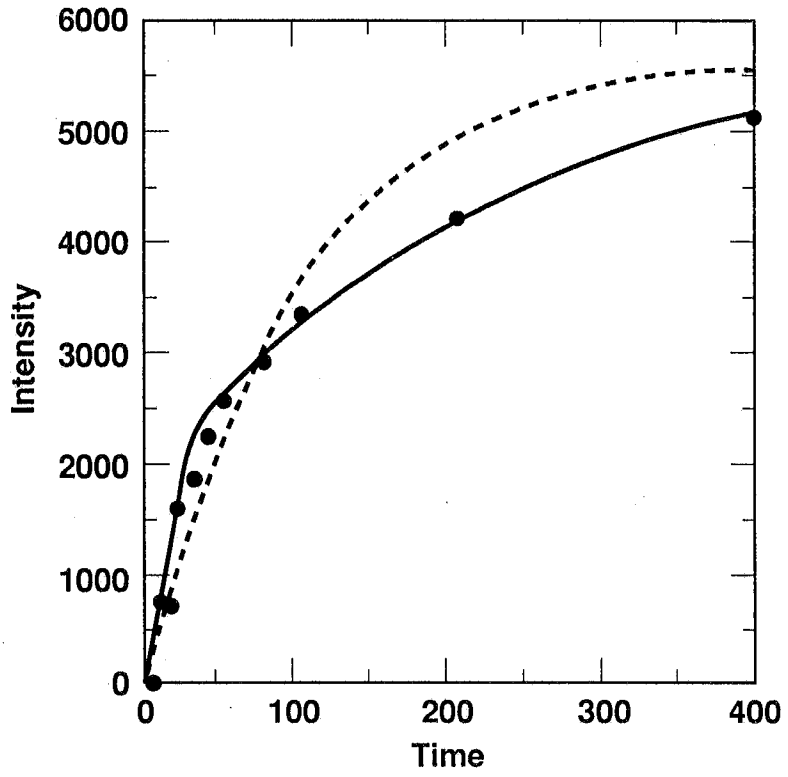

Figure 3.1 Short time (μs) behavior in a variable contact time measurement for the aromatic region of PSOC-1507D Beulah Zap lignite. Fit of data (circles) with the simple VC model using one T_{CH} (dashed line) and with T_{GCH} and T_{LCH} accounting for two stage cross polarization for carbons with directly attached protons (solid line).

Dipolar dephasing data were employed to separate the aromatic Gaussian (C-H) component from the Lorentzian (non-protonated) component of the carbon magnetization. The dipolar dephasing pulse sequence has been described previously [Alemany, et al., 1983], and the version used here has 180° refocusing pulses in both the carbon and proton channels. There were 23 interrupted decoupling delays in this analyses, ranging from 2 to 200 μs for the aromatic region. The decay of the carbon magnetization was fit to the following four parameter equation [Sethi, et al., 1988]:

$$M(\tau) = M_{OL}\, e^{-\tau / T_L} - M_{OG}\, e^{-0.5\,(\tau / T_G)^2} \qquad (3.3)$$

In Eq. 3.3, T_L and M_{OL} are the Lorentzian decay constant and initial magnetization, respectively, for the weakly coupled spins. The variables T_G and M_{OG} are the Gaussian decay constant and initial magnetization, respectively, for the strongly coupled spins. The sum of M_{OG} and M_{OL} has been normalized to unity.

Segmental motion in the aliphatic region of the ^{13}C CP/MAS spectrum of coals creates some uncertainty in the relative contributions of CH_3 and CH_2/CH groups [Soderquist, et al., 1987; Vassola, et al., 1987], as measured in the dipolar dephasing experiments. The methyl contribution was therefore approximated from the integrated intensities of the 0-22 (alkyl and aryl methyl groups) and 50-60 (methoxy group) ppm regions of the spectrum.

Using parameters from the above ^{13}C NMR analyses, twelve structural parameters relating to the carbon skeletal structure can be obtained. The average aromatic cluster size and the number of attachments on an aromatic cluster can also be estimated. This procedure for data analysis, including the cluster size estimation model, has been described by Solum, et al. [1989].

The high mineral content of the Zap lignite and associated char samples caused a low signal to noise level in the NMR analyses. This signal to noise difficulty was reduced by demineralizing the lignite samples; all solid-state NMR data presented here for the lignite and associated chars are from the demineralized samples. Demineralization was achieved by leaching the samples successively in HCl, HF, and then HCl again (all at 50-60°C), with warm water rinses between acid leaching steps. It is thought that the organic skeletal structure is not significantly altered by the acid leaching procedure. The bituminous coal and chars were not demineralized, since adequate signal to noise levels were achieved with the native samples.

The ^1H and ^{13}C NMR data for each tar sample were obtained with a Varian VXR-500 spectrometer. Tars were removed from the tar filter and dissolved in 1 ml samples of deuterated (98%) dimethyl sulfoxide (DMSO). The ^{13}C NMR data on tars were obtained by using a 30° carbon pulse with an acquisition time of 1.2 s and a 0.5 s pulse delay. These conditions provide semi-quantitative data that slightly underestimate the carbon aromaticity. Small amounts of particulate matter were observed in the

tar/DMSO solutions, but no serious degradation of spectral resolution was observed due to the presence of colloidal material.

Curie-Point GC/MS and Low-Voltage MS Analyses

Analyses of the tar samples by combined gas chromatography and mass spectrometry (GC/MS) were performed at the University of Utah's Center for Micro Analysis and Reaction Chemistry under the direction of Professor Henk Meuzelaar. Techniques used were similar to those reported by Chakravarty, et al. [1988] and Yun, et al. [1991]. The analyses were performed using a Hewlett Packard 5890 chromatograph with a 15 m x 0.25 mm i.d. x 0.25 μm film thickness DB-5 column (J&W Scientific). A schematic of the Curie point GC/MS system is provided in Fig. 3.2. The conditions used in GC/MS were as follows: electron energy 70 eV, ion trap detector (ITD, Finnigan MAT) scanned from m/z 40-450 at 1 scan/sec, pyrolysis time 2 sec, 883K Curie-point wires in an inlet set at 523 K. The column was temperature programmed from 313-573K at 15 K/min.

Low-voltage mass spectrometry (LV/MS) experiments were carried out using an extranuclear Model 5000-1 Curie-point pyrolysis MS system (see Fig. 3.3). Twenty-five microgram quantities of tar were coated on ferromagnetic wires from methanol suspensions. The wires were inserted into borosilicate glass reaction tubes and introduced into the vacuum system of the mass spectrometer. The ferromagnetic wires were inductively heated at approximately 100 K/s to an equilibrium temperature of 883 K. Total heating time was 10 sec. Low-voltage MS conditions were as follows: electron ionization at 12 eV (set value), scanning rate 1000 amu/s, total scanning time 20 s, mass range scanned m/z 40-260. The LV/MS system allows for a relatively quick, first-order analysis of the types of species that occur in tar samples, whereas the GC/MS system is used to confirm results from the LV/MS system and to provide further detail on specific species.

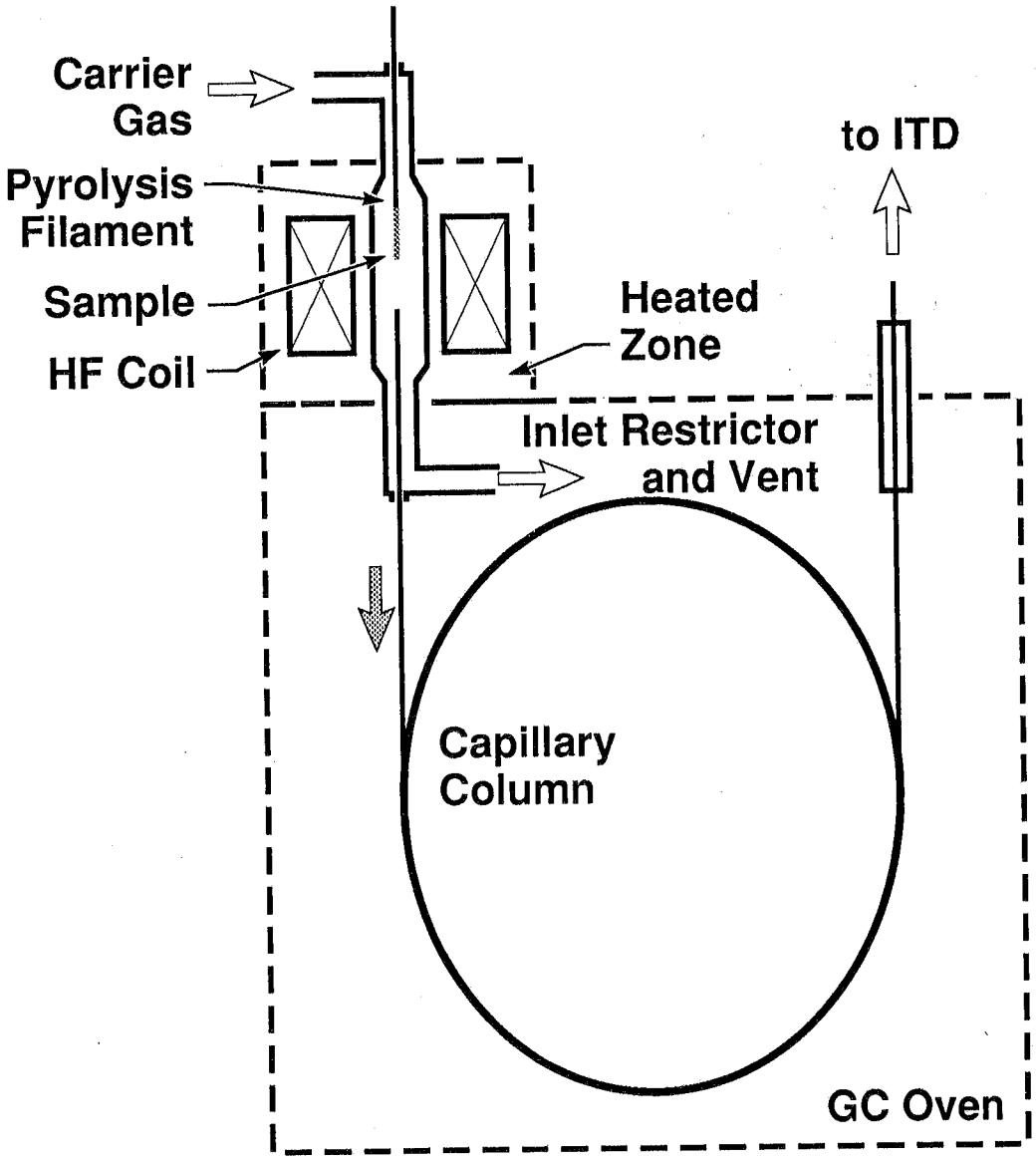

Figure 3.2 Schematic of the Curie-point desorption GC/MS system used at the University of Utah.

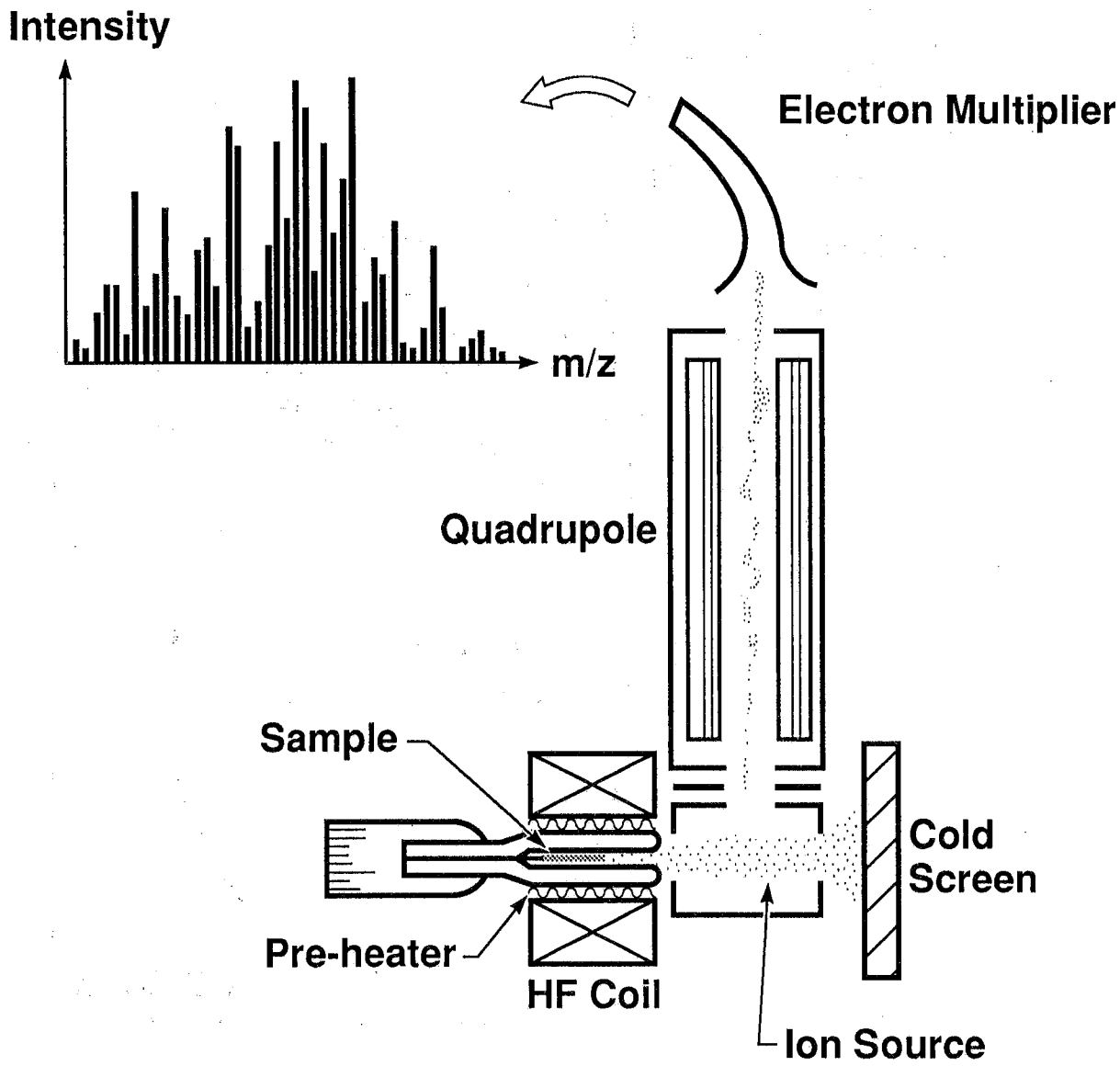

Figure 3.3 Schematic of the Curie-point desorption LV/MS system used at the University of Utah.

Nomenclature for Chapter 3

f_a	carbon aromaticity (fraction of carbons contained in aromatic groups)
m_p	particle mass
M	magnetization parameter in NMR analysis
T	time constant in NMR analysis
$T_{1\rho}{}^H$	spin relaxation time in NMR analysis
τ	contact time in NMR analysis
x_i	mass fraction of species i

Subscripts

G, OG	Gaussian component of NMR signal from dipolar dephasing analysis
GCH	Gaussian component of NMR signal from variable contact time analysis
L, OL	Lorentzian component of NMR signal from dipolar dephasing analysis
LCH	Lorentzian component of NMR signal from variable contact time analysis

Superscripts

o	parent coal

References for Chapter 3

Alemany, L. B., D. M. Grant, T. D. Alger, and R. J. Pugmire, *J. Am. Chem. Soc.*, **105**, 6697 (1983).

Chakravarty, T., W. Windig, G. R> Hill, and H. L. C. Meuzelaar, *Energy and Fuels*, **2**, 400 (1988).

Gan, H., S. P. Nandi, and P. L. Walker, *Fuel*, **51**, 2722 (1972).

Müller, L., A. Kumar, T. Baumann, and R. R. Ernst, *Phys. Rev. Lett.*, **32**, 1402 (1974).

Sethi, N. K., R. J. Pugmire, J. C. Facelli, and D. M. Grant, *Anal. Chem.*, **60**, 1574 (1988).

Soderquist, A., D. J. Burton, R. J. Pugmire, A. J. Beeler, D. M. Grant, B. Durand, and A. Y. Huk, *Energy and Fuels*, **1**, 50 (1987).

Solum, M. S., R. J. Pugmire, and D. M. Grant, *Energy and Fuels*, **3**, 187 (1989).

Tsai, C., and A. W. Scaroni, *Fuel*, **66**, 200 (1987).

Vassola, A. M., M. A. Wilson, P. Vollin, J. M. Oades, A. G. Waters, and R. L. Malcolm, *Anal. Chem.*, **59**, 558 (1987).

Wu, Z., S. Zhong, and X. Wu, *Phys. Rev. B.*, **37**, 9827 (1988).

Yun, Y., H. L. C. Meuzelaar, N. Simmleit, and H.-R. Schulten, *Energy and Fuels*, **5**, 22 (1991).

4. OVERVIEW OF EXPERIMENTS PERFORMED

Experiments in the CDL in 100% N_2

The main body of experiments in the Sandia Coal Devolatilization Laboratory (CDL) were conducted on five coals from the PETC suite, ranging from a lignite to a low volatile bituminous coal. Elemental compositions and other properties for the parent coals, as determined by the Penn State coal bank, are shown in Table 4.1 (copies of the complete Penn State analyses for these coals are found in the Appendix). The coals were size classified under nitrogen using a sieve tray and Rho-Tap shaker assembly, and then aerodynamically classified under nitrogen using a Vortec classifier. The resulting samples were distributed to several investigators under PETC funding.

The coal devolatilization experiments were performed in parallel with a series of char combustion experiments at Sandia for the same coals. The sizing-pyrometer systems used in these two laboratories are limited to particles with diameters greater than ~ 50 μm, and work best with particles greater than 100 μm. Although 100 μm particles are greater than the mass mean particle diameter typically used in pulverized coal furnace applications (~ 50 μm), the rates and mechanisms for the two particle sizes are thought to be similar under the temperature and gas conditions explored in the two laboratories. For instance, total volatiles yields from Pittsburgh seam coal particles heated at 1000 K/s differed by less than 1% (daf basis) over this size range [Anthony, et al., 1974], which is well within the experimental accuracy of the determination of volatiles yields.

Three of the size fractions that were provided by PETC were compatible with the optical systems used in coal experiments at Sandia: 63 to 75 μm; 75 to 106 μm; and 106 to 125 μm. Only limited supplies of certain size fractions from some coals were available, due to grinding tendencies. The 106 to 125 μm size fraction was used extensively in the Sandia char combustion experiments. Therefore, the 106 to 125 μm size fraction was used in the Sandia coal devolatilization experiments when sufficient quantities of that size fraction were available after the char combustion experiments. For the PSOC-1507D Beulah Zap lignite samples, sufficient quantities of the 106 to 125 μm size fraction were not available, so the 75 to 106 μm size fraction was used. For the PSOC-1451D Pittsburgh #8 hva bituminous coal, a set of experiments were performed on two different size fractions (63 to 75 μm and 106 to 125 μm).

The analyses of the size-graded coals used in the Sandia devolatilization experiments are shown in Table 4.2. The differences in composition between the Penn State analyses on the unpulverized coal and the analyses of the pulverized and size-graded coal are due to particle size. A large effect of particle size is seen in comparing the analyses of the two size fractions of the Pittsburgh #8 coal. The ash content changes from 11.2% for the 106-125 μm size fraction to 3.7% for the 63-75 μm size fraction.

Table 4.1
Characteristics of the Five Coals Examined in the CDL
(Analyses from the Penn State coal bank)

PSOC- Seam name Reported rank State	1445 Blue #1 subbituminous New Mexico	1451 Pittsburgh #8 hva bituminous Pennsylvania	1493 Illinois #6 hvb bituminous Illinois	1507 Beulah Zap lignite North Dakota	1508 Pocahontas #3 lv bituminous West Virginia
Proximate Analysis (% as received)					
Moisture	12.22	2.54	9.43	33.57	1.14
Ash	4.04	13.32	13.74	8.30	7.36
Volatile Matter	40.33	33.56	34.34	27.08	15.52
Fixed Carbon	43.41	50.58	42.50	31.06	75.98
Calorific Value (Btu/lb, ash free)	13,814	14,891	14,102	12,144	15,711
Ultimate Analysis (% daf)					
Carbon	74.97	83.26	78.07	71.55	91.48
Hydrogen	5.64	5.41	4.92	5.04	4.38
Nitrogen	1.40	1.58	1.50	0.95	1.10
Sulfur	0.75	1.58	5.87	1.63	0.69
Chlorine	0.03	0.09	0.04	0.02	0.06
Oxygen (by diff.)	17.20	8.10	9.61	20.81	2.30
Ash Analysis (% of dry coal)					
SiO_2	0.82	3.36	2.75	0.8	1.66
Al_2O_3	0.45	1.71	1.19	0.43	0.99
TiO_2	0.02	0.09	0.07	0.02	0.08
Fe_2O_3	0.25	0.85	2.39	0.78	0.44
MgO	0.03	0.07	0.08	0.28	0.06
CaO	0.16	0.28	0.76	1.44	0.40
Na_2O	0.01	0.06	0.04	0.38	0.06
K_2O	0.02	0.22	0.20	0.05	0.03

Table 4.2
Characteristics of the Five Coals Examined in the CDL
(Analyses of the Size Fractions Used in Sandia Experiments)

PSOC- Seam name Reported rank State	1445D Blue #1 subbituminous New Mexico	1451D Pittsburgh #8 hva bituminous Pennsylvania		1493D Illinois #6 hvb bitum. Illinois	1507D Beulah Zap lignite North Dakota	1508D Pocahontas #3 lv bituminous West Virginia
Size Fraction (μm)	106-125	106-125	63-75	106-125	75-106	106-125
Moisture (mass %)	9.31	1.51	1.44	3.28	18.04	0.70
C (mass %, daf)	75.6	81.92	84.23	74.12	66.56	88.83
H	5.26	6.45	5.54	4.96	4.26	4.37
O	17.33	8.72	7.56	13.18	25.16	5.14
N	1.32	1.65	1.65	1.45	1.12	1.06
S	0.49	1.26	1.01	6.29	2.89	0.6
Ash (mass %, dry)	3.48	11.2	3.73	11.3	18.7	16.7
SiO2 (% of dry coal)	1.68	5.20	1.90	4.77	2.50	8.48
K2O	0.05	0.18	0.07	n.a.	0.42	0.07
TiO2	0.05	0.12	0.06	0.10	0.03	0.31
Fe2O3	0.28	0.66	0.31	3.58	8.1	0.95
Al2O3	0.84	2.60	1.20	1.78	2.50	3.83
CaO	0.14	0.29	0.11	n.a.	7.66	1.29
Na2O	0.01	0.06	0.01	n.a.	1.51	0.12
MgO	0.01	n.a.	0.03	n.a.	0.76	0.30

The smaller size fraction also contains more carbon and less oxygen than the larger size fraction.

The size-graded Illinois #6 hvb bituminous coal contains less carbon than the unpulverized coal. In fact, the size-graded Illinois #6 coal contains less carbon than the Blue #1 subbituminous coal, making carbon content a poor indicator of coal rank for these two coals. Perhaps this is why the standard coal rank classification uses heating value for low rank coals to bituminous coals, and then switches to carbon content. However, for research purposes, it is useful to have one scale to indicate coal rank. The oxygen content of the parent coal provides a distinctive index of rank for this suite of coals, and is therefore used to indicate coal rank in this report.

Two gas temperature conditions were used in this series of experiments, with maximum centerline gas temperatures of 1050 K and 1250 K. Typical centerline gas temperature profiles, measured as a function of the distance from the coal injection tube, were shown in Section 2 of this report. Due to small, day-to-day changes in heater performance, gas temperature profiles were measured for each gas condition before each set of experiments on a particular coal. The measured gas temperature profiles, corrected for radiation, are therefore tabulated in the appendix for each coal.

The majority of the coal devolatilization data was obtained over a period of three years (1987 to 1990), after the infrared sizing-pyrometer system was fully operational. However, during the time when the pyrometer system was being developed, a series of solid sampling experiments for PSOC-1451D Pittsburgh #8 hva bituminous coal particles were conducted in the inert gas flow reactor under gas temperature conditions similar to those encountered in later experiments. This early set of experiments was conducted in collaboration with Steve Hsu, a doctoral student (at that time) studying under Professor Jack Howard at MIT. Although most of the early sampling experiments were repeated after the development of the sizing-pyrometer system, the mercury porosimetry and internal surface area analyses were not performed on the most recent samples (due to cost considerations). Elemental analyses and the extent of mass release are not available for these early samples. The mercury porosimetry and internal surface area data for this coal are therefore provided in this report for reference, but do not directly correspond to the rest of the data for this coal. Some of these early data were reported elsewhere [Hsu, 1989, thesis; Seery, et al., 1989].

Particle temperature histories, elemental organic and inorganic analyses of char samples, and apparent densities are available for each coal and temperature environment. However, the NMR analyses, GC/MS analyses, mercury porosimetry, and N_2 BET analyses were only performed on a select set of samples. The data available for each coal in 100% N_2 at each temperature condition in the coal devolatilization laboratory are summarized in Table 4.3, and the data are tabulated in the appendix as a function of coal type. The numbers in this table represent the number of samples for which data are available at that temperature condition. Numbers after a comma indicate duplicate experiments. In this table, ash analysis

Table 4.3
Data from the Coal Devolatilization Laboratory in 100% N_2

	1445D		1451D		1451D		1493D		1507D		1508D	
Size range (μm)	106-125		106-125		63-75		106-125		75-106		106-125	
Temperature Condition	1250 K	1050 K	1250 K	1050 K	1250 K	1050 K	1250 K	1050 K	1250 K	1050 K	1250 K	1050 K
Elemental composition	7	7	7	6	7	7,3	7,5	7	7,4	7,4	7	7
Ash analysis	7	7	7	6	7	7,3	7,5	7	7,4	7,4	7	7
Mass release	7	7	7	6	7	7,3	7,5	7	7,4	7,4	7	7
Internal surface area	7	7	6*	6*		6*			7			
Porosity	7	7	6*	6*		6*			7			
Apparent Density	7	7	7		7	7,3	7	7,4	7,4	7,4	7	7
Average diameter	7	7	7		7	7,3	7	7,4	7,4	7,4	7	7
SEM					10	5	5					
Cross-section micrographs					8	3						
^{13}C NMR analysis of char	2	4			4		6		6		3	3
^{1}H NMR analysis of tar	2	4			3	2	5,3	5	4	3		
^{13}C NMR analysis of tar	2	4					0,4	5	4	3		
GC/MS analysis of tar					2	1			2			
LV/MS analysis of tar		3			1		2		1			
Mass release rates	x	x	x	x	x	x	x	x	x	x	x	x
Elemental mass release rates	x	x	x	x	x	x	x	x	x	x	x	x
Gas temperatures	x	x	x	x	x	x	x	x	x	x	x	x
Pyrometer data	5	(3),4	5	4	5	4	4	4	4	3	5	4
Temperature history	x	x	x	x	x	x	x	x	x	x	x	x

*Data from early experiments with Steve Hsu in similar reactor environments.

refers to the elemental composition of the ash as well as the total amount of ash; mass release refers to the extent of mass release using inorganic tracers from the ash analyses; mass release rates refer to the extent of mass release as a function of residence time, including comparison with kinetic models, and elemental mass release rates refer to the fractional mass release of the major organic elements (C, H, N, S, and O) as a function of time and as a function of the total mass release.

Experiments in the CDL in 0 to 10% O_2

Two types of experiments were conducted in the Sandia Coal Devolatilization Laboratory (CDL) where up to 10 mole-% oxygen was added to the nitrogen in the flow reactor. The first set of experiments was performed at the request of PETC personnel as a consistency check on some char combustion experiments performed at the University of North Dakota Energy and Environmental Research Center (UNDEERC). In this set of experiments, particle temperatures for two coal types were examined at a gas temperature of ~ 1000 K and an oxygen concentration of ~ 10 mole-%. This work involved only sizing-pyrometer experiments without solids sampling experiments, and is described in Section 6.

A second set of experiments was performed in the CDL in 0 to 10 mole-% O_2 to determine the effect of oxygen on particle swelling characteristics. This purpose of these experiments was to investigate possible reasons for notable differences in particle swelling behavior between samples collected in 100% N_2 in the CDL and samples collected in post-flame combustion environments of 3 to 12% O_2 in the Char Combustion Laboratory (CCL). The experiments in the CDL were conducted mainly with the solids sampling apparatus, and did not involve the sizing-pyrometer. These data are discussed in Section 6.

Experiments in the CCL with 0% post-flame O_2

A series of coal devolatilization experiments were performed in the Char Combustion Laboratory (CCL) in order to examine particle swelling properties as a function of the ambient oxygen concentration. As part of this project, a new gas operating condition was developed in the laminar flame-fired flow reactor in the CCL that had 0% O_2 in the post-flame region. Modifications were also made to the sampling system in the CDL in order to aerodynamically separate tar from char, including temporary use of the cyclone system from the CDL. This set of experiments involved mainly solids sampling studies. Data available for these samples include elemental organic and inorganic composition, apparent densities, N_2 BET internal surface areas, and NMR analyses of chemical structure. Samples in this set of experiments were obtained only at one location in the flow reactor, corresponding to the end of volatiles combustion and the beginning of char combustion. These experiments in the CCL were conducted as part of the devolatilization project, and hence are not included in the milestone report for the coal char combustion project [Hurt, et al., 1992]. The results of the devolatilization experiments in the CCL are discussed in Section 6, and the data are tabulated in the appendix.

References for Chapter 4

Anthony, D. B., J. B. Howard, H. C. Hottel, and M. P. Meissner, *Fifteenth Symp. (Int.) on Comb.*, The Combustion Institute, p. 1303 (1974).

Hsu, J., "Swelling, Mass Transport, and Chemical Kientics in Bituminous Coal Pyrolysis," Ph. D. Thesis, Chemical Engineering Department, Massachusetts Institute of Technology (1989).

Hurt, R. H., R. E. Mitchell, and D. R. Hardesty, "Compilation of Sandia Coal Char Combustion Data and Kinetic Analyses," Milestone Report for DOE/PETC Contract FWP 0709 (in press, 1992).

Seery, D. J., J. D. Freihaut, W. M. Proscia, J. B. Howard, W. Peters, J. Hsu, M Hajaligol, A. Sarofim, R. Jenkins, J. Mallin, B. Espindola-Merin, R. Essenhigh, and M. K. Misra, "Kinetics of Coal Pyrolysis," Final Report for DOE Contract No. DE-AC22-84PC70768 (1989).

5. RESULTS AND DISCUSSION OF EXPERIMENTS IN 100% N_2

This section describes the results of the main body of coal devolatilization experiments preformed in the Sandia Coal Devolatilization Laboratory (CDL). As described in the Apparatus section, these experiments were performed in 100% N_2 in a laminar flow reactor at two different gas temperature operating conditions. The data are discussed in this section by topic: particle temperature histories, extent of mass release, devolatilization rates, physical structure characteristics, elemental mass release rates, chemical structure of char and tar, and spectral emissivities.

Particle Temperature Histories

One of the principal issues in the devolatilization literature at the start of this project was the temperature at which coal particle devolatilize (see Chapter 1). The determination of particle temperature histories during devolatilization is therefore one of the major contributions of this work, and distinguishes these experiments from any other devolatilization experiment. These results were published by Fletcher [1989a and 1989b].

A. Theory

The energy conservation equation of a spherical particle in an inert laminar flow, assuming negligible internal temperature gradients, is written as follows:

$$v_p\, m_p\, c_p \frac{dT}{dz} = h\, A_p \left(T_g - T_p\right) \frac{B}{e^B - 1} - \sigma\, \varepsilon_p\, A_p \left(T_p^4 - T_w^4\right) - v_p \frac{dm}{dz} \Delta H \qquad (5.1)$$

where $h = Nu\ k_g / d_p$. This equation expresses the thermal inertia in terms of convective heat transfer from the surrounding gas, radiative heat transfer, and the global heat of reaction during devolatilization. The θ term represents the effects of high mass transfer on the convective heat transfer coefficient [Spalding, 1955], and is defined by the following two equations:

$$\theta = B / (e^B - 1) \qquad (5.2)$$

where the transfer number B for heat transfer is defined by:

$$B = \frac{c_{pg}}{2\, \pi\, d_p\, k_g} \left(\frac{dm_p}{dt}\right) \qquad (5.3)$$

For small spheres near the gas velocity, the Nusselt number is 2. The gas thermal conductivity k_g is calculated based on the local film temperature $(T_p + T_g)/2$. At long residence times, the thermal inertia term on the left side of Eq. 5.1 becomes negligible, devolatilization is completed, and the equation reduces to a balance between the convection term and the radiation term.

Moisture Evaporation Rate

The evaporation of water from lignites and high-moisture coals must be modeled correctly in order to determine particle temperature histories and hence reaction rate coefficients. The rate of evaporation of a spherical drop of water can be expressed as:

$$\frac{dm_w}{dt} = \dot{W} = k_m \pi d_p^2 \left(\frac{x_{w,o} - x_{w,\infty}}{1 - x_{w,o}} \right) \tag{5.4}$$

(see Eq. 21.1-12, p. 641, ref. [Bird, et al., 1960]). The mass transfer coefficient is obtained from a correlation with the Sherwood number:

$$Sh = \frac{k_m d_p}{\rho_g D_w} = 2 + 0.6 Re^{0.5} Sc^{0.333} \tag{5.5}$$

For most practical problems involving evaporation of water from pulverized coal particles, the particle Reynolds number is low enough to assume that Sh = 2.0. At high rates of mass transfer, typical of rapid heating experiments, the rate of evaporation (Eq. 5.4) becomes:

$$\dot{W} = \theta_w k_m \pi d_p^2 \left(\frac{x_{w,o} - x_{w,\infty}}{1 - x_{w,o}} \right) \tag{5.6}$$

(Eq. 21.5-62, ref. [Bird, 1960]), where:

$$\theta_w = B_w / (e^{B_w} - 1) \tag{5.7}$$

A derivation of this expression is given in Appendix A. The transfer number B_w for water evaporation is defined as:

$$B_w = \frac{\dot{W}}{2 \pi d_p D_w \rho_g} \tag{5.8}$$

The mole fraction of water at the particle surface, $x_{w,o}$, used in Eq. 5.6, is calculated from the vapor pressure of water and the total pressure:

$$x_{w,o} = P_w / P_{tot} \tag{5.9}$$

The Antoine vapor pressure correlation is used to obtain P_w:

$$ln\, P_w = A - \frac{B}{T + C} \tag{5.10}$$

The Antoine vapor pressure coefficients for water are: A = 18.3036 mm Hg; B = 3816.44 mm Hg-K; and C = -46.13 K. When moisture effects are considered, the rate of evaporation is coupled with the particle energy equation through the heat of vaporization term, and Eq. 5.1 becomes:

$$m_p c_p \frac{dT_p}{dt} = \theta h A_p (T_g - T_p) - \sigma \varepsilon_p A_p \left(T_p^4 - T_w^4\right) + \sum_i \dot{r}_i \Delta H_i \qquad (5.11)$$

where the reactions i represent moisture evaporation, devolatilization, and char oxidation. In practice, this equation is solved using a predictor-corrector technique with time steps small enough to minimize computational errors. Gas and particle properties are varied as a function of time and temperature.

Rapid Heating Effects on Heat Transfer

At rapid heating conditions for large particles, significant internal temperature gradients may exist. It is difficult to quantitatively evaluate the effect of internal temperature gradients, due to the uncertainty in the thermal conductivity as a function of particle temperature, composition, and morphology. Gat [1986] used values of k_p between 0.14 and 0.36 W m^{-1} $°C^{-1}$ to show the probable existence of internal temperature gradients of several hundred degrees in 35 μm coal particles heated at 2 x 10^5 K/s to 2040 K. At more moderate heating rates typical of drop tube reactors (less than 10^4 K/s), internal temperature gradients of a 100 μm particle injected directly into a 1200 K gas stream were calculated to be on the order of 40 K using the Heisler charts [Heisler, 1947]. For softening coals, cenosphere formation obscures the standard thermal conductivity analysis, since large voids are formed inside the particle early in the pyrolysis process, after which heat transfer through a relatively thin shell should be treated.

In addition to effects of internal particle temperature gradients, some investigators claim that the rapid particle heating is significantly influenced by transient boundary layer effects. The rapid heating reportedly enhances the effective Nusselt number, allowing more efficient heat transfer to the particle. These claims were based on a quasi-analytical model of temperature gradients in the boundary layer of a rapidly-heated particle. In an effort to further understand this mechanism, and the effects it has on devolatilization rates, a detailed numerical model of heat transfer in and near rapidly-heated particles was developed at Sandia by Fletcher and Baxter [see Fletcher and Hardesty, 1990a]. A finite difference form of the energy equation was used to calculate the temperature profile in the boundary layer near a particle and throughout the interior of the particle. Only the inert particle case was considered. The results of the full numerical model indicate that there is no significant contribution to the particle temperature history due to an enhancement of the Nusselt number at rapid heating conditions; claims to the contrary are erroneous. The temperature profile in the boundary layer of the particle generally relaxes to the quasi-steady profile in a few milliseconds. The full numerical model was compared to the simple approach outlined above, where the Nusselt number is set to 2 and the internal particle

temperature gradients are neglected; results indicate no significant differences related to the assumption that the Nusselt number is 2. Results also indicate that the particle surface is a maximum of 40 K higher than the particle center for a 100 μm particle heated at 10^4 K/s to 1200 K, in accordance with results obtained using the Heisler charts. Internal particle temperature gradients and transient boundary layer effects are therefore ignored in this work.

Sensitivity Analysis

A sensitivity analysis was performed to examine the influence of the various terms in Eq. 5.1. The gas temperature profile used for this study (the 1250 K gas temperature profile shown in Fig. 2.2) is typical of drop tube reactors, as discussed previously. During the particle heating period, the thermal inertia and convective heat transfer terms are important, emphasizing the need to know the particle heat capacity and the local gas temperature. The base calculation was for a 115 μm diameter particle with c_p as a function of temperature, elemental composition, and ash content [Merrick, 1983]. The heat of reaction ΔH was set to -100 cal/g, which is slightly endothermic. Figure 5.1 shows the differences in calculated temperature due to (a) assuming the gas temperature is constant at 1250 K, (b) assuming c_p = 0.3 cal g^{-1} K^{-1}, and (c) for different particle diameters representing the sieve sizes. Note that the temperature dependence of the heat capacity was extrapolated from coal data at 300-500 K. The rate model used in these calculations is the two-step model with coefficients recommended by Ubhayakar et al. [1976] to fit the data of Badzioch and Hawksley [1970] and Kimber and Gray [1967]. Similar particle temperatures are predicted if other rate models are used, since ΔH is small. The wall temperature in this case was 500 K. Particles were allowed to swell by 40% as a linear function of the fraction of volatiles released [Smoot and Pratt, 1979], and the apparent density was adjusted accordingly.

Note that the calculated particle temperatures during the heating period (30-50 ms) differ by as much as 75 K at a given residence time, depending on the treatment of the particle heat capacity. If the gas temperature is assumed to be isothermal, even near the coal injector, calculated particle temperatures can differ by 250 K. If the particles stray from the centerline of the flow reactor, the temperature will be somewhere between these two extremes. For example, Tsai and Scaroni [1984] attempted to measure the degree of radial particle dispersion using a honeycomb apparatus, performed two-dimensional calculations of the gas temperature and velocity, and averaged the gas temperature over the region of particle dispersion. Their calculations were sensitive to the degree of radial particle dispersion during particle heatup, since significant radial gas temperature gradients exist near the coal injector in typical drop tube reactor studies.

The effect of particle diameter, even from a narrow size distribution (say 105-125 μm, or -140 to +120 mesh), can result in temperature differences as large as 100 K during heatup. Additional calculations have shown that the predicted temperatures are only

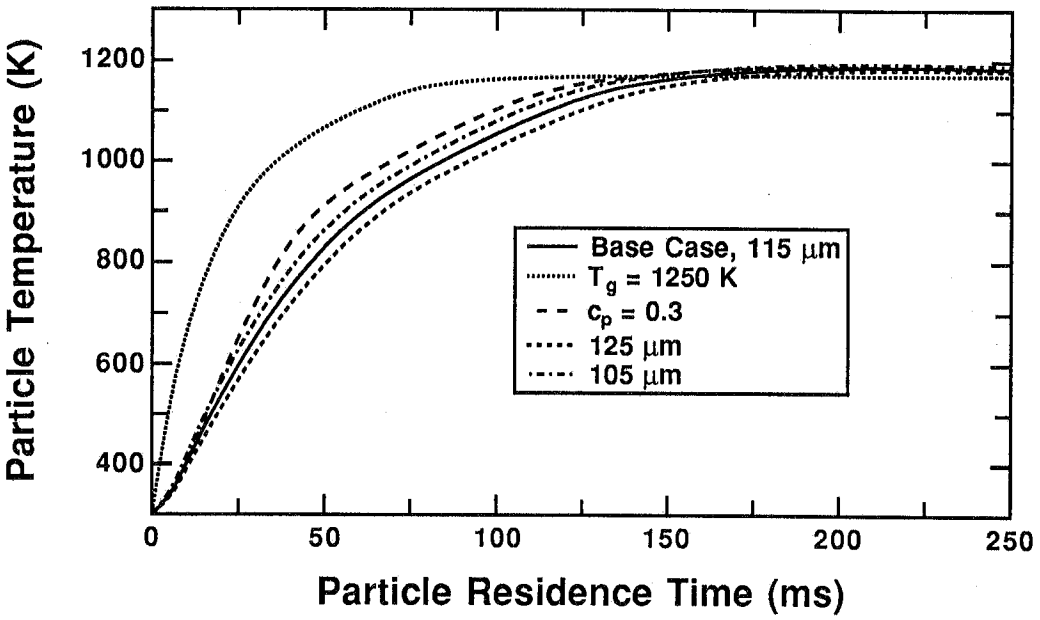

Figure 5.1 Effect of local gas temperature, particle heat capacity, and particle diameter on calculated particle temperature in the 1250 K gas condition in the CDL.

mildly sensitive to particle swelling (less than 50 K difference), and are relatively insensitive to particle velocity (less than 25 K difference when constant particle velocity was used), or heat of reaction (changing ΔH from -100 to 0 cal/g caused less than a 25 K difference in particle temperature). The reduction in heat transfer from the blowing parameter (Eq. 5.2) is negligible at these temperatures and heating rates. When the initial apparent density of the particles (grams per particle volume based on the diameter) was changed from the commonly used value of 1.3 g/cm^3 [Smoot and Pratt, 1979] to 0.65 g/cm^3, differences in calculated particle temperature as high as 125 K were observed.

This analysis demonstrates the need for careful determination of the particle time-temperature profile as a function of particle size, even if the particles have been tightly screened and aerodynamically classified. Cloud measurements assuming a mean particle size may be skewed towards the smallest sizes, since the number density of small particles affects the optical measurement rather than the mass fraction. A physically unrealistic description of the time-temperature profile causes large differences in kinetic parameters derived from the experimental data, emphasizing the need for careful experimental verification of the time-temperature profile.

B. Results and Discussion

Particle Velocities

The size, temperature and velocity of individual Spherocarb particles (non-reacting carbon spheres) were measured as a function of vertical distance in the flow reactor in order to calibrate the sizing-pyrometer system. Knowing the gas temperature, along with particle size and velocity, the local gas velocity can be calculated from the particle momentum equation assuming quasi-steady behavior, as follows:

$$v_g = v_p - \left(\frac{\rho_p \, d_p^2 \, g}{18 \, \mu_g} \right) \tag{5.12}$$

Gas and particle velocities at the injector tip were 72 cm/s. Figure 5.2 shows particle velocity measurements for Spherocarb particles and calculated gas velocities as a function of distance in the flow reactor. It can be seen that the local gas velocity is low in the cool region near the coal injector (0-75 mm). If the radial gas temperature and velocity profiles were uniform, the gas velocity would be 77 cm/s. The velocity decrease at the flow reactor exit is caused by a local pressure increase due to buoyant forces; the hot buoyant gas from the flow reactor is compressed against the cooler dense air at the exit of the flow reactor, and the exhaust suction was inadequate to compensate. Pressure differences on the order of a few pascals can cause noticeable velocity gradients in high temperature flows. The measured particle velocities are integrated numerically in order to convert vertical distances in the flow reactor to particle residence times.

Signal Conditioning

Emission signals from multiple particles in the optical path are occasionally detected; emission signals with extraneous peaks are discarded. At the particle loadings used in this study (5-10 mg/min), relatively few multiple particle events were detected. As an additional method to screen particle emission signals, particle emissivity was calculated from the signal intensity of the 2.2 μm channel using the measured particle temperature and diameter. This calculation of emissivity reflects all of the errors associated with both the size and temperature measurement [Mitchell, 1987]; a calculated emissivity outside the normal range represents an erroneous emission signal. The emissivity calculation includes one system calibration constant, which was set such that the average Spherocarb emissivity was close to 0.85. In a typical screening procedure, particles with calculated emissivities greater than 1.1 and less than 0.6 are ignored.

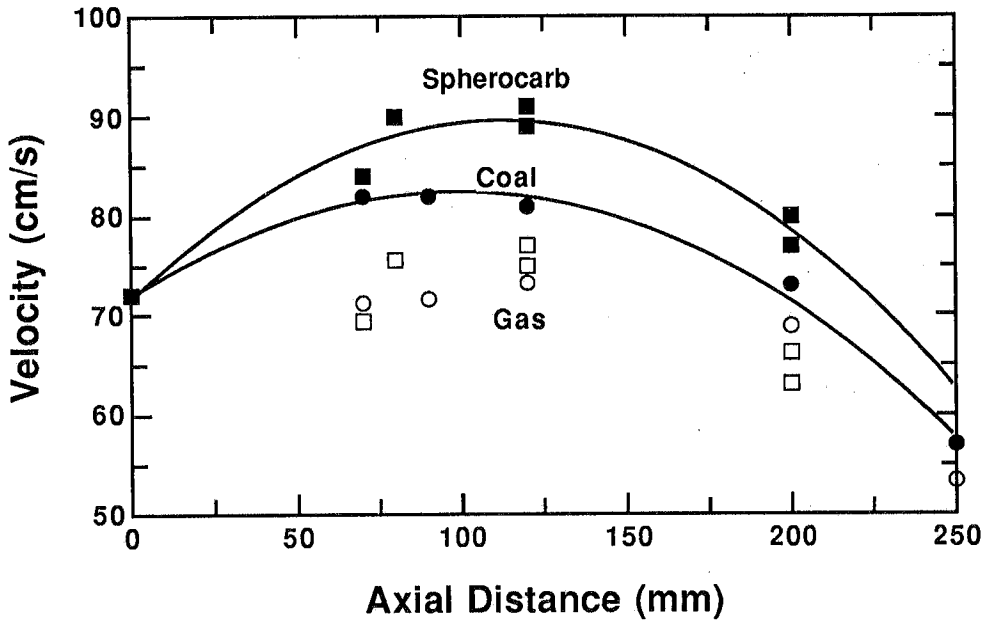

Figure 5.2 Measured Spherocarb and coal particle velocities as a function of vertical distance in the 1050 K gas condition in the CDL. Gas velocities calculated from the respective Spherocarb and coal particle velocities are also shown. Solid lines are the curve fits used in the particle temperature calculations.

Spherocarb Particle Temperatures

Spherocarb particle temperatures at axial locations of 200-250 mm were used to determine the system spectral response factor for the detection optics. In this region of the reactor, gas and particle temperatures are in quasi-steady equlibrium, and particle temperatures can be calculated from the gas temperature based on the particle diameter and emissivity. Spherocarb emissivities of 0.85 were employed. The system response factor is a combination of the optical response of each optical component (windows, mirrors, lenses, and detectors) as well as the response of the amplifiers and electronic filters used in conjunction with the detectors. The voltage signal recorded on the oscilloscope is the combination of all of these response functions, as well as the optical properties of the coal particle and surrounding gas. Nitrogen is transparent at the wavelengths examined in this study. The system response factor is therefore used a calibration constant to account for the spectral response of the particle, optical system, and electronic system, and is determined experimentally.

The measured particle temperatures and velocities are grouped into size bins of 10 μm, and each size bin is analyzed for mean properties as well as standard deviations. Typical standard deviations in the Spherocarb particle temperature were 20 K at T_p = 900 K and 5 K at T_p = 1200 K. The temperature threshold of approximately 850 K is

due to the lack of signal on the 1.36 μm channel. Standard deviations in the particle velocity are typically 2 to 3 cm/s.

Calculations of Spherocarb temperature in the flow reactor were performed for both 125 and 149 μm diameter particles, which represents the maximum and minimum sieve sizes. Measured particle velocities and gas temperatures were used in the calculations. The particle heat capacity expression used in these calculations is that recommended for pure carbon [Merrick, 1983].

The dominant mode of heat transfer in this reactor is convection, especially during particle heatup. However, a small amount of radiative heat is transferred from the interior of the heater system to particles near the coal injector. Radiation from the heater section above the flow reactor is modeled as if from a flat disk at the same temperature located at the coal injection plane. The view factor from a disk to a particle [Siegell and Howell, 1981] is:

$$F_{1\text{-}2} = 1 - \frac{1}{\sqrt{1 + R^2}} \tag{5.13}$$

where R is defined as the ratio of the separation distance (z) to the disk radius (r_d). The radiation loss to the coal injection tube is modeled in a similar fashion. The radiation term in Eq. 5.1 is changed to contain contributions from the heater, the coal injection tube, and the flow reactor walls, as follows:

$$Q_{rad} = \varepsilon \sigma A \left[(1 - F_{p\text{-}h})(T_w^4 - T_p^4) + (F_{p\text{-}h} - F_{p\text{-}i})(T_h^4 - T_p^4) + F_{p\text{-}i}(T_i^4 - T_p^4) \right] \tag{5.14}$$

where T_h and T_i are the temperatures of the heater section and the coal injection tube, respectively. The view factors between the particle and the heater ($F_{p\text{-}h}$) and between the particle and the injector tube ($F_{p\text{-}i}$) are calculated as a function of axial position. At the 1250 K gas condition, the heater radiation raised the particle by as much as 100 K in regions of the reactor near the coal injector. The thermocouple measurements are corrected in a similar fashion in order to obtain gas temperature.

Measured Spherocarb particle temperatures are compared in Fig. 5.3 with predictions from Eq. 5.1 for two different gas temperature conditions. Duplicate data points represent a combination of repeat measurements and the range of particle temperatures for the size distribution. It can be seen that predicted and measured particle temperatures agree to within 50 K at long residence times, although agreement is not as good during the heating region.

Coal Particle Temperatures

A careful study was performed to determine the errors in the particle size and temperature measurements induced by the tar cloud surrounding each coal particle. The particle sizes determined from the emission signal are close to the sizes expected

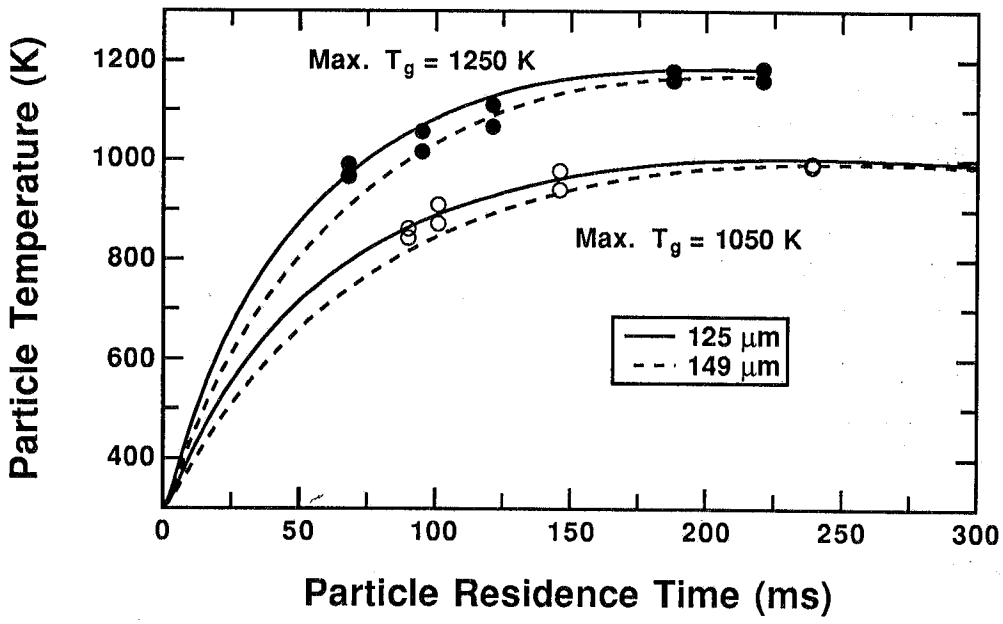

Figure 5.3 Comparison of measured (discrete points) and calculated (curves) Spherocarb particle temperatures as a function of residence time in the two gas conditions in the CDL. Multiple points here represent the range of three particle size bins.

for coal particles and not representative of the particle cloud (observed visually to be at least 10 times the particle diameter). This is strong evidence that the tar cloud does not interfere with the particle emission signal. The emission intensities per unit surface area (i.e. detector signal) for Spherocarb and bituminous coal are very similar in magnitude, indicating that the emissivities are similar. The calculated emissivity is generally used as a self-consistency check, as mentioned above. However, the fact that the calculated emissivities are similar for the Spherocarb and bituminous coal is additional evidence that the tar cloud does not influence particle temperature measurements. Measurements reported by Fletcher et al. [1987] show that Spherocarb and partially reacted char particles have similar emissivities (0.9 and 0.7, respectively).

Since the tar cloud is expected to exhibit a diameter of at least 10 times that of a coal particle, any partial tar cloud interference on signals from the infrared sizing-pyrometer would be observed in the baseline signal before and after the particle emission signal. Examination of numerous coal particle emission signals indicates that no baseline deviations are present in the region before or after the particle, indicating that the tar cloud emission is not observed by the infrared detectors. Based on the facts that no baseline deviations due to the tar cloud are observed, measured particle diameters are in the appropriate range for particles and not tar clouds, and that the emission intensity for Spherocarb and coal particles are similar, tar cloud effects are though to be negligible in this system.

Table 5.1 shows representative particle temperature and velocity measurements as a function of particle size for the 105-125 μm size fraction of PSOC-1451D hva Pittsburgh bituminous coal. The broad size distribution in Table 5.1 is indicative of particle swelling, and agrees with recent size distribution measurements for the same coal at similar conditions [Mallin and Jenkins, 1987]. Standard deviations in the measured particle temperature are higher than for Spherocarb, indicative of non-sphericity and of particle to particle differences in composition. Calculated emissivities are similar to those obtained for Spherocarb particles. Coal particle velocities are slightly lower than those measured for Spherocarb particles, since the apparent density of the coal decreases significantly due to devolatilization (from 1.27 to 0.27 g/cc). Gas velocities calculated from the coal particle data, using Eq. 5.12 and measured apparent densities, agree to within 5% of the gas velocities calculated from the measured Spherocarb particle velocities. The open symbols in Fig. 5.2 are measured coal particle velocities and the corresponding gas velocities are calculated from Eq. 5.12.

Table 5.1
Representative Particle Temperature and Velocity Measurements as a Function of Particle Size
(PSOC-1451D, 106-125 μm, 1250 K gas condition, 120 mm)

Size (μm)	#	T_p (K)	σ_T (K)	v_p (cm/s)	σ_v (cm/s)	ε	σ_ε
115	6	983	23	0.80	0.02	0.69	0.09
125	15	953	23	0.81	0.03	0.86	0.16
135	17	966	23	0.81	0.02	0.73	0.13
145	10	948	29	0.83	0.02	0.72	0.11
155	11	951	17	0.83	0.03	0.61	0.12
165	12	951	18	0.82	0.02	0.64	0.09

Coal particle temperatures are calculated from Eq. 5.1 using measured gas temperatures, particle velocities, and apparent particle densities. The heat of reaction ΔH was set to -100 cal/g, according to the recommendations of Freihaut [1980]. As mentioned earlier, these calculations were found to be relatively insensitive to the value used for ΔH. The particle heat capacity is calculated as a function of temperature and ash content according to Merrick [1983]. Particle swelling was calculated as a linear function of the extent of volatiles release [Smoot and Pratt, 1979]. Based on the apparent density and weight loss determinations, as well as the measured particle sizes, the final particle diameter was increased by 40% due to swelling.

Figure 5.4 shows a comparison of calculated and measured coal particle temperatures as a function of particle residence time at two different gas temperature flow

conditions, based on the measured centerline gas temperature profile. The system response factor which matched predicted coal particle temperatures after heatup was 15% lower than that used for the Spherocarb particles. This may indicate a different spectral emissivity ratio for the two types of particles.

The assumption made here is that the ratio of the spectral emissivities of the coal particles at the two wavelengths of interest (1.3 and 2.2 μm) does not change as a function of residence time or extent of reaction. Release of functional groups is known to change spectral emissivities in certain infrared wavelength regions [Fletcher et al., 1987; Baxter et al., 1988]. Emission from specific functional groups begins at wavelengths of 3.0 μm due to -OH and -NH stretching, but emission peaks from specific functional groups are not found in the near infrared region (1.0-2.7 μm). Spectral characteristics of coal particles in the near infrared region should therefore not change as different functional groups are released into the gas phase, but may possibly change as a function of coal type.

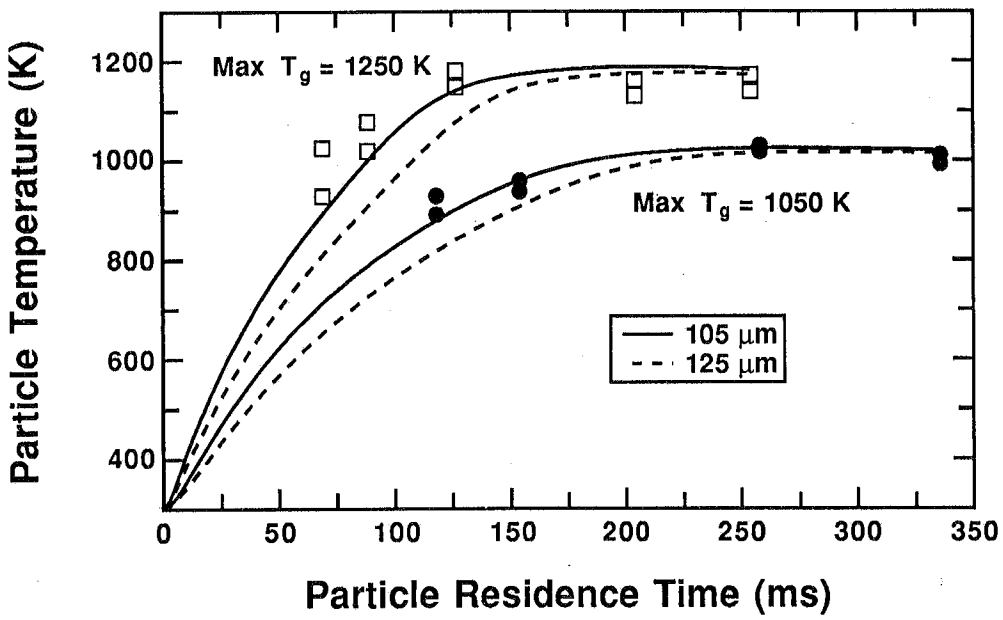

Figure 5.4 Comparison of measured (discrete points) and calculated (curves) particle temperatures as a function of residence time in the two gas conditions in the CDL for PSOC-1451D, Pittsburgh #8, coal (106-125 μm size fraction).

The particle temperature calculation is mildly sensitive to the mass of the particle m_p during the heating period (see left-hand term of Eq. 5.1), hence the devolatilization rate used to model the temperatures can affect calculations. Calculated temperature histories are shown in Fig. 5.4 for two different initial particle sizes, representing the bounding screen mesh sizes. The data points represent the range of average particle

temperatures measured for the different size bins. The spread in measured particle temperatures at any given residence time is roughly equivalent to the spread in the predicted particle temperatures due to differences in particle size. The predicted particle temperatures are much lower than the measured temperatures during the heating region, indicating that particles heat faster than expected based on the centerline gas temperature.

Possible reasons for this increased heat transfer are (1) radial particle dispersion in regions of severe gas temperature gradients near the coal injector, (2) local flow disturbances generated by rapid devolatilization, and (3) changes in the Nusselt number due to non-uniform boundary effects and/or particle spinning effects on non-spherical particles. It is interesting that the measured and calculated particle temperatures are in better agreement for Spherocarb than for the coal. The particle loading and apparent degree of particle dispersion (based on visible emission and laser scattering observations) are very low in this study, suggesting that the gas temperatures experienced by the coal particles is close to the measured centerline gas temperature. The Nusselt number is derived assuming steady flow conditions and an infinite, fully-developed boundary layer. In regions of large radial and axial gas temperature gradients and transient gas and particle temperatures, the Nusselt number may not adequately describe convective particle heating. Regardless of the reason for the increased heat transfer, the value of performing the particle temperature measurements is very apparent.

Since particle temperatures below 850 K are not possible with this apparatus, it is necessary to fit the measured particle temperature history using the correct form of the particle energy equation. Particle heating is governed by a characteristic heating time τ_p, where:

$$\tau_p = \frac{\rho_p \, d_p^2 \, c_p}{12 \, k_g} \tag{5.15}$$

when $Nu = 2.0$. Since τ_p is really a function of time and the extent of reaction, only the initial value ($\tau_p{}^o$) is changed to fit the experimentally measured particle temperature history. Changes in $\tau_p{}^o$ can be interpreted as changes in the convective heat transfer coefficient (or Nusselt number) for the particle, or changes in the particle diameter, apparent density, or heat capacity not accounted for in the calculations using the methods described above.

Figures 5.5 and 5.6 show a comparison of the calculated and measured particle temperatures when $\tau_p{}^o$ is adjusted to obtain agreement with the measured particle temperatures. The mean particle size is used in these calculations, rather than the range of particle sizes. Best agreement for the Spherocarb particles was obtained by lowering $\tau_p{}^o$ by 22% at both temperature conditions. Best agreement for the coal particles was obtained by lowering $\tau_p{}^o$ by 42% and 17% at the 1250 K and 1050 K gas

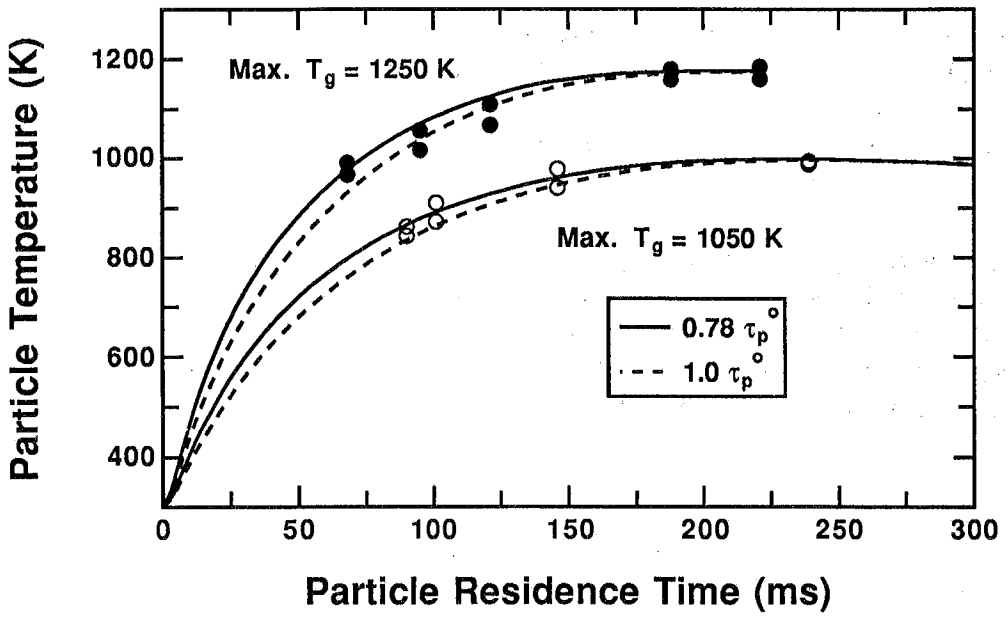

Figure 5.5 Comparison of measured (discrete points) and calculated (curves) Spherocarb particle temperatures as a function of residence time in the two gas conditions in the CDL, showing the effect of τ_p^o. Initial particle diameter in these calculations is 140 μm.

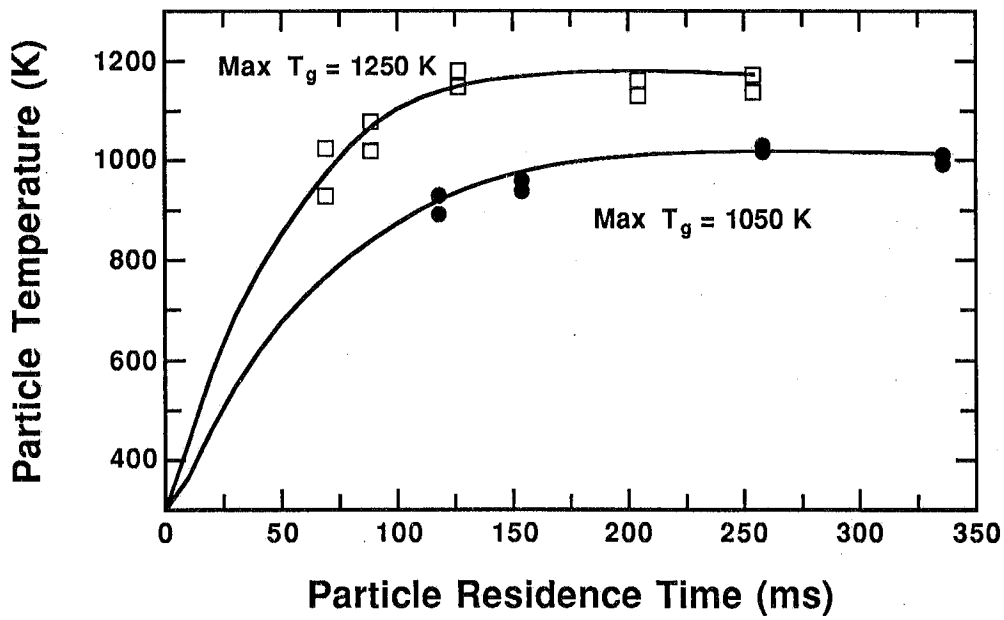

Figure 5.6 Comparison of measured (discrete points) and calculated for PSOC-1451D, Pittsburgh #8, coal particle temperatures as a function of residence time in the two gas conditions in the CDL, using 0.58 τ_p^o for the 1250 K gas condition and 0.83 τ_p^o for the 1050 K gas condition. Initial particle diameter in these calculations is 115 μm.

conditions, respectively. The most severe heat transfer correction was required to match the coal particle temperatures at the 1250 K gas condition. This implied change in heating characteristics is thought to be within the combined uncertainties of estimates for the apparent density and heat capacity of the particles as a function of temperature and reaction history.

This method for fitting the measured particle temperature history attempts to account for changes in local gas temperature and radiant heat transfer as well as changes in particle properties. Since the particle temperature history of this system is well characterized, future determination of devolatilization kinetic parameters from weight loss measurements should be physically realistic.

Other Coals

The procedure to obtain a particle temperature history was repeated for all of the other coals in each temperature condition. The measured gas and particle temperatures, along with the calculated temperature histories, are shown in the Appendix for all five coals. For all of the coals examined, the initial characteristic particle heating time τ_p^o had to be lowered from published values in order to obtain good agreement with measured particle temperatures. Good agreement was achieved with the sizing-pyrometer data from all five coals in both temperature conditions by lowering the value of τ_p^o by 58%.

C. Conclusions

The large differences in reported devolatilization rates can be attributed to the difficulty in determining accurate particle time-temperature profiles during devolatilization under rapid heating conditions. This difficulty arises because a major portion of volatiles are released during particle heating. Particle temperature histories are acutely sensitive to the local gas temperature and to the diameter, heat capacity, and apparent density of the particles.

In order to avoid the difficulties associated with inferred particle temperatures, an optically accessible entrained flow reactor and infrared sizing-pyrometer system was used to measure simultaneously the size, temperature, and velocity of individual particles in the flow reactor at different residence times. This is the first time that this measurement technique has been applied to the study of coal devolatilization. Comparison of measured sizes and temperatures of pure carbon spheres with those of pyrolizing coal particles shows that the temperature measurement is not influenced significantly by the tar cloud surrounding each particle. Gas and particle temperatures and velocities in the flow reactor are significantly influenced by local cooling near the point of injection, which may be a cause for the large discrepancy in reported devolatilization rates measured in conventional drop tube reactors.

Key assumptions made in the determination and analysis of particle temperatures are as follows:

1. Particle emissivities at the two wavelengths of interest do not change during devolatilization ($\varepsilon_{\lambda 1}/\varepsilon_{\lambda 2}$ = constant).

2. The population of particles for which temperatures are measured is representative of all particles.

3. Temperature differences between the surface of the particle and the center are small in these experiments, and can be neglected.

4. Inteference from the surounding tar cloud is negligible in these flow reactor conditions.

Temperatures as low as 850 K were measured for 100 μm diameter particles. Spherocarb and coal particle temperatures, measured as a function of particle size, were compared with calculated temperatures as a function of residence time. Measured particle temperatures were found to be higher than predicted using on the centerline gas temperatures and published particle properties (i.e., heat capacities), emphasizing the need for the particle temperature measurements. These temperature measurements are being combined with solid sampling experiments in order to determine coal devolatilization rates. Rates determined in this apparatus should be physically meaningful since particle temperature histories are well understood.

Extent of Mass Release

The devolatilization behavior of five coals was studied in a 100% nitrogen environment. Samples of PSOC-1507D, PSOC-1445D, and PSOC-1493D were collected in the CDL in two different gas conditions (1050 K and 1250 K) at various stages of devolatilization. The samples were analyzed for elemental composition of organic and inorganic material, as discussed in Section 3. These analyses are listed in the Appendix. The choice of particle sizes is discussed in Section 4.

The major mineral elements are used as tracers to determine the fraction of mass released as volatile matter. The elemental mineral matter data for the PSOC-1507D samples were widely scattered, however, and only the total ash determination is suitable for use as a tracer. The elemental mineral matter for the PSOC-1508D samples were also widely scattered, including the total ash content. This is a low volatile coal, which exhibits a very low reactivity, and the standard ASTM ashing technique may be at too low of temperature to obtain adequate data for this coal. Mass balances (amount fed to the reactor minus amount collected in the probe) were therefore used to determine the extent of mass release for this coal. A collection efficiency of 93% was determined for this coal by sampling at early residence times where no devolatilization occurs. Tracers used for the other three coals (PSOC-1445D, PSOC-1451D and PSOC-1493D) include titanium, aluminum, and silicon, as well as total ash. The mass release on a dry, ash-free (daf) basis is shown in

Figures 5.7-5.11 for these five coals, along with the average value for each sample. The ASTM volatiles matter determination is also shown in these figures.

The total volatiles yields obtained at the 250 mm sampling position in each gas condition to the ASTM volatile matter content are shown in Table 5.2 for the five coals examined. At the 1250 K gas condition, this ratio corresponds directly to the Q factor, since it is thought that little or no volatile matter remains in these samples. However, at the 1050 K gas condition, devolatilization is not complete, and this ratio must be factored by the volatile matter remaining in order to compute Q factors. The ASTM volatile matter was not determined on these samples, and hence Q factors are not presented.

Table 5.2
Comparison of Volatile Yields Measured in the CDL to the ASTM Volatile Matter Content

Coal Type	V_{ASTM} (% daf)	V_{1050} (% daf)	V_{1050}/V_{ASTM}	V_{1250} (% daf)	V_{1250}/V_{ASTM}
PSOC-1507D (Zap lignite, 75-106 μm)	49.6	52.5	1.06	53.7	1.08
PSOC-1445D (Blue #1 subbituminous,106-125 μm)	46.8	39.6	0.85	53.6	1.15
PSOC-1493D (Illinois #6 hvb bituminous, 106-125 μm)	43.4	43.5	1.00	52.9	1.22
PSOC-1451D (Pittsburgh #8 hva bituminous, 63-75 μm)	38.7	55.5	1.43	53.1	1.37
PSOC-1508D (Pocahontas #3 lv bituminous, 106-125 μm)	17.2	6.6	0.38	16.1	0.94

The mass of volatile matter released in the CDL exceeds the ASTM volatile matter content for four coals at the 1250 K gas condition. The mass release measured in the CDL for the low volatile coal is comparable to the ASTM yield, within the limits of experimental error for this coal. The data shown for the 106-125 μm size fraction of the Pittsburgh #8 coal are not shown here, since these were the first samples obtained in the CDL and analyzed by Coors Analytical Laboratories, and the yields seem to be low compared to the 63-75 μm size fraction. Volatiles yield data as a function of particle size [Anthony, et al., 1974] indicate that no such trend should exist. The data for the 106-125 μm size fraction are therefore thought to be incorrect and are ignored in this analysis.

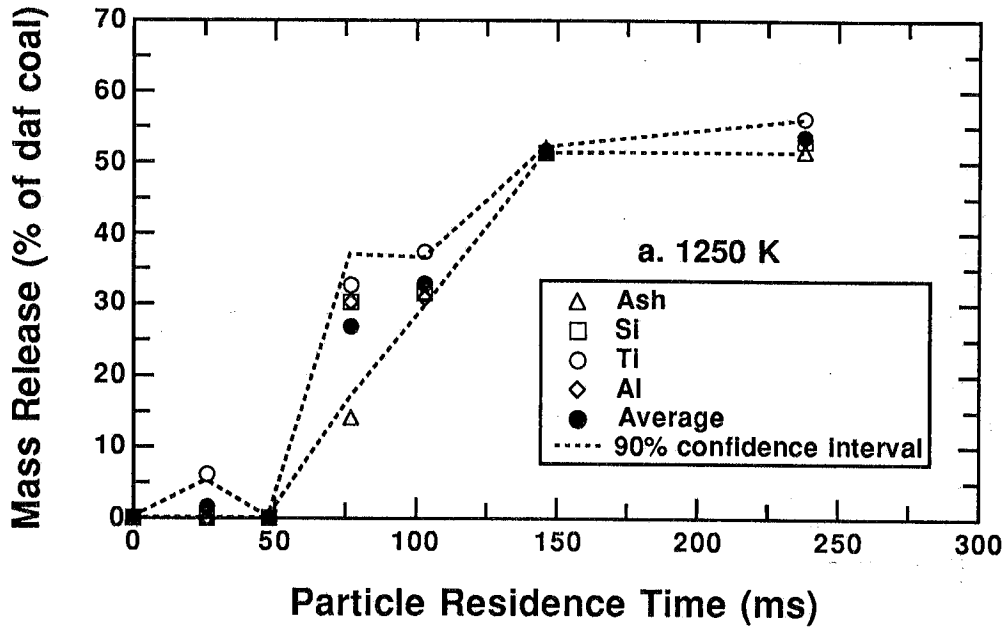

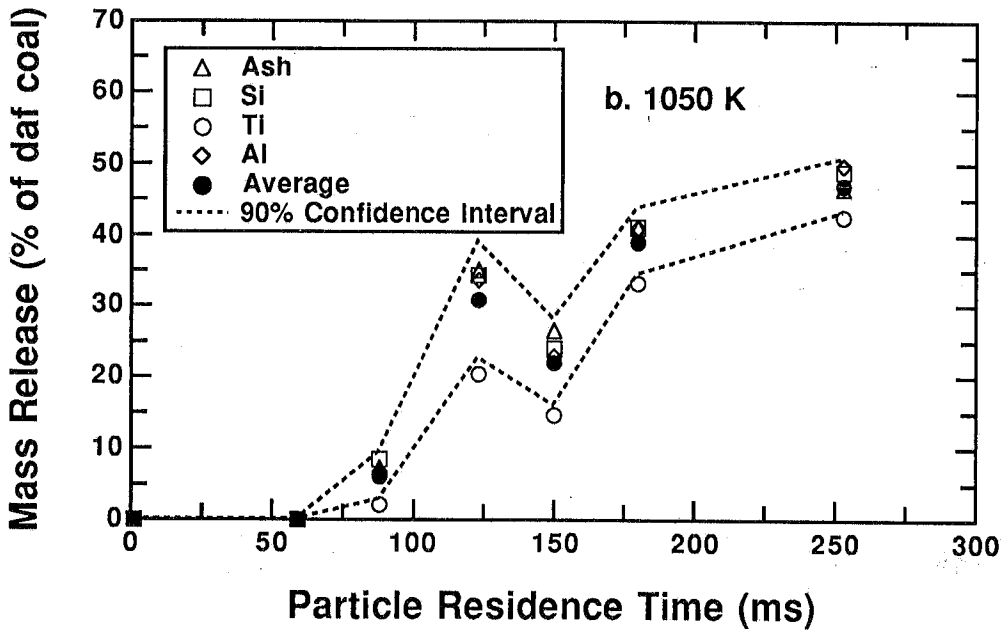

Figure 5.7 Mass release due to devolatilization for PSOC-1445D New Mexico Blue #1 subbituminous coal particles in 100% N_2 in the CDL. (a) 1250 K gas condition, (b) 1050 K gas condition.

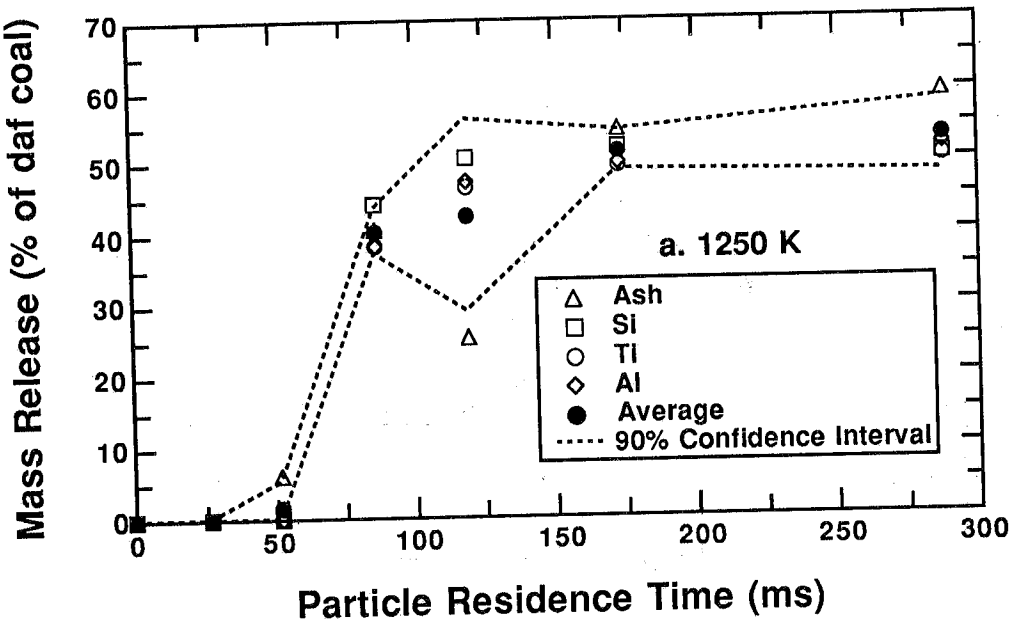

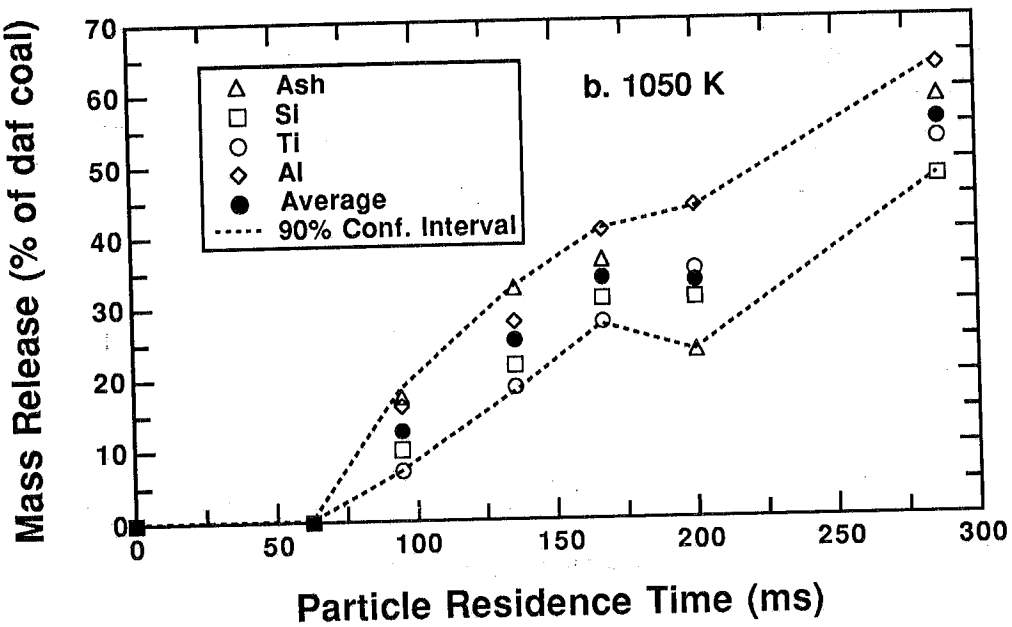

Figure 5.8 Mass release due to devolatilization for PSOC-1451D Pittsburgh #8 hva bituminous coal particles (63-75 μm size fraction) in 100% N_2 in the CDL. (a) 1250 K gas condition, (b) 1050 K gas condition.

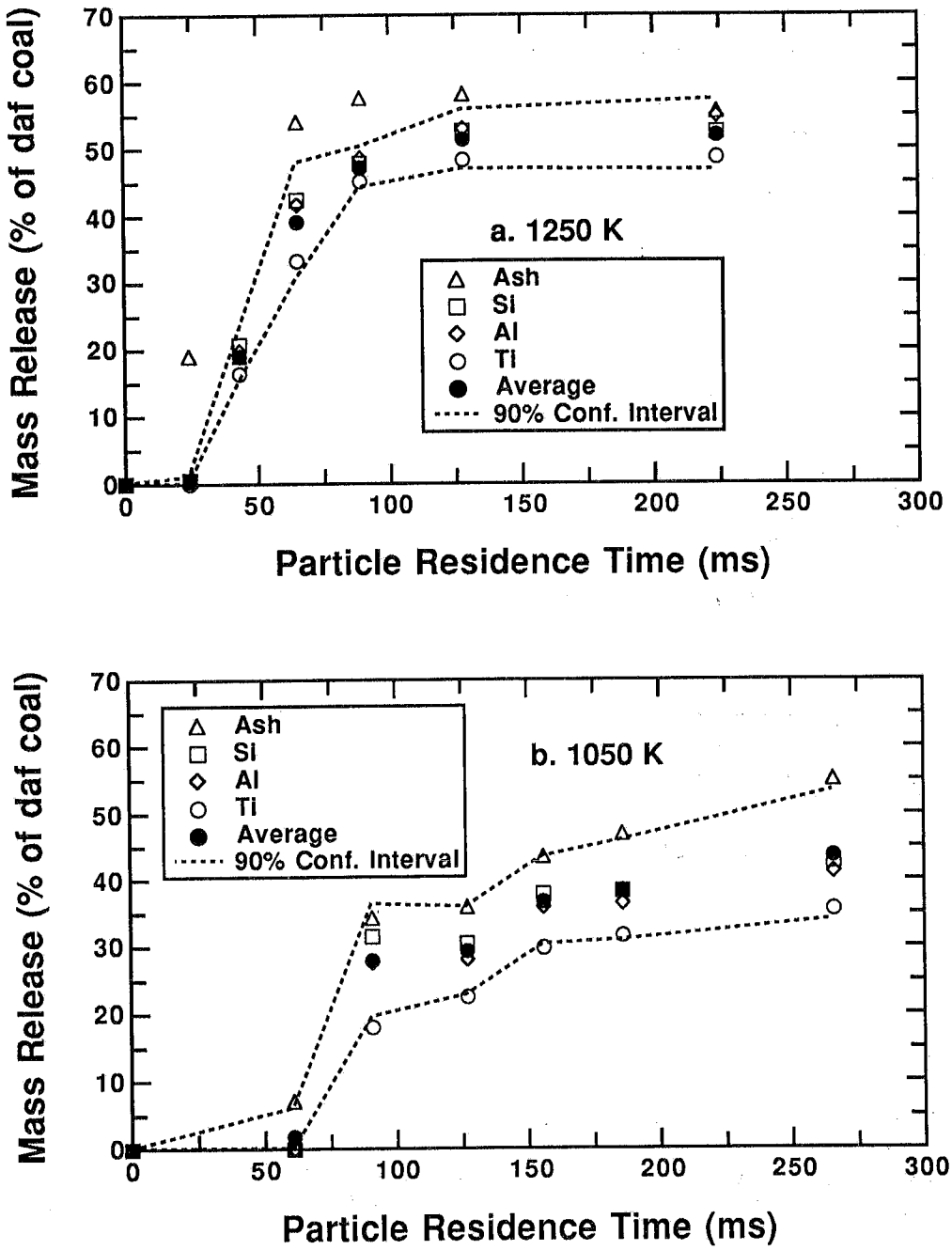

Figure 5.9 Mass release due to devolatilization for PSOC-1493D Illinois #6 hvb bituminous coal particles in 100% N_2 in the CDL. (a) 1250 K gas condition, (b) 1050 K gas condition.

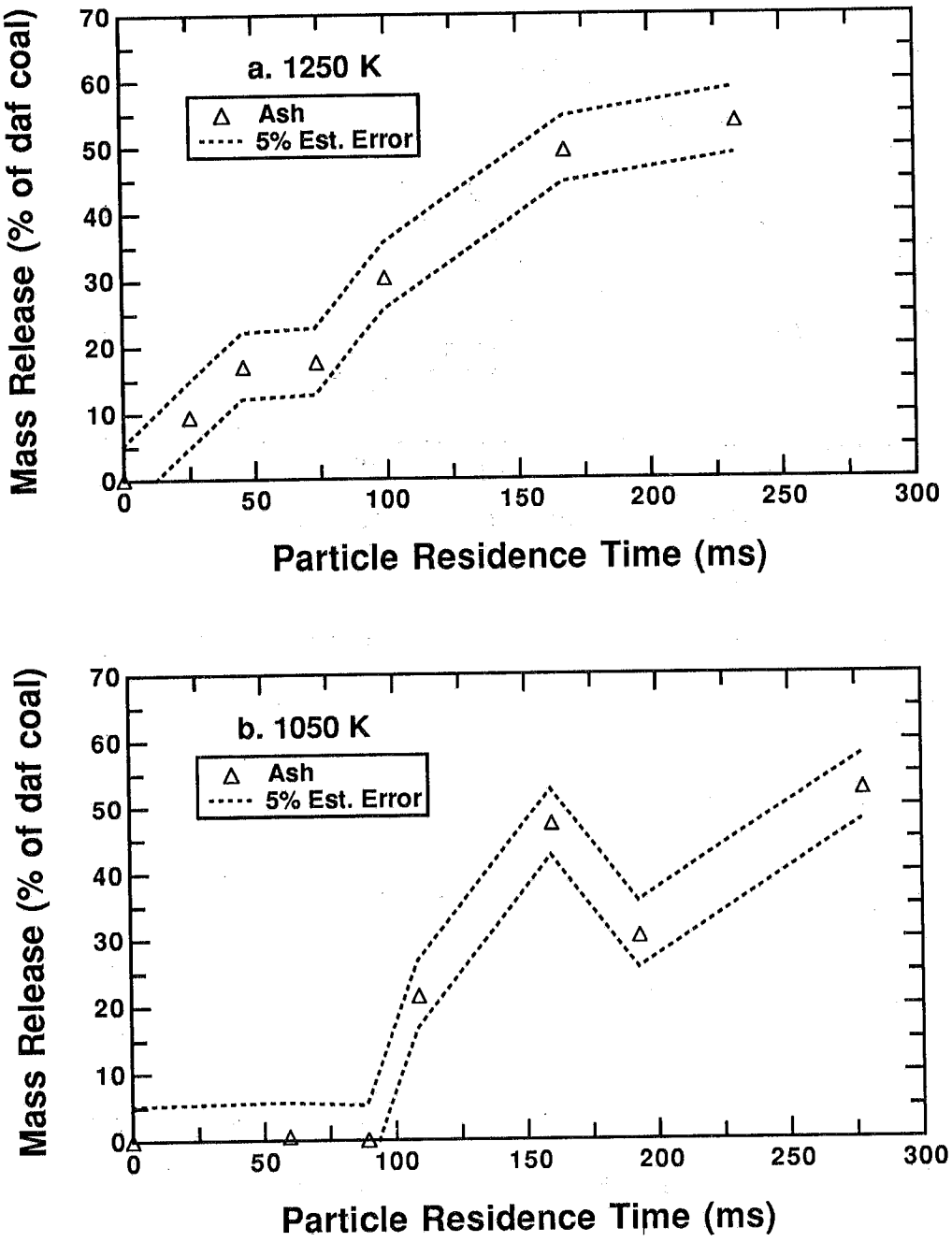

Figure 5.10 Mass release due to devolatilization for PSOC-1507D North Dakota Beulah Zap lignite particles in 100% N_2 in the CDL. (a) 1250 K gas condition, (b) 1050 K gas condition.

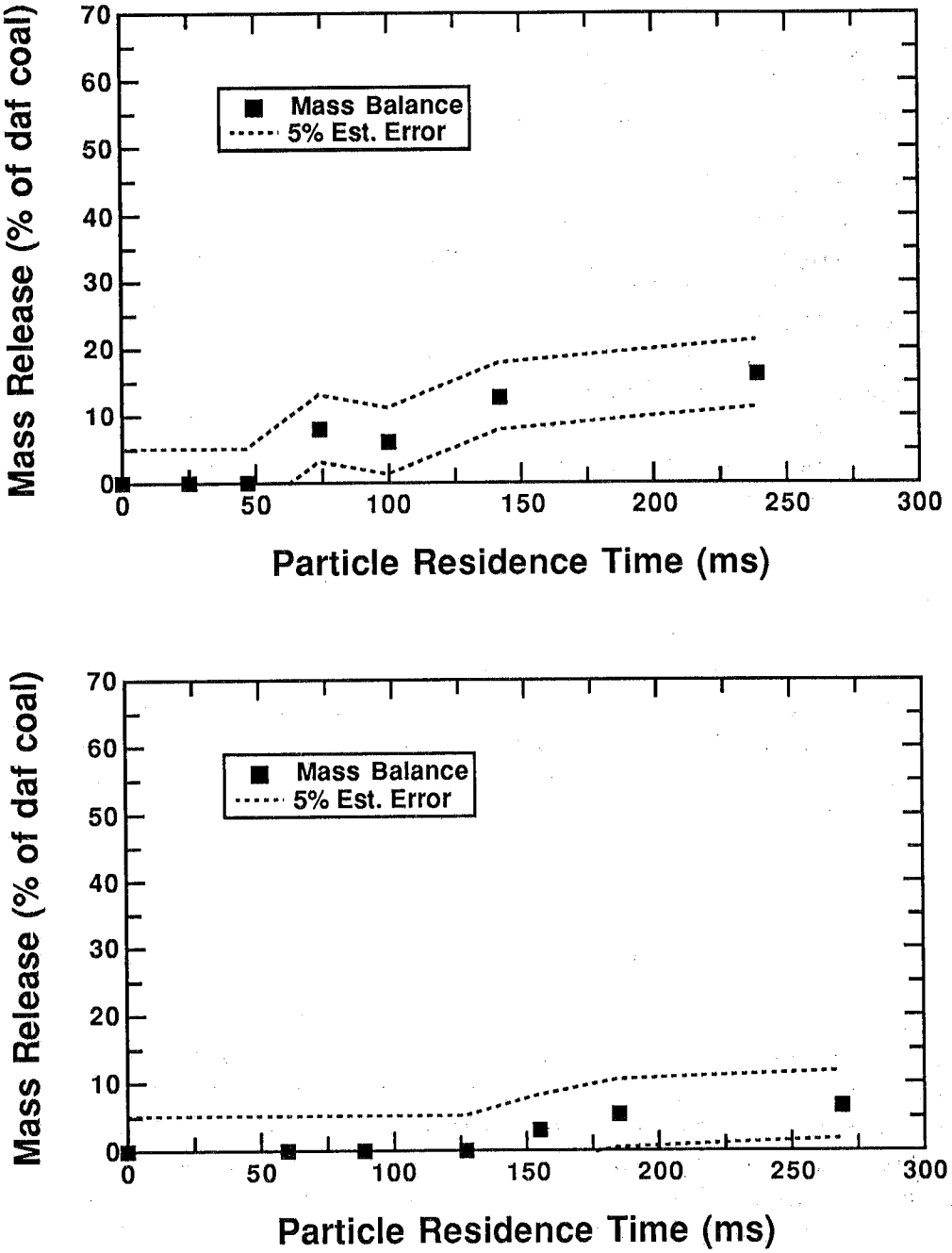

Figure 5.11 Mass release due to devolatilization for PSOC-1508D West Virginia Pocahontas #3 lv bituminous coal particles in 100% N_2 in the CDL. (a) 1250 K gas condition, (b) 1050 K gas condition.

The ratio of volatile matter released in the CDL to the amount of volatile matter determined using the ASTM method increases as the rank increases from lignite to bituminous coal; the hva bituminous coal exhibits the largest ratio, while the lignite ratio is close to unity. However, at even higher rank (i.e., the low volatile bituminous coal), the yield in the entrained flow experiment again approaches the ASTM yield. Maximum particle temperatures in the 1250 K gas condition are approximately 1150-1200 K due to radiative loss through the transparent flow reactor walls, and the heating rate is approximately 10^4 K/s. The temperature of the ASTM proximate analysis is 950°C (1223 K), which is a comparable temperature. The difference in yield is therefore due to differences in heating rate and the lack of tar redeposition in the flow reactor experiments. Three of the coals (PSOC-1507D, 1493D, and 1451D) investigated here exhibited volatile yields exceeding the ASTM volatile content at the 1050 K gas condition (maximum gas temperatures of 1000 K), which is 200 K lower than the ASTM analysis condition.

The inadequacy of the ASTM proximate analysis has been known for many years [Howard, 1981]. The data in Table 5.2 provide evidence that the proximate analysis does not even correctly reflect the trends in the amount of volatile matter released from different coals of different rank. The coal with the second lowest ASTM volatile content (PSOC-1451D) exhibits the same yield at the 1250 K gas condition as the coal with the highest ASTM volatile content (PSOC-1507D). In fact, four of these coals exhibit nearly identical volatile yields on a dry ash-free (daf) basis, even though the ASTM volatile contents, ash contents, and elemental compositions are markedly different.

Devolatilization Rates

Measured kinetic rates of devolatilization must be compared using some type of rate model. Under high heating rate conditions, tars are rapidly released from the coal particles followed by a slower release of gases. These two mechanisms of mass release can be seen in the data for PSOC-1451D coal particles in the 1250 K gas condition. For means of comparison, a 1-step Arrhenius rate expression was used to fit all four sets of data for this coal (two gas conditions, two particle size fractions) simultaneously. The computational model involves a predictor-corrector technique to solve Eqs. 5.1 to 5.11 and 5.13 to 5.14 as a function of residence time. This method of comparison is independent of the mechanisms proposed by more sophisticated models, which are often a cause for disagreement among investigators. The tar yield for this hva bituminous coal has been reported to be 25% [Freihaut, et al., 1987], and the majority of the tar is released before substantial gas release. The total mass release rate should therefore be similar to the tar release rate during the majority of devolatilization for this coal.

A. Comparison with 1-Step Model

The best agreement between the 1-step model and the mass loss data, as determined from the average of the four tracers, was achieved using $A = 2.3 \times 10^{14}$ s^{-1} when the activation energy E was set to 55 kcal/mole. These 1-step calculations are represented by the solid lines in Figures 5.12-5.13. The ultimate yields in the calculations were adjusted to match the average measured yield of each size fraction. These kinetic coefficients are very similar to the 1-step Arrhenius coefficients for tar release presented by Solomon, et al. [1986] of E = 55 kcal/mole and $A = 4.3 \times 10^{14}$. It is well known that the 1-step kinetic formulation does not adequately describe devolatilization rates over a wide range of temperatures and heating rates. The particle heating rates in Solomon's entrained flow reactor are similar to those encountered in this experiment. It is interesting to note the agreement between these data and those of Solomon, which are the only other published kinetic rates which have been obtained using particle temperature measurements during rapid devolatilization. This small difference in reported rates can be explained by a 50 K difference in particle temperatures, which is comparable to the accuracy of the pyrometry experiment.

B. Comparison with Other Rates

It is well known that the one-step Arrhenius expression is not applicable to pyrolysis rates over a wide range of temperatures or heating rates. Several engineering models of devolatilization, developed from a wide range of temperatures and heating rates, have been commonly used in combustion applications, i.e., the 2-step model [Kobayashi, et al., 1976; Ubhayakar, et al., 1976], the distributed activation energy model (DAEM) [Pitt, 1962; Anthony, et al., 1974], and the distributed-energy chain statistics model (DISCHAIN) [Niksa, et al., 1987]. The four-tracer mass loss data are compared in Figs. 5.14-5.15 with data from three other investigators using the models developed to fit those data: Kobayashi's flow reactor data [Kobayashi, et al., 1976] (2-step model), Ubhayakar's fit to two sets of flow reactor data [Ubhayakar, et al., 1976] (2-step model), and Niksa's screen heater data [Niksa, et al., 1984] (DISCHAIN). The DAEM with coefficients by Anthony [Pitt, 1962; Anthony, et al., 1974] yields rates very similar to those calculated using DISCHAIN, and hence are not presented here. This comparison is intended to compare the proposed rate coefficients; new coefficients can be generated for any of these models to fit these data.

The continuous lines in Figs. 5.14-5.15 represent the different model predictions using the measured particle velocities and temperatures, as outlined previously. The 2-step model with coefficients proposed by Ubhayakar et al. [1976] seems to agree most closely with the experimental data, while the coefficients of Kobayashi et al. [1976] yield poor agreement. A representative time scale for the different kinetic models is calculated by the difference in time between $V/V^* = 0.1$ and 0.9. For the 106-125 μm size fraction at 1050 K, these time scales are shown in Table 5.3. From this

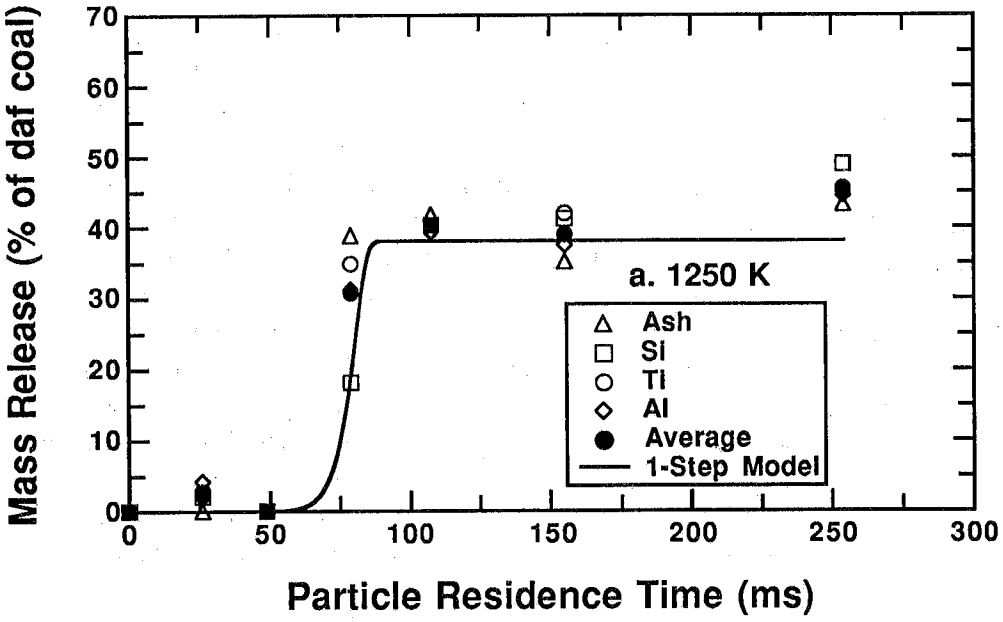

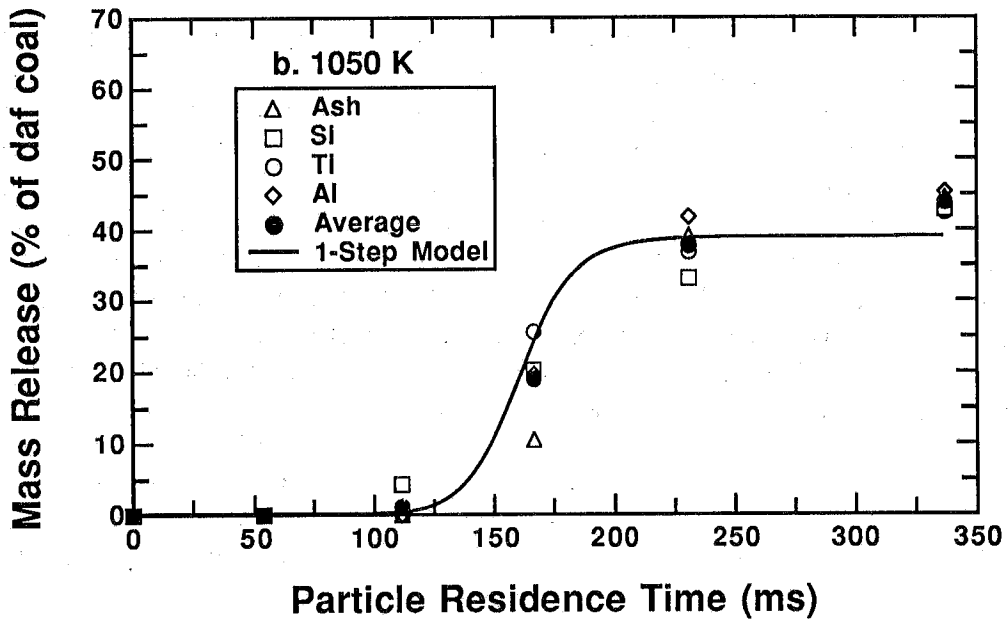

Figure 5.12 Mass release calulated using a 1-step Arrhenius rate expression versus measurements for 106-125 μm, PSOC-1451D, Pittsburgh #8 coal particles (a) 1250 K, (b) 1050 K.

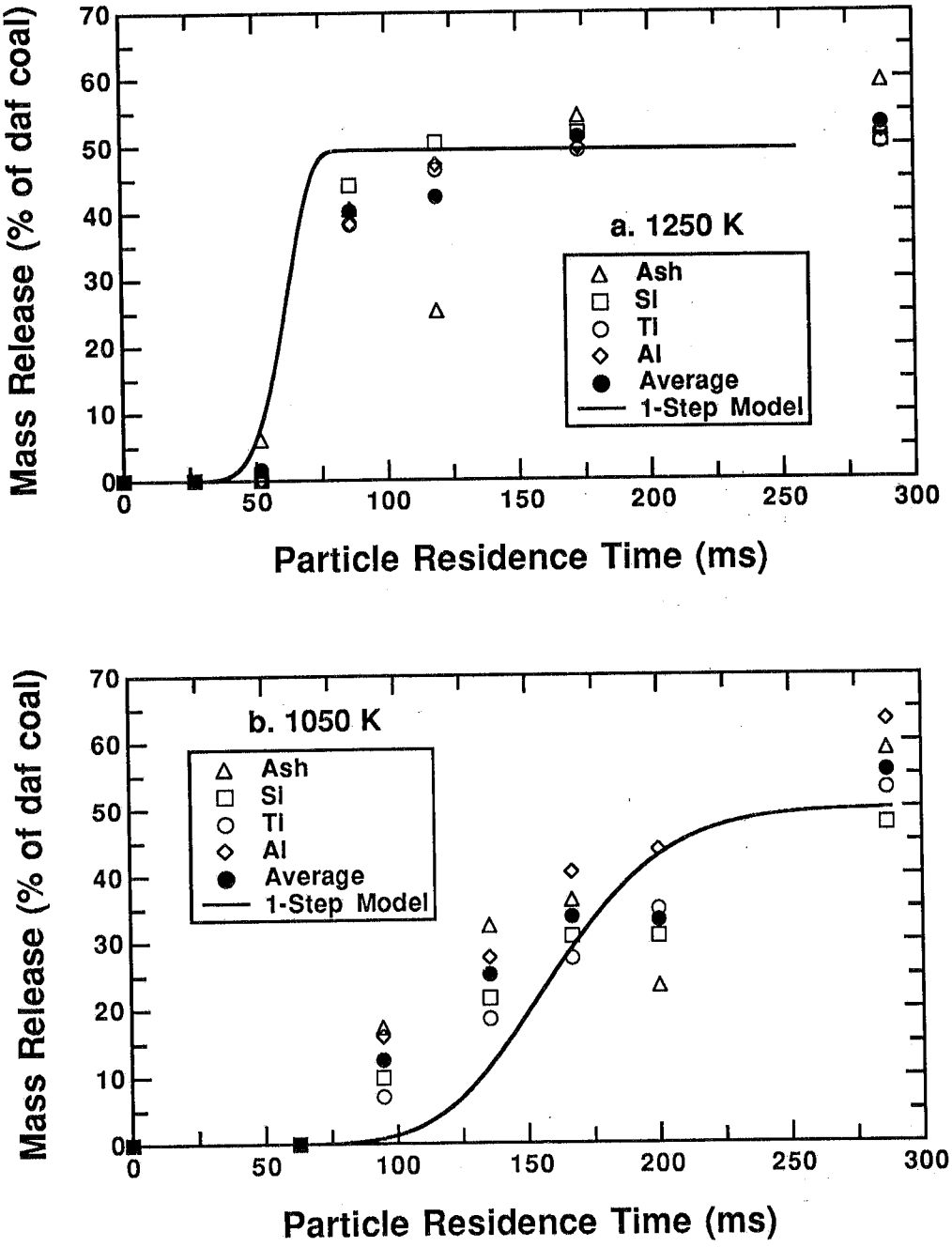

Figure 5.13 Mass release calulated using a 1-step Arrhenius rate expression versus measurements for 63-75 μm, PSOC-1451D, Pittsburgh #8 coal particles (a) 1250 K, (b) 1050 K.

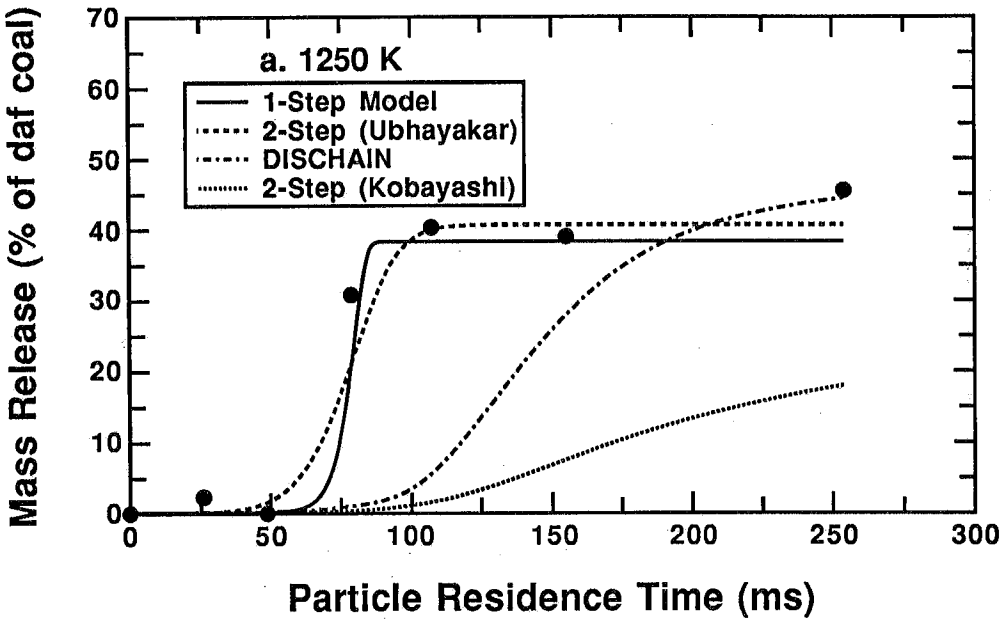

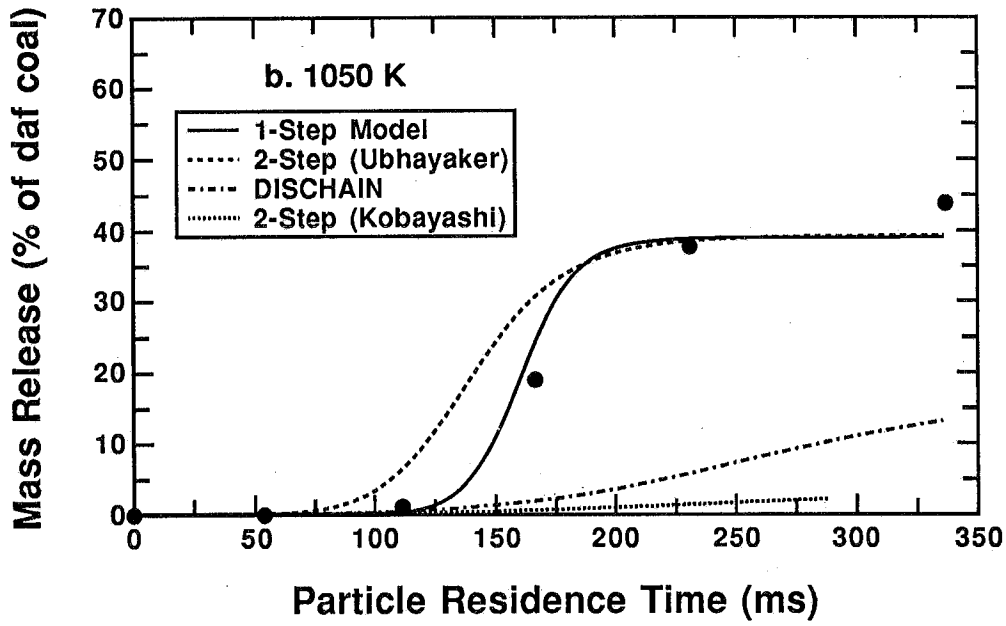

Figure 5.14 Meaured and predicted mass release as a function of residence time for 115 μm diameter, PSOC-1451D, Pittsburgh #8 coal particles using different reported kinetic expressions in the (a) 1250 K gas condition, and (b) 1050 K gas condition. Data points represent the volatiles release determined from the average of four tracers.

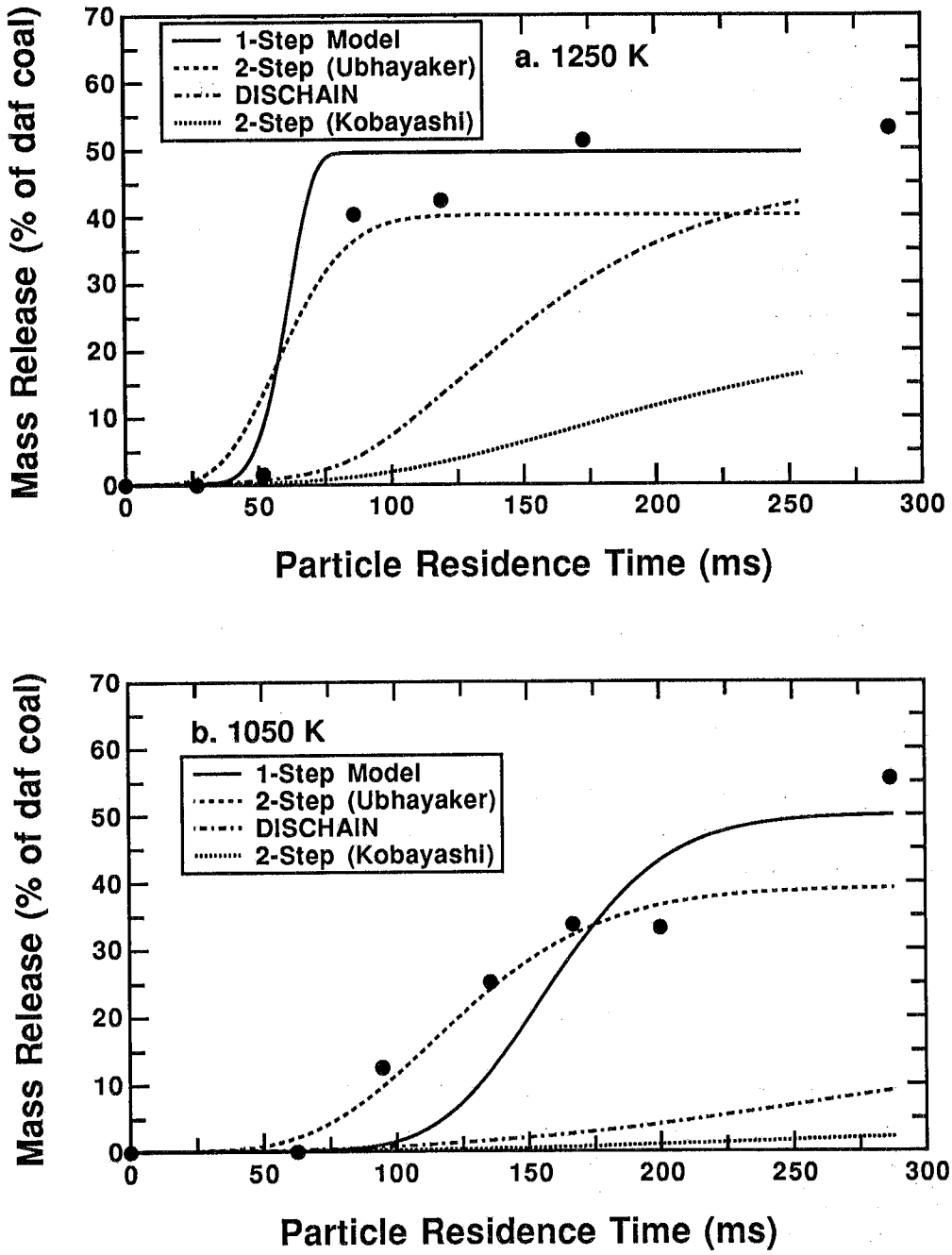

Figure 5.15 Meaured and predicted mass release as a function of residence time for 69 μm diameter, PSOC-1451D, Pittsburgh #8 coal particles using different reported kinetic expressions in the (a) 1250 K gas condition and (b) 1050 K gas condition. Data points represent the volatiles release determined from the average of four tracers.

comparison, the differences in the predicted time scales for this condition are indicative of the large variation in rates obtained from devolatilization experiments where particle temperatures are not measured.

Table 5.3
Reported Times Scales for Devolatilization

Model	V^*	$t_{0.1\ V^*}$	$t_{0.9\ V^*}$	Δt
2-Step (Kobayashi)	28.2	342	5560	5218
2-Step (Ubhayakar)	34.7	104	189	85
DISCHAIN (Niksa)	37.7	209	3440	3231
Present work	33.0	128	280	152

C. Determination of Coefficients for Other Models

The well-characterized temperature histories and mass release data during devolatilization allows determination of rate coefficients for proposed models. The two-step model consists of two reactions which compete for the raw coal material:

$$\text{Coal} \Rightarrow y_1\ V + (1 - y_1)\ C \qquad (5.16)$$

$$\text{Coal} \Rightarrow y_2\ V + (1 - y_2)\ C \qquad (5.17)$$

where "Coal" represents unreacted coal, V represents volatile matter, and C represents char. The factors y_1 and y_2 represent different yield factors for the two competing reactions. The low yield reaction is favored at low temperatures, while the high yield reaction is favored at high temperatures. This also allows prediction of changes in ultimate yield as a function of heating rate.

The determination of coefficients for the two-step devolatilization model from the Sandia data uses experimentally-measured particle velocities, temperatures, and apparent densities in the manner described earlier for the description of the particle temperature histories. Particle properties such as heat capacity, diameter, and apparent density are estimated as a function of time, temperature, and reaction history. Kinetic coefficients for the devolatilization model are determined by matching the mass release data in terms of both rates of release and final yields. The yield factors y_1 and y_2 which permit the best fits of the two-step model to the Sandia devolatilization data for all five coals are listed in Table 5.4. The same activation energies and pre-exponential factors are used to describe the devolatilization

behavior of all five coals; only the yield factors were changed as a function of coal type. The activation energies E_1 and E_2, and the pre-exponential factors A_1 and A_2, in these calculations are taken from Ubhayakar, et al. [1976]. The yield coefficient for the high activation energy reaction (y_2) was set to 1.0 for all five coals, and the other yield factor (y_1) was essentially 0.53 for coal ranks from lignite to bituminous. The yield factor y_1 for the low volatile bituminous coal was 0.14.

Table 5.4
Coefficients Determined for the Two-Step Devolatilization Model for Five Coals

$$dm/dt = (k_1 + k_2)\, m$$
$$dV/dt = (y_1 k_1 + y_2 k_2)\, m$$
$$dC/dt = \{(1-y_1)k_1 + (1-y_2)k_2\}\, m$$

A_1 (s^{-1})	3.75×10^5
E_1 (kcal/mole)	17.6
A_2 (s^{-1})	1.46×10^{13}
E_2 (kcal/mole)	60.0

PSOC-	y_1	y_2
1507D	0.53	1
1445D	0.53	1
1493D	0.51	1
1451D	0.53	1
1508D	0.14	1

The fits of the devolatilization data using the two-step devolatilization model are shown in Figs. 5.16 to 5.20. These figures show the data on a daf basis. The data shown here is the average of the different tracers, except for the PSOC-1507D data which is taken only from the ash tracer, and the PSOC-1508D data, which is from a mass balance. The agreement between experimental data and model predictions is fairly good in terms of the ultimate yield and the residence time at which rapid devolatilization occurs. However, the 2-step model does not seem to accurately predict the gradual tapering of the devolatilization rate at 75 to 125 ms indicated by the data at the 1250 K gas condition for the two low rank coals (PSOC-1445D and PSOC-1507D). The two-step model predicts a higher volatiles yield than indicated by the data for the high rank coal (PSOC-1508D) at the 1050 K gas condition. The 2-step model is a simple empirical expression, and is not expected to capture all of the features of coal rank. Most of these features are related to the product distribution of gases and tar, and must be modeled using more detailed descriptions of the chemical structure of the coal and the resulting reaction rate mechanisms.

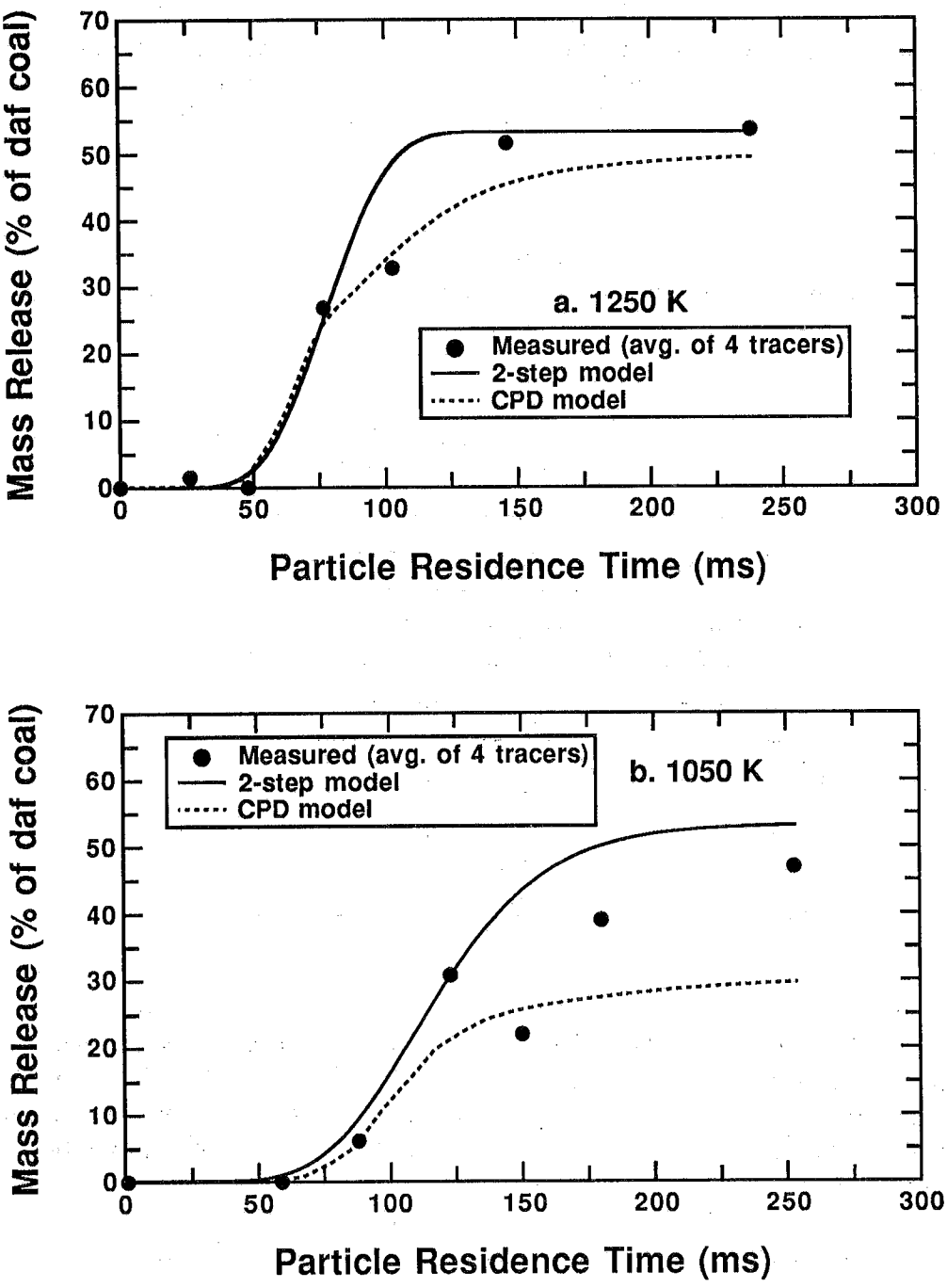

Figure 5.16 Meaured and predicted mass release as a function of residence time for PSOC-1445D subbituminous coal particles using the 2-step model with adjusted yield coefficients and the CPD model for the (a) 1250 K gas condition and (b) 1050 K gas condition.

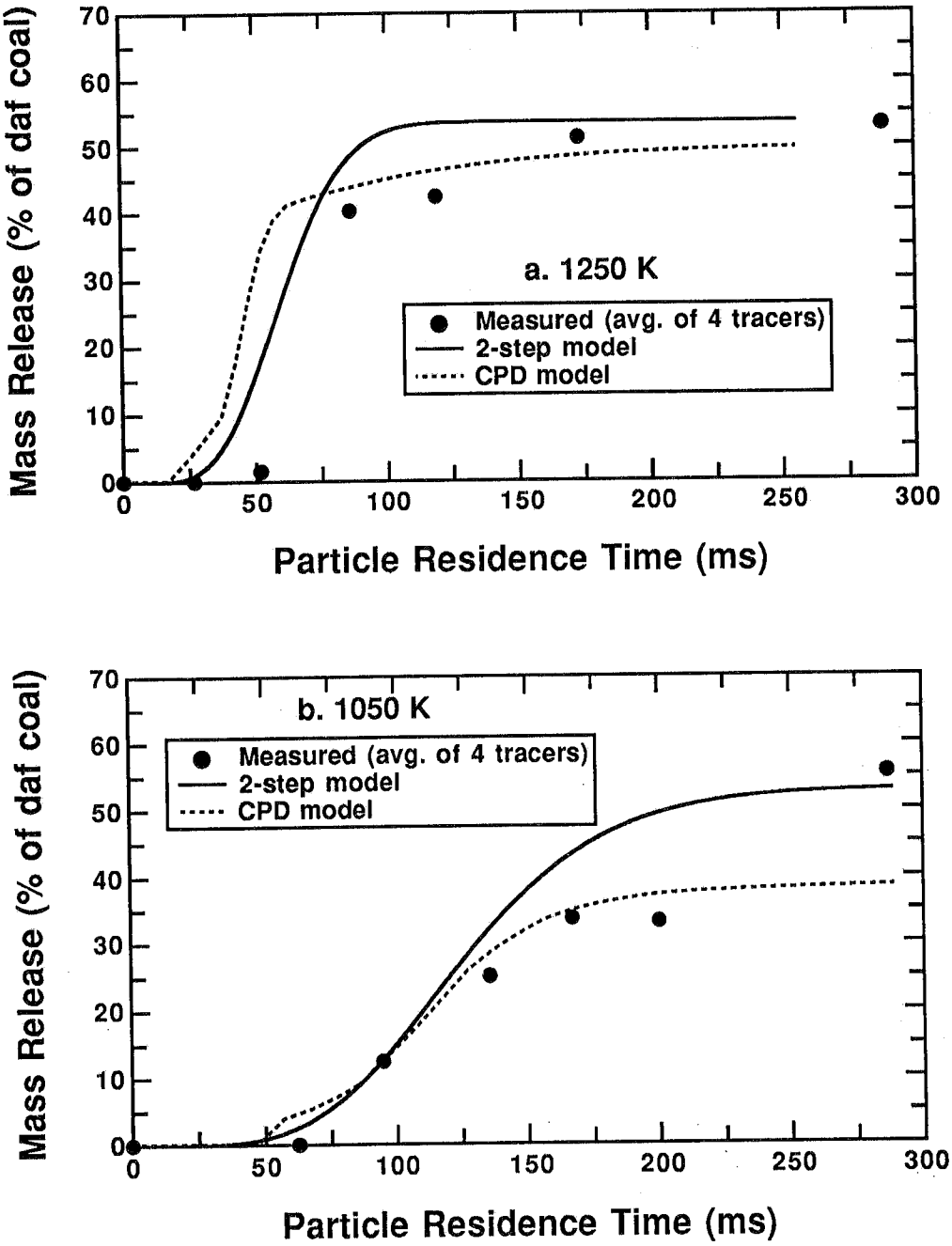

Figure 5.17 Meaured and predicted mass release as a function of residence time for PSOC-1451D hva bituminous coal particles (63-75 μm size fraction) using the 2-step model with adjusted yield coefficients and the CPD model for the (a) 1250 K gas condition and (b) 1050 K gas condition.

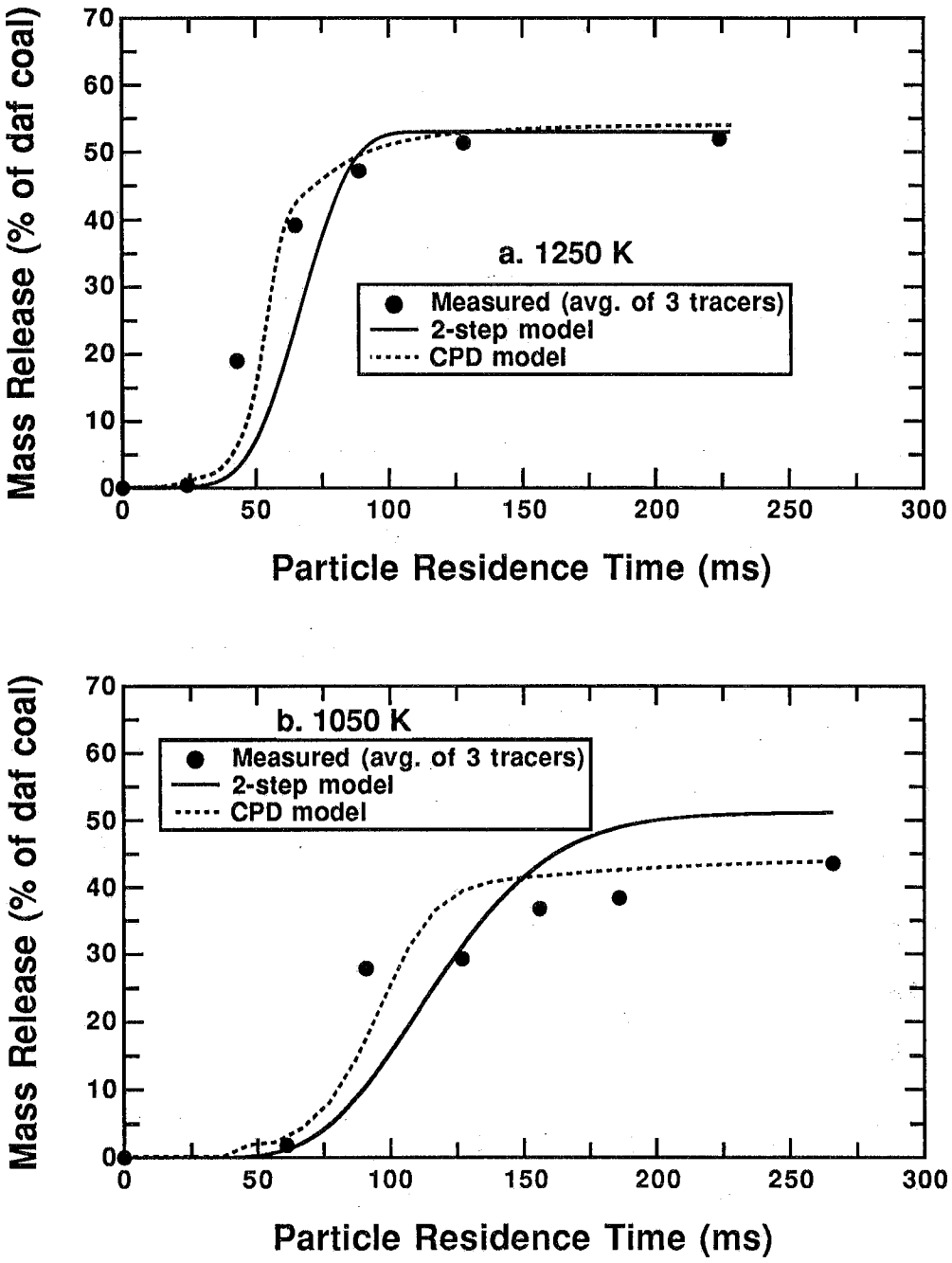

Figure 5.18 Meaured and predicted mass release as a function of residence time for PSOC-1493D hvb bituminous coal particles using the 2-step model with adjusted yield coefficients and the CPD model for the (a) 1250 K gas condition and (b) 1050 K gas condition.

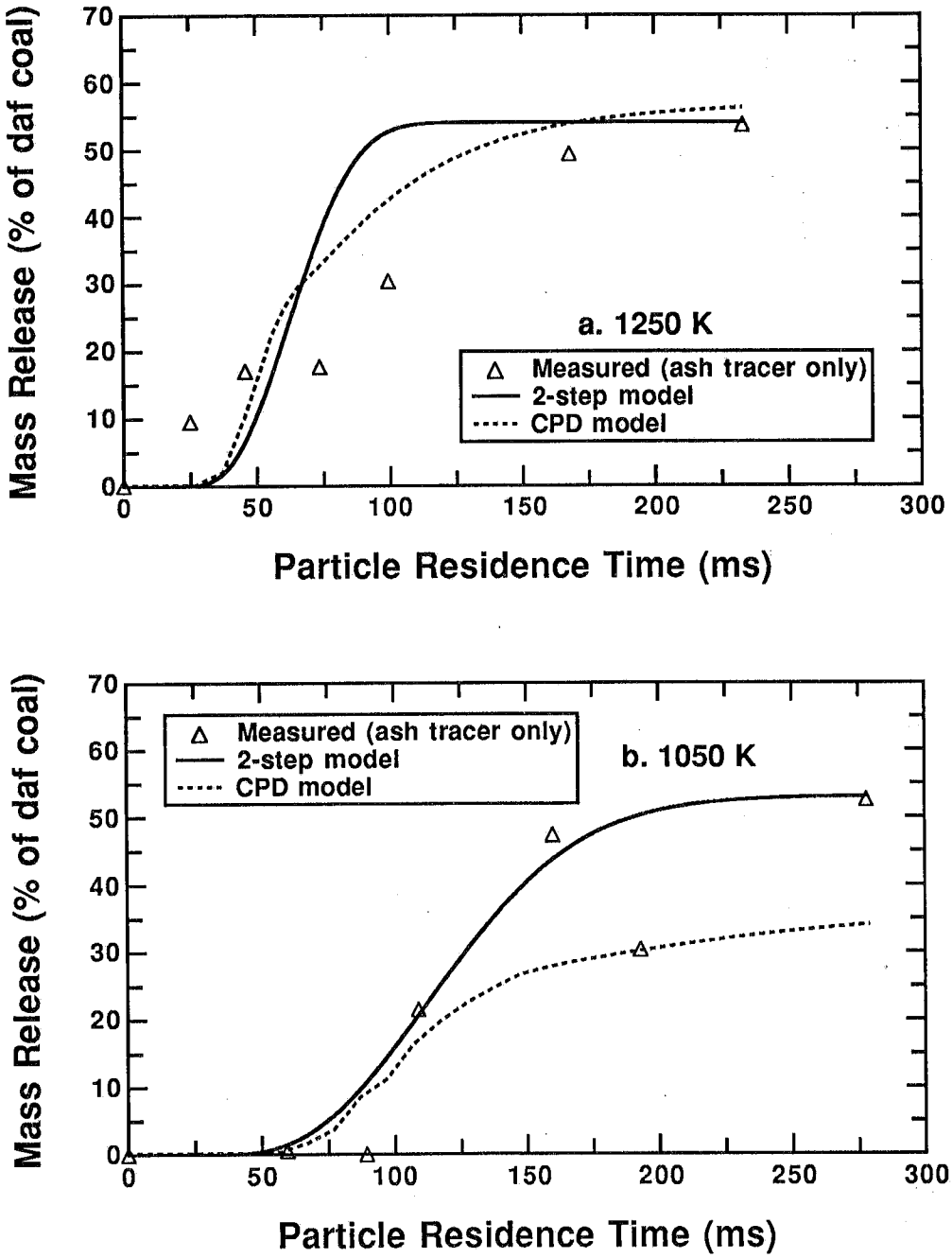

Figure 5.19 Meaured and predicted mass release as a function of residence time for PSOC-1507D lignite particles using the 2-step model with adjusted yield coefficients and the CPD model for the (a) 1250 K gas condition and (b) 1050 K gas condition.

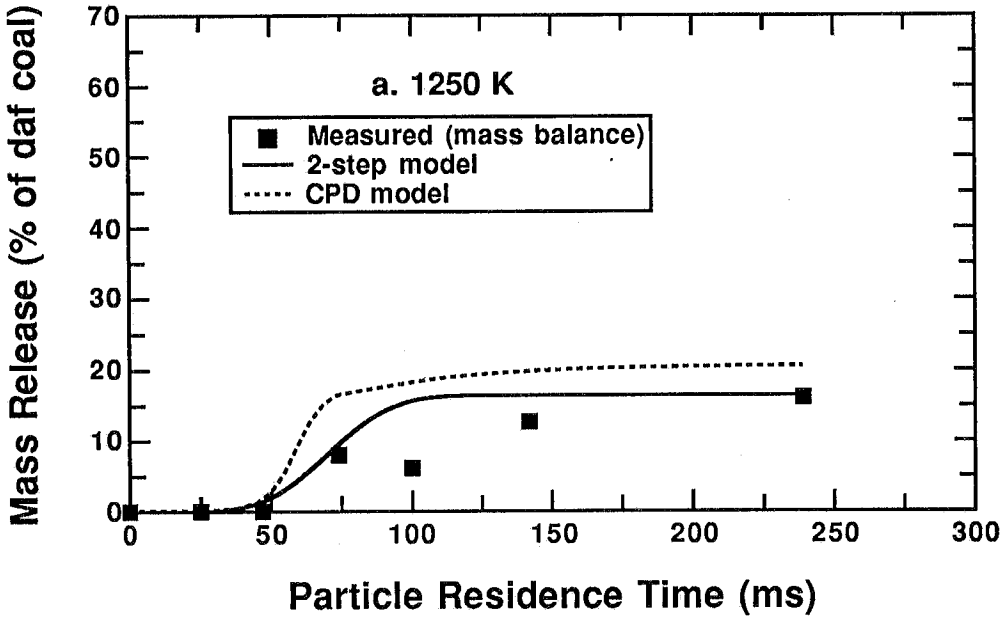

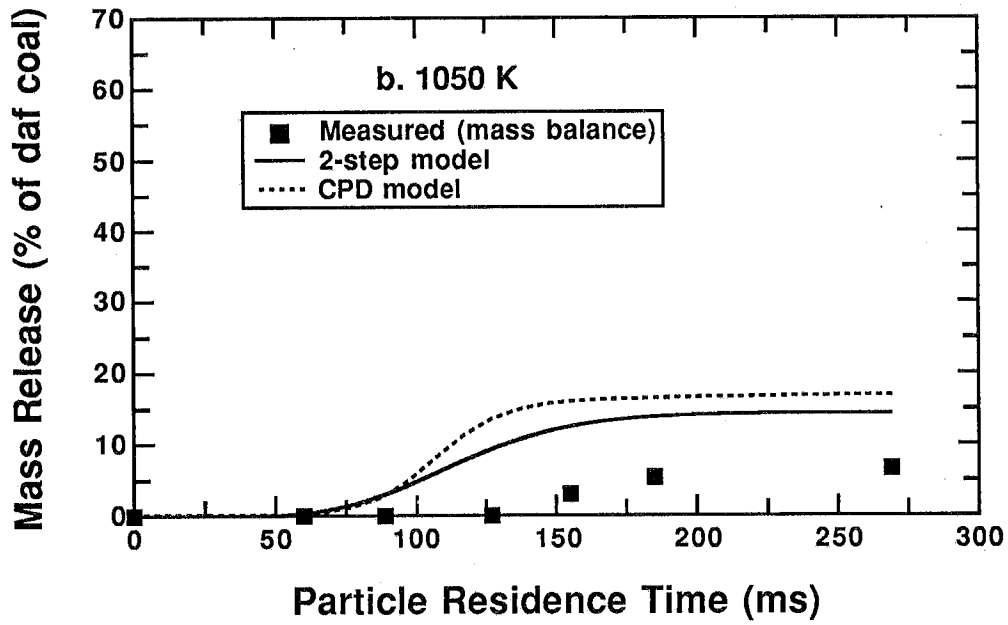

Figure 5.20 Meaured and predicted mass release as a function of residence time for PSOC-1508D lv bituminous coal particles using the 2-step model with adjusted yield coefficients and the CPD model for the (a) 1250 K gas condition and (b) 1050 K gas condition.

More sophisticated devolatilization models have been developed to describe differences in devolatilization rates as a function of coal rank based on chemical mechanisms rather than empirical formulations. The chemical percolation devolatilization (CPD) model [Grant, et al., 1989; Fletcher, et al., 1990; Fletcher, et al., 1991] was developed at Sandia to describe coal devolatilization behavior as a function of coal rank, based on the chemical structure of the parent coal. Coal-dependent input parameters relating to chemical structure are selected from recent analyses performed using ^{13}C nuclear magnetic resonance (NMR) spectroscopy. Two yield parameters are currently specified from measured gas and tar yields [Fletcher, et al., 1991]. The CPD model uses one set of kinetic rate parameters that are assumed to be independent of coal type. The model quantitatively describes tar yields and molecular weight distributions as a function of temperature, heating rate, ambient pressure, and coal type. Predicted total volatiles yields for the five coals in two different gas temperature conditions are shown in Figs. 5.16 to 5.20. Input parameters for these predictions are shown in Table 5.5, along with the source for each input parameter.

Table 5.5
Coefficients Determined for the CPD Model for Five Coals

a. Determined from tar yield data

	Beulah Zap lignite[a]	New Mexico Blue #1 subbitum.[b]	Illinois No. 6 hvb bituminous[c]	Pittsburgh No. 8 hva bituminous[d]	Pocahontas No. 3 lv bituminous[e]
$\pounds_0$	0.44	0.53	0.62	0.47	0.82
c_0	0.16	0.04	0.00	0.00	0.00
$f_{gas,\infty}$	0.55	0.47	0.33	0.25	0.10

b. Determined from NMR measurements

$\sigma+1$	4.5	5.8	4.1	4.8	4.3
m_a	145	195	145	195	260

[a]Coal samples and data for a Zap lignite from Serio, et al. [1987]; NMR analyses by Solum, et al. [1989]

[b]Coal samples and data for a Montana Rosebud subbituminous coal from Serio, et al. [1987]; NMR analyses on Rosebud coal by Solum, et al. [1989]; $f_{gas,\infty}$ raised to better match yield for PSOC-1445D.

[c]Coal samples and data for PSOC-1493D, with the tar/gas ratio set to equal that measured for an Illinois #6 by Serio, et al. [1987]; NMR analyses by Fletcher, et al. [1990b]

[d]Coal sample from Argonne premium coal sample bank, pyrolysis data from Gibbins-Matham and Kandiyoti [1988]; NMR analyses by Solum, et al. [1989]

[e]Coal sample from Argonne premium coal sample bank; NMR analyses by Solum, et al. [1989]; data from Solomon, et al. [1990]

Best agreement between the CPD model and the data is observed for the two bituminous coals (PSOC-1451D and PSOC-1493D), where this model has been extensively validated by comparison with data over a large range of heating rates. For the Illinois #6 coal (Fig. 5.18a), the CPD model explains the gradual tapering of the measured total mass release curve by allowing rapid tar release followed by degassing of the char at a slower rate. The lower yield observed at the 1050 K condition for this coal is also quantitatively predicted by the CPD model (and not the 2-step model). The CPD model predictions also agree well with the observed time scales of the onset of rapid mass release (tar evolution) and the completion of mass release for this coal. For the Pittsburgh #8 coal, the CPD model predicts a region of gas evolution at the 1250 K gas condition (Fig. 5.17a) following the initial mass release period, which is also observed in the data. At the 1050 K gas condition, the CPD model agrees with all but the data point at 290 ms, whereas the 2-step model agrees with the data point at 290 ms at the expense of disagreement with the data points at 175 and 200 ms. Repeat experiments for the Pittsburgh #8 coal at the 1050 K gas condition, especially at late or extended residence times, are recommended in order to verify the data points at 175, 200, and 290 ms.

The CPD model agrees well with the mass release data at the 1250 K gas condition for the two low rank coals (PSOC-1507D and PSOC-1445D), as shown in Figs. 5.16a and 5.17a. In particular, the CPD model predicts a low tar yield for these coals, and hence a significant amount of light gas release. This is evidenced by a significant rounding of the mass release curve predicted by the CPD model, as compared to the 2-step model. Both of these sets of data for the low rank coals at the 1050 K gas condition contain a data point that seems out of place, suggesting repeat experiments. However, at the 1050 K gas condition, the CPD model predicts significantly lower total yields than observed experimentally. The fact that the CPD model predicts lower yields than the data at the 1050 K gas condition suggests that coal-dependent kinetic parameters must be used.

Comparison of CPD model predictions with data for the high rank coal (PSOC-1508D Pocahontas #3) support the notion that pyrolysis kinetics may be dependent on coal rank. The yield coefficients for this coal were taken from comparison with TGA data [Solomon, et al., 1990a] for the Argonne premium coals. The predicted yield at the 1250 K gas condition (Fig. 5.20a) is ~ 5% higher than the data on a daf basis, but this may be due to the fact that the Pocahontas coal from the PETC suite is slightly different than the Argonne coal. However, the predicted yield at the 1050 K gas condition is 10% daf *higher* than the data, indicating that the predicted reaction rate is too fast for this coal at 1050 K. When coupled with the observations for the low rank coals, the trend is seen that the pyrolysis rates predicted by the CPD model at 1050 K are (i) too slow for low rank coals; (2) accurate for bituminous coals; and (iii) too fast for high rank coals. This is consistent with the postulate that the activation energies for gas release and/or tar release increase as a function of increasing coal rank.

Coal-dependent activation energies (and standard deviations) have been suggested by Burnham, et al. [1989] and by Solomon et al. [1990; Serio, et al., 1990; Solomon, et al., 1991; Carangelo, et al., 1991] based on thermogravimetric analyses (TGA) of coal pyrolysis products. The temperature of maximum mass release at slow heating rates in these TGA studies steadily increases as a function of increasing coal rank. Activation energies extracted from TGA data for a simplistic model also increase by as much as 15 kcal/mole with increasing coal rank [Burnham, et al., 1989]. Based on similar TGA data, Solomon, et al. [1991] use coal-dependent activation energies for evolution of specific gases, such as CO and CO_2, that vary by as much as 10 kcal/mole. The Sandia data presented here as a function of coal rank may be the first published indication of coal-dependent kinetic rates at rapid heating conditions ($\sim 10^4$ K/s). It is recommended that the effect of coal-dependent reaction rate parameters should be studied in the future, and that some of the Sandia experiments should be repeated to eliminate some of the scatter in the data.

D. Summary

Gas and particle temperatures and velocities in the flow reactor are significantly influenced by local cooling near the point of injection, which may be a cause for the large discrepancy in reported devolatilization rates measured in conventional drop tube reactors. Particle size, temperature, and velocity measurements were therefore performed in a laminar flow reactor to study coal devolatilization rates of a bituminous coal. Comparisons of measured sizes and temperatures for pure carbon spheres and pyrolyzing coal particles show that the temperature measurement is not influenced significantly by the tar cloud surrounding each particle. Temperatures as low as 850 K were measured for 100 μm diameter particles. Measured coal particle temperatures and velocities are fit using the general form of the particle energy equation in order to extrapolate to particle temperatures lower than 850 K.

Char particles were collected from the flow reactor using a helium quench probe with an on-line aerodynamic separation of tars and gases from char particles. Char samples were analyzed for elemental inorganic composition, and several elements were used as tracers to determine the extent of mass release during devolatilization. The statistical uncertainty in the mass release data is reduced by using the average of four independent tracers. The measured mass of volatiles released in the flow reactor has been compared with several commonly used rate models.

The data show evidence that the volatiles release is very rapid, and agrees quite well with the 1-step Arrhenius expression for tar release reported by Solomon, et al., [1986] for coals experiencing similar heating rates. Three simple rate models, with constants taken from other experiments, have also been compared with these temperature-resolved experimental data. Only the 2-step model with coefficients recommended by Ubhayakar et al. [1976] gives pyrolysis time scales comparable with this set of data. A more sophisticated model based on the chemical structure of the coal (the CPD model) used these data as a basis to determine rate coefficients.

The particle temperature measurements are viewed as critical to the determination of pulverized coal pyrolysis rates under rapid heating conditions. Kinetic coefficients derived from this experiment should be more universally applicable than previous data where particle temperature measurements were not performed. The facts that the minimum particle temperature measurement threshold is 850 K, and that devolatilization commences at lower temperatures than 850 K, do not impede the use of these data. On the contrary, if the kinetic rates were slower, as proposed by other investigators, 850 K would be the temperature at which devolatilization begins. The data presented here, however, indicate that 850 K corresponds to the middle of devolatilization, and hence kinetic rates obtained from these data are higher than initially expected. These data therefore serve as a good indication of the kinetics of devolatilization, even though temperature measurements over the entire extent of mass release are not available. When this project started, the range of devolatilization rates at any temperature was on the order of 10^5 s^{-1}. As a result of these experiments, the current uncertainty in devolatilization rates at rapid heating rates is thought to be less than a factor of five.

Physical Structure Characteristics of Char Particles

One of the most important products of coal devolatilization is char, which must be characterized in order to determine the heterogeneous burning rate. Char may burn in several regimes, depending on the particle size, temperature, and ambient oxygen concentration. At low temperatures, referred to as Zone I combustion, the oxygen penetrates the entire interior of the coal particle, and the overall reaction rate is controlled by the surface reaction in the pores. At moderate temperatures (Zone II), the overall reaction rate is controlled by the combined effects of diffusion of oxygen from the particle surface through the pore structure and the chemical reaction rate on the surface. At high temperatures (Zone III), the overall reaction rate is controlled by diffusion of oxygen from the ambient environment to the particle surface, and little or no penetration of oxygen past the particle surface occurs.

In Zone II and Zone III combustion, the principal physical characteristics of the char formed during devolatilization that affect heterogeneous reaction are: (1) size; (2) density; and (3) internal surface area. These three features of the char change as a function of the parent coal type and the pyrolysis conditions. For example, low rank coals are thermal-setting materials, and are not expected to swell during devolatilization. On the other hand, bituminous coals are thermal-plastic materials, resulting in particle softening and swelling behavior that is related to the heating conditions.

A. Internal Surface Area

Internal surface area measurements were performed using nitrogen BET adsorption, as discussed in Section 3. The samples obtained in the CDL in 100% nitrogen were

analyzed at the Lawrence Livermore Particle Characterization Laboratory. As indicated in Section 4 (Table 4.2), internal surface area measurements are available for three of the five coals, although the Pittsburgh #8 coal samples were from preliminary sampling experiments conducted in collaboration with Steve Hsu before the sizing-pyrometer and the technique for organic and inorganic elemental analysis were completely developed. Some of these data were reported in publications involving Steve Hsu and Jack Howard [Hsu, 1989; Seery, et al., 1989].

The internal surface area of the low rank coal chars obtained in the 1250 K gas condition increase dramatically at long residence times, corresponding to the late stages of devolatilization, as shown in Fig 5.21. The N_2 BET surface area increases from ~ 5 m^2/g in the parent coal to ~ 200 to 300 m^2/g in the fully-pyrolyzed char for the subbituminous coal and the lignite in the 1250 K gas condition. No such increases in internal surface area are observed for coal samples obtained in the 1050 K gas condition. The bituminous coal particles exhibited only a slight increase in internal surface area during devolatilization; the 63-75 μm particles exhibits an increase in internal surface area from 4 to 17 m^2/g in the 1050 K gas condition, while no increase in internal surface area is observed in either gas condition for the 106-125 μm size fraction.

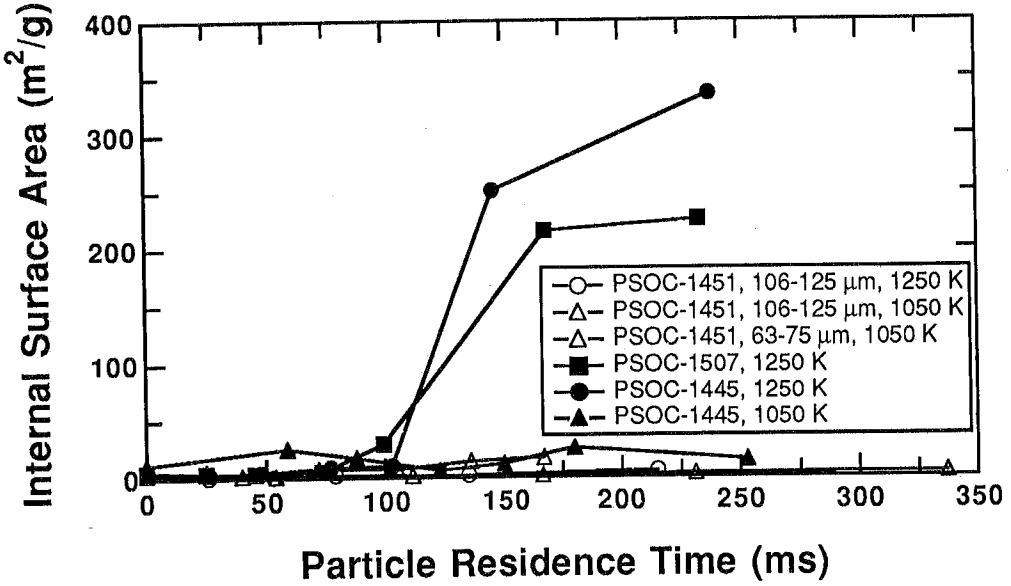

Figure 5.21 Internal surface areas of char particles from different coals as a function of residence time, as measured by the N_2 BET method.

The increase in the internal surface area of the low rank coals is caused by light gas evolution form a rigid matrix, which tends to fracture the coal structure to create escape paths for trapped gases. Bituminous coals soften during devolatilization, closing up the underlying pore structure and then solidyfing. The chars of bituminous

coals exhibit large macropores (pores in the 10 to 50 μm diameter range), but very few micropores which contribute to internal surface area. The macroporous structure is observed with optical and SEM micrographs, as discussed later.

B. Apparent Density and Average Diameter

The apparent density of a coal particle is defined here as the mass of the particle divided by its outer surface volume ($\rho_a = 6m_p/\pi d_p^3$). The particle mass, apparent density, and diameter are therefore all related, and only two can be specified independently. Since the extent of mass release is determined from inorganic tracers, measurement of the apparent density also specifies the average particle diameter. The apparent density of char samples is measured relative to that of the parent coal using a volumetric technique (referred to as tap densities), assuming that packing factors for the parent coal are similar to those of the char (see Section 3). The apparent density ratio (ρ/ρ_o) is therefore related to the fraction of mass remaining (m/m_o) and the swelling ratio (d/d_o).

A few of the samples obtained early in the experimental sequence were analyzed by mercury porosimetry, before the tap density technique was used. The mercury porosimetry data gives volume of pores filled as a function of pressure, and the pressure is interpreted as the pore size. For particles with no macropores, such as unreacted coal particles, the pore sizes greater than 3 μm are attributed to interparticle voids, and not counted as porosity. However, for pulverized coal chars, the macropores on the surface of the particles are of the same size as the interparticle voids, and interpretation of the apparent density is impossible. However, the apparent density ratio can still be estimated from the mercury porosimetry experiments by assuming that the interparticle voids are of the same size for the raw coal particles and the macroporous char particles. The ratio of the measured bulk densities (uncorrected for interparticle voids) therefore is the same as the ratio of the apparent densities of the coal and char.

A comparison of the apparent density ratios obtained for the identical char samples by the tap density and mercury porosimetry techniques is shown in Fig. 5.22. The apparent density ratios obtained by both techniques agree to within 5%, which is probably the accuracy of wither measurement. Since the tap density technique is significantly easier to perform (i.e., less costly) than the the mercury porosimetry measurements, only tap densities were measured for the majority of the collected char samples.

The apparent density ratios and diameter ratios for the coal and char samples from five coals in the 1050 K and 1250 K gas conditions are shown in Figs. 5.23 to 5.28. The diameters of Pittsburgh #8 coal particles increase by as much as 62% during devolatilization in 100% N_2 in the CDL. The typical swelling behavior observed in the samples collected in the CDL is a rapid diameter increase during or just after the tar release period, followed by a decrease in diameter as the internal pressure decreases and crosslinking reactions change the coal from a thermal plastic-material to a

thermal-setting material. The existence of particle shrinkage after the maximum swelling period is also observed in the SEM micrographs, as shown in the next section.

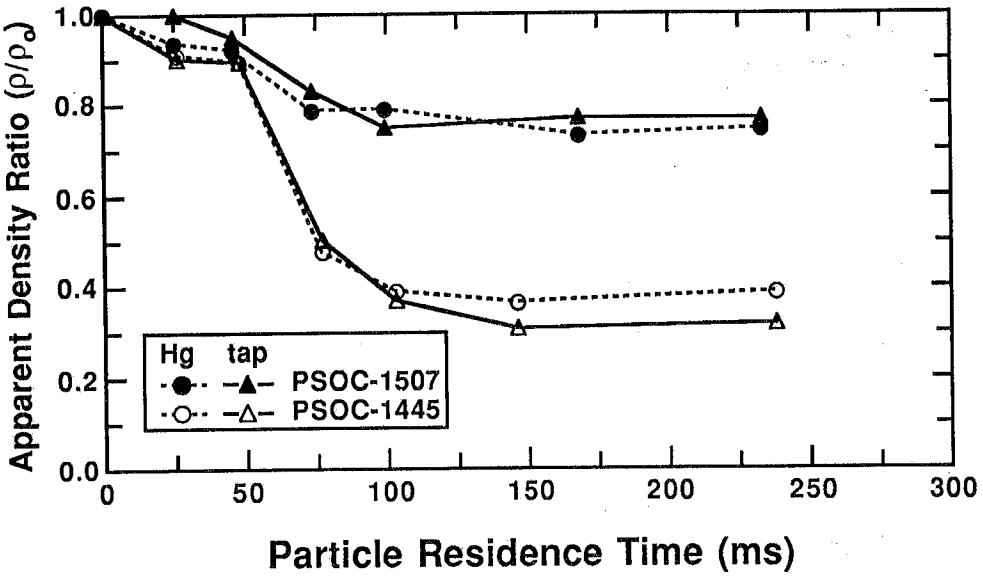

Figure 5.22 Comparison of apparent density ratios measured by Hg porosimetry and by the tap density technique for PSOC-1445D subbituminous char and PSOC-1507D lignite char samples obtained in the 1250 K gas condition.

Hsu [Hsu, 1990, thesis; Seery, et al., 1989, final report] attributed the large changes in particle diameter in the Pittsburgh #8 coal to particle coalescence. The probability of particle collisions in the lightly-loaded entrained flow reactor is very low, especially during the optical experiments where single particle behavior is observed. Inside the helium quench probe, the gas stream is further diluted by at least a factor of five, which even further decreases the probability of particle collisions. The particles are quenched long before reaching the cyclone, so coalescence after collection is not possible. Since particle collisions are thought to be highly improbable, changes in particle diameter are therefore attributed to swelling in this report.

For comparison as a function of coal rank, the maximum degree of swelling, the final degree of swelling, and the final apparent density of the char for five coals are listed in Table 5.6 and illustrated in Fig. 5.29. The Pittsburgh #8 coal exhibits the highest degree of swelling in these experiments. The degree of swelling decreases uniformly as rank either increases or decreases from Pittsburgh #8 coal. The degree of swelling observed in the CDL as a function of coal rank mirrors the trend observed in the free swelling index, even for the lv bituminous coal. However, the quantitative swelling behavior of the coal particles in the rapid heating experiments in the CDL do not correlate with the free swelling index.

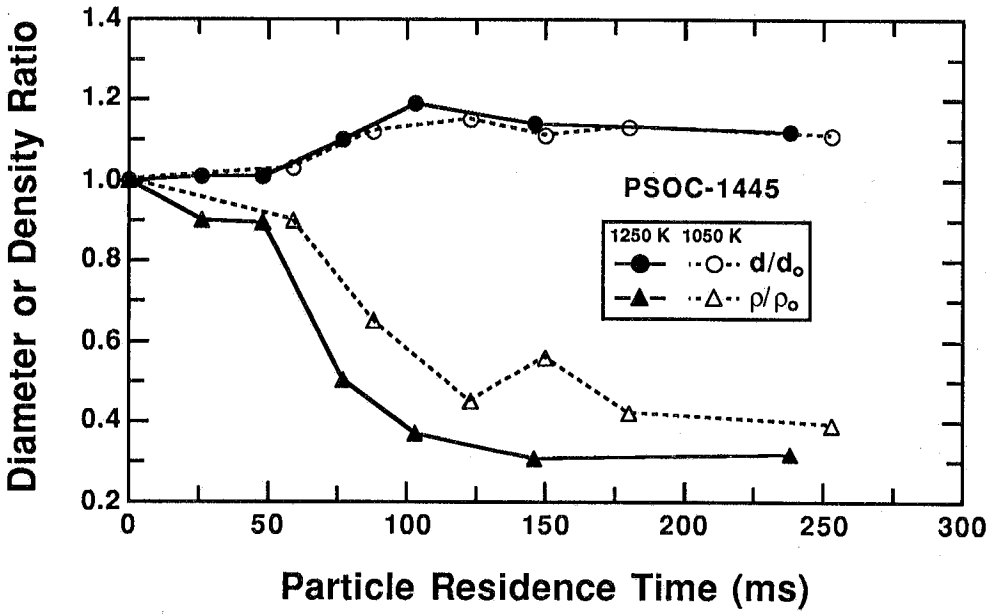

Figure 5.23 Apparent density ratios (ρ/ρ_o) and diameter ratios (d/d_o) as a function of particle residence time for PSOC-1445D subbituminous coal in 100% N_2 in the CDL.

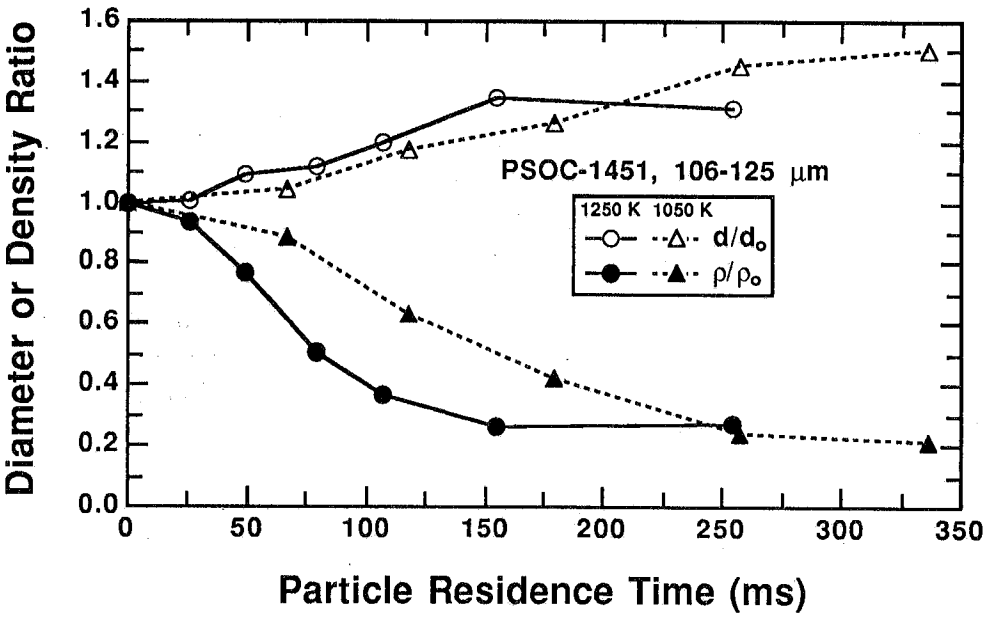

Figure 5.24 Apparent density ratios (ρ/ρ_o) and diameter ratios (d/d_o) as a function of particle residence time for the 106-125 μm size fraction of PSOC-1451D hva bituminous coal in 100% N_2 in the CDL.

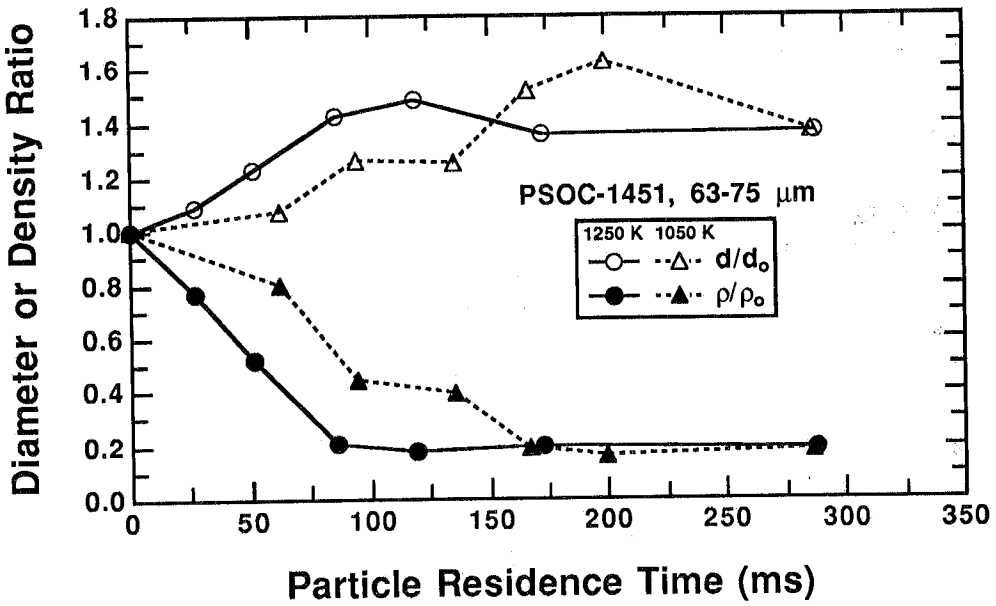

Figure 5.25 Apparent density ratios (ρ/ρ_o) and diameter ratios (d/d_o) as a function of particle residence time for the 63-75 μm size fraction of PSOC-1451D hva bituminous coal in 100% N_2 in the CDL.

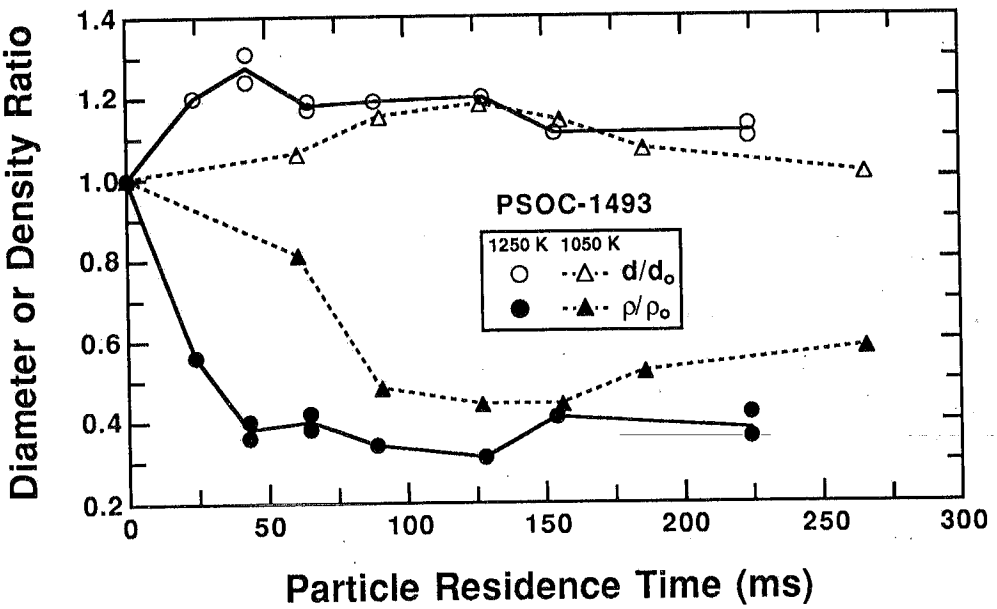

Figure 5.26 Apparent density ratios (ρ/ρ_o) and diameter ratios (d/d_o) as a function of particle residence time for PSOC-1493D hvb bituminous coal in 100% N_2 in the CDL.

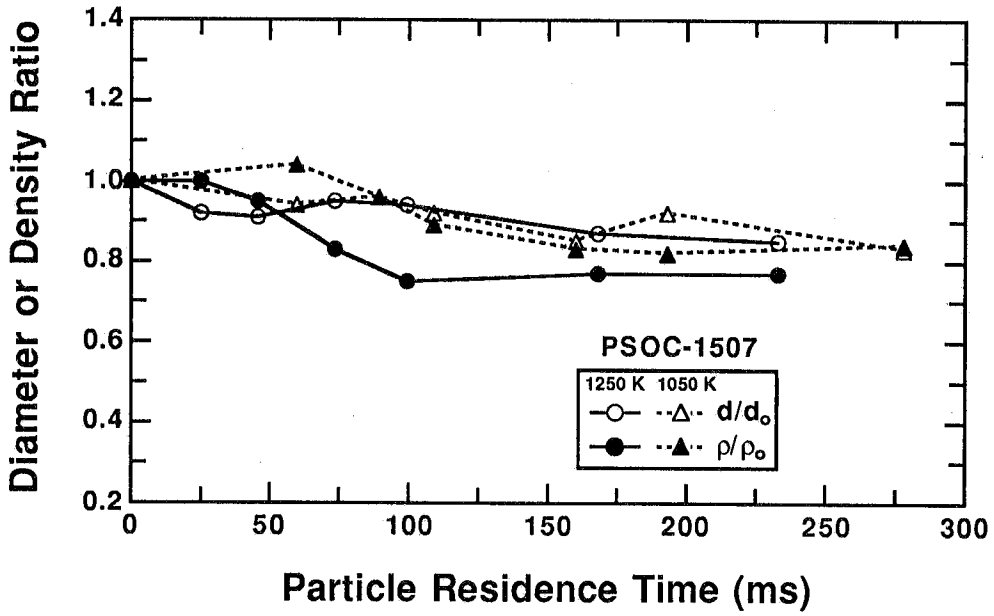

Figure 5.27 Apparent density ratios (ρ/ρ_o) and diameter ratios (d/d_o) as a function of particle residence time for PSOC-1507D lignite in 100% N_2 in the CDL.

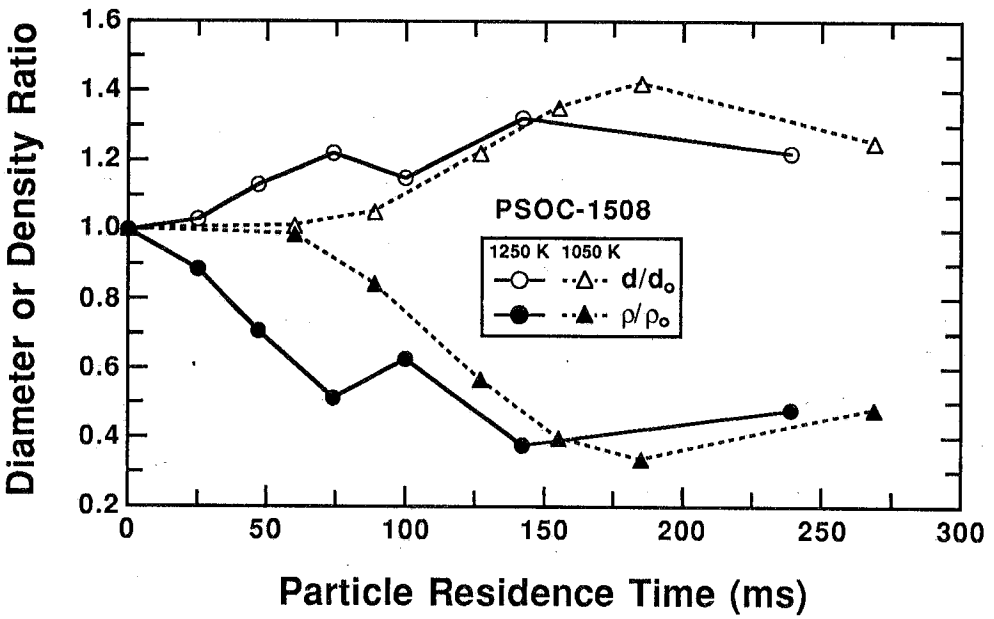

Figure 5.28 Apparent density ratios (ρ/ρ_o) and diameter ratios (d/d_o) as a function of particle residence time for PSOC-1508D lv bituminous in 100% N_2 in the CDL.

Table 5.6
Swelling Characteristics and Apparent Densities of Coal Particles in 100% N_2 in the CDL

PSOC-	Free Swelling Index[a]	Maximum d/d_o		Final d/d_o		Final ρ/ρ_o	
		1250 K	1050 K	1250 K	1050 K	1250 K	1050 K
1507D	0.0	1.0	1.0	0.85	0.83	0.77	0.84
1445D	0.0	1.19	1.15	1.12	1.11	0.32	0.39
1493D	3.0	1.28	1.18	1.12	1.01	0.38	0.58
1451D[b]	7.5	1.35	1.50	1.31	1.50	0.27	0.21
1451D[c]	7.5	1.49	1.62	1.37	1.37	0.19	0.18
1508D	6.5	1.32	1.42	1.22	1.25	0.48	0.48

[a]from Penn State coal data base for PSOC-1451 (unsized).
[b]106-125 μm size fraction; [c]63-75 μm size fraction

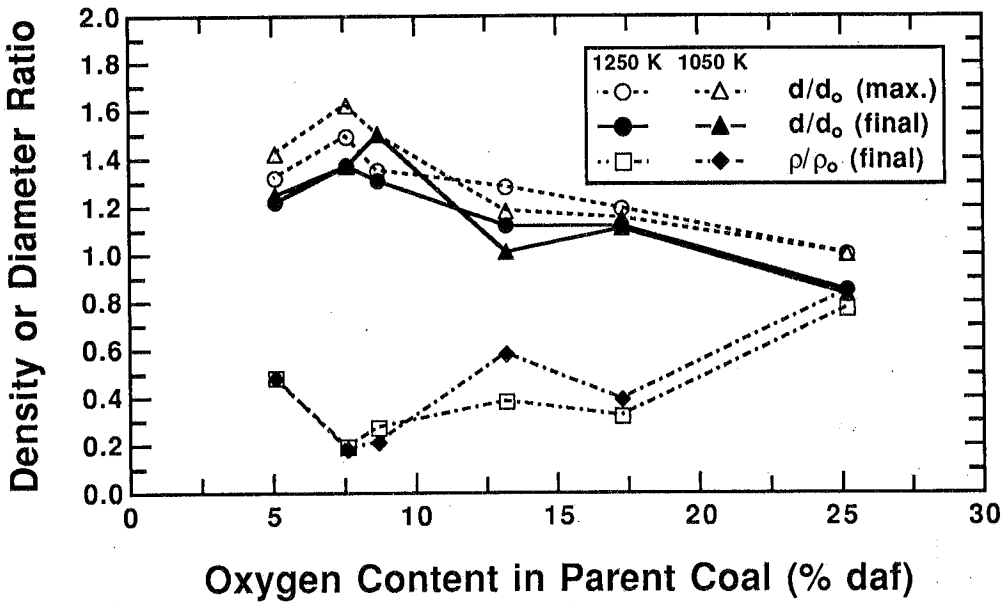

Figure 5.29 Apparent density ratios (ρ/ρ_o) and diameter ratios (d/d_o) as a function of coal rank (oxygen content in the parent coal) in 100% N_2 in the CDL.

The maximum degree of swelling is observed in the 1050 K gas condition, rather than in the 1250 K gas condition. This may indicate that in the 1050 K condition, crosslinking reactions are not as rapid compared to the tar release, and the coal has more time to swell. However, the final states of the char from the two gas conditions seem to coincide, meaning that if the particle swells more at a lower temperature, it then shrinks to the same final state that is observed at higher temperatures.

The lignite shows only small decreases in apparent density, which correspond to slight *decreases* in diameter (i.e., shrinkage). The final char particle diameter is 15% less than the unreacted lignite particles. It is interesting to compare the swelling data with the measurements of internal surface areas (discussed previously). The lignite chars exhibit a large increase in internal surface area in the late stages of devolatilization, even though the particle diameter decreases. In contrast, the highly-swelling coals show little or no increase in internal surface area during devolatilization. The subbituminous coal shows a modest degree of swelling along with a significant increase in internal surface area.

The apparent density of the char from the hva bituminous coal (PSOC-1451D) in the experiments in 100% N_2 decreases by over 80%, resulting in a very porous material. The SEM analyses in the next section confirm that most of these particles are cenospheres with large internal voids with diameters in the 30 to 50 μm range. The apparent density of the lignite char particles decreases by only 20%, although the extent of mass release during devolatilization is approximately the same as for the bituminous coal. This is consistent with the increases in internal surface area for the lignite chars, and the fact that the lignite chars exhibit layered fissures rather than large bubble-like internal voids.

Diameter changes during devolatilization are shown as a function of mass release in Fig. 5.30. Particle swelling for the bituminous coals occurs before significant mass release occurs, as metaplast is generated inside the coal particle. The Pittsburgh #8,

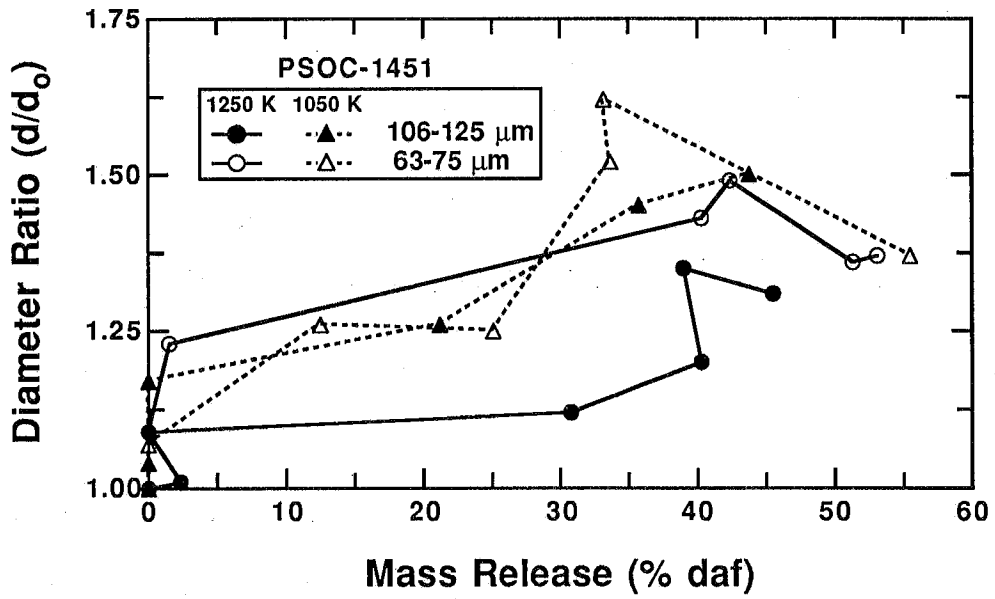

Figure 5.30a Diameter change due to swelling during devolatilization as a function of mass release for PSOC-1451D hva bituminous coal.

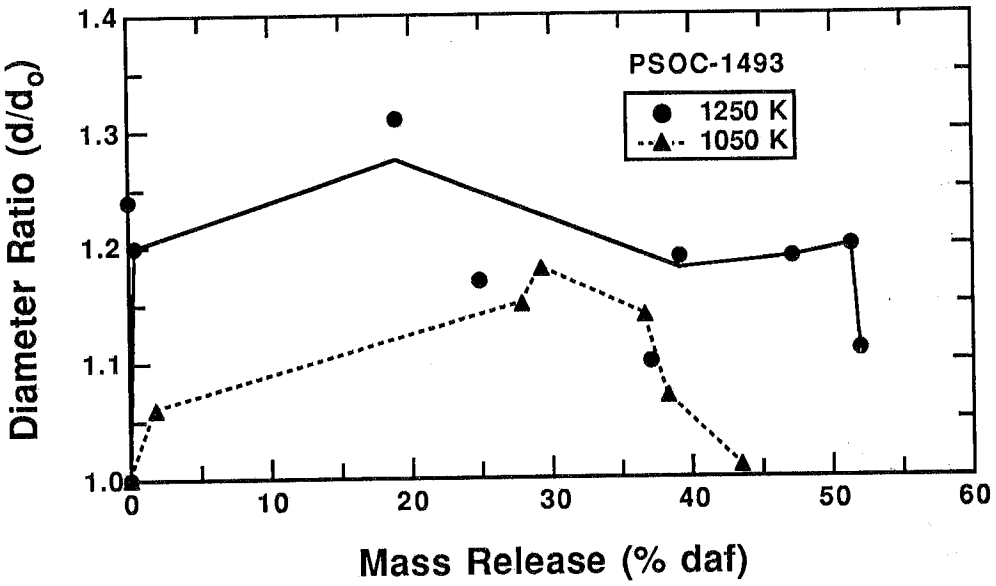

Figure 5.30b Diameter change due to swelling during devolatilization as a function of mass release for PSOC-1493D, hvb bituminous coal.

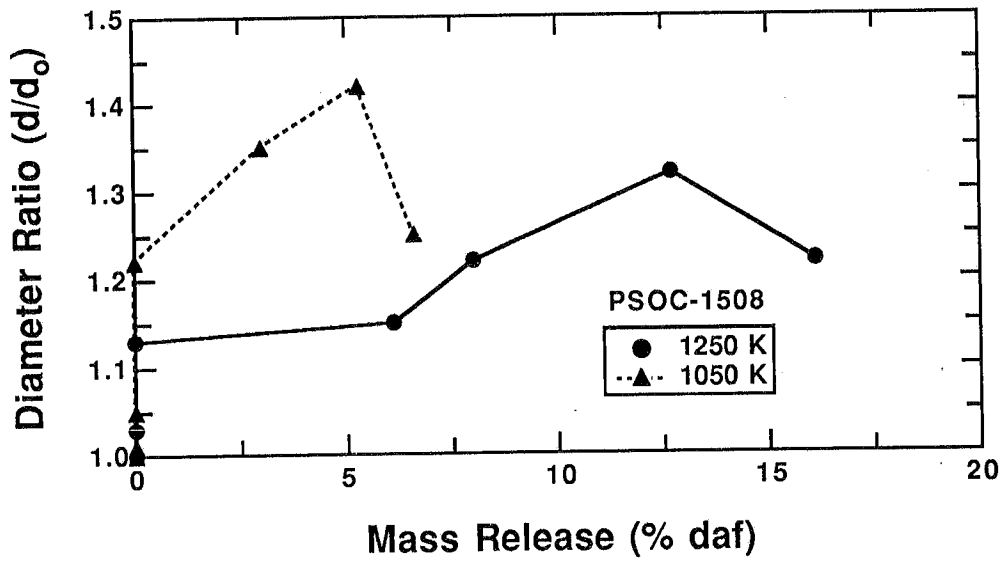

Figure 5.30c Diameter change due to swelling during devolatilization as a function of mass release for PSOC-1508D, lv bituminous coal.

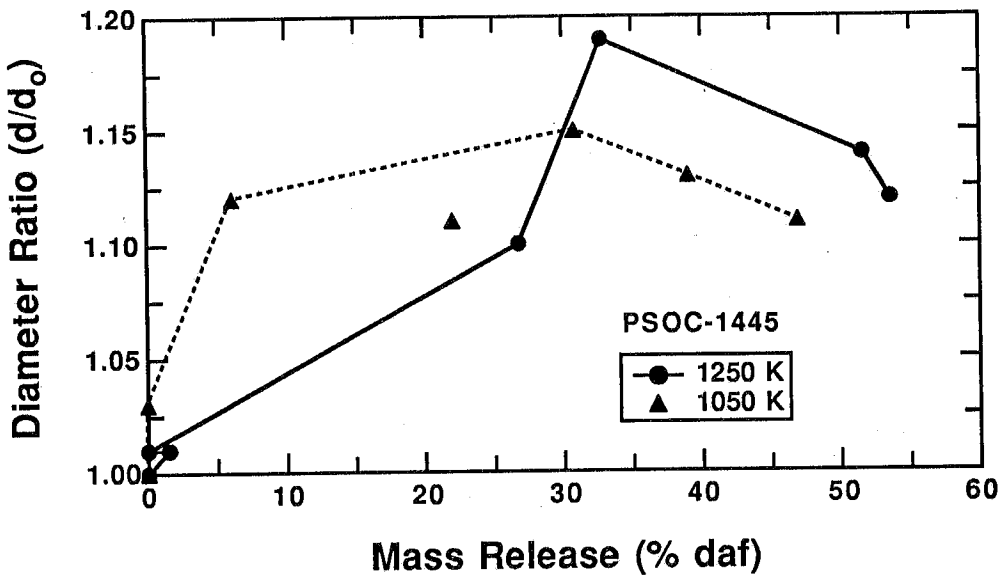

Figure 5.30d Diameter change due to swelling during devolatilization as a function of mass release for PSOC-1445D, subbituminous coal.

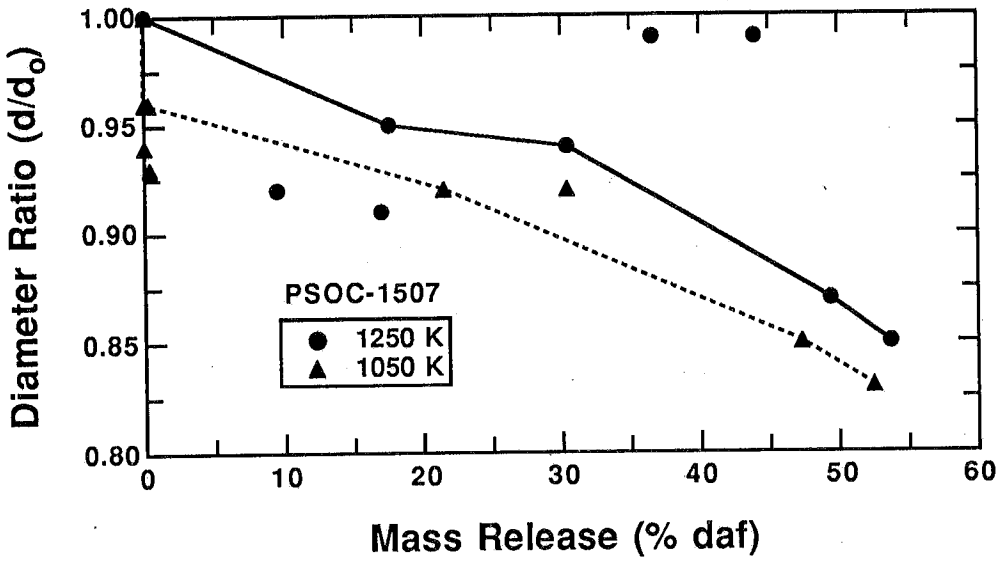

Figure 5.30e Diameter change due to shrinkage during devolatilization as a function of mass release for PSOC-1507D, lignite.

Illinois #6, and Pocahontas #3 coals exhibit diameter changes of 10 to 20% before 5% daf mass release. Particle shrinkage is observed in these plots in the late stages of mass release, after the peak swelling occurs. This means that particle swelling is a complicated function of the transient chemical and physical features of the coal particle, rather than a simple linear function of the extent of mass release, as commonly used in combustion calculations [Smoot and Pratt, 1979].

Low rank coals do not swell before principal mass release period (the lignite actually shrinks). However, for the subbituminous coal (PSOC-1445D), the degree of swelling during the principal mass release period is followed by a shrinkage period in a manner similar to that observed for the bituminous coals. It has been suggested [Suuberg, et al., 1985; Solomon, et al., 1990b] that crosslinking reactions occur early in the pyrolysis of low rank coals, which prevent any softening behavior. Early crosslinking would explain the lack of early swelling behavior observed here in the low rank coals.

It is important to remember that these data regarding swelling and apparent density are from rapid heating experiments in 100% nitrogen, with particle heating rates of approximately 10^4 K/s. These data will be compared in Section 6 with other experiments performed in the CDL with different amounts of oxygen added to the flow reactor gas, and to pyrolysis experiments performed in the Sandia Char Combustion Laboratory (CCL) at slightly higher heating rates. The goal is to describe the physical and chemical properties of coal particles during devolatilization under current typical combustion conditions *and* under possible future alternative conditions.

C. SEM Analysis

The physical characteristics of PSOC-1451D coal chars were examined using scanning electron microscopy (SEM) and optical microscopy of cross sections of particles. The samples analyzed by SEM were collected before the sizing-pyrometer was completed, and hence no residence times are available for these samples. However, the particle temperature histories are thought to be similar to those for the 1050 K condition. Due to the lack of precise residence times, the samples from this early study are referred to here by their axial distance from the coal injection tube.

Figure 5.31 shows changes in physical structure of PSOC-1451D (106-125 μm) coal particles in the 1050 K gas environment in 100% N_2 in the CDL as a function of residence time. Early in the devolatilization process, (z=70 mm), large fissures appear in the particle which may be caused by thermal expansion of the carbon matrix. At 90 mm, surface bubbles appear near the corners of the particles, but the particles still retain their jagged edges. At 120 mm, significant rounding of the particle has begun, and the surface is seen to be full of individual bubbles that are approximately 5 to 10 μm in diameter. Some of these surface bubbles have ruptured but a large number of bubbles remain intact. At 140 mm, many of the particles are almost spherical with large blowholes on the surface. A large particle is shown that has different light scattering properties than the surrounding coal, indicating some type of mineral

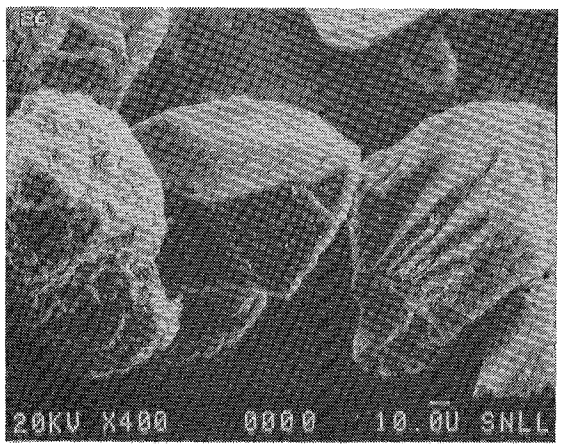

30 mm

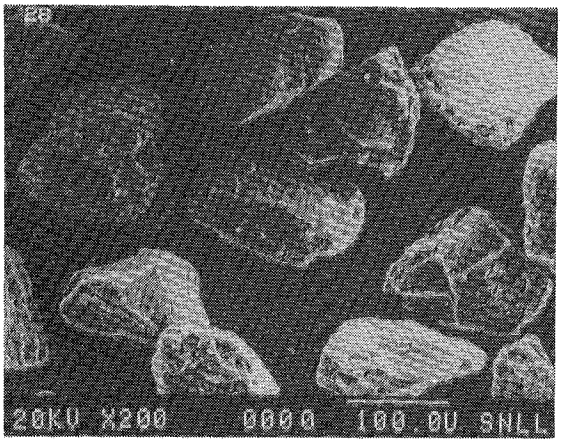

70 mm

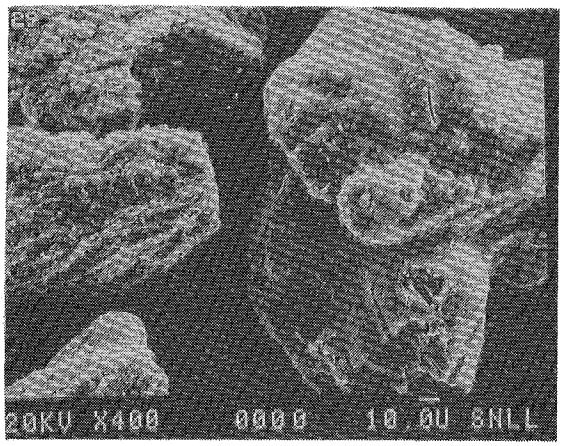

90 mm

Figure 5.31 Scanning electron micrographs of 106-125 µm PSOC 1451d hva Pittsburgh bituminous coal particles collected at 30 mm, 70 mm and 90 mm from the injector for the 1050 K gas temperature condition.

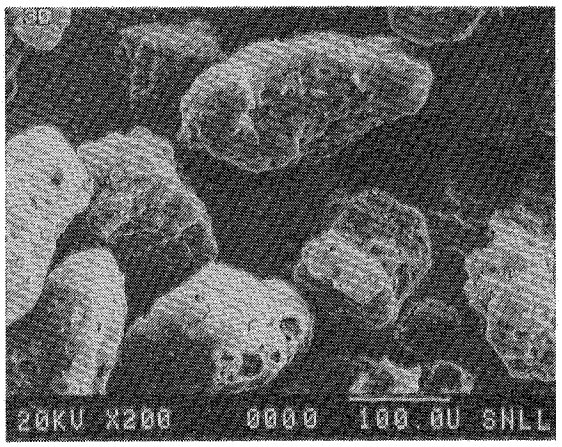

120 mm

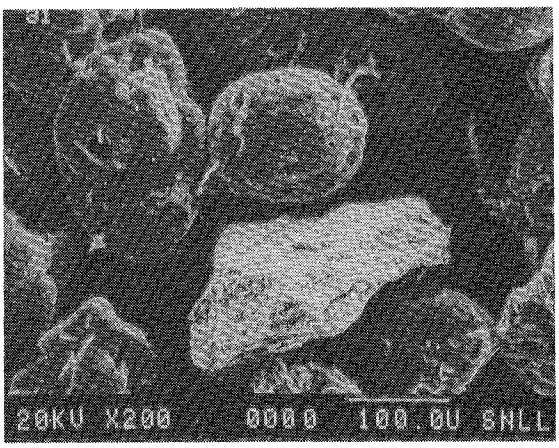

140 mm

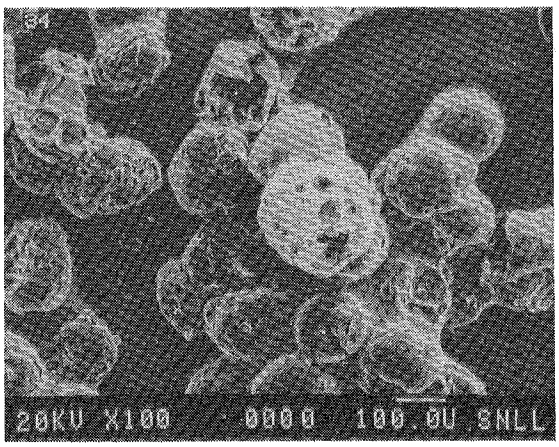

160 mm

Figure 5.31 Scanning electron micrographs of 106-125 μm PSOC 1451d hva Pittsburgh bituminous coal particles collected at 120 mm, 140 mm and 160 mm from the injector for the 1050 K gas temperature condition.

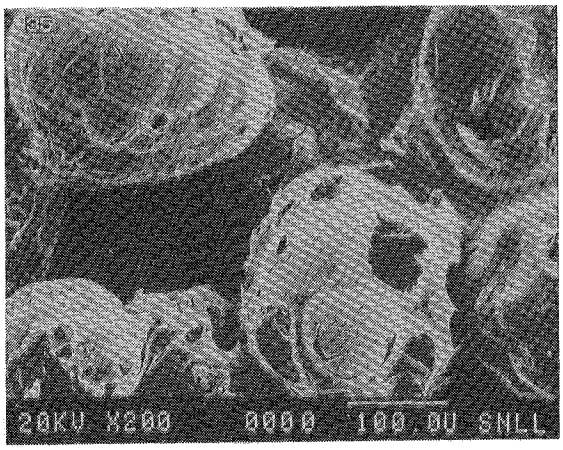

180 mm

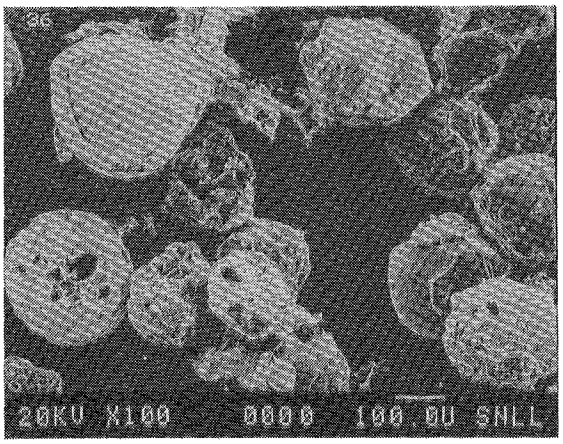

200 mm

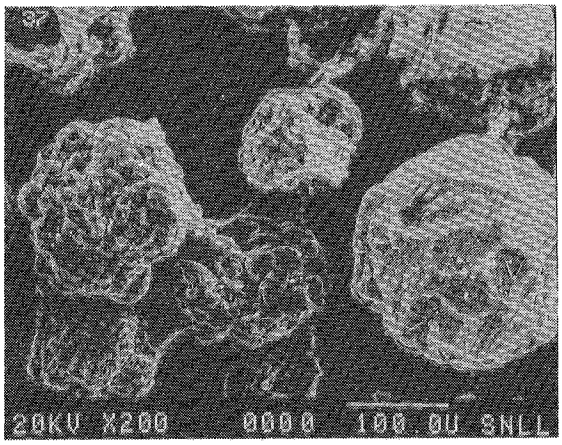

250 mm

Figure 5.31 Scanning electron micrographs of 106-125 μm PSOC 1451d hva Pittsburgh bituminous coal particles collected at 180 mm, 200 mm, and 250 mm from the injector for the 1050 K gas temperature condition.

particle that has not passed through a molten stage. As devolatilization proceeds, the surface bubbles merge and form large central bubbles and particles with thin shells. Finally, at 250 mm, there is evidence for particle shrinkage as the metaplast inventory is depleted and as the particle cools slightly from the peak temperature.

The internal structure of these coal particles is shown in in the cross-section micrographs in Fig. 5.32 for the same char samples examined in Fig 5.31. Small voids begin to form at 30 mm, and significant voidage appears at 90 mm. The fissures in the particle are visible in the 90 mm sample, but have disappeared and coalesced with the surrounding interior bubbles in the 140 mm sample.

The significant voidage seen in the cross-section micrograph of the 90 mm sample is not apparent in the surface SEM of the same sample. Under no conditions, in fact, is there any visual evidence of changes in surface structure without changes in internal structure. This fact supports the argument that internal thermal gradients are not important under these flow reactor conditions.

Elemental Mass Release Rates

Samples collected in the CDL at various stages of devolatilization were analyzed for elemental composition of C, H, N, S, and O. The analysis for each element was performed independently, and the closure was generally within 5%. The elemental analyses presented in Appendices D-H. It is useful to compare the release of each element to the amount of mass release. The fractional mass release of each element i is calculated as follows:

$$f_i = \frac{x_i\, m}{x_{i,o}\, m_o} \tag{5.18}$$

where f_i is the fraction of the initial amount of element i remaining in the char, x_i is the mass fraction of elemental in the char sample, and m represents the mass of the particle. The subscript o represents the parent coal. This equation holds true on either a moisture-free basis or on a DAF basis.

The percentage of each element released as a function of the mass released during devolatilization for all five coals, as calculated from Eq. 5.18, is shown in Figs. 5.33-37. The solid 45° line in each plot represents the total mass release rate ($1\text{-}m/m_o$). As expected, the carbon is released from the Pocahontas #3 coal (PSOC-1508D), Pittsburgh #8 hva bituminous coal (PSOC-1451D), Illinois #6 hvb bituminous coal (PSOC-1493D), and New Mexico Blue subbituminous coal (PSOC-1445D) in a manner directly proportional to the total mass release, and hence the data points fall on the 45° line. Carbon is the principal component in these coals, and hence should be released proportionally to the total mass. The data for the North Dakota lignite, however, show that the carbon is not released at the same rate that the total mass is

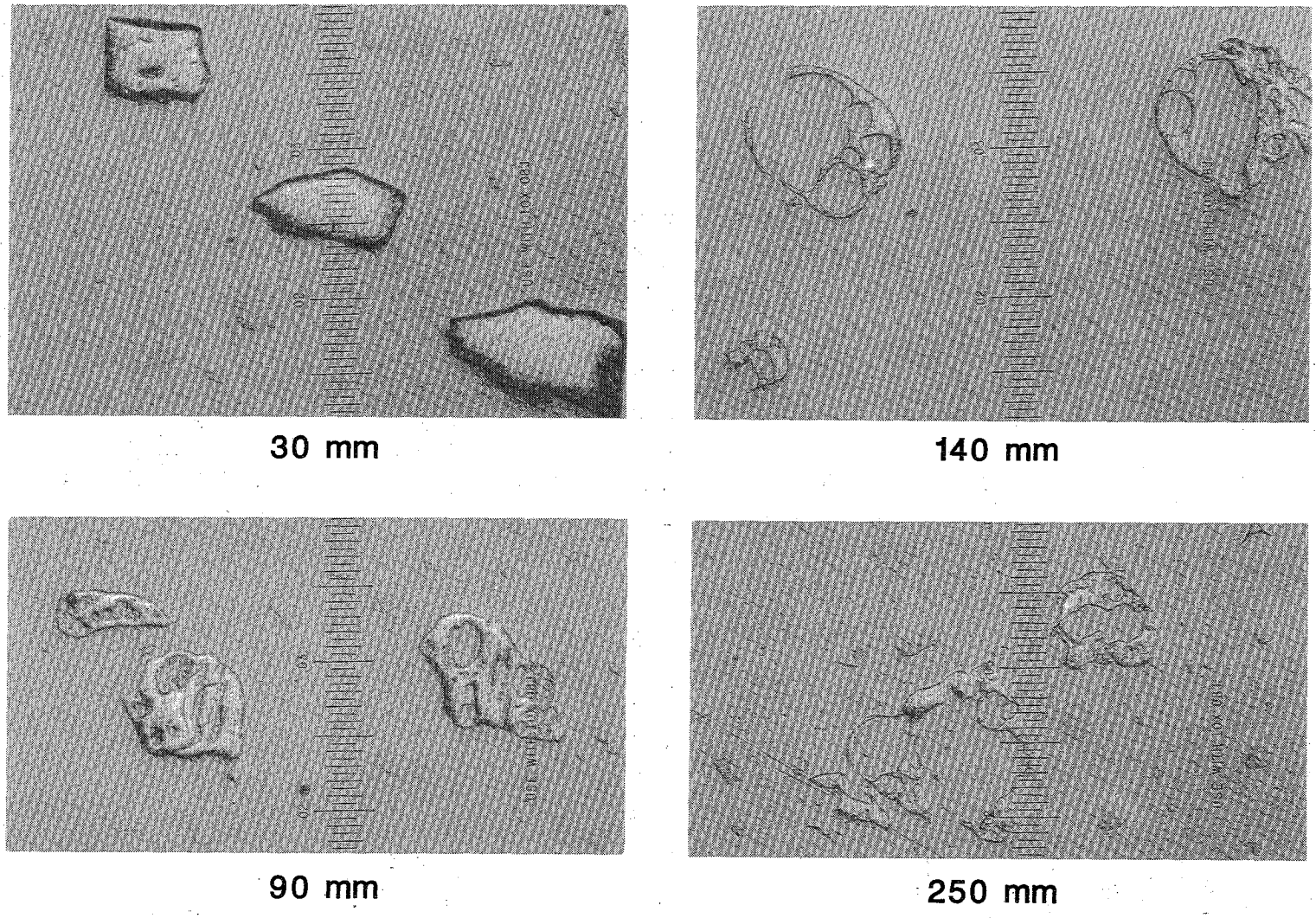

Figure 5.32 Cross-section micrographs of 106-125 μm PSOC 1451d hva Pittsburgh bituminous coal particles collected at different position in the flow reactor at the 1050 K gas temperature condition.

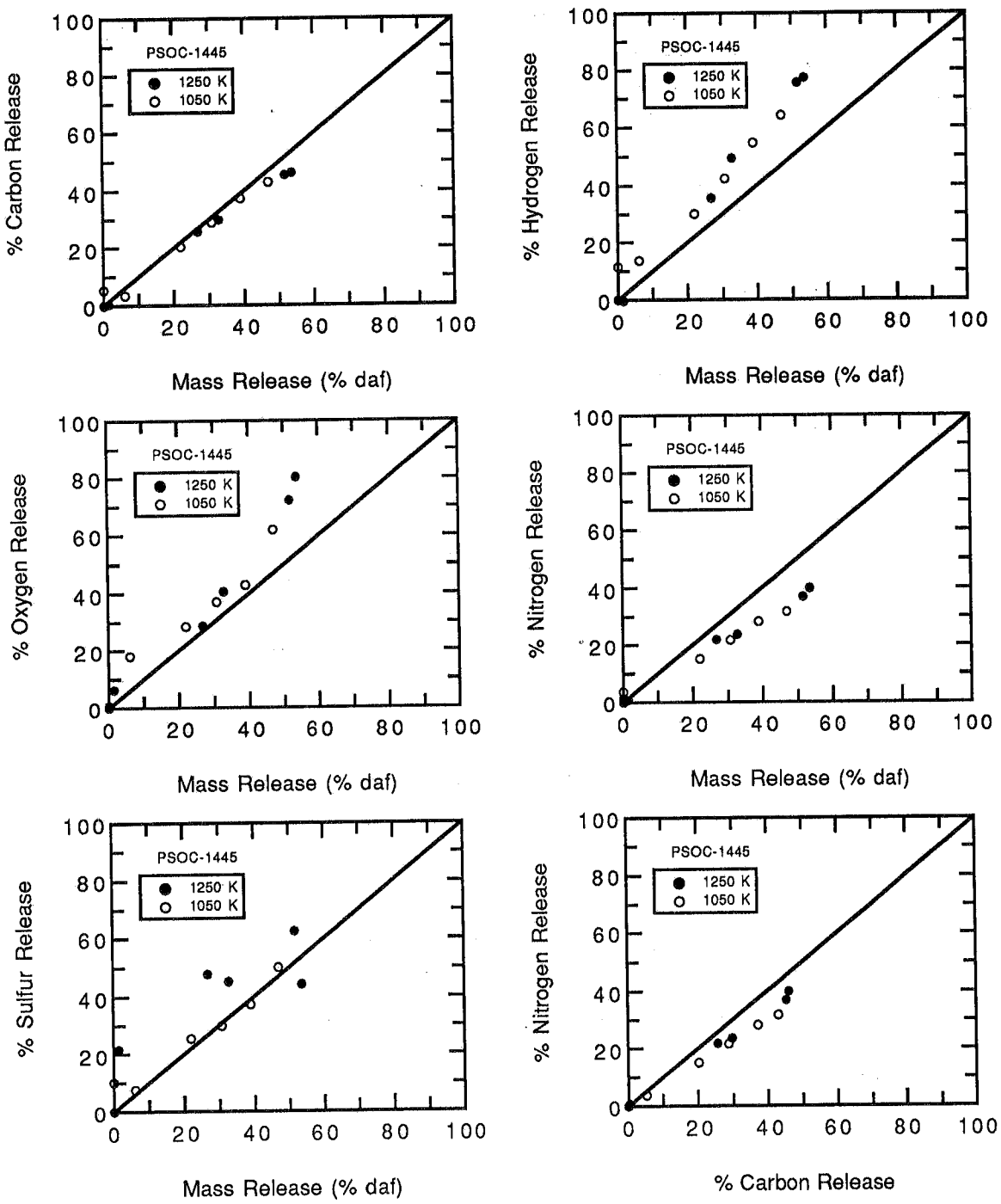

Figure 5.33 Elemental mass release rates for PSOC-1445D New Mexico Blue #1 subbituminous coal particles (106-125 μm) during devolatilization in 100% N_2 in the CDL.

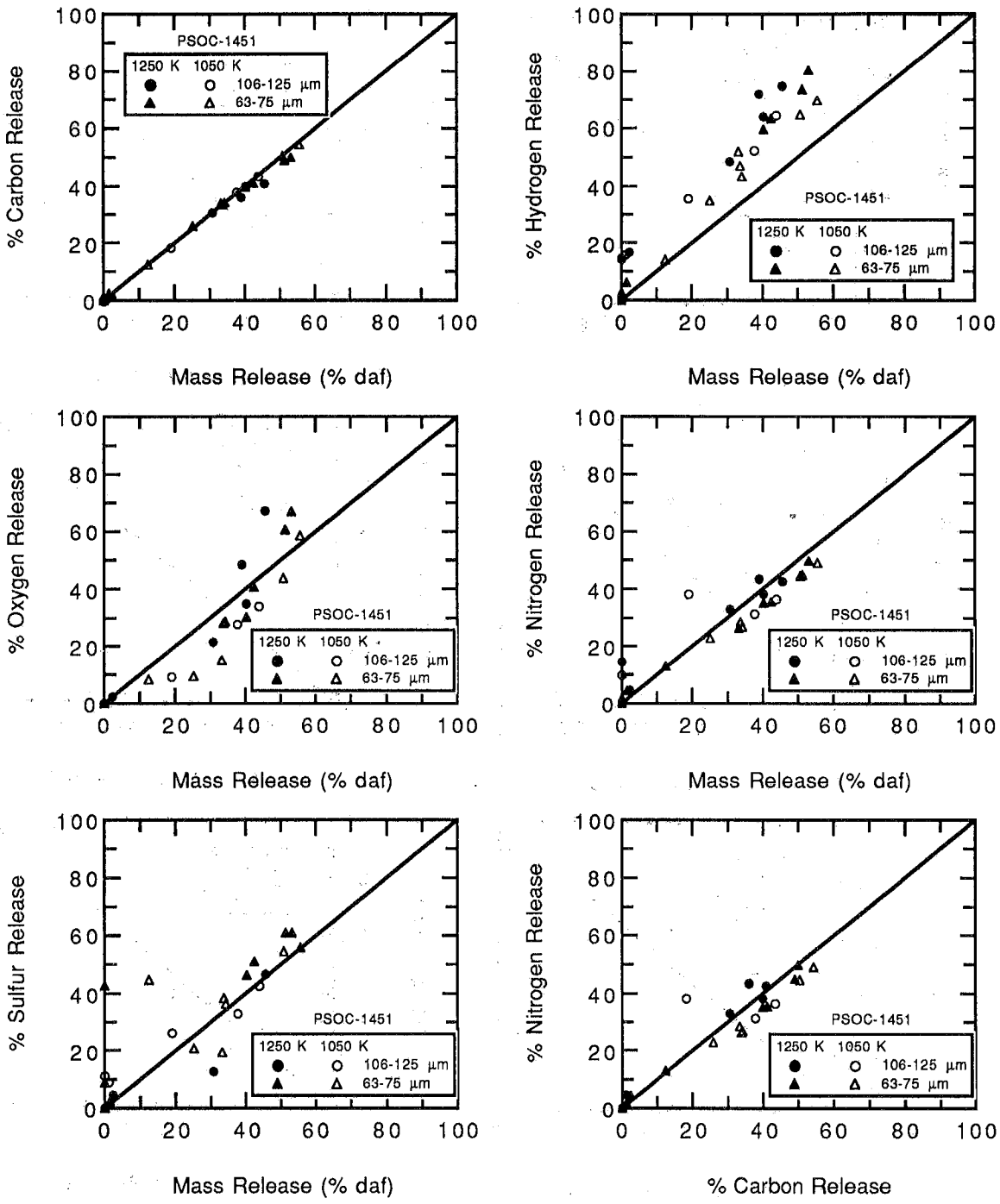

Figure 5.34 Elemental mass release rates for PSOC-1451D Pittsburgh #8 hva bituminous coal particles (106-125 and 63-75 µm) during devolatilization in 100% N_2 in the CDL.

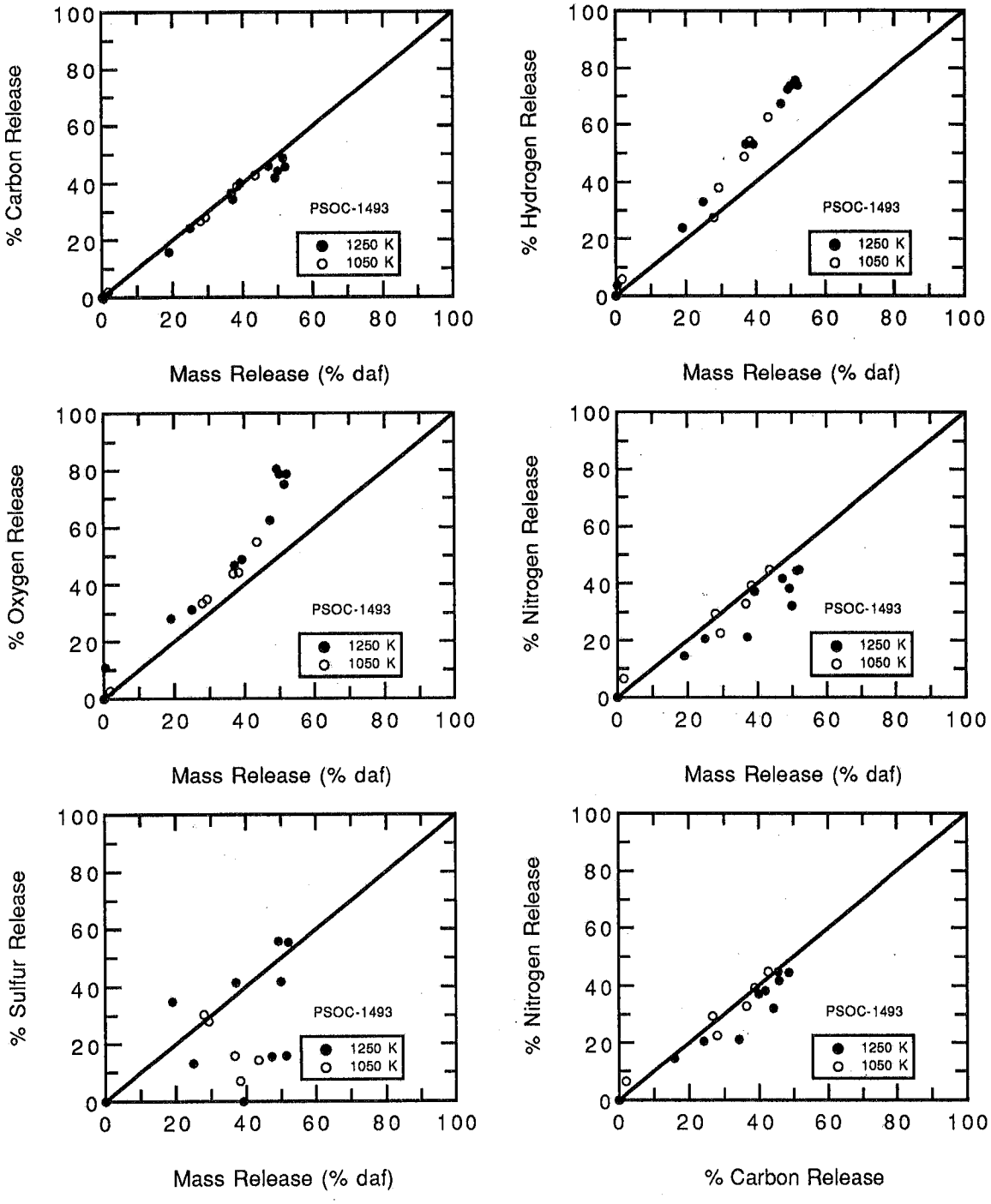

Figure 5.35 Elemental mass release rates for PSOC-1493D Illinois #6 hvb bituminous coal particles (106-125 μm) during devolatilization in 100% N_2 in the CDL.

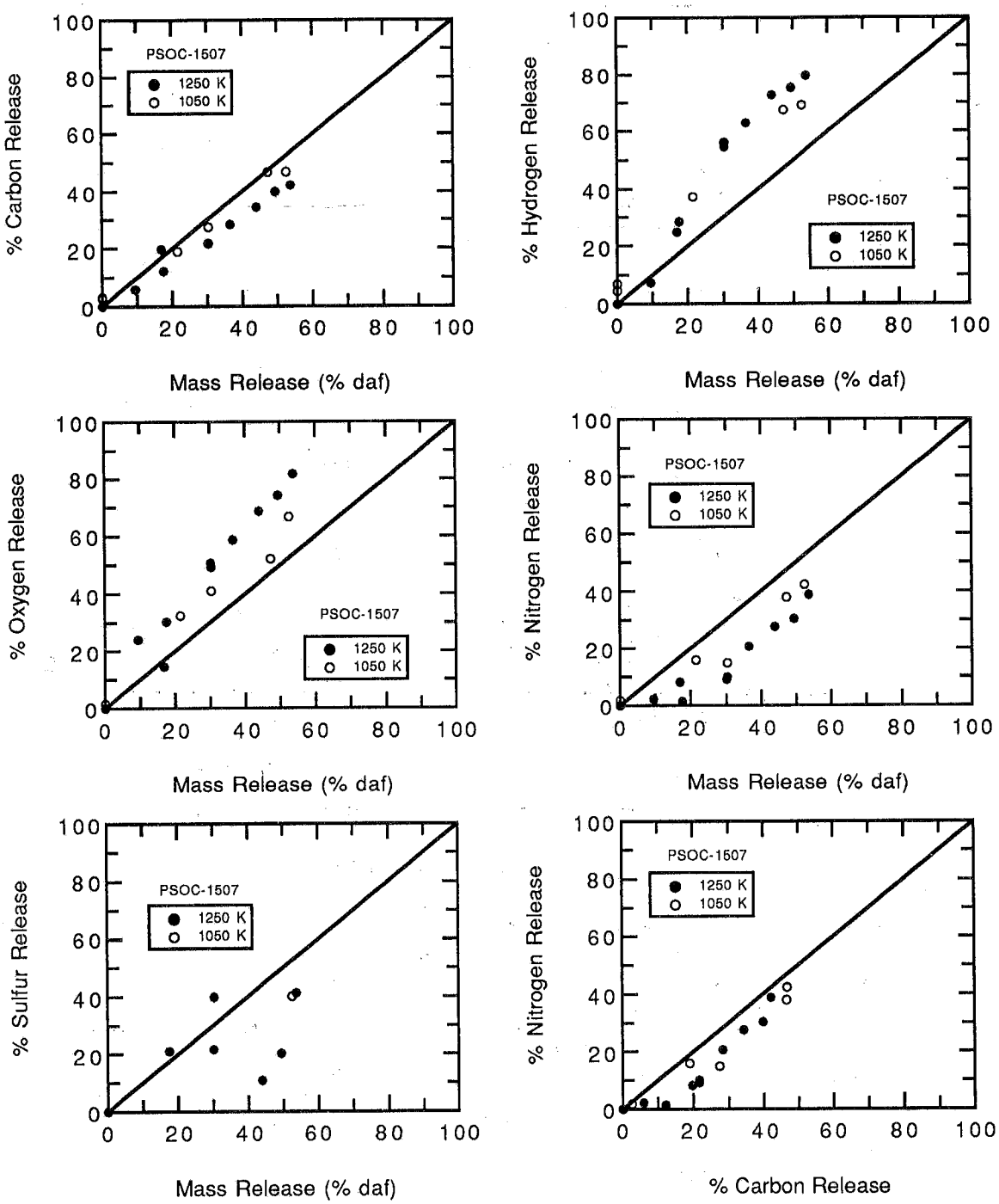

Figure 5.36 Elemental mass release rates for PSOC-1507D North Dakota Beulah Zap lignite particles (75-106 μm) during devolatilization in 100% N_2 in the CDL.

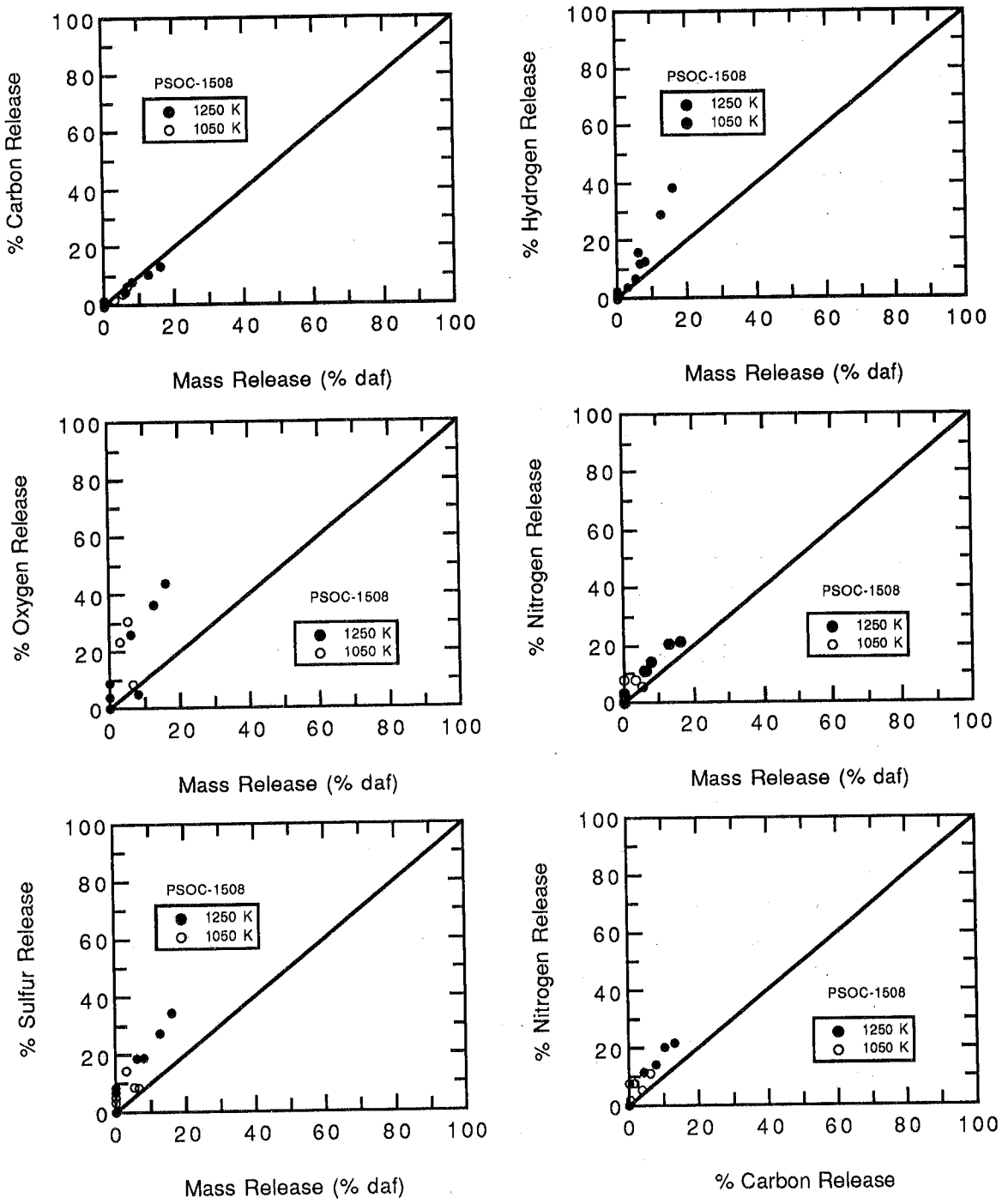

Figure 5.37 Elemental mass release rates for PSOC-1508D West Virginia Pocahontas #3 lv bituminous coal particles (106-125 μm) during devolatilization in 100% N_2 in the CDL.

released. The lignite contains more oxygen than the three coals (see Table 4.1), and the oxygen seems to be released preferentially to the carbon. The rapid release of CO_2 in the early stages of the devolatilization process is characteristic of lignites [Suuberg, et al., 1970].

A small amount of preferential oxygen release is observed in the early stages of devolatilization for the Illinois #6 and New Mexico Blue #1 coals. In contrast, the oxygen is released at a lower rate than carbon in the early stages of devolatilization for the Pittsburgh #8 coal. This is consistent with known occurrences of oxygen in coals as a function of rank. In low rank coals, such as lignites and subbituminous coals, oxygen is found in carbonyl groups, which release CO_2 early in the pyrolysis process since the C=O bonds are generally peripheral chain ending groups and not very strong. In the bituminous coals, oxygen is bound in aliphatic and aromatic ether groups, and significant scission of carbon bonds must occur before such strongly bound oxygen can be released. These three coals exhibit an increase in the rate of oxygen release during the late stages of devolatilization (40 to 60% daf mass release), with the most pronounced effect observed for the Illinois #6 coal. The late oxygen release is most likely caused by breaking ether linkages in the coal molecule, which are more stable than the carbonyl groups.

The hydrogen in all five coals is initially released faster than the the other elements, and hence the data points lie above the 45° line representing the total mass release. This results from the fact that the molecular weight of hydrogen-rich pyrolysis products is low enough to vaporize at the temperatures studied here. Pyrolysis products that are low in hydrogen content, such as polycyclic ring structures, have higher molecular weights and remain in a solid or liquid state, with a high probability of cross-linking to the solid matrix. For example, light gases such as methane and ethane are enriched in hydrogen, and are released as volatiles. The resultant char, after volatiles are completely released, consists mainly of carbon (on a mass basis). The hydrogen release seems to be somewhat independent of the rank of the coal, and also correlates to some degree with the oxygen release.

In the low volatile bituminous coal (PSOC-1508D), the oxygen, hydrogen, nitrogen, and sulfur are all released preferentially to carbon. The carbon aromaticity in the low volatile coal is higher than in the other coals, as is the carbon content. This means that the labile bridges are very small, and the the entire coal molecule is more tightly bound than the lower rank coals. The non-carbon elements are present in such low concentrations that they almost behave as impurities, rather than significant features of the coal structure.

The data from all five coals indicate that nitrogen is released from the coal at a rate only slightly different than the carbon release. This is better seen when the nitrogen release is plotted versus the carbon release, as shown for all five coals in Fig. 5.38. The strong correlation between carbon and nitrogen release as a function of coal rank indicates that the nitrogen is primarily bound in secondary amine structures with the carbon, such as cyclic ring heteroatoms, rather than in loosely bound NH_2 groups. The

correlation between release of carbon and nitrogen is strongest for the mid-rank coals (subbituminous through bituminous); the nitrogen release is slightly lower than the carbon release in the lignite, while the nitrogen release is slightly higher in the low volatile coal.

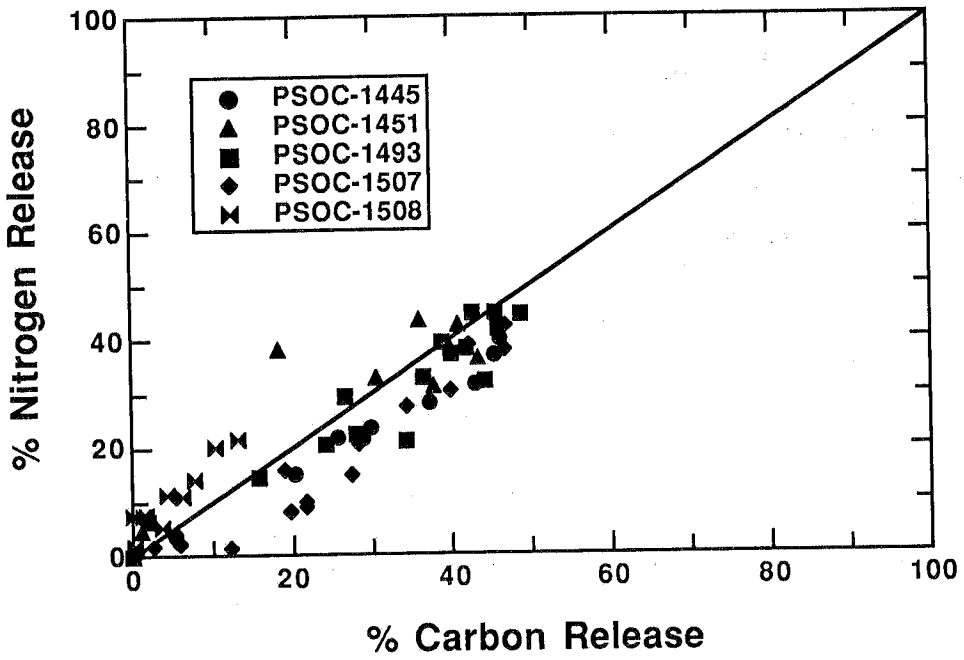

Figure 5.38 Correlation between elemental release of nitrogen and carbon for five coals.

The sulfur release data seem to be more scattered than the release data for the other elements. This is due in part to the small sample sizes analyzed and to the low sulfur contents of the parent coal. The trends seem to be that the sulfur is released early in the devolatilization process for the low volatile bituminous and the subbituminous coals, late in the devolatilization process for the Illinois # 6 coal and the North Dakota lignite, and roughly proportional to the total mass release for the Pittsburgh #8 coal. The sulfur release is obviously related to the proportion of pyrite present in the coal, which was not measured in these samples.

It is interesting to consider the elemental mass release in terms of the process of coalification. Elemental compositions of parent coals lie in a coalification band when the hydrogen to carbon ratio is plotted versus the oxygen to carbon ratio. As low rank coals age, the oxygen is given up preferentially to hydrogen. However, after coals reach the bituminous coal stage, hydrogen is lost preferentially to oxygen, causing a bend in the coalification band. When coals devolatilize, the elemental release profiles do not follow the coalification band, as shown in Fig. 5.39 for chars collected at

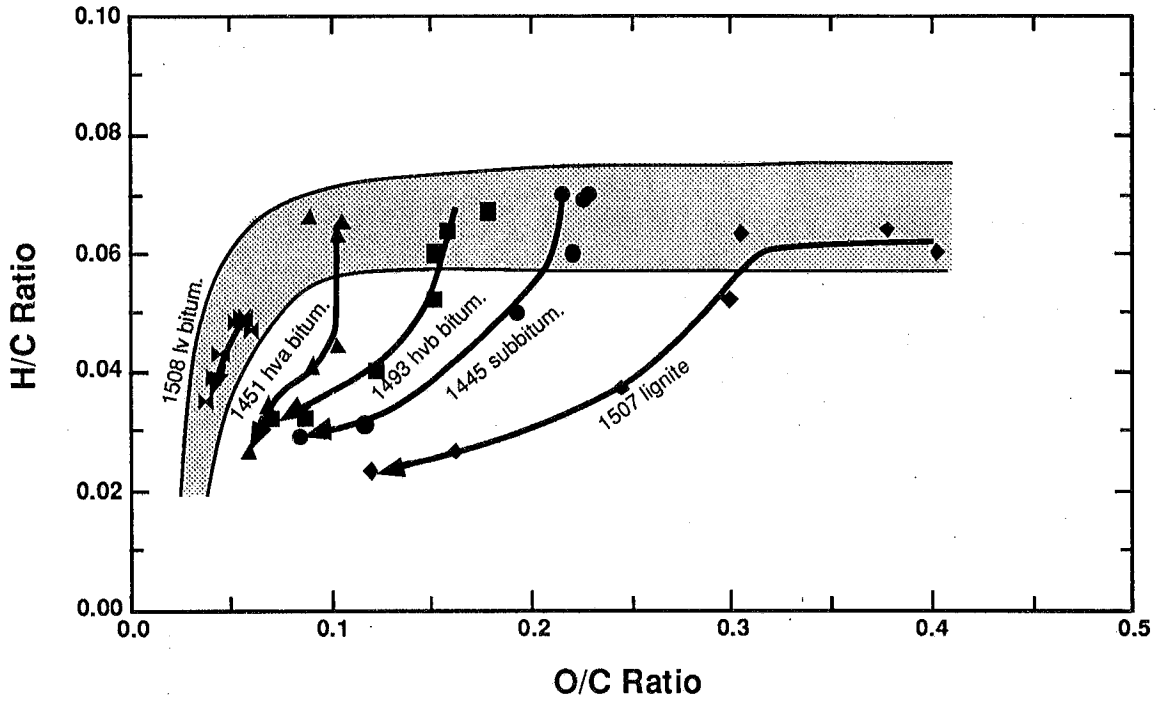

Figure 5.39 Coalification chart showing locations of initial coals and progress of chars during devolatilization, based on elemental composition.

different residence times in 100% N_2 in the CDL. Oxygen and hydrogen are released during devolatilization at similar rates, and hence the low rank coal char profiles bypass the bend in the coalification band. The fully-devolatilized coal chars all lie in a small region of the coalification chart compared to the diversity of the parent coals. However, the fully-devolatilized chars collected do exhibit slight differences, and none have approached the composition of graphite, which is located at (0,0) on the coalification chart.

Chemical Structure of Char and Tar Determined from NMR Analysis

The chemical structures of coal char and tar samples from devolatilization experiments are examined using ^{13}C NMR spectroscopy. The data for two coals have been published [Fletcher, et al., 1990a; Pugmire, et al., 1991]. The data from these two coals are presented here along with the data from the other three coals examined at Sandia.

A. Evolution of Char Structure

Representative chemical structures identified in the ^{13}C NMR analyses of coal and char samples are illustrated in Fig. 5.40. The measured variations in several of these parameters are shown in Fig. 5.41 as a function of residence time during

devolatilization in the 1250 K gas condition for two coals. The data shown at 0 ms residence time are for the parent coal; analyses of two separate samples of lignite indicate the experimental error involved in each chemical structure parameter. For clarity, only the carbon aromaticities (fraction of carbon contained in aromatic structures) with the carbonyl subtracted (f_a', not f_a) will be discussed in this section.

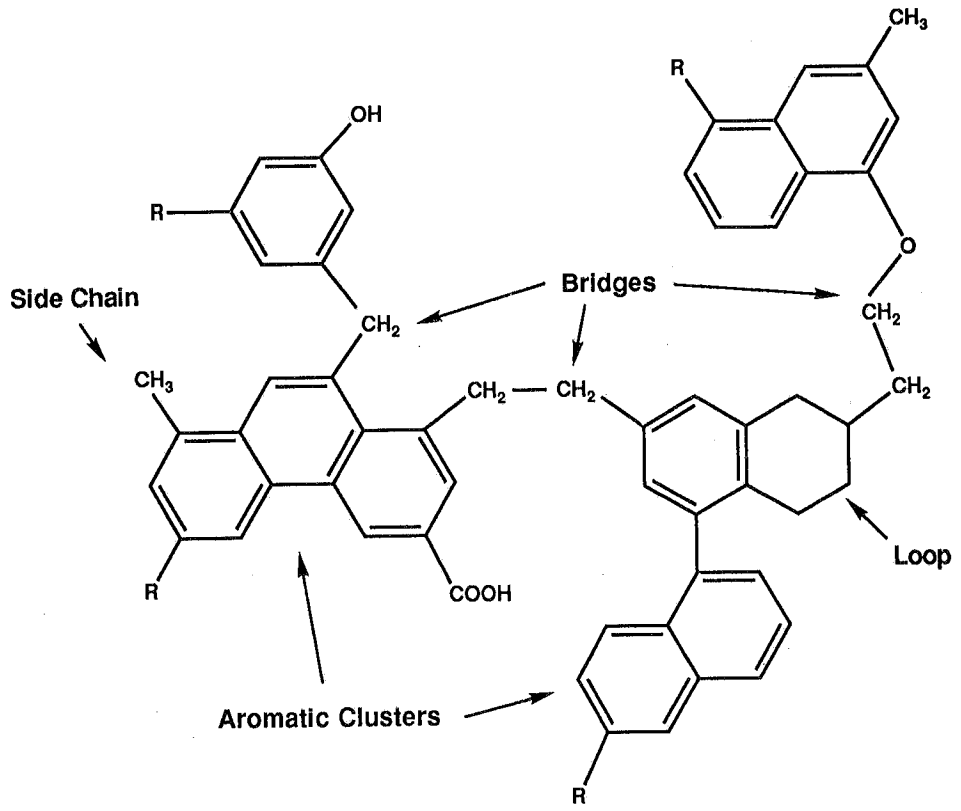

Figure 5.40 Representative chemical structures identified in ^{13}C NMR analyses of coal and coal chars.

The ultimate volatiles yield at the 1250 K gas condition was 51% on a dry ash free (daf) basis for the Illinois No. 6 coal, and 53.7% for the Zap lignite. Approximately 40% of the volatiles from Illinois No. 6 are released by 43 ms, and 75% of the total mass release occurs by 65 ms. Tar is released at residence times from ranging from 30 to 65 ms, based on model predictions [Fletcher, et al., 1990b] and comparison with similar data [Serio, et al., 1987]. During this tar release period, the percentage of aromatic carbon for the bituminous coal char has changed by less than 5% (see Fig. 5.41), suggesting that the carbon aromaticity of the initial tar is similar to that of the coal.

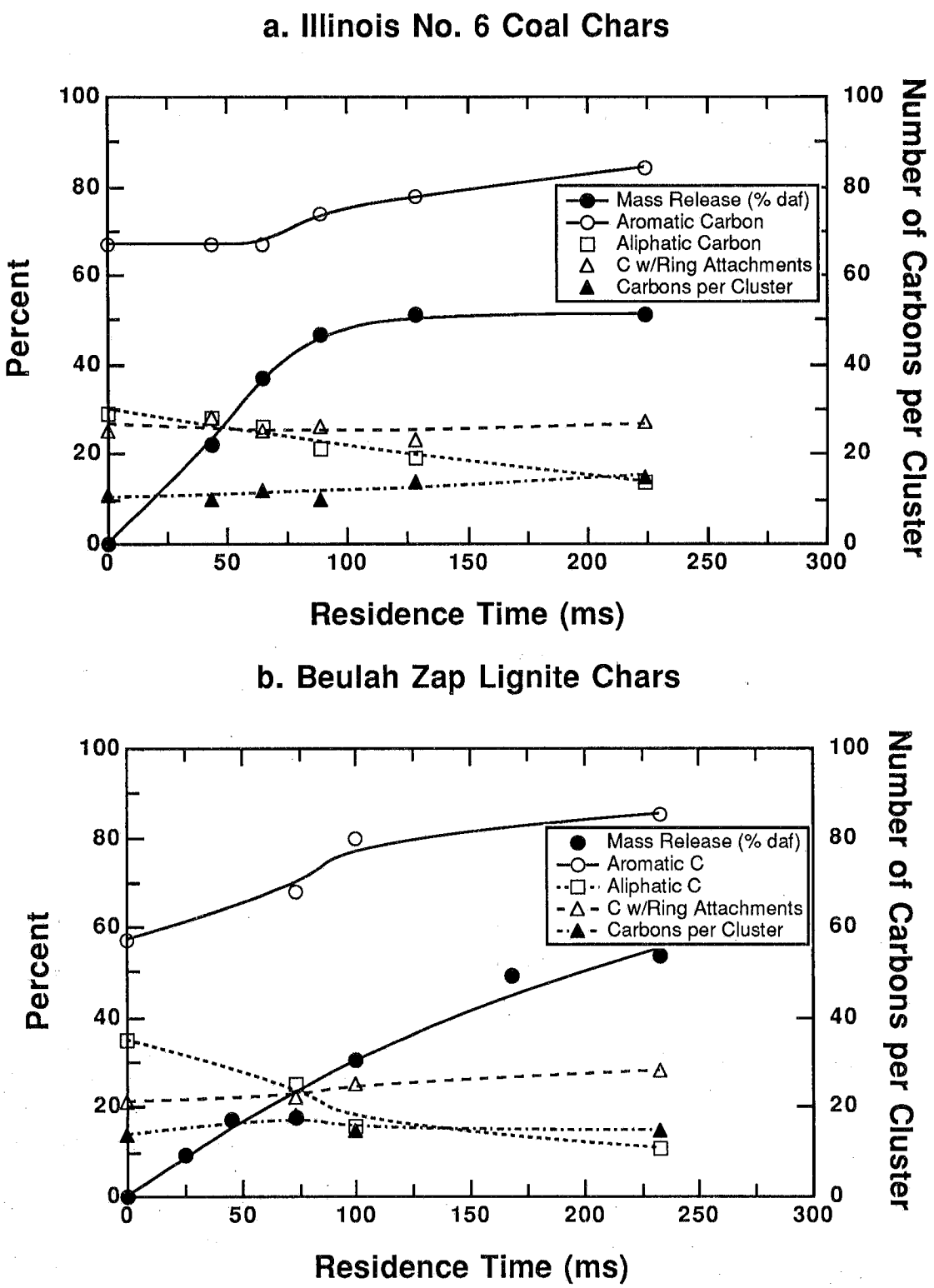

Figure 5.41 Char structure parameters and mass release profiles for (a) Illinois No. 6 coal and (b) Beulah Zap lignite, as a function of residence time at the 1250 K gas temperature condition.

The number of aromatic carbons per cluster in the bituminous coal char at 223 ms reaches a final value of 15, a modest 40% increase in cluster size when compared to anthracite coals and graphitized samples where the number of aromatic carbons per cluster may be in the range of 50 to 350 [Sethi, et al., 1988; Orendt, et al., 1990]. The number of aliphatic carbons per cluster in the bituminous coal char remains relatively constant until the late stages of devolatilization, and then decreases. The number of aliphatic carbons per cluster in the bituminous coal char at 223 ms is almost a factor of two lower than in the parent coal, but has changed by less than the experimental error at the point where 75% of the volatiles have been released (65 ms).

As shown in Fig. 5.41b, the chemical structure of the Zap lignite changes in a manner similar to the changes exhibited by the Illinois No. 6 coal. The other three coals also exhibit similar behavior, and hence data for these coals are not shown in this type of plot. A careful examination of the relationship between mass release and carbon aromaticity for the lignite (Fig. 5.41) clearly indicates differences from those observed for Illinois No. 6. Approximately 20 to 25% of the total mass release for the lignite occurs over the time period where 75% of the mass release was noted for the bituminous coal. On the other hand, the carbon aromaticity in the lignite char changes in the early stage of pyrolysis as compared to the bituminous coal chars, indicating that the structural relationship between the initial lignite tars and chars is quite different from those observed in the Illinois No. 6 samples. The carbon aromaticities for both sets of chars ultimately reach comparable values, but the parent lignite has a lower carbon aromaticity value ($f_a' = 0.57$) than the parent bituminous coal ($f_a' = 0.67$). Hence, some of the restructuring of the aromatic species occurs earlier in the lignite than in the Illinois No. 6 coal.

The number of aromatic carbons per cluster in the lignite chars shows no significant change with residence time, within experimental error. However, the total number of carbons per cluster decreases as the result of the release of aliphatic carbons, as indicated by the number of aliphatic carbons per cluster. The high number of aliphatic carbons per cluster in the parent Zap lignite, relative to Illinois No. 6 coal, correlates with the higher gas release of the lignite during pyrolysis.

Attachments to aromatic clusters (see Fig. 5.40) consist of alkyl groups and oxygen functional groups (e.g., phenols and/or alkyl and aryl ethers). These attachments are bridges and loops between aromatic clusters or side chains that are not connected on one end to another aromatic cluster. The bond strengths of the aromatic rings are much greater than the bond strengths of the labile bridges and loops. During devolatilization these labile bridges break, generating finite-size fragments containing one or more aromatic clusters. The light fragments are released as tar, while the heavier fragments stay in the char as metaplast and eventually reattach to the infinite char matrix. Broken bridge fragments (i.e., side chains) are eventually released as light gas. In this analysis, it is assumed that the fractured bridge fragments may be distinguished from intact bridges by the presence of methyl groups. Hence, the number of side chains per cluster can be estimated together with the number of intact bridges and loops per cluster. It is important to note that aliphatic carbons still remain

at the end of the pyrolysis process and represent the presence of stable aliphatic bridge material and/or side chains that have not been expelled at the pyrolysis temperatures employed.

In the Illinois #6 coal and char samples, the total number of carbons per cluster (aromatic plus aliphatic) has not changed relative to the experimental error (estimated at ±3). Furthermore, in the bituminous coal chars, the number of aromatic carbons with attachments remains essentially constant as a function of residence time, even though the number of aliphatic carbons in the 223 ms sample is a factor of two lower than in the parent coal. The number of attachments to aromatic rings for the lignite chars increases by approximately 25% while the number of aliphatic carbons decreases by 65%. These data suggest that the pyrolysis process eliminates functional groups from the aromatic clusters in the lignite, with a net loss of aliphatic carbons. At the same time, however, additional crosslinking sites are formed.

The total number of attachments per cluster (referred to as the coordination number, $\sigma+1$) is shown in Fig. 5.42 for char samples from all five coals. The coordination number either remains relatively constant or decreases during devolatilization for all five coals. This means that no new attachment sites are generated during pyrolysis; any reattachment of metaplast occurs at existing side chain sites. Decreases in the coordination number can be explained by the release of side chains with no subsequent crosslinking at that site. The implication of the data in Fig. 5.42 is that crosslinking does not generate any new attachment sites, and occurs only at existing sites that are occupied by a side chain.

The number of bridges and loops (i.e., bridges between aromatic rings and aliphatic loops on aromatic rings, such as tetralin) per cluster does not change significantly in the Illinois #6 coal char until the end of the mass release period, as shown in Fig. 5.43. The increase in the number of bridges and loops per cluster is an indication of the extent of crosslinking that occurs between neighboring aromatic clusters. The total number of attachments per aromatic cluster ($\sigma+1$), however, does not change significantly, indicating that bridge material is released at a rate proportional to the formation of crosslinking bridges. These stable char bridges likely are formed at the site of the original bridge. These data at rapid heating conditions clearly indicate that the average molecular structure of the Illinois No. 6 coal does not undergo major changes in functional group distribution until after most of the tar is released, at which time reactions occur in the char/metaplast that are associated with gas release.

However, the crosslinking behaviors of the chars from other coals are different from that observed in Illinois No. 6. The changes in the number of bridges and loops per cluster in the late stages of mass release for the other bituminous coal (PSOC-1451D) are more scattered, and do not exhibit the clear indication of crosslinking observed in the Illinois #6 coal (PSOC-1493D). The number of bridges and loops is slightly higher in the parent lignite, and increases in a monotonic progression with the extent of mass release. The lignite data reflect the early crosslinking that is observed

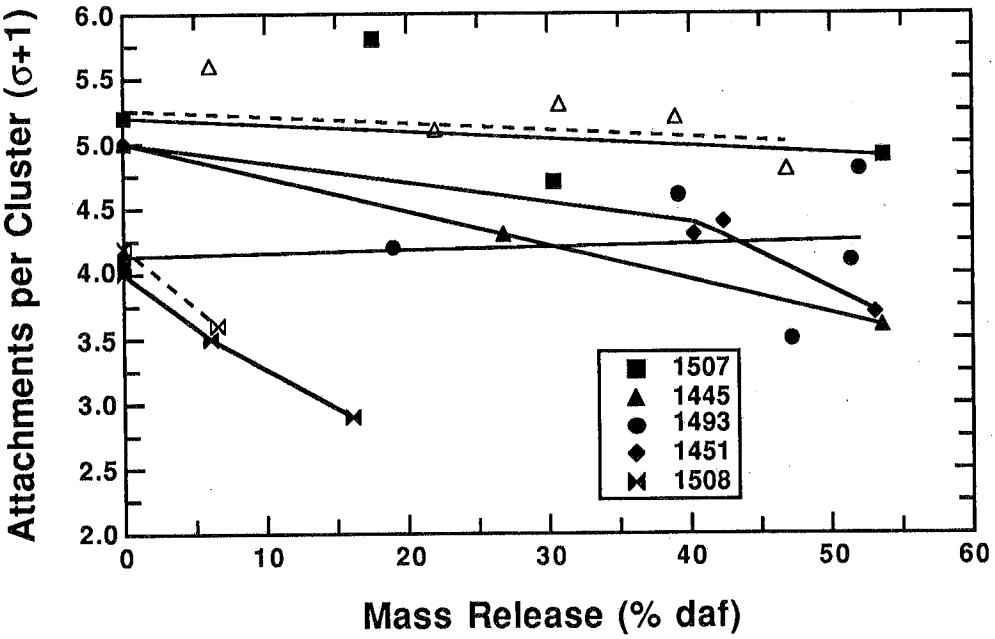

Figure 5.42 The total number of attachments per cluster vs. the extent of mass release due to devolatilization for chars collected at different residence times in the 1050 K (dashed lines and open symbols) and 1250 K (solid lines and filled symbols) gas temperature conditions.

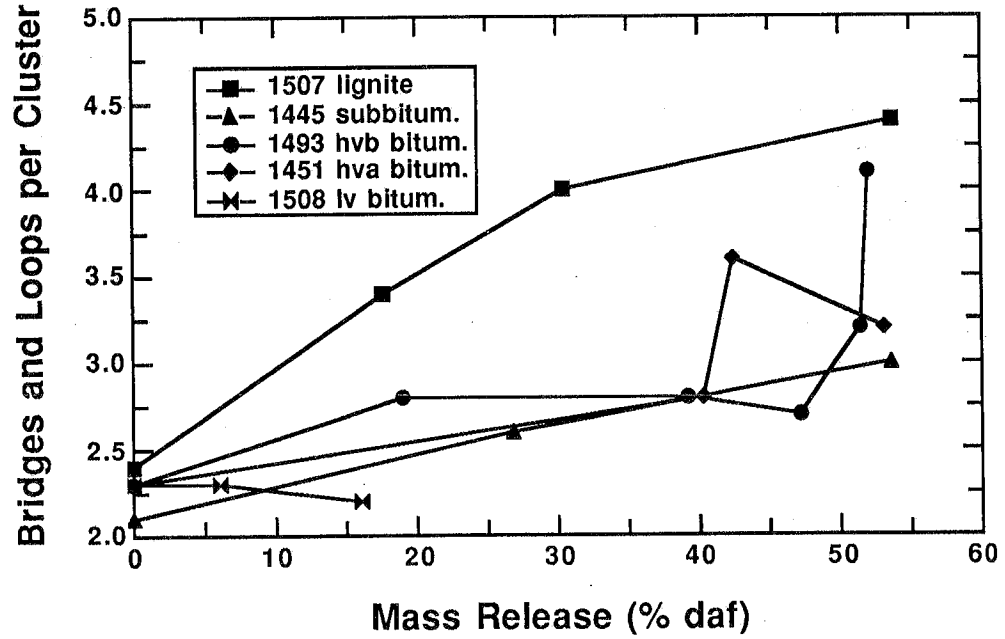

Figure 5.43 The number of bridges and loops per cluster vs. the extent of mass release due to devolatilization for chars collected at different residence times in the 1250 K gas temperature condition.

swelling measurements of lignites as compared to the high volatile bituminous coals [Suuberg, et al., 1985; Solomon, et al., 1990b; Solum, et al., 1990]. This early crosslinking is only indicated in Fig. 5.43 for the lignite; none of the other coals show significant increases in the number of bridges and loops per cluster until the late stages of mass release (including the subbituminous coal). The highest rank coal (PSOC-1508D Pocahontas lv bituminous) shows a slight decrease in the number of bridges and loops per cluster as mass release proceeds.

Coordination numbers for char samples obtained in the 1050 K gas condition in the CDL are shown as dashed lines and open symbols in Fig. 5.43. In the 1050 K gas condition, the coordination number determined for the chars from the subbituminous coal (PSOC-1445D) does not decrease as much with mass release as indicated at 1250 K. The lower temperature condition does not permit the same degree of gas release as the higher temperature condition, and hence more side chains remain attached to the clusters. The coordination number data at 1050 K for the high rank coal (PSOC-1508D) follow the data indicated at 1250 K. In general, the data at 1050 K support the conclusion inferred from the 1250 K data; no increases in the number of attachments per cluster are seen, indicating that crosslinking occurs only at existing side chain sites.

The relationships between the carbon aromaticity and the fractional elemental mass release of C,H,O,N, and S for the Illinois No. 6 coal and the Zap lignite at the 1250 K gas temperature environment are shown in Fig. 5.44. For the Illinois No. 6 coal, hydrogen and oxygen are released at a higher rate than carbon in the early and intermediate stages of mass release (0 to ~ 45%), corresponding to the release of light hydrocarbons, CH_4, H_2O and CO_2 [Solomon, et al., 1990a] at the same time tar is released. The sulfur and nitrogen release also correspond to the carbon release, although there is some scatter due to the small samples used for elemental analysis. During the late stages of mass release (~ 45 to 51%), corresponding primarily to release of side chains as light gases, the loss of carbon seems to reach a plateau at a value of 40%, while rapid hydrogen and oxygen release continues. The increase in carbon aromaticity, rapid release of hydrogen and oxygen, and plateau in carbon release are indicative of dehydrogenation of aliphatic ring structures. Possible gases evolving from the char during the later stages of devolatilization are H_2, CO, CO_2, and C_2H_4 [Suuberg, et al., 1978].

For the lignite, the oxygen, carbon, and hydrogen release are comparable in the early stage of mass release (0-10%), where light gases are evolved. A slight rise in hydrogen release is noted at approximately 15% mass release, which occurs at the point where tar release begins. The rates of oxygen and hydrogen release are consistently higher than the release rate of carbon through all stages of devolatilization. The carbon aromaticity increases rapidly in the early to mid-point ranges of the mass release and then begins to level off during the latter stage of pyrolysis. The elemental mass release and aromaticity data for the lignite in the latter stage of pyrolysis is associated with loss of peripheral oxygen containing groups on

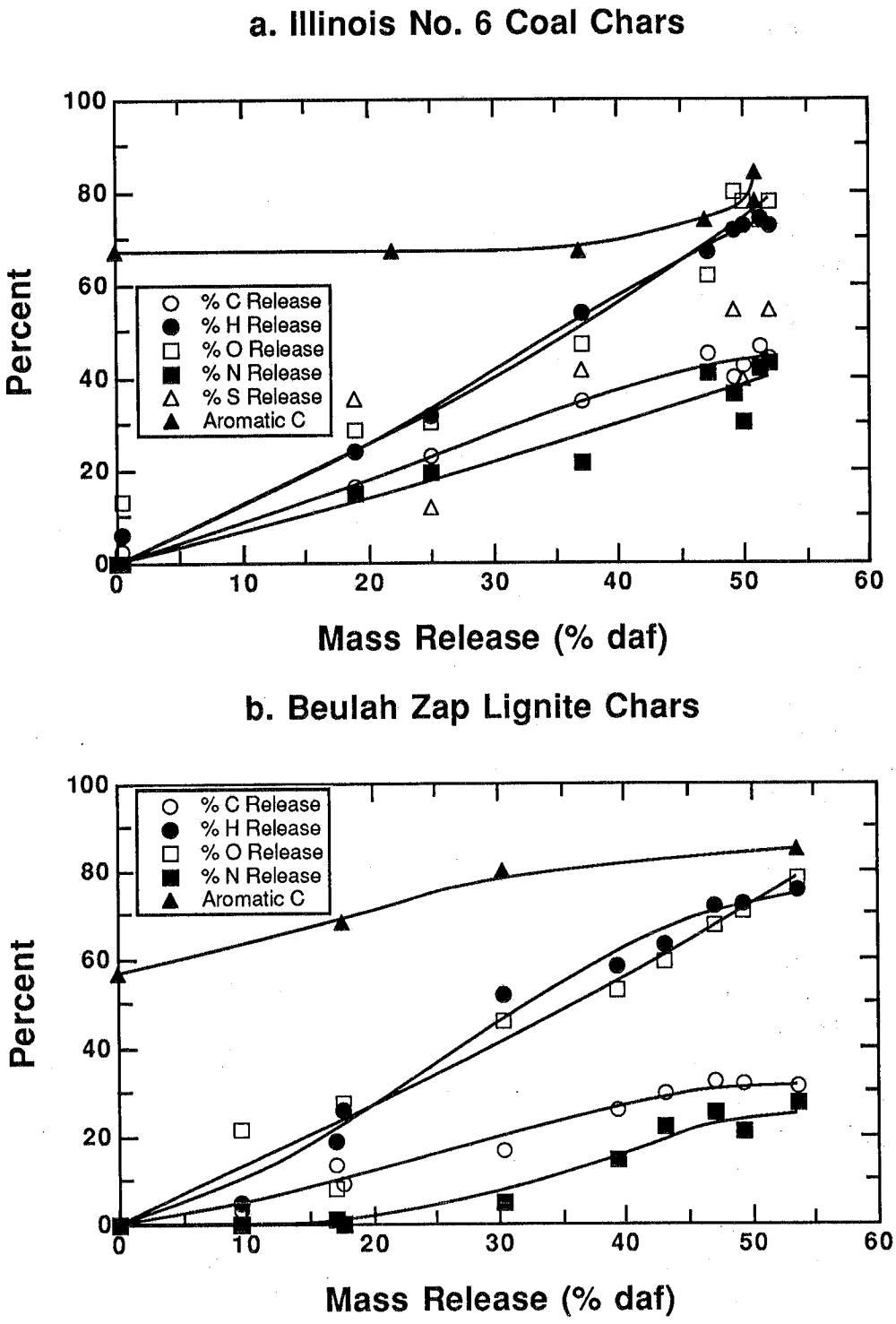

Figure 5.44 Fractional elemental mass release of C, H, N, O, and S relative to the total mass release during devolatilization for the Illinois No. 6 coal and Beulah Zap lignite. Carbon aromaticity is also shown. Solid lines represent curve fits to the data.

the aromatic cluster, as opposed to the apparent ring dehydrogenation noted in Illinois No. 6 coal. It appears that major changes in functional group distribution and restructuring of the aromatic rings occurs in the lignite at an earlier stage in the pyrolysis process than was noted for Illinois No. 6 coal.

The proton spin relaxation time constant $T_{1\rho}^{Har}$ is a complex function of the motion within the lattice and the effects of free electrons that are present. This parameter may therefore be related to the concentration of metaplast in the coal char. The value of $T_{1\rho}^{Har}$ in the rotating frame passes through a minimum in the chars and then rises to values similar to or higher than those observed in the parent coals. Similar behavior has been noted in other chars prepared at both rapid (~ 10^4 K/sec) and slow (~ 0.5 K/sec) heating conditions [Solum, et al., 1990]. The relationship between $T_{1\rho}^{Har}$ and the free electrons present in coals and chars has been discussed by Jurkiewicz, et al. [1990]; the variations in the value of $T_{1\rho}^{Har}$ and the relationship the the amount of metaplast present in the char warrant further study.

B. Chemical Structures of Fully-Devolatilized Coal Chars

One of the interesting chemical structure features determined in the NMR analyses is the molecular weight per cluster in the char. The coal macromolecule is thought to consist of a number of fused aromatic rings connected by aliphatic bridges, as illustrated earlier in Figure 5.40. The average cluster molecular weight determined from the NMR analyses includes the average number of aromatic carbons per cluster plus the average number of attachments (bridges and side chains) per cluster, i.e. the contributions from both the aromatic and aliphatic material in the vicinity of a cluster.

NMR analyses of chars collected in the CDL at the 1250 K gas condition as a function of residence time are shown in Fig. 5.45. The average cluster molecular weight for parent coals ranges from 270 amu for the Illinois No. 6 coal to 440 amu for the Zap lignite, as shown in Fig. 5.45 at a residence time of 0 ms. However, as these coals are heated and the volatiles are released, average cluster molecular weights for the chars of these different coals become very similar. This is consistent with the similarity observed in the elemental compositions of the fully-devolatilized coal chars discussed earlier and shown in Fig. 5.39.

The fraction of carbon contained in aromatic rings (i.e., the carbon aromaticity) is shown as a function of residence time in Fig. 5.46 for all five coals. The carbon aromaticities of the fully-devolatilized chars only range from 79% for the subbituminous coal to 88% for the Pittsburgh No. 8 and the Pocahontas coals, whereas f_a' in the parent coals range from 53% for the subbituminous coal to 77% for the Pocahontas coal. The carbon aromaticity measured for the subbituminous coal and char is uniformly lower than measured in the other four coals (and their chars). The carbon aromaticities of the fully-devolatilized chars from the other four coals lie in a narrow range from 84% to 88%.

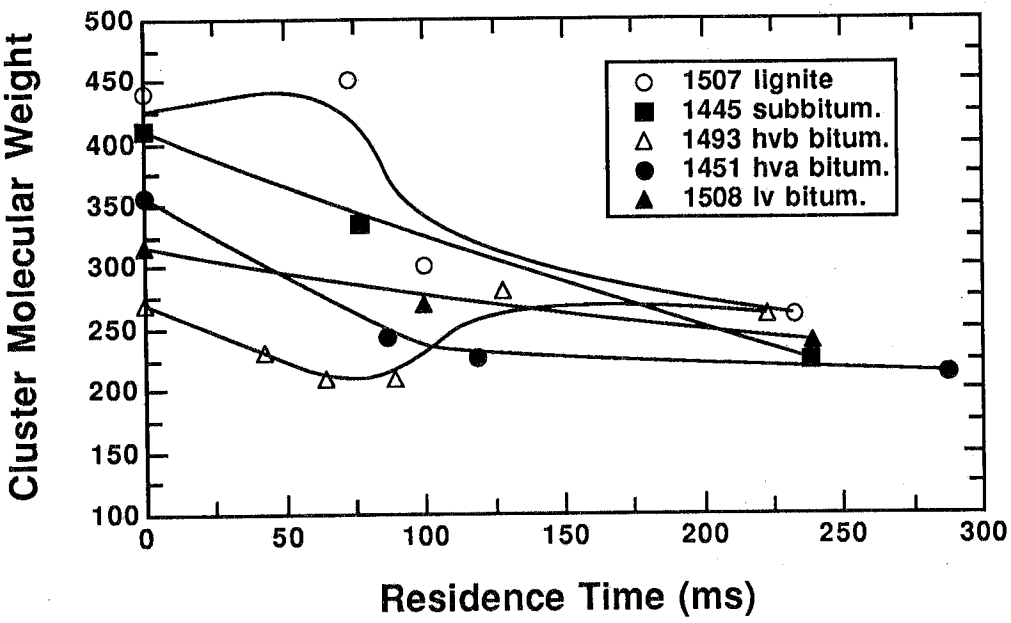

Figure 5.45 Average cluster molecular weights in coals and chars collected in the 1250 K gas condition in the CDL, determined from ^{13}C NMR analyses. Parent coals are represented at 0 ms residence time.

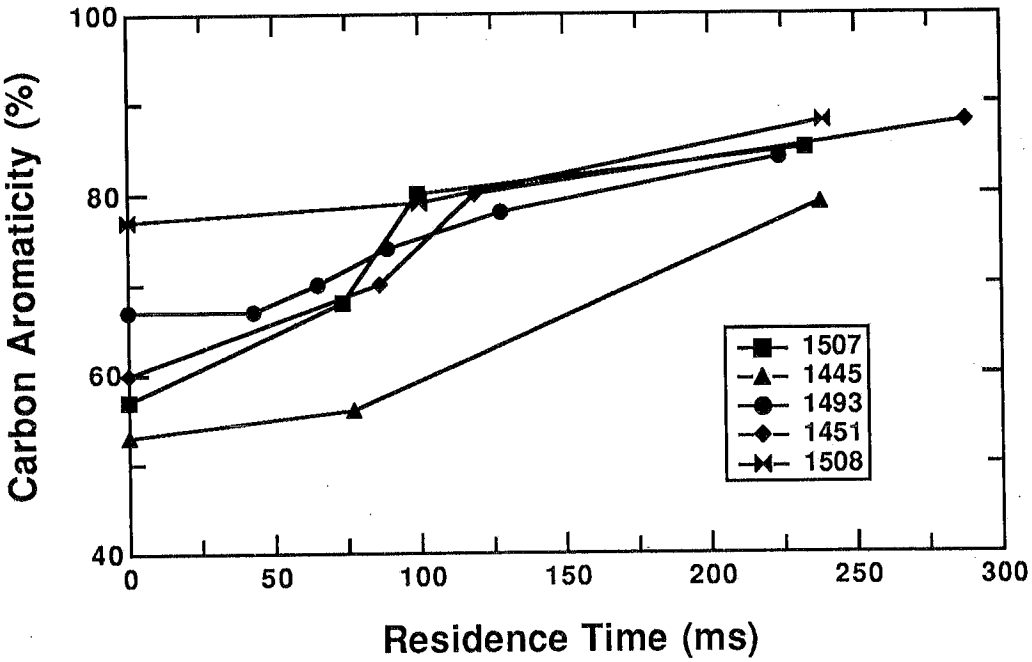

Figure 5.46 Carbon aromaticities in coals and chars collected in the 1250 K gas condition in the CDL, determined from ^{13}C NMR analyses. Parent coals are represented at 0 ms residence time.

It is well known that the physical structures (i.e., apparent densities and internal surface areas) of these chars vary significantly, causing a difference in the *apparent* reactivities of these chars (based on external surface area). However, the similarity in chemical structure of the fully-devolatilized chars from different coals may imply that the *intrinsic* chemical reactivities of these chars are similar. The exact relationship between cluster molecular weight, carbon aromaticity, and intrinsic chemical reactivity is not yet clear.

The fact that the chemical structure of these chars are similar is somewhat surprising because the chemical compositions of these chars are different. The carbon contents of the fully-devolatilized chars vary from 83% on a dry ash-free (daf) basis for the lignite char to 92% daf for the Pocahontas char. The oxygen contents of these chars range from 9.9% daf for the lignite char to 3.3% daf for the Pocahontas char. The NMR chemical structure data on chars are new; further examination of these data is needed, along with comparison with char composition, physical structure, and reactivity data.

Another comparison of chemical structure as a function of coal rank is the average molecular weight of attachments to clusters in the parent coal. Attachments to clusters include labile bridges (£), char bridges (c), and side chains (δ). As explained by Fletcher, et al. [1991], the molecular weight of attachments m_{att} can be calculated from the cluster molecular weight by subtracting the mass in the aromatic fused structure (the number of aromatic carbons per cluster multiplied by the molecular weight of carbon) and dividing by the number of attachments per cluster:

$$m_{att} = \frac{M_{clust} - C_{clust} M_C}{\sigma + 1} \tag{5.19}$$

The definition of the molecular weight per cluster (M_{clust}) used here includes the mass in the aromatic part of the cluster plus the surrounding aliphatic material. The cluster molecular weight therefore includes the mass of side chains, and one-half the molecular weights of labile bridges and char bridges attached to the cluster, as follows:

$$m_{att} = \frac{£ \frac{m_b}{2} + c \frac{m_{char}}{2} + \delta m_\delta}{£ + c + \delta} \tag{5.20}$$

where £, c, and δ represent the populations of labile bridges, char bridges, and side chains, respectively. The factor of 2 in the m_b and m_c terms reflects the fact the only one-half of an intact bridge is attributed to a cluster. Unreacted coals contain very few char bridges (i.e., $c = 0$), and hence Eq. 5.20 reduces to the relation $m_{att} = m_\delta$, assuming that $m_\delta = m_b/2$. For fully-devolatilized chars, £ = 0, and Eq. 5.20 becomes:

$$m_{att} = \frac{c \frac{m_{char}}{2} + \delta m_\delta}{c + \delta} \tag{5.21}$$

Attachment molecular weights have been thus determined for all five coals examined in the Sandia devolatilization experiments, as well for chars at different residence times, as shown in Fig. 5.47. Attachment molecular weights for other parent coals are also shown, as reported by Solum, et al. [1989] for the Argonne premium coals [Vorres, 1989] and for three coals examined at Advanced Fuel Research (AFR) [Serio, et al., 1987]. The continuous lines in this figure represent linear correlations of the data. The oxygen content of the parent coal is an indicator of coal rank; the oxygen content of the parent coal decreases as coal rank increases. The attachment molecular weights of the parent coals exhibit a definite trend as a function of coal rank; values of m_{att} range from 52 amu in the lignite and subbituminous coal (25% daf oxygen) to 13 amu for the highest rank coal (Pocahontas #3 lv bituminous, Argonne sample).

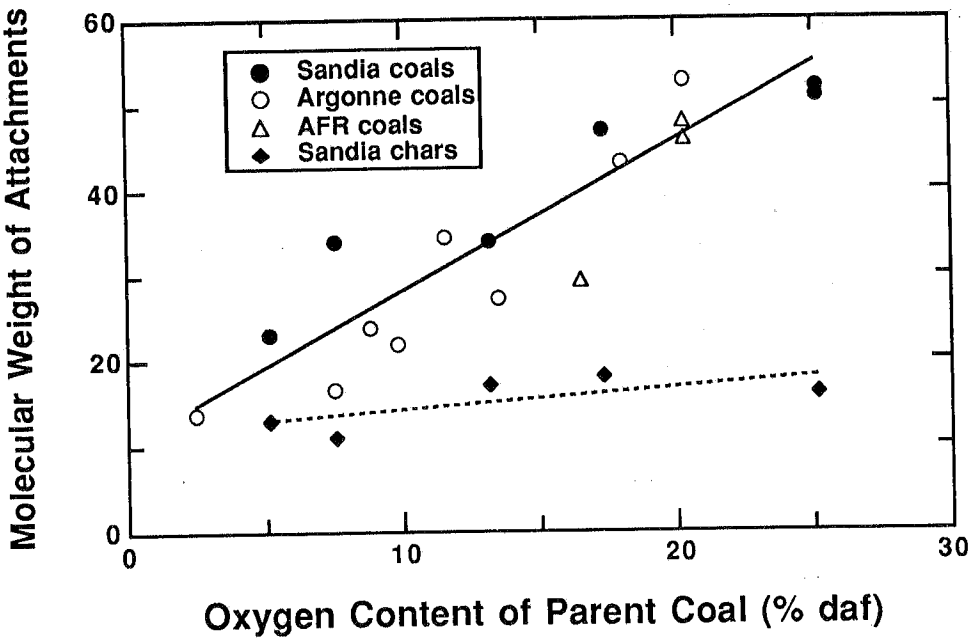

Figure 5.47 Average molecular weight of attachments to aromatic clusters in unreacted and fully-devolatilized coals as a function of coal type. Data for non-Sandia coals are taken from Solum, et al. [1989]. Fully-devolatilized chars are from the longest residence time (~ 250 ms) in the 1250 K gas condition in the CDL.

The fully-devolatilized chars are from the longest residence time (~ 250 ms) in the 1250 K gas condition in the CDL (in 100% N_2). The molecular weights of attachments for the fully-devolatilized chars vary from 18 to 11 amu, which is not a significant dependence on coal rank. The fully-devolatilized chars do not contain any labile bridges, and hence the attachments to the cluster consist solely of char bridges and side chains. The fact that the average molecular weight of attachments to aromatic clusters in the fully-devolatilized chars is low enough (11 to 18 amu) to compare with

bridges consisting of one atom (12 amu for carbon, 16 amu for oxygen). Low molecular weight side chains may consist mainly of methyl groups (15 amu) and OH groups (17 amu), which are more stable than longer side chains such as COOH or ethyl groups (C_2H_5).

Stable char bridges are thought to mainly consist of three types: (a) biphenyl bridges, where a bridge is formed between neighboring carbons on different aromatic clusters (Ar-Ar); (b) ether-type bridges where a single oxygen atom forms a bridge between neighboring clusters (Ar-O-Ar); and (c) a carbon bridge, thought to mainly consist of single carbon atoms between clusters (Ar-C-Ar). These three types of char bridges are illustrated in Fig. 5.48. Two bridges may link the same two aromatic clusters, and are defined here as a loop. Only the sum of bridges and loops is determined in the NMR analysis. The molecular weights of these three types of bridges are low enough to be consistent with the NMR data: 0 amu for the biphenyl bridge; 16 amu for the oxygen bridge; and 12 amu for the carbon bridge.

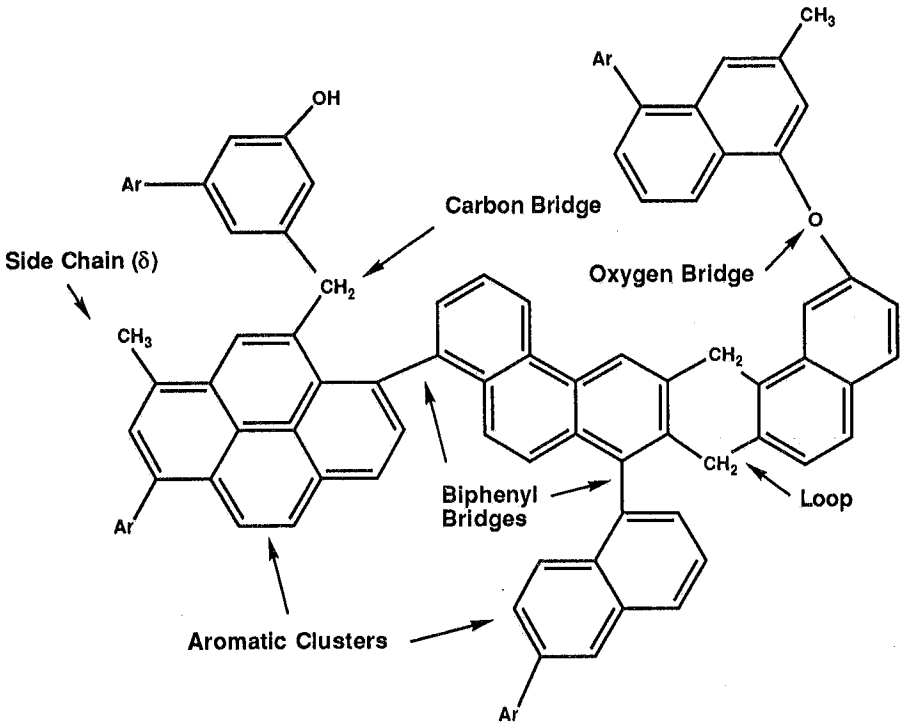

Figure 5.48 Characteristic chemical structures found in fully-devolatilized coal chars, illustrating the postulated forms of char bridges.

The NMR data obtained thus far from the coal and char samples obtained in the Sandia devolatilization experiments seem to be self consistent, and are of value in determining the chemical transformations that occur in the char and tar. The differences in chemical structure of the parent coal, such as the average cluster molecular weight and the average molecular weight of attachments, are smoothed

during the devolatilization process, and the chemical structures of the fully-devolatilized chars become remarkably similar. These data are currently being used as a test for the CPD model, so that the model agrees with tar and total volatiles mass release data of tar based on measured chemical mechanisms rather than empirical interpretation.

C. Evolution of Tar Structure

The devolatilization experiments conducted at Sandia were performed on the same coals used in a parallel set of experiments conducted at United Technologies Research Center (UTRC) [Freihaut, et al., 1989; Freihaut and Proscia, 1989; Seery et al., 1989]. The focus of the UTRC work was to characterize the tars produced during devolatilization using Fourier transform infrared (FTIR) spectroscopy. The tars produced in the Sandia experiments are analyzed using ^{1}H and ^{13}C NMR spectroscopy. This section describes the results of both ^{1}H and ^{13}C NMR analysis of the tars from both the bituminous coal and the lignite, collected as a function of residence time in the two gas conditions. The results for the Illinois #6 coal and Zap lignite have been published [Fletcher, et al., 1990b; Pugmire, et al., 1991]; data are shown here for tars from all five coals examined at Sandia.

Aromatic Structure

Perhaps the best indication of the extent of pyrolytic transformation of evolved tars is the changes in the carbon and hydrogen aromaticity. The carbon and hydrogen aromaticities of tars collected at the two gas temperature conditions, measured by standard ^{13}C and ^{1}H NMR spectroscopic techniques, are shown as a function of residence time in Figs. 5.49 for tars from the Illinois No. 6 coal. The fraction of coal released as volatile material is also shown for reference. The data points shown in these figures at zero residence time correspond to the aromaticities derived from solid-state ^{13}C NMR analyses of the parent coal. The hydrogen aromaticity $f_{a,H}$ of the parent coal is easily estimated from the the measured fraction of aromatic carbon with proton attachments f_a^H and the measured C/H ratio in the char, as follows:

$$f_{a,H} = \frac{f_a^P x_C}{M_C x_H} \tag{5.22}$$

where M_C is the molecular weight of carbon. For the Illinois No. 6 tar samples at 1250 K, the carbon aromaticity rises rapidly during the period of initial mass release and then continues to rise gradually to a final value of 0.97. The hydrogen aromaticity of the tars follows a similar pattern to that of the carbon aromaticity values. This continual rise in the aromaticity of the tar is in dramatic contrast to that observed for the char residue, where the carbon aromaticity (f_a') remains largely unchanged until the last stages of pyrolysis. The carbon and hydrogen aromaticities of tars from long residence times in the 1050 K gas condition are considerably lower than those seen in

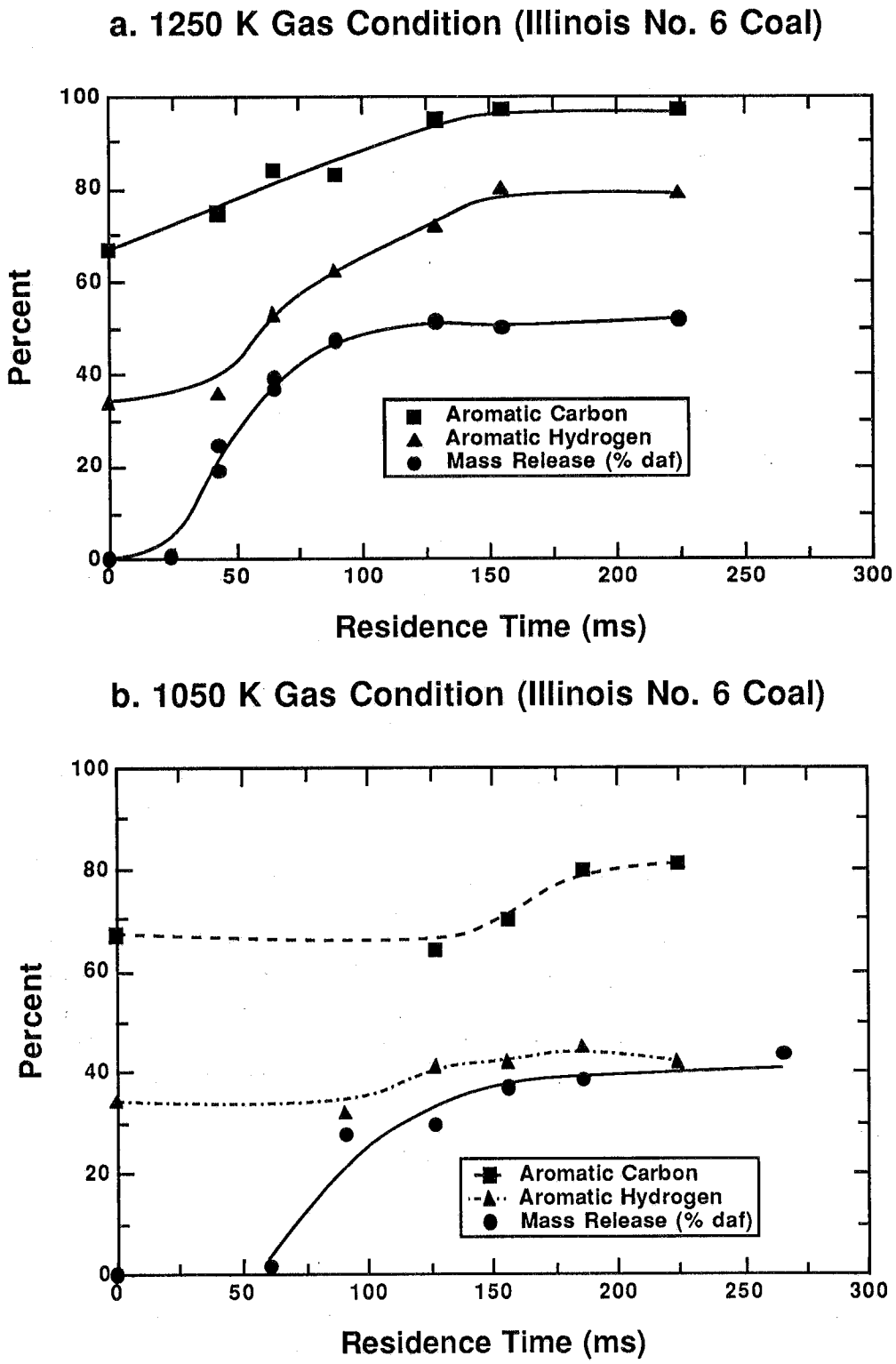

Figure 5.49 Percentages of hydrogen and carbon contained in aromatic groups in Illinois No. 6 coal tars vs. residence time in the 1250 K and 1050 K gas conditions. The hydrogen and carbon aromaticities at 0 ms are derived from NMR analyses of the parent coal.

the 1250 K gas condition. The hydrogen aromaticities actually double in tars at long residence times in the 1250 K gas condition. These data imply that gas phase secondary reactions occur in the evolved tars in the 1250 K gas environment but not in the 1050 K gas environment.

The hydrogen and carbon aromaticities in tars from four coals as a function of residence time are shown in Fig. 5.50. Tar data for the high rank coal (PSOC-1508D) are not available due to the small quantities of tar produced by this coal. The same trends appear in Fig. 5.50 as shown in Fig. 5.49 for the Illinois #6 coal. At the 1050 K gas condition, the hydrogen aromaticities rise gradually from about 30% in the initial tars released to 40% in the long residence times. The carbon aromaticities in the 1050 K gas condition increase from approximately 60% to a final state of ~ 75%. The aromaticity values for tars from the high temperature experiments (1250 K) exhibit a rapid initial increase similar to that observed in the Illinois No. 6 tars. However, the final carbon and hydrogen aromaticity values of the subbituminous coal and lignite tars are generally 10% (absolute scale) lower than those of the bituminous coal tars at both temperature conditions. This observation suggests that the fundamental differences in the structures of the parent coals are still manifest in the final pyrolysis products. Some of the differences between the components of these tars have been noted in the pyrolysis mass spectroscopy data of Lo et al. [1990], which are presented later in this report.

The aromaticities of the initial tars evolved at the 1250 K gas condition and the tars evolved at the 1050 K condition are very similar to the aromaticities of the parent coal. For example the tar from the Illinois #6 coal at 50 ms in the 1250 K condition exhibits carbon and hydrogen aromaticities that are within ~ 5% of the aromaticities of the parent coal and of the tars from the 1050 K condition. However, by 75 ms, the aromaticities of the tars start to increase due to cracking and polymerization reactions. The similarity of the coal tar to the parent coal structure is expected for the bituminous coals, but not expected for the low rank coals [Freihaut, et al., 1989; Solomon, and Hamblen, 1985].

The percentage of hydrogen in the tar attached to 1-ring, 2-ring, and 3-ring or greater condensed aromatic species can be estimated from the ^{1}H NMR data, as shown in Figs. 5.51 for the tars from Illinois #6 coal collected at the two different gas temperature conditions. These data reveal some of the more subtle changes that occur in the tars in the gas phase. The percentage of hydrogen in aromatic structures with three or more rings increases in the Illinois No. 6 tars as a function of residence time at the 1250 K gas condition (Fig. 5.51), seemingly at the expense of the hydrogen in 1-ring aromatic structures, which decreases as a function of residence time. Tars collected at a residence time of 223 ms contain twice as much hydrogen in aromatic structures with three or more rings than the initial tars evolved during the 40-70 ms residence time period. The hydrogen in 2-ring aromatic structures also increases substantially at this temperature condition. In contrast, the data obtained from tars collected at the 1050 K gas condition, although somewhat scattered, do not show any such trend.

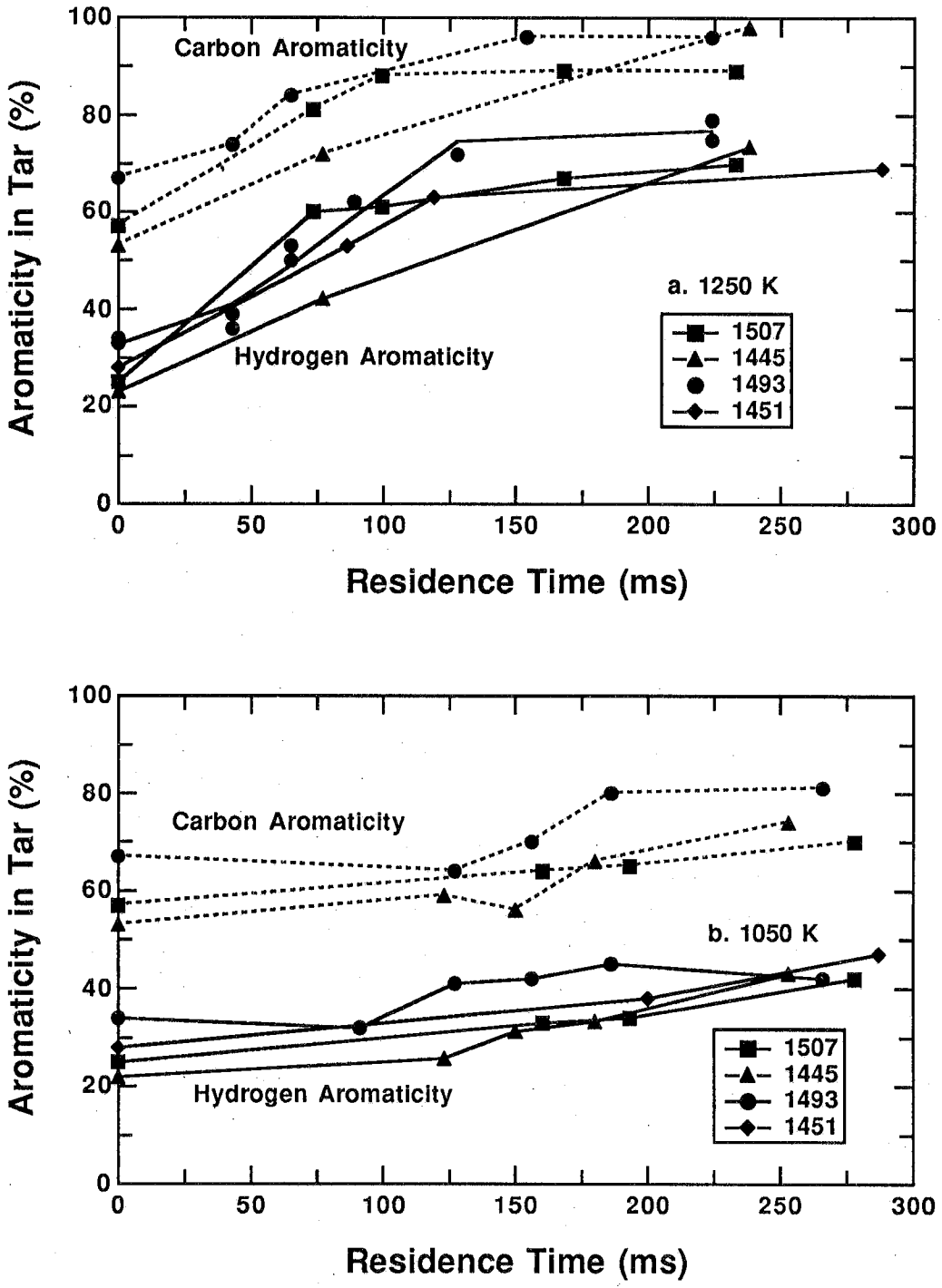

Figure 5.50 Percentages of hydrogen and carbon contained in aromatic groups in coal tars vs. residence time in the 1250 K and 1050 K gas conditions. The hydrogen and carbon aromaticities at 0 ms are derived from NMR analyses of the parent coal.

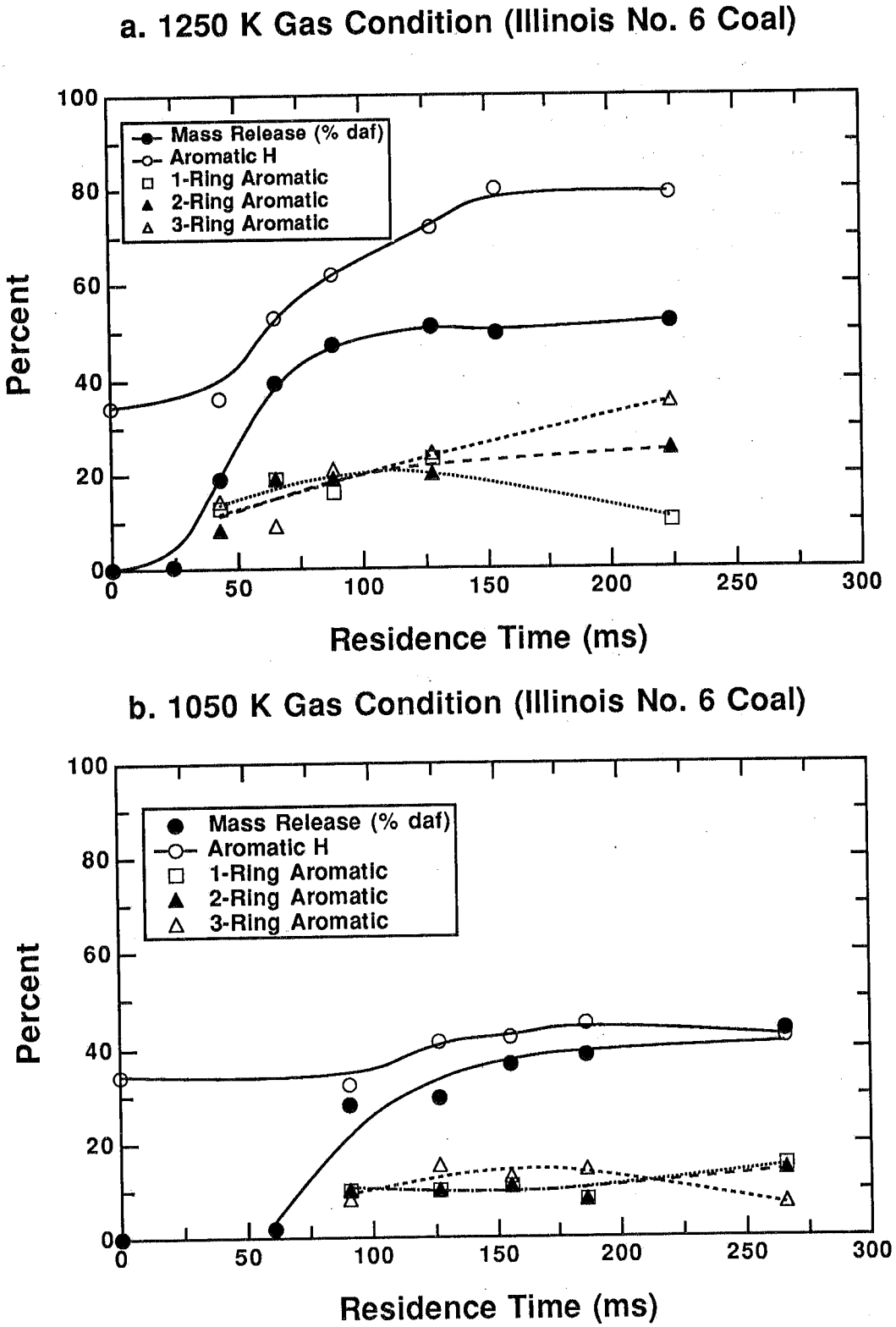

Figure 5.51 Percentage of hydrogen contained in aromatic structures in Illinois No. 6 coal tars consisting of one, two, and three or more rings vs. residence time in the 1250 K and 1050 K gas conditions.

The hydrogen aromatic ring data (Fig. 5.52) for subbituminous coal and lignite tars exhibit patterns similar to those observed in the bituminous coal tars. However, the decrease in the concentration of one-ring aromatic compounds in tars collected from the lignite at long residence times in the 1250 K gas condition is not quite as great as observed in the bituminous and subbituminous coal tars. However, the pyrolysis mass spectroscopy data for the lignite tars [Lo, et al., 1990; Fletcher and Hardesty, 1990b] show decreases in 1-ring compounds and increases in multi-ring compounds as a function of residence time in the 1250 K gas condition. The implication is that gas phase secondary reactions of coal tar may be somewhat independent of coal type.

The evolution of condensed polynuclear aromatic species can occur by two different processes: 1) dehydrogenation reactions such as the conversion of tetralin type species to napthalenes, etc.; and 2) ring condensation reactions such as those associated with the formation of soot precursors where aliphatic side chains serve as sites for polymerization and subsequent dehydrogenation to form condensed polynuclear aromatic species.

Aliphatic structure

The aliphatic hydrogen attached to carbons at the α–, β–, and γ–positions (relative to an aromatic group as defined in Fig. 5.53) and measured by ^1H NMR is classified into methyl groups (CH_3) and the combination of CH and CH_2 groups. For tars from the Illinois No. 6 coal in the 1250 K gas condition, the hydrogen in the β– and γ-positions decreases from 19% to 4% during the period of mass release, as shown in Fig. 5.54a. These data indicate preferential release, at 1250 K, of β- and γ-hydrogen relative to α-hydrogen, and suggest that CH_3 or remote CH and CH_2 groups are released preferentially to the α-CH and CH_2 groups. The release of aliphatic chain ends is more energetically favored than breakage of fairly stable aliphatic bridges and loops between aromatic structures. The number of hydrogens associated with γ-CH_3 groups decreases quite rapidly in the gas phase to only approximately 1% of the total hydrogen present in the tar. The decrease in α-methyl hydrogen concentration by a factor of four indicates a low concentration of methyl groups attached to aromatic rings at the final stage of pyrolysis. On the other hand, the total hydrogen present at the α-position only drops approximately 50% and a relatively large fraction of the total protons observed in the final tar are present on functional groups (i.e., CH, CH_2 and CH_3) adjacent to the aromatic rings. The low concentration of α-CH_3 and β- and γ-groups requires the presence of three- to four- fold more CH and CH_2 groups than methyl groups at the α-position. The CH and CH_2 groups are probably present in the form of bridges between aromatic rings or loops (hydroaromatic structures), as shown earlier in Fig. 5.48 for coal chars. These data are consistent with the processes associated with formation of condensed polynuclear aromatic species discussed previously.

The bituminous coal tars from the 1050 K gas condition exhibit different behavior as a function of residence time than the tars from the 1250 K condition. The concentration

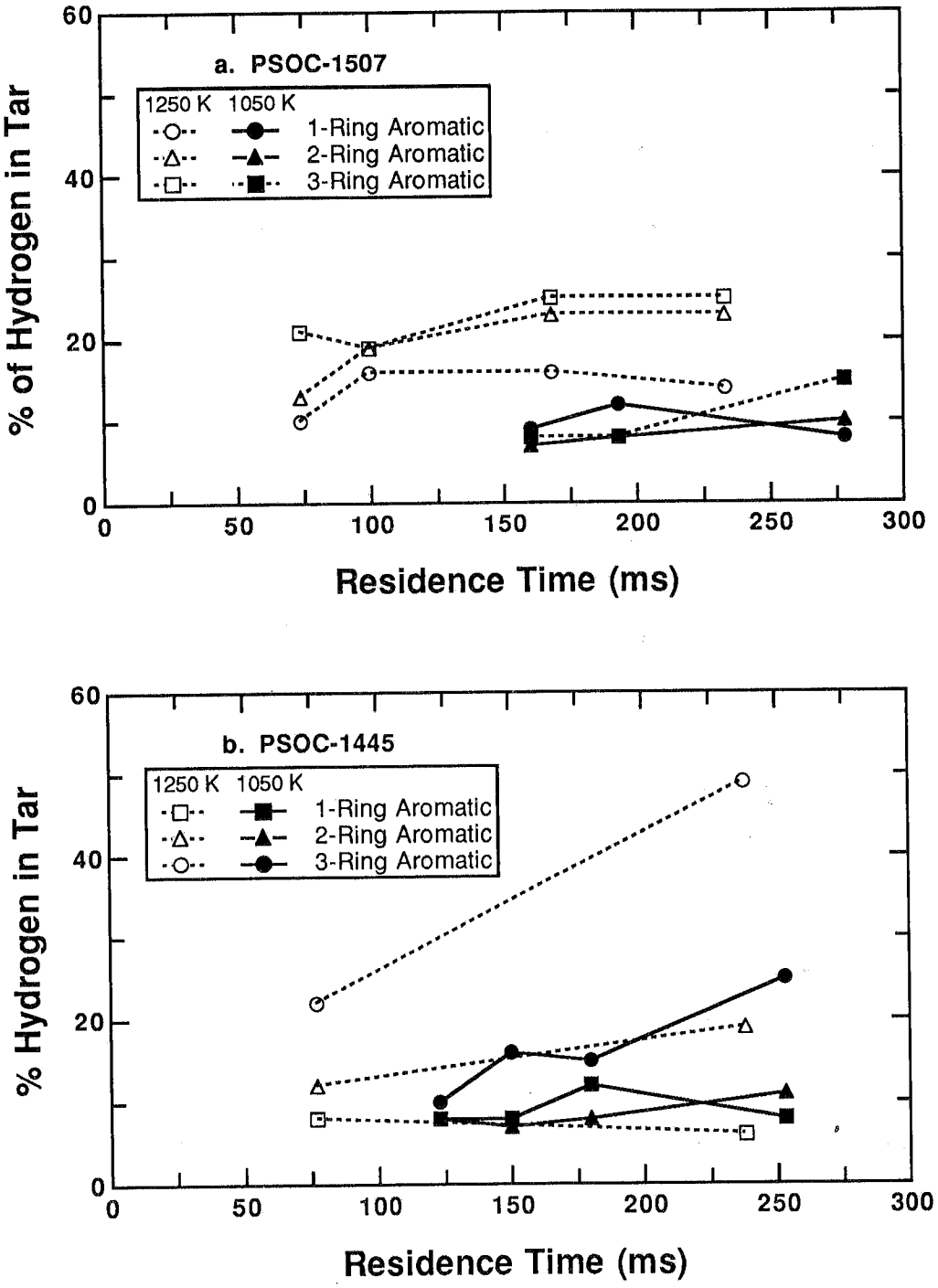

Figure 5.52 Percentage of hydrogen contained in aromatic structures in the tars from (a) Beulah Zap lignite and (b) Blue #1 subbituminous coal consisting of one, two, and three or more rings vs. residence time at the 1250 K and 1050 K gas conditions.

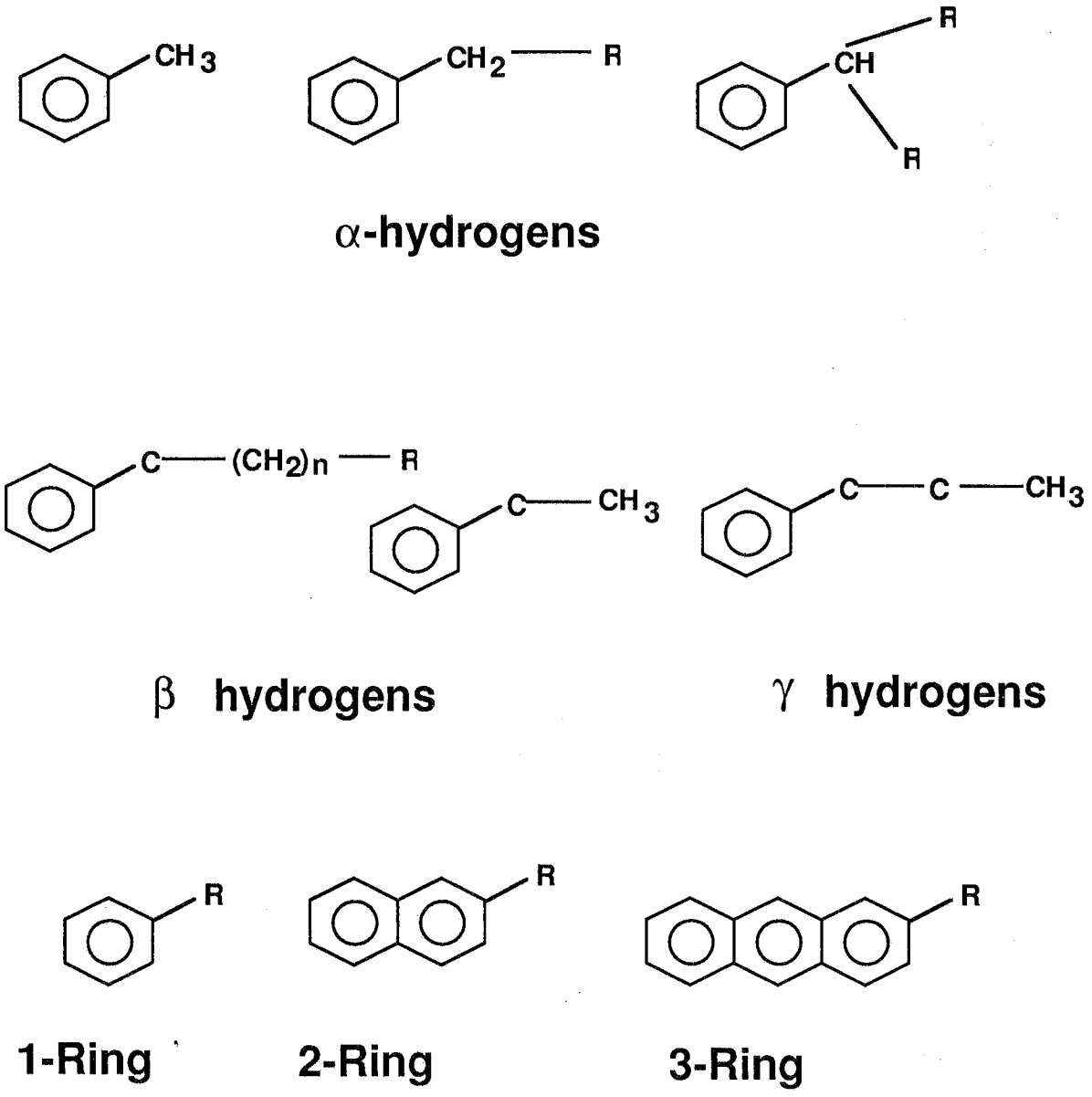

Figure 5.53 Representative chemical structures detected by ^{1}H NMR spectroscopy.

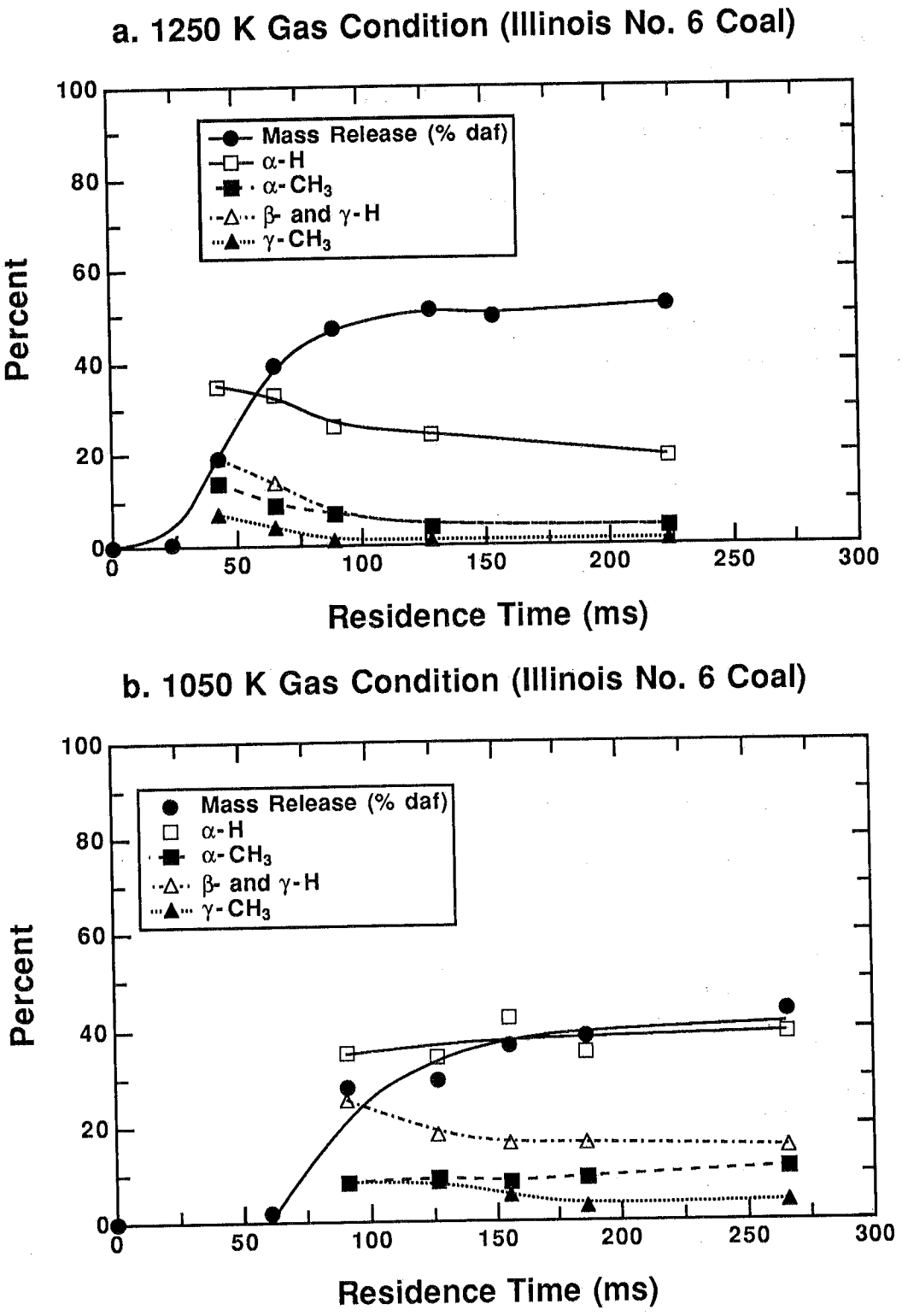

Figure 5.54 Percentage of hydrogen contained in aliphatic structures in Illinois No. 6 coal tars, with hydrogen in the α, β, or γ position relative to the aromatic ring, vs. residence time in the 1250 K and 1050 K gas conditions.

of β- and γ- hydrogens decrease by only 50% in the gas phase. The concentration of γ-CH_3 groups drops by a factor of two, but the amount of α-CH_3 groups present actually increases slightly. This observation, together with the overall increase in α-hydrogen, indicates that the cracking of β- and γ- groups from the aromatic rings leaves an increasing amount of α-CH_3 groups intact. Furthermore the overall increase in α-hydrogen demonstrates that structures such as ethylene bridges and loops (two α-carbons per bridge) are not substantially disrupted in the gas phase reactions at 1050 K.

Tars obtained from other coals exhibit similar characteristics to the tars obtained from the Illinois #6 coal, and the results are summarized in Figs. 5.55 and 5.56. The initial tar from the 1050 K gas condition is compared with the long residence time tar from the 1250 K condition to show the effects of gas phase reactions of tar. The decrease in α-hydrogen in the 1250 K gas condition is rank-dependent; the lignite tar does not lose α-hydrogen while the Pittsburgh #8 coal tar shows the most severe decrease in α-hydrogen. The decrease in α-H is greater than the decrease in α-CH_3; hence, the initial release of tar appears to be rich in CH and/or CH_2 groups present as ethylene bridges or in hydroaromatic species. The chemical structures of the initial tars produced exhibit a dependence on coal rank; the initial tars from the low rank coals contain more β- and γ-hydrogen, while the initial tars from the high rank coals are enriched in α-hydrogen. The tars from all of the coals in the 1250 K condition exhibit a 30 to 80% decrease in the concentration of β- and γ-hydrogen, based on the concentrations measured in the initial tars.

The chemical structures in the final tars produced in the 1250 K condition do not vary significantly as a function of coal rank. A significant amount of α-hydrogen remains in the final tars from the 1250 K condition, as opposed to the drastic reduction in β- and γ-hydrogen in these same tars. Since the α-CH_3 concentration in the final tars from the 1250 K condition is low, the majority of the α-H is present in CH and CH_2 groups. Since the final tars at the 1250 K condition contain very little β- and γ-hydrogen, these CH and CH_2 groups are most likely contained in one-carbon bridges between aromatic clusters, in a manner similar to the carbon bridges in fully-devolatilized coal chars (see Fig. 5.48).

In the tars obtained at 1050 K, the β- and γ-hydrogen content decreases by nearly 30% while the γ-CH_3 and α-CH_3 groups are essentially invariant. Furthermore, the concentration of α-hydrogen containing groups increases slightly in some of the coal tars from the 1050 K condition at long residence times. The loss of material associated with relatively long chain functional groups (i.e., chains with three or more carbons) without a concomitant loss of γ-CH_3, α-CH_3, and α-hydrogens suggests the loss of substances such as paraffins and/or biomarkers that are released at the lower temperature [Meuzelaar, et al., 1989; Yun, et al., 1989] whereas, at higher temperatures, they may become incorporated into the metaplast before the material can be released into the gas phase.

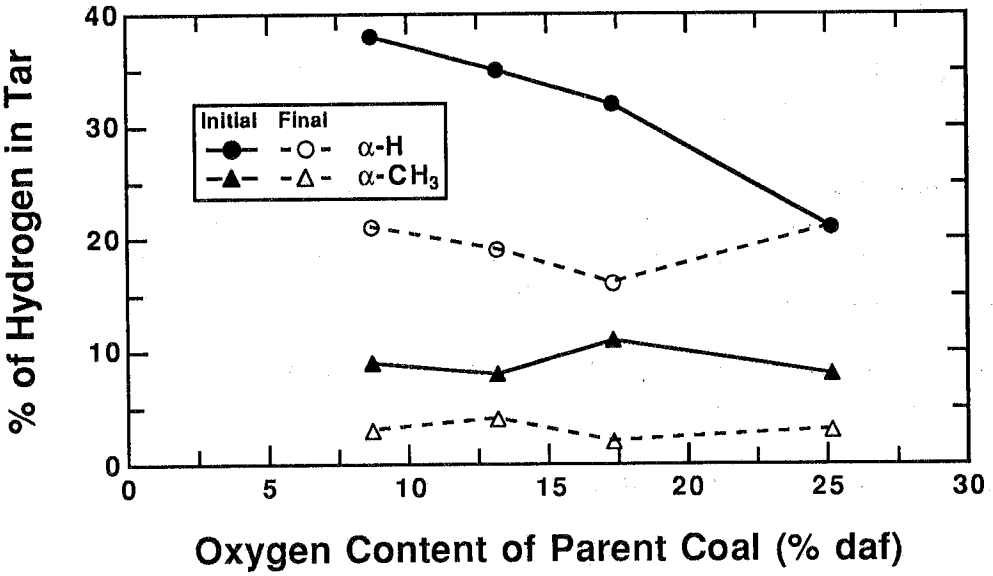

Figure 5.55 Reduction in the percentage of α-H and α-CH_3 in tars from four coals in the 1250 K gas condition. The initial tar is taken from the earliest residence time in the 1050 K gas condition; the final tar is taken from the longest residence time in the 1250 K gas condition.

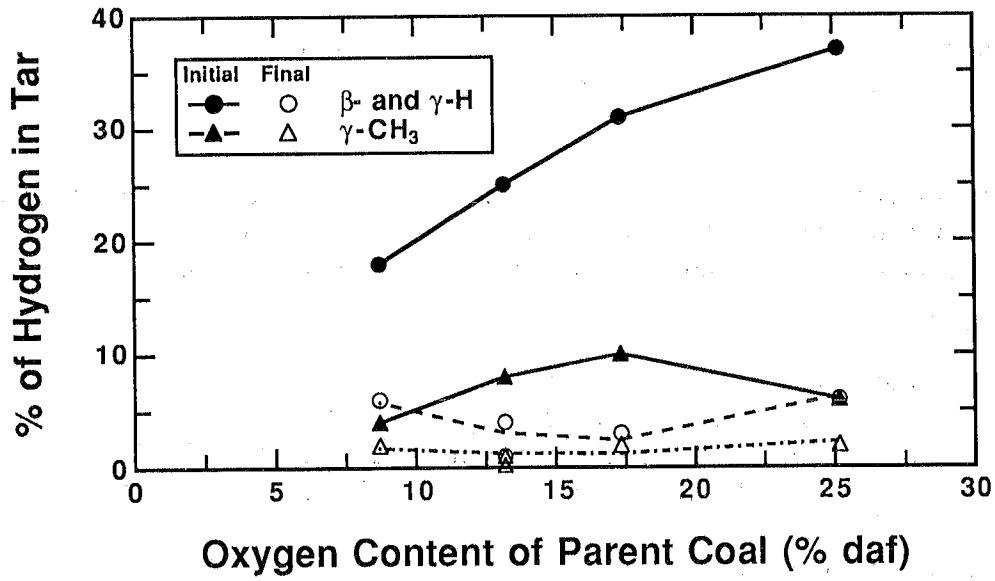

Figure 5.56 Reduction in the percentage of β- and γ-H in tars from four coals in the 1250 K gas condition. The initial tar is taken from the earliest residence time in the 1050 K gas condition; the final tar is taken from the longest residence time in the 1250 K gas condition.

D. Conclusions

Char Structure

Based on the NMR analysis of the chars formed during devolatilization of five coals of different rank at the 1250 K gas condition, the following conclusions are reached:

1) NMR data can be used to track lattice parameters associated with average cluster size and cross linking reactions. Under rapid heating conditions the NMR data demonstrates that the Zap lignite undergoes early cross linking behavior, while higher rank coals exhibit a slower overall rate of crosslinking.

2) Under rapid heating conditions (10^4 K/sec), the data exhibit: a) little evidence of cluster size growth in the macromolecular structure; b) crosslinking at the same time that aliphatic carbons are released; c) little evidence for graphitization under the temperature and residence time conditions of these experiments.

3) In the Illinois No. 6 coal, most of the mass release has occurred before significant changes in carbon aromaticity has occurred. In chars from Zap lignite, the changes in carbon aromaticity occur much earlier than for the bituminous coal.

4) The carbon skeletal structure of the final chars from coals of all ranks are quite similar, even though the structures of the initial coals are quite different.

Tar Structure

Based on the ^1H and ^{13}C NMR analysis of the tars collected from four coals of different rank in the 1250 K and 1050 K gas conditions, the following conclusions are reached:

1) The pyrolysis temperature has a major effect on the tar structure. The proton and carbon aromaticities of the tars from a given coal in the 1250 K gas condition are higher than for samples collected at comparable extents of mass release in the 1050 K gas condition.

2) The carbon aromaticities of the bituminous and subbituminous coal tars at 1250 K are higher than the values for the corresponding chars collected at the same residence time. On the other hand, the carbon aromaticities found in the Zap lignite tars are comparable to those observed in the chars.

3) The proton NMR data suggest that in the 1250 K gas condition, hydrogens associated with 2- and 3-ring aromatic compounds increase, while that of 1-ring compounds decrease for the Illinois No. 6 tars. Similar but less compelling evidence is noted for the lignite and subbituminous coal tars. These data may suggest the conversion of hydroaromatic species to condensed polynuclear aromatic species and/or ring polymerization.

4) The α-hydrogen content in the initial tars evolved increases as a function of coal rank. The α-hydrogen in the tars from the three non-lignitic coals decreases with residence time at the 1250 K condition but not at the 1050 K condition. This observation suggests that relatively stable CH and/or CH_2 bridges exist at the 1050 K gas condition in the higher rank coals. However, at 1250 K substantial bond rupture may be occurring.

5) The α-methyl groups are released early in tars from all four coals at 1250 K, but do not decrease significantly at 1050 K.

6) The γ-methyl groups in both tars are the most susceptible to cracking reactions in the gas phase, but the extent of release of the β- and γ-hydrogens is based on gas temperature conditions and residence time. The percentage of γ-methyl groups in the initial tar evolved decreases as coal rank increases.

The NMR data presented here for char and tar samples from the CDL have led to greater understanding of the pyrolysis process. The chemical percolation devolatilization (CPD) model [Grant, et al., 1989; Fletcher, et al, 1990a; Fletcher et al., 1991] currently uses such information on the chemical structure of coal as input parameters.

Chemical Structure of Tar Determined from Mass Spectrometry

Tars collected in the CDL were analyzed at the University of Utah using two different mass spectrometric techniques, in collaboration with Professor Henk Meuzelaar. Curie-point desorption low voltage mass spectrometry (LV/MS) was used to provide a first-order analysis of the composition of the tar samples. Tar samples were subsequently analyzed by Curie-point gas chromatography/mass spectrometry (GC/MS) to confirm the LV/MS results and to provide further detail. These MS data are presented in graphical form only, and are not tabulated in the appendix.

A. Curie-Point Desorption Low-Voltage Mass Spectrometry Analyses

Low-voltage mass spectra of tars obtained by Curie-point desorption directly in front of the ion source are shown in Fig. 5.57a-e for two different coals. Beulah Zap tar samples obtained in the 1250 K gas condition at 70 ms and 250 ms are compared in Figs. 5.57a and 5.57b. Comparison of these two samples shows (1) a marked decrease in hydroxyaromatic signals (e.g., alkylsubstituted phenols, dihydroxybenzenes, and naphthalenes) accompanied by (2) a strong increase in polycondensed aromatic hydrocarbons (e.g., phenanthrenes and pyrenes) in the 250 ms sample (organic structures are illustrated in Fig. 5.58). The marked change in the nature of the tars collected at 70 and 250 ms is attributed to secondary reactions of tar in the gas phase, subsequent to release from the coal particle. Especially significant

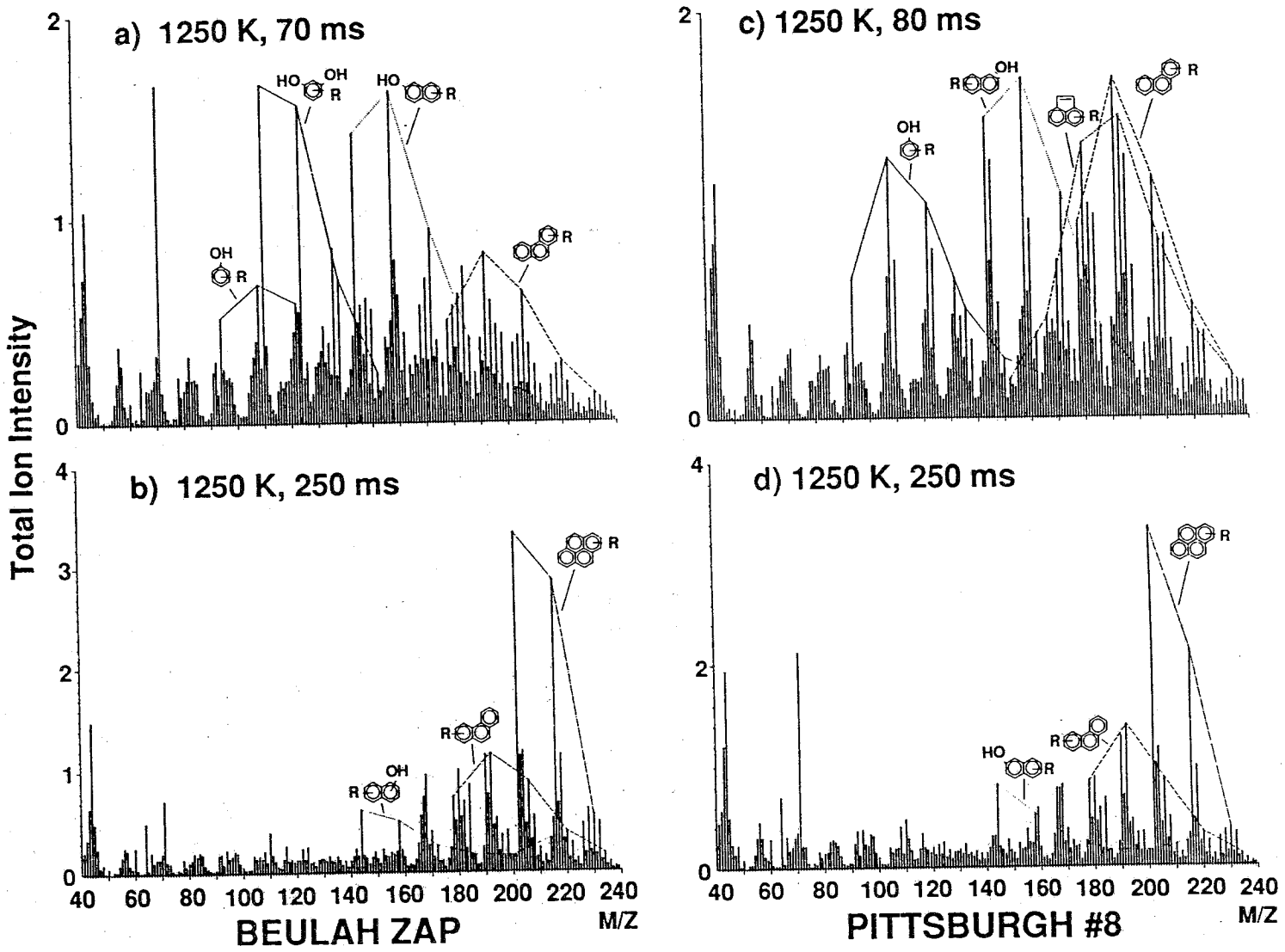

Figure 5.57a-d Curie-point desorption mass spectra of Beulah Zap and Pittsburgh #8 tars showing the effects of coal rank (a and b vs c,d, and e), residence time (a and c vs. b,d, and e) and gas temperature (e vs. a,b, c, and d).

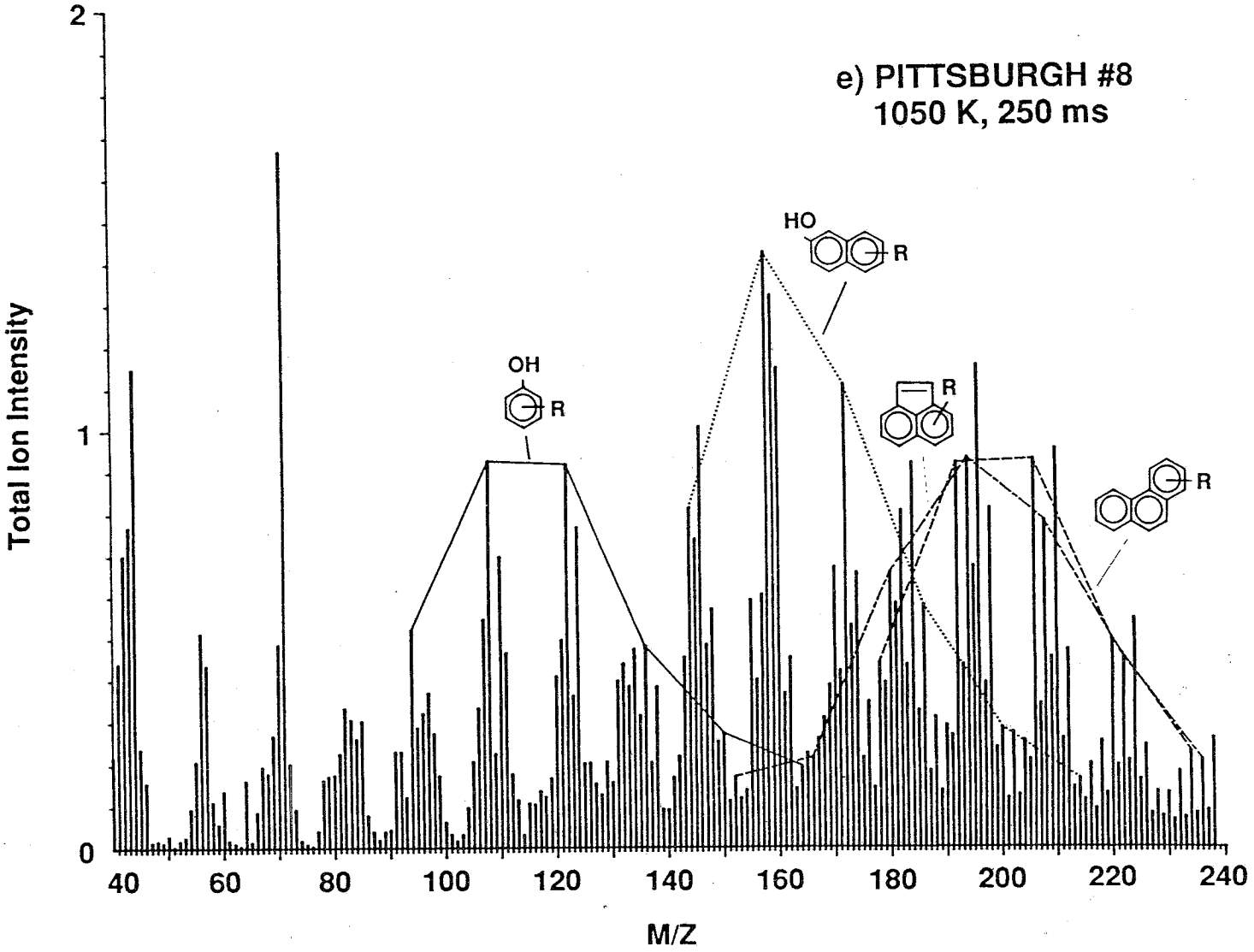

Figure 5.57e Curie-point desorption mass spectra of Pittsburgh #8 tar from the 1050 K gas condition. Compare with Figures 5.57a, b, c, and d.

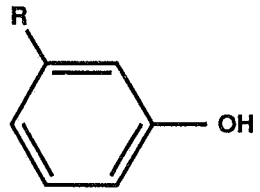

alkyl phenol

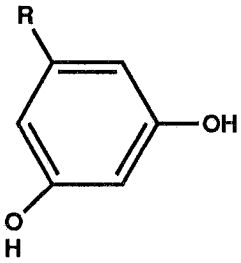

dihydroxybenzene

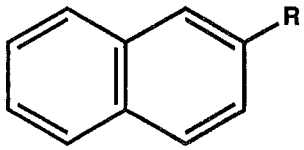

naphthalenes

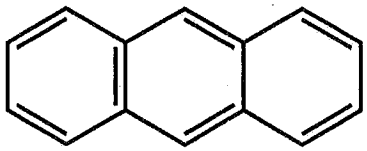

anthracene

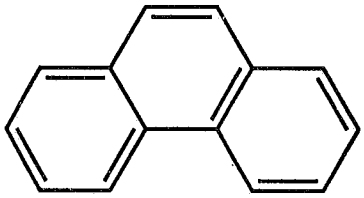

phenanthrene

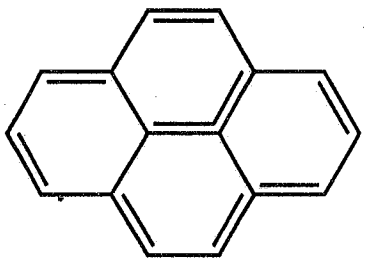

pyrene

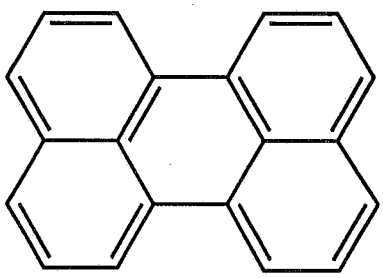

perylene

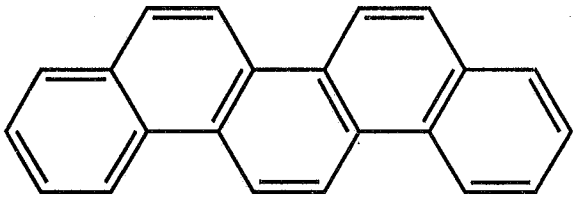

picene

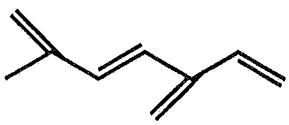

terpene

Figure 5.58 Structures of organic compounds referred to in the mass spectrometric analyses of coal tars.

is the dominance of unsubstituted pyrene among the various alkylsubstituted homologs. This is a telltale sign of high temperature gas phase reactions and may perhaps be seen as a first step in the direction of soot formation.

The Beulah Zap tar pattern at 70 ms, on the other hand, compares well with direct Curie-point pyrolysis mass spectra of North Dakota coal [Metcalf, et al., 1987]. This indicates that at 70 ms, primary pyrolysis products (e.g., dihydroxybenzenes) still dominate, although the yield of polycondensed aromatic hydrocarbons (e.g., alkyl phenanthrenes) is already higher than would be observed under vacuum micropyrolysis conditions.

The tar patterns of Pittsburgh #8 coal at 1250 K (Figs. 5.57c and d) are in excellent agreement with the observations from tars from the Beulah Zap lignite. The short residence time pattern (80 ms) corresponds quite well with the Curie-point pyrolysis mass spectrum, as reported by Chakravarty et al. [1988], whereas the long residence time (250 ms) tar shows a pronounced shift towards polycondensed aromatic hydrocarbon. Due to the higher rank (hva bituminous) of the Pittsburgh #8 coal, however, the short residence time spectrum (Fig. 5.57c) is clearly different from that of the Beulah Zap lignite. For example, the tar from the Pittsburgh #8 coal exhibits lower (alkyl) dihydroxybenzene intensities and increased (alkyl) naphthalene series than tar from the Beulah Zap lignite. This is in agreement with trends observed in earlier LV-MS studies of coals of different rank [Meuzelaar, et al., 1984]. The higher oxygen content of the lignite tar is consistent with the increased oxygen content of low rank coals.

Finally, the effect of temperature is briefly illustrated by comparison of Figs. 5.57c and 5.57e (Pittsburgh #8, 70 ms at 1250 K vs. 250 ms at 1050 K). In spite of the long residence time (250 ms), the MS pattern in Fig. 5.57e is highly similar to that in Fig. 5.57c, indicating the absence of marked secondary reactions at this lower temperature.

B. Curie-Point Desorption Gas Chromatography/Mass Spectrometry Analyses

The Curie-point desorption GC/MS technique confirms and further elucidates the trends observed in the LV/MS analyses, as illustrated in Figs. 5.59 and 5.60. Illinois #6 tar sampled at 250 ms (Fig. 5.60) in the 1250 K gas condition shows an approximate 100-fold reduction in the relative abundance of (alkyl) phenols (intensities in left-hand panels of Fig. 5.60 are multiplied by 100) relative to the tar sampled at 70 ms (Fig. 5.59). A corresponding ten-fold increase in selected polycondensed (4-6 ring) aromatic hydrocarbons is observed in the 250 ms sample (compare scaling factors of right-hand panels of Figs. 5.59 and 5.60).

Changes in relative composition as a function of residence time are illustrated for New Mexico Blue tars at 1050 K in Fig. 5.61 and for Beulah Zap, Illinois #6, and Pittsburgh #8 tars in Figs. 5.62a, b, and c, respectively. At 1050 K, fragment ions of aliphatic

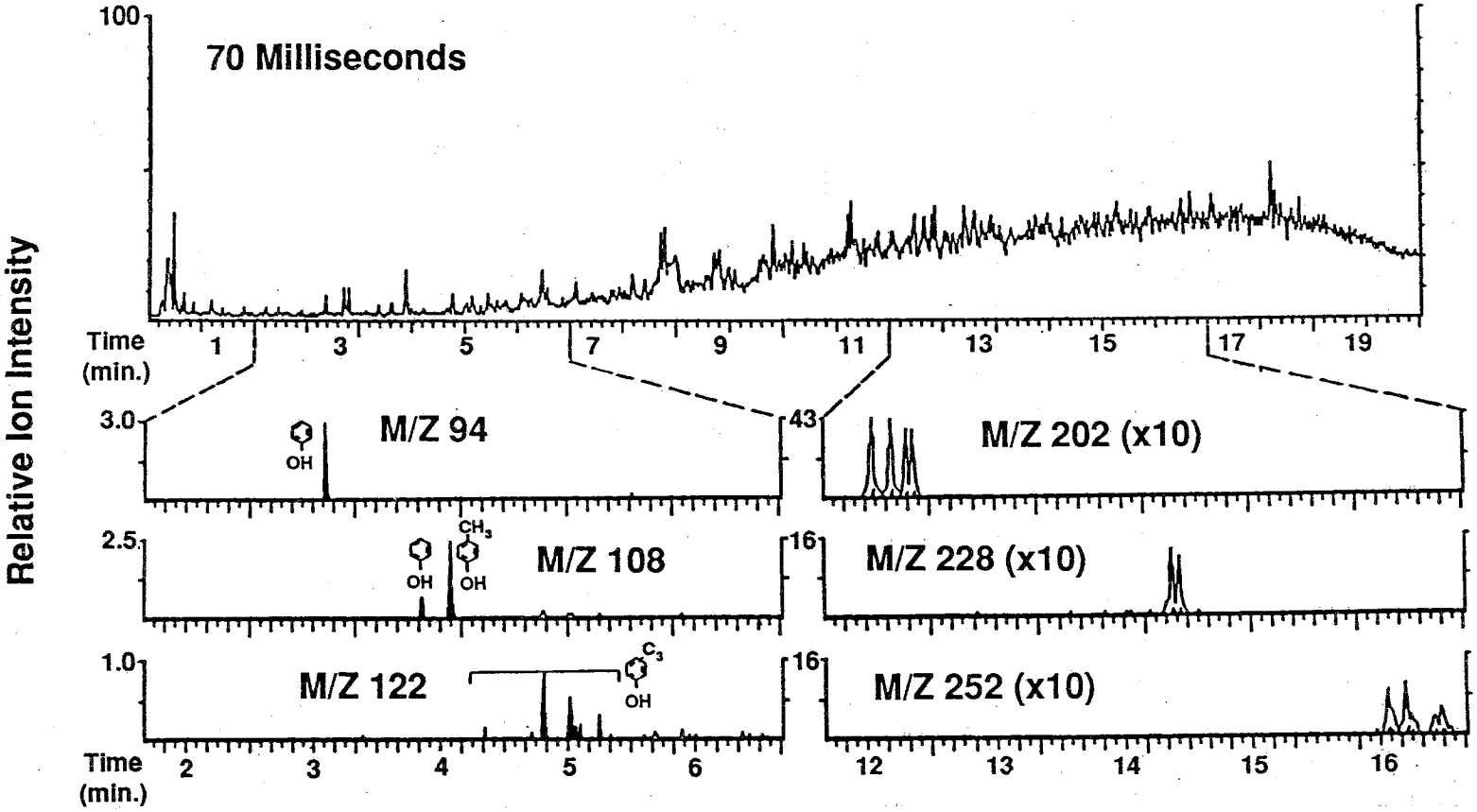

Figure 5.59 Curie-point desorption GC/MS profiles of Illinois #6 tar obtained at 1250 K after 70 ms. Total ion chromatogram (upper profile) and selected ion chromatograms (lower profiles) show relative abundance of (alkyl) phenols vs. pyrenes, perylenes, and picenes.

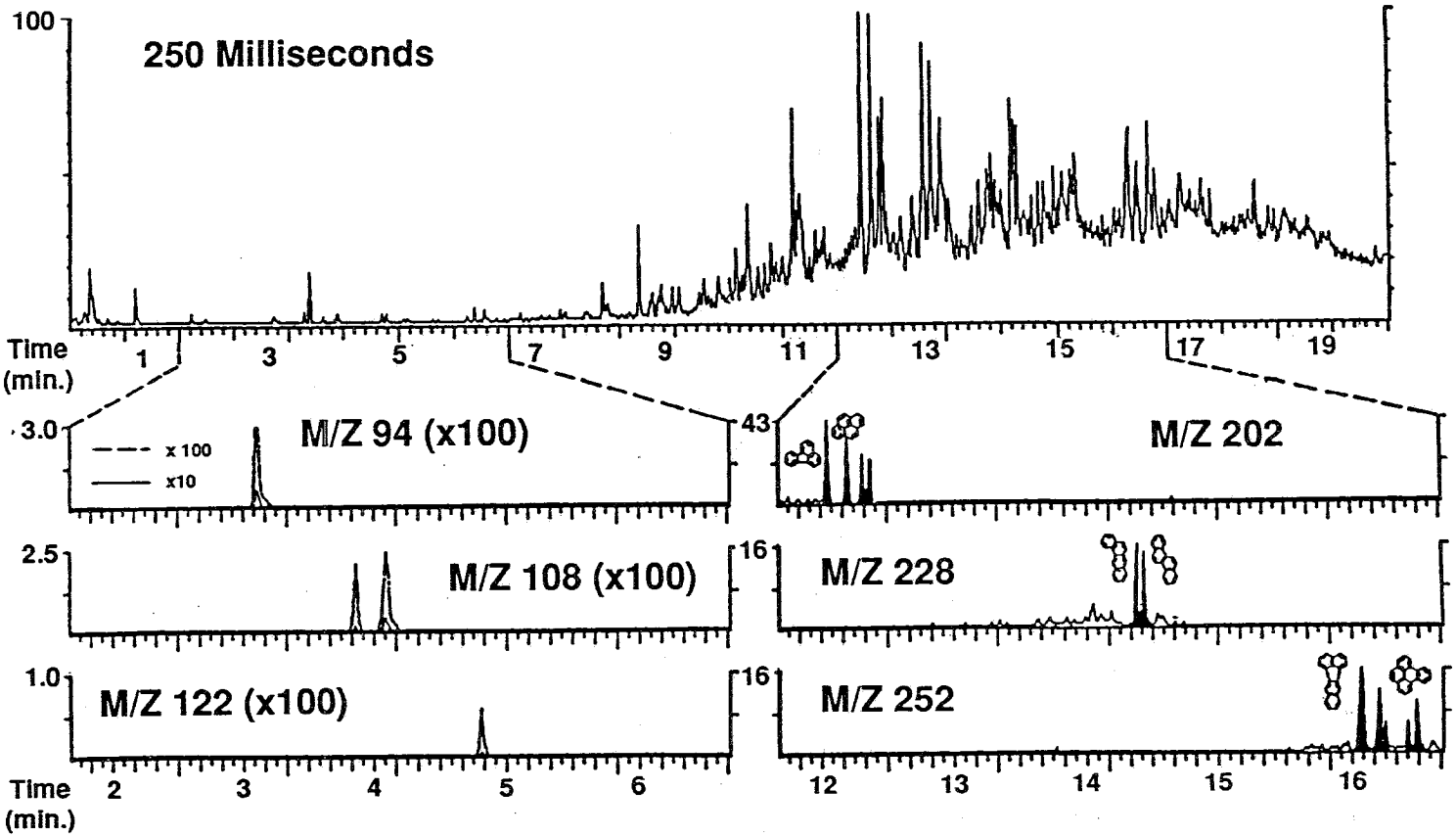

Figure 5.60 Same as Fig. 5.59 but obtained after 250 ms. Note 100-fold decrease in (alkyl) phenol as opposed to 10-fold increase in polynuclear aromatic hydrocarbons.

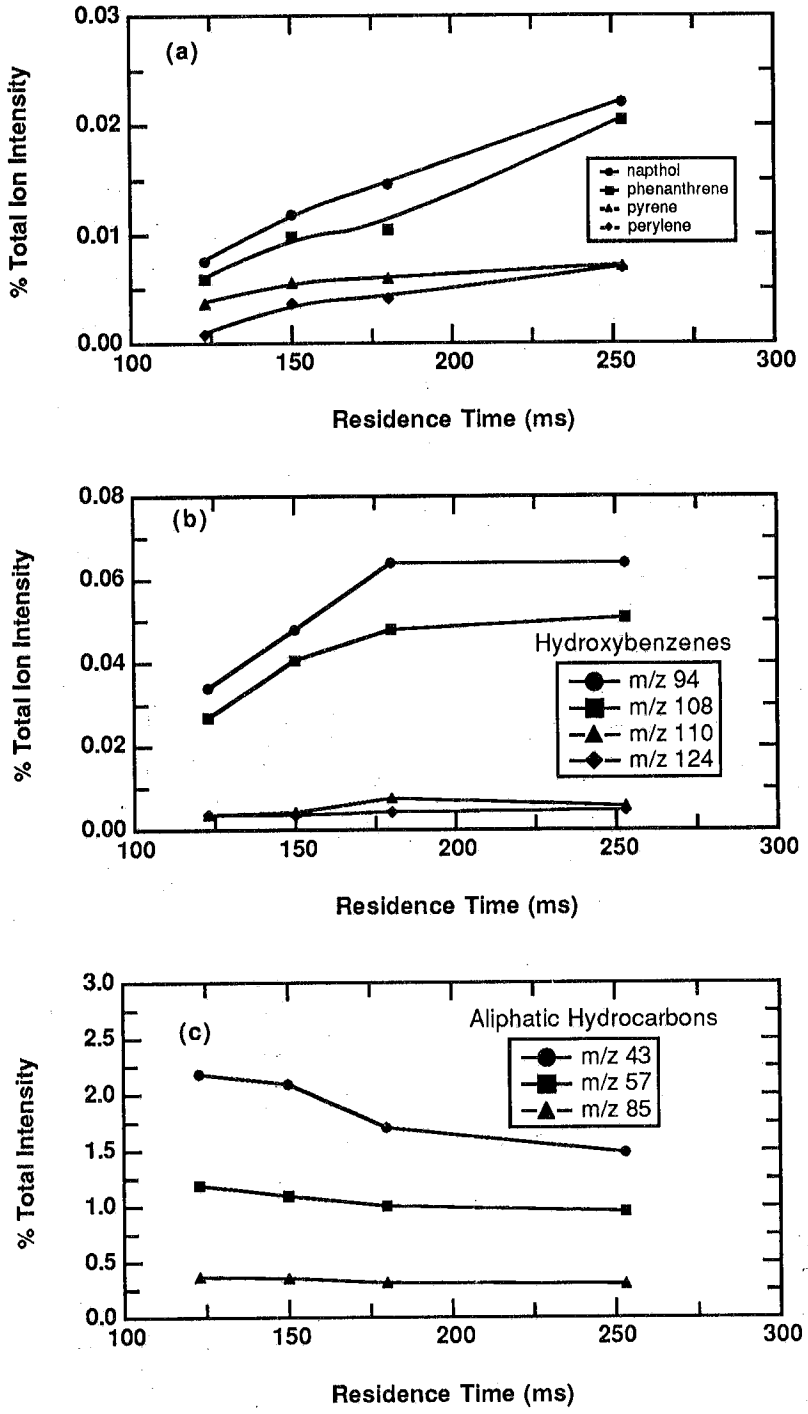

Figure 5.61 Relative abundance of selected ion profiles in Curie-point desorption GC/MS data on New Mexico Blue tar samples obtained in the 1050 K gas condition at different residence times.

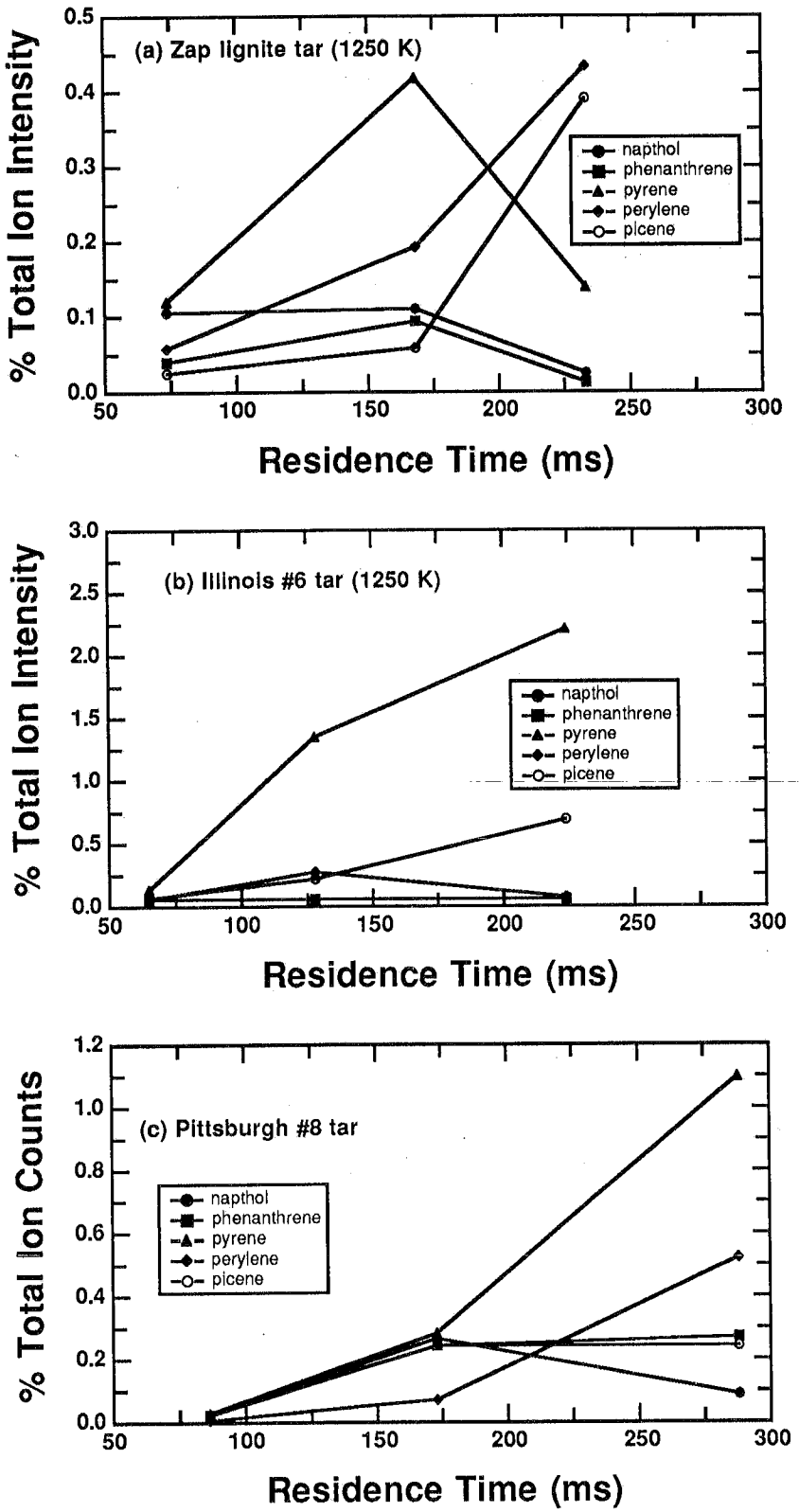

Figure 5.62 Same as Fig. 5.61 but representing tars from three different coals obtained in the 1250 K gas condition.

hydrocarbons (e.g., at m/z 85, 57, 43, in Fig. 5.62c) dominate the short residence time (120 ms) tar. Based on previous, time-resolved pyrolysis field ionization MS studies [Yun, et al., 1990], early evolution of aliphatic hydrocarbon moieties during devolatilization of low-rank coals is likely to represent the desorption of low MW biomarker-type compounds (e.g., branched and/or alicyclic terpenoids). At 150 ms the relative intensities of the aliphatic hydrocarbon moieties start to decrease due to the strong increase in hydroxyaromatics (e.g., dihydroxybenzenes at m/z 110 and 124, Fig. 5.61b). At 250 ms, the relative abundance of compounds such as naphthols are still increasing, suggesting that the devolatilization process may not yet be fully completed. However, suspected secondary reaction products such as pyrenes and perylenes are starting to increase slightly. Nevertheless, the relative abundance of the highly reactive dihydroxybenzenes appears to be more or less stable. Altogether, the conclusion is that at 1050 K the devolatilization process of New Mexico Blue coal is close to being complete after 250 ms.

A much different picture is obtained at 1250 K, as illustrated for the three coals in Fig. 5.62. Concentrations of compounds such as pyrenes, perylenes, and even picenes appear to increase continuously after the first sampling position, whereas the relative abundances of naphthols and even phenanthrenes decrease after approximately 100-150 ms. This is further evidence of marked secondary gas-phase reactions. The above observations at 1050 and 1250 K suggest that devolatilization at 1150 K should be completed within 100-200 ms, and that the onset of secondary gas-phase reactions should become clearly visible at longer residence times. A set of experiments will be performed during the next quarter to collect and analyze tar and char samples at (a) an 1150 K gas condition, and (b) longer residence times in the 1050 K gas condition.

C. Comparison with ^{1}H and ^{13}C NMR Analyses

The same tars examined in this study were analyzed previously by ^{1}H and ^{13}C NMR spectroscopy [Fletcher, et al., 1990b, Pugmire, et al., 1991]. The NMR data indicate that tars evolved from the Illinois #6 coal are similar in chemical structure to the parent coal. In the 1250 K gas condition, the NMR data indicate that tar reacts in the gas phase, while little or no evidence of gas phase reaction of tars is indicated in the 1050 K gas condition. The tar samples collected at long residence times (250 ms) in the 1050 K gas condition were similar in chemical structure to the initial tar evolved in the 1250 K gas condition (70 ms). The tar samples collected at long residence times (250 ms) in the 1250 K gas condition exhibited: (1) a decrease in 1-ring aromatic compounds; (2) an increase in aromatic ring compounds with 3 or more rings; (3) an increase in the carbon and proton aromaticity (at the expense of aliphatic material); and (4) a decrease in the aliphatic carbons in the β and γ positions relative to the aromatic rings.

The LV/MS and GC/MS data presented here are consistent with the NMR data, and show further detail regarding gas phase reaction of specific organic compounds in the tar. For example, one ring compounds indicated in the MS analyses of the tars are alkyl phenols and dihydroxybenzenes; these compounds were shown to decrease in

abundance in the long residence times in the 1250 K gas condition. Similarly, the MS data for tar samples collected at long residence times in the 1250 K gas condition indicate an increase in polycondensed aromatic compounds with 3 or more aromatic rings, such as phenanthrenes and pyrenes. The detail provided by the MS analyses helps to interpret the coarse but quantitative chemical groups identified in the NMR analyses.

D. Conclusions

Based on the Curie-point GC/MS and low-voltage MS analyses of the tar formed during devolatilization of Beulah Zap, New Mexico Blue, Illinois #6, Pittsburgh #8, and Pocahontas #3 coals, the following conclusions are reached:

1. The degree of aromaticity increases rapidly in tars from all five coals as a function of residence time at the 1250 K gas temperature. However, little increase in aromaticity in the tars is detected at the 1050 K gas temperature.

2. At a gas temperature of 1250 K, devolatilization is complete within 70 msec and secondary gas-phase reactions of tar vapors can be observed within 100 msec. At 1050 K, the devolatilization process appears to be more or less complete after 250 msec.

3. In order to study the complete devolatilization process and the possible onset of secondary reactions, further experiments should be conducted at an intermediate temperature, e.g., 1150 K.

These conclusions are consistent with the ^{1}H and ^{13}C NMR analyses performed previously on these same tars [Fletcher, et al., 1990b].

Nomenclature for Chapter 5

A	area; pre-exponential rate constant
B	blowing coefficient (transpiration parameter)
c	char bridge population
C	char
C_{clust}	carbons per aromatic cluster
c_p	heat capacity
d	diameter
D	diffusivity
E	activation energy
f_i	fraction of element i remaining in the char
f_a'	carbon aromaticity
$f_{a,H}$	hydrogen aromaticity
f_a^P	fraction of aromatic carbopn with hydrogen attachments
$F_{1\text{-}2}$	radiation view factor from surface 1 to surface 2
h	convective heat transfer coefficient
H	heat of reaction
k	thermal conductivity
£	labile bridge population
m	mass
M	molecular weight
P	pressure
Q	radiation heat transfer rate
$\dot{r}_i$	reaction rate for reaction i
r_d	disk radius for radiation correction to particle heating
R	ratio of the separation distance to the disk (z/r_d)
Re	Reynolds number
Sc	Schmidt number
Sh	Sherwood number
t	time
T	temperature
$T_{1\rho}^{Har}$	spin relaxation time in NMR analysis
v	velocity
V	volatiles
V^*	ultimate volatiles yield
$\dot{W}$	moisture evaporation rate
x	mass fraction
y	yield factor for two-step devolatilization rate
z	distance from injection point

Nomenclature for Chapter 5 (cont.)

Greek

ε	emissivity
δ	side chain population
ρ	density
σ	Stefan-Boltzman radiation constant; standard deviation
$\sigma+1$	coordination number (number of total attachments per cluster)
θ	Correction factor for blowing
μ	viscosity
τ	time constant

subscripts

att	attachments to clusters
b	labile bridge
C	carbon
clust	aromatic clusters
δ	side chains
ε	emissivity
g	gas
h	heater
H	hydrogen
i	i^{th} reaction; injection tube
m	mass
o	surface
p	particle
T	temperature
tot	total
v	velocity
w	water; wall
∞	bulk gas condition (distance from surface = ∞)

References for Chapter 5

Anthony, D. B., J. B. Howard, H. C. Hottel, and M. P. Meissner, *Fifteenth Symp. (Int.) on Comb.*, The Combustion Institute, p. 1303 (1974).

Badzioch, S., and P. G. W. Hawksley, *Ind. Eng. Chem.*, **9**, 521 (1970).

Baxter, L. L., T. H. Fletcher, and D. K. Ottesen, D. K., *Energy & Fuels*, **2**, 423 (1988).

Bird, R. B., W. E. Stewart, and E. N. Lightfoot, *transport Phenomena*, Wiley and Sons, New York (1960).

Burnham, A. K., M. S. Oh, R. W. Crawford, and A. M. Samoun, *Energy and Fuels*, **3**, 42 (1989).

Carangelo, R. M., M. A. Serio, P. R. Solomon, S. Charpenay, Z. Yu, and R. Bassilakis, *ACS Div. Fuel Chem. prepr.*, **36**:2, 796 (1991).

Chakravarty, T., Windig, W., Taghizadeh, K., and Meuzelaar, H. L. C., *Energy & Fuels* **2**, 191 (1988).

Fletcher, T. H., L. L. Baxter, and D. K. Ottesen, *1987 International Conference on Coal Science* ,J. A. Moulijn, Eds., Elsevier Science Publishers B. V., Amsterdam, p. 945, 1987.

Fletcher, T. H., *Comb. Sci. Tech.*, **63**, 89 (1989a).

Fletcher, T. H., *Comb. Flame*, **78**, 223 (1989b).

Fletcher, T. H. and D. R. Hardesty, "Coal Combustion Science: Task 1, Coal Devolatilization," DOE/PETC Quarterly Progress Report for January to March, 1990, edited by D. R. Hardesty, Sandia Report No. SAND90-8223, available NTIS (1990a).

Fletcher, T. H. and D. R. Hardesty, "Coal Combustion Science: Task 1, Coal Devolatilization," DOE/PETC Quarterly Progress Report for April to June, 1990, edited by D. R. Hardesty, Sandia Report No. SAND90-8245, available NTIS (1990b).

Fletcher, T. H., A. R. Kerstein, R. J. Pugmire, and D. M. Grant, *Energy & Fuels*, **4**, 54 (1990a).

Fletcher, T. H., M. S. Solum, D. M. Grant, S. Critchfield, and R. J. Pugmire, *Twenty-Third Sym. (Int.) on Comb.*, The Combustion Institute, Pittsburgh, PA, p. 1231 (1990b).

Fletcher, T. H., A. R. Kerstein, R. J. Pugmire, and D. M. Grant, "A Chemical Percolation Model for Devolatilization: 3. Chemical Structure as a Function of Coal Type," in press (1991). See also Fletcher, T. H. and D. R. Hardesty, "Coal Combustion Science: Task 1, Coal Devolatilization," DOE/PETC Quarterly Progress Report for October to December, 1990, edited by D. R. Hardesty, Sandia Report No. SAND91-8210, available NTIS (1991).

Freihaut, J. D., Ph. D. Thesis, Dept. of Materials Sci. and Eng., Penn. State Univ. (1980).

Freihaut, J. D., W. M. Proscia, and D. J. Seery, *ACS Div. of Fuel Chem. Preprints*, **32**(3):129-141 (1987).

Freihaut, J. D., and W. M. Proscia, *Energy & Fuels*, **3**, 625 (1989).

Freihaut, J. D., W. M. Proscia, and D. J. Seery, *Energy & Fuels*, **3**, 692 (1989).

Gat, N., *Comb. Sci. Tech.*, **49**, 297 (1986).

Grant, D. M., R. J. Pugmire, T. H. Fletcher, and A. R. Kerstein, *Energy & Fuels*, **3**, 175 (1989).

Heisler, M. P., *Trans. ASME*, **69**, 227 (1947).

Howard, J. B., "Fundamentals of Coal Pyrolysis and Hydropyrolysis," in *Chemistry of Coal Utilization*, ed. by M. A. Elliott, Wiley and Sons, New York, p. 689 (1981).

Hsu, J., "Swelling, Mass Transport, and Chemical Kientics in Bituminous Coal Pyrolysis," Ph. D. Thesis, Chemical Engineering Department, Massachusetts Institute of Technology (1989).

Jurkiewicz, A., Wind, R. A., Neevel, G. E., *Fuel*, **69**, 830 (1990).

Kimber, G. M., and M. D. Gray, M. D., *Comb. Flame*, **11**, 360 (1967).

Kobayashi, H., J. B. Howard, and A. F. Sarofim, *Sixteenth Symp. (Int.) on Comb.*, The Combustion Institute, 411 (1976).

Lo, R., Pugmire, R. J., Fletcher, T. H., and Meuzelaar, H. L. C, *ACS Div. of Fuel Chem. Preprints*, **35**:3 697 (1990).

Mallin, J. R. and R. G. Jenkins, "Pyrolysis of Lignitic and Bituminous Coals in an Entrained Flow Reactor," A Topical Report to UTRC for DOE Contract No. DE-AC22-84PC70768, Dept. of Mat. Sci. and Eng., Penn. State (1987).

Merrick, D., *Fuel*, **62**, 540 (1983).

Metcalf, G. S., Windig, W., Hill, G. R., and Meuzelaar, H. L. C., *Int. J. of Coal Geology* **7**, 245 (1987).

Meuzelaar, H. L. C., Harper, A. M., Hill, G. R., and Given, P. H., *Fuel* **63**:5, 640-652 (1984).

Meuzelaar, H. L. C., Yun, Y., Simmleit, N., and Schulten, H. R., *ACS Div. of Fuel Chem. Preprints*, **34**:3, 693 (1989).

Niksa, S., L. E. Heyd, W. B. Russel, and D. A. Saville, *Twentieth Symp. (Int.) on Comb.*, The Combustion Institute, p. 1445 (1984).

Niksa, S., A. R. Kerstein, and T. H. Fletcher, *Comb. Flame*, **69**, 221 (1987).

Orendt, A. M., Solum, M. S., Sethi, N. K., Hughes, C. D., Pugmire, R. J., and Grant, D. M., "^{13}C NMR Techniques for Structural Studies of Coal and Coal Chars," in Advances in Coal Spectroscopy, H. L. C. Meuzelaar, Ed., Plenum Press, (in press, 1990).

Pitt, G. J., *Fuel*, **41**, 267 (1962).

Pugmire, R. J., M. S. Solum, D. M. Grant, S. Critchfield, and T. H. Fletcher, *Fuel*, **70**, 414 (1991).

Seery, D. J., J. D. Freihaut, W. M. Proscia, J. B. Howard, W. Peters, J. Hsu, M Hajaligol, A. Sarofim, R. Jenkins, J. Mallin, B. Espindola-Merin, R. Essenhigh, and M. K. Misra, "Kinetics of Coal Pyrolysis," Final Report for DOE Contract No. DE-AC22-84PC70768 (1989).

Serio, M. A., D. G. Hamblen, J. R. Markham, and P. R. Solomon, *Energy & Fuels*, **1**, 38 (1987).

Serio, M. A., P. R. Solomon, S. Charpenay, Z. Yu, and R. Bassilakis, *ACS Div. Fuel Chem. prepr.*, **35**:3, 808 (1990).

Sethi, N. K., Pugmire, R. J., Facelli, J. C., and Grant, D. M., *Anal. Chem.*, **60**, 1574 (1988).

Siegell, R. and J. R. Howell, J. R. *Thermal Radiation Heat Transfer*, Hemisphere Publishing Corporation, Washington (1981).

Smoot, L. D., and D. T. Pratt, *Pulverized Coal Combustion and Gasification*, Plenum Press, New York (1979).

Solomon, P. R. and D. G. Hamblen, "Pyrolysis," in *Chemistry of Coal Conversion*, ed. Schlosberg, R. H., Plenum Press, New York, 121 (1985).

Solomon, P. R., M. A. Serio, R. M. Carangelo, and J. R. Markham, *Fuel*, **65**, 182 (1986).

Solomon, P. R., M. A. Serio, R. M. Carangelo, R. Bassilakis, D. Gavel, M. Maillargeon, F. Baudais, and G. Vail, *Energy and Fuels*, **4**, 319 (1990a).

Solomon, P. R., Serio, M. A., Despande, G. V., and Kroo, E., *Energy & Fuels*, **4**, 42 (1990b).

Solomon, P. R., D. G. Hamblen, M. A. Serio, Z. Yu, and S. Charpenay, *ACS Div. Fuel Chem. prepr.*, **36**:1, 268 (1991).

Solum, M. S., Gan, Z., Pugmire, R. J., Grant, D. M., and Solomon, P. R., (manuscript in preparation, 1990).

Spalding, D. B. *Some Fundamentals of Combustion*, Butterworths Scientific Publications, London (1955).

Suuberg, E. M., W. A. Peters, and J. B. Howard, *Seventeenth Symposium (International) on Combustion*, The Combustion Institute, p. 117 (1970).

Suuberg, E. M., Peters, W. A., and Howard, J. B., *17th Symp. (Int.) on Comb.*, The Combustion Institute, 117 (1978).

Suuberg, E. M., D. Lee, and J. W. Larsen, *Fuel*, **64**, 1668 (1985).

Tsai, C. and Scaroni, A. W., *Twentieth Symp. (Int.) on Comb.*, The Combustion Institute, p. 1455 (1984).

Ubhayakar, S. K., D. N. Stickler, C. W. von Rosenberg, and R. E. Gannon, *16th Symp. (Int.) on Comb.*, The Combustion Institute, Pittsburgh, PA, 427 (1976).

Vorres, K. S., "Users' Handbook for the Argonne Premium Coal Sample Bank," Argonne National Laboratory, supported by DOE contract W-31-109-ENG-38 (September, 1989). Also Vorres, K. S., *ACS Div. Fuel Chem. prepr.*, **32**:4, 221 (1987).

Yun, Y., Maswadeh, W., Meuzelaar, H. L. C., Simmleit, N., and Schulten, H. R., *ACS Div. of Fuel Chem. Preprints*, **34**:4, 1308 (1989).

Yun, Y., Meuzelaar, H. L. C., Simmleit, N., and Schulten, H.-R., T*he Mobile Phase in Coal Viewed from a Mass Spectrometric Perspective*, ACS Symposium Series, (in press, 1990).

6. RESULTS OF ADDITIONAL EXPERIMENTS

Transition from Coal Devolatilization to Char Combustion

A. Introduction

Coal devolatilization affects the combustion performance of pulverized fuel boilers in many different ways. The primary influences of coal devolatilization on combustion performance are the amount of mass released as volatile matter and the heating value of the pyrolysis products. The volatile matter is released quickly compared to the subsequent heterogeneous char oxidation, and significantly influences near-burner gas temperatures and stoichiometry. Equally important is the amount of mass remaining in the char, since this is the mass that must be oxidized in the available residence time in the furnace. The physical structure of the char subsequent to devolatilization (i.e., internal surface area, pore size, and porosity) determines the rate of char oxidation. Many devolatilization experiments have been conducted at moderate temperatures (800 to 1300 K) and moderate heating rates (10^3 to 10^4 K/s), since this regime allows definition of primary devolatilization products and rates of evolution. At higher temperatures and heating rates, the primary devolatilization products decompose in the gas phase. Secondary devolatilization products formed from gas phase decomposition of primary volatiles include additional light gases as well as soot. The physical and chemical nature of the char is dependent on the devolatilization conditions, which are dependent on the heating rate and oxygen concentration. In order to understand the transition from coal devolatilization to char oxidation, the effect of high temperatures (1300 to 2000 K) and rapid heating rates (> 10^5 K/s) on devolatilization must be characterized.

Coal particle swelling must be understood as a function of heating rate and temperature before a description of the transition from coal devolatilization to char oxidation can be completed. As high volatile bituminous coals are heated, the aliphatic bonds between the aromatic clusters are broken, and fragments are formed with small enough molecular weight to become liquid. The liquid in the coal is termed metaplast. Further increases in temperature raise the vapor pressures of the lower molecular weight species in the metaplast, and tar vapor is released from the particle. Light gases are formed from the aliphatic bridge material. High volatile bituminous coals contain enough metaplast for the particle to exhibit liquid properties in certain temperature regimes. As internal gases (light gases and tar vapors) are generated, bubbles are formed. With sufficient bubble formation, the internal pressure becomes larger than the surface tension of the particle, and the particle diameter increases. In low rank coals, crosslinking reactions scavenge much of the metaplast before it can be released as tar, and no particle swelling is observed.

The degree of particle swelling during devolatilization may affect the particle temperature in a practical coal combustion system; thermal radiation to the particles is significant in large combustors. Heat transfer to and from particles is a function of the particle surface area, which is proportional to the square of the particle diameter.

Particle size, density, and internal surface area also significantly affect the rate of char oxidation. Small particles may burn in a regime where oxygen penetrates the pores of the particles (Zone I), and hence the reaction rate is controlled by the intrinsic chemical reactivity of the char. Intermediate size particles may burn in a regime where time scales of internal diffusion of oxygen through the pores and the intrinsic chemical reactivity are of the same order (Zone II). Large particles may burn in a regime where the rate is controlled by the diffusion of oxygen to the particle surface from the ambient gas stream (Regime III).

The physical properties of a coal char are rank dependent. Chars from low rank coals do not swell, and exhibit high internal surface areas. Chars from bituminous coals may soften, resulting in large internal voids caused by bubbles in the particle during pyrolysis. The large internal voids generated in softening coals reduce the diffusion resistance in the particle in Zone II combustion conditions, although for simplicity most char combustion studies assume a continuous pore structure throughout the particle.

In an oxidizing atmosphere, devolatilized gases and tar vapors combust with the oxygen. At rapid heating conditions typical of pulverized fuel furnaces, the mass release from the particle is high enough to reduce the amount of heat transfer to the particle (particle blowing). The oxygen is partially consumed by combustion with the volatiles, and the mass flux of volatiles is large enough to prevent diffusion of oxygen to the surface. However, during the late stages of devolatilization, the mass flux is not as high, and it is therefore possible that oxygen may react heterogeneously with the char before complete devolatilization.

The purpose of this study is to investigate the transition from coal devolatilization to char oxidation, including the differences in the physical and chemical char structures formed during devolatilization and combustion experiments. This study also includes investigation of the total mass release attributable to devolatilization as a function of temperature, and possible regimes where devolatilization and char oxidation at rapid heating conditions may occur simultaneously.

In the following section, a literature review of previous research on high temperature devolatilization yields and particle swelling behavior is presented. Results of Sandia experiments in the CDL and CCL in different gas phase oxygen environments are then presented.

B. Background

High Temperature Coal Devolatilization ($T_p > 1300$ K)

Many coal devolatilization experiments have been conducted at temperatures less than 1300 K. However, relatively few detailed studies of devolatilization have been performed at temperatures higher than 1300 K. The results of experiments performed without an aerodynamic separation of tars and soot from char particles [e.g.,

Kobayashi, et al., 1976; Ubhayakar, et al., 1976] are questionable, since the redeposition of pyrolysis products onto the char makes interpretation difficult. Wornat, et al. [1987] studied the soot/tar ratio from a bituminous coal at temperatures ranging from 1100 to 1500 K; total mass release was not reported as a function of temperature. Serio, et al. [1987] reported volatiles yield for a lignite at 1073 K (V = 55% daf) and 1873 K (V = 68% daf), although the lignite was not held at 1073 K long enough to achieve complete devolatilization. The most notable high temperature products from the 1873 K experiment were CO and H_2. Kimber and Gray [1967] used a plasma torch for a heat source in a drop tube furnace, with graphite resistance heaters for walls. Samples were collected in a water cooled probe equipped with a cyclone separator. The total volatiles yields (% daf) reported for a low rank coal were 48% at 1370 K, 60% at 1720 K, and 72% at 2170 K.

Tamhankar, et al. [1984] used a modified thermogravimetric analyzer (TGA) to study the pyrolysis behavior of lignite at heating rates ranging from 100 to 1000 K/s and temperatures between 973 and 1873 K in N_2, CO_2, and H_2O. A plateau in the volatiles yield was observed at 1473 K, followed by additional rapid rise at 1700 K. Morgan and Dekker [1987] used a drop tube to measure volatiles yields for three coals (hvb, mvb, lvb) at 1473, 1673, and 1773 K. A gas quench probe and a cyclone separator were used in these experiments. Residence times were estimated at 80 ms maximum. All three coals showed increase in yield at each increase in temperature. Blair, et al. [1976] studied nitrogen evolution from coal using a graphite ribbon. The experiments were conducted at high heating rates, with temperatures ranging to 1400 K. The data show increases in yield with increasing temperature for Illinois #6, Wyodak and one other coal. Pohl and Sarofim [1976] used an entrained flow reactor and a crucible heater to examine nitrogen evolution during pyrolysis. Temperatures as high as 2300 K were achieved in their experiments. Continual increases in yield with temperature were observed for a bituminous coal and a lignite.

Particle Swelling Behavior

Lightman and Street [1968; Street, et al., 1969] examined the characteristics of chars from pyrolysis of high volatile bituminous coals in a drop tube furnace with air or nitrogen as the carrier gas. Their findings indicated a sequence of swelling that included: (i) fissures in the particles (~ 573 K); (ii) larger fissures, with internal gas bubbles evident (~ 723 K); (iii) large interconnected internal voids, with surface bubbles apparent (~ 773 K), (iv) ignition (~ 913 K). They classified the particles into four categories: (a) relatively solid particles with fissures and ash sandwiches; (b) lacy cenospheres with many internal partitions; (c) thin-walled balloons; and (d) thick walled cenospheres. Particles treated in nitrogen possessed a more open structure and were more swollen than those treated in air. Swelling was shown to be influenced by the duration and temperature of treatment. Swelling ratios were obtained for four different coals, with furnace temperatures of 1073 K, as summarized in Table 6.1.

Table 6.1
Summary of Swelling Data from Lightman and Street (1968)

Coal	Size (μm)	B.S. Swelling Number	Swelling Ratio	
			Air	Nitrogen
Rawdon	63-75	1/2	1.04	
	53-63			1.16
Ackton Hall	24-30	5	1.09	
	53-63		1.10	
	90-105		1.09	1.57
Grange Ash	53-63	8	1.16	
Yniscedwyn	63-63	0	1.00	

The data for the bituminous coal (Ackton Hall) indicated 57% diameter change when particles were heated in nitrogen, but only 10% diameter change when heated (and combusted) in air. The lower rank coal (Rawdon) exhibited less diameter change when heated in the nitrogen environment. These data suggest that the devolatilization of coal in oxidizing atmospheres may inhibit particle swelling for bituminous coals.

Tsai and Scaroni [1987] studied the structural changes in bituminous coal particles heated in a drop tube furnace to 1200 K (estimated heating rate of 10^4 K/s). Data were presented for 112 μm diameter particles heated in nitrogen and in air. Diameter increases were determined by combining measurements of apparent density (tap density technique) with measurements of mass release (ash tracer technique). Pyrolysis in nitrogen showed a swelling region with particle diameter increases of up to 20%, followed by shrinkage region with subsequent deceases in diameter of approximately 10%. In the combustion tests with the same coals, the swelling was more pronounced (up to 30% swelling), with subsequent large extents of shrinkage (partially due to combustion). The internal particle surface area was characterized by CO_2 adsorption. Particles heated in air and in N_2 exhibited identical changes in internal surface area as a function of mass release, until the onset of char oxidation in the combustion experiment.

Melia and Bowman [1983] suggested a three zone model for particle swelling during devolatilization: (1) a rigid coal matrix; followed by (2) a low viscosity plastic state; followed by (3) a rigid char matrix. Their model suggests that the extent of swelling is dependent on particle heating rate. At low heating rates (~1 K/s), little swelling occurs, while maximum swelling occurs at heating rates of 10^4 to 10^5 K/s. At even higher heating rates, little swelling occurs. This model relies heavily on data obtained by Pohl, et al. [1978], where particle diameter increases of 1000% were reported. However, diameter increases reported in the literature are generally less than 100%; the large diameter increases reported by Pohl and coworkers may have been caused by particle agglomeration.

C. Approach to the Present Experiments

Recent coal combustion research at Sandia includes both devolatilization experiments (discussed in this report) and char oxidation experiments [Hurt, et al., 1992]. A description of both of the Sandia Coal Devolatilization Laboratory (CDL) and the Sandia Coal Combustion Laboratory (CCL) is presented in Section 2 of this report. The goal of this research effort is to describe the reaction behavior of coal particles throughout their lifetime in a typical pulverized coal-fired boiler. The devolatilization experiments have been conducted in 100% nitrogen to isolate the pyrolysis reactions, with typical particle heating rates of 10^4 K/s and particle temperatures as high as 1200 K. The char combustion experiments have been conducted in oxidizing environments (6-12 mole-% oxygen) after the pyrolysis process is complete, with minimum particle heating rates of approximately 10^5 K/s and particle temperatures of approximately 1500 K [Hurt, et al., 1992]. In order to adequately describe combustion behavior in a large scale system, it is important to bridge the gap between the devolatilization experiments and the char oxidation experiments.

Common coal samples were used in the coal devolatilization and char oxidation experiments. Char samples collected in the two laboratories were analyzed for organic and inorganic elemental composition. The ratio of the apparent density of the char sample to that of the parent coal is measured using a tap density technique. The mass mean diameter of the char sample is determined from the combination of the extent of mass release and the apparent density, using the following relationship:

$$\left(\frac{\rho}{\rho_o}\right)\left(\frac{d}{d_o}\right)^3 = \left(\frac{m}{m_o}\right), \tag{6.1}$$

where d is the particle diameter, m is the mass of the particle, ρ is the apparent density of the particle, and the subscript o refers to the parent coal sample.

The differences in swelling behavior between experiments conducted in the CDL and the CCL are attributed to three independent reactor parameters: (a) gas phase oxygen concentration;(b) particle heating rate; and (c) the presence of post-flame combustion products (i.e., H_2O, CO_2, and radicals such as OH). The experiments described here were performed to investigate the effects of gas phase oxygen concentration on coal particle swelling behavior during devolatilization. In particular, the effect of oxygen is studied by performing experiments in the CDL with controlled amounts of oxygen added to the nitrogen environment, and by performing experiments in the CCL with little or no oxygen present in the post-flame environment. The particle temperature histories in the two flow reactors are not changed significantly by adding or subtracting oxygen. Future experiments should characterize the effects of heating rate and post-flame combustion products on coal particle swelling during devolatilization.

The CCL experiments with no post-flame oxygen required modifications to the sampling system to aerodynamically separate tars, soot and aerosols from char

particles. The cyclone from the CDL was therefore used in these experiments to prevent the tar and soot from recondensing on the char particles. The extent of mass release from the char particles was determined from the trace mineral species (Si, Al, Ti, and total ash). Apparent density was determined as described above. Samples were obtained in the CDL at two different residence times in the 1250 K gas condition: 130 ms (subsequent to tar release) and 250 ms (reactor exit). Samples were taken just subsequent to the pyrolysis zone (47 ms, 6.4 cm above the burner) in the CCL. Maximum gas temperatures in the CCL experiments were approximately 1600 K, corresponding to the temperatures used in previous char combustion experiments.

D. Results

Analyses of char and tar samples obtained during devolatilization in the CDL in 100% N_2 are tabulated in the appendix. Also included in a separate appendix are the analyses of char samples collected in the CCL in the 0% post-flame oxygen condition. This section discusses the results obtained in the devolatilization experiments in the CDL and the CCL.

Total Volatiles Yield

The total volatiles yield data from the experiments performed in the CDL and in the CCL are shown in Table 6.2 for five different coals. The percentage of oxygen in the parent coal is used as an indicator of rank. The terms CCL-0, CCL-6 and CCL-12 denote experiments in the CCL with 0, 6, or 12% oxygen in the post flame gas. All of the data shown for CCL-6 and CCL-12 were obtained for the size fraction 106-125 μm (see Hurt, et al. [1992]). The 106-125 μm size fraction was also used for the CDL-0 and CCL-0 experiments on PSOC-1445D, 1493D, and 1508D. In the CDL-0 and CCL-0 experiments, however, due to insufficient quantities of the 106-125 μm size fraction, the 75-106 μm size fraction of PSOC 1507D and the 63-75 μm size fraction of PSOC-1451D were used.

Table 6.2
Comparison of Total Volatiles Yields in the CDL and CCL Experiments

Coal Type (PSOC-)	Oxygen (% daf)	ASTM *V* (% daf)	CDL-0 *V* (% daf)	CCL-0 *V* (% daf)	CCL-6* *V* (% daf)	CCL-12* *V* (% daf)
1507D	25.2	49.6	53.7	58.6	61.7	61.7
1445D	16.3	46.8	53.4	56.2	64.2	69.3
1493D	13.6	43.4	53.5	58.3	58.0	58.0
1451D	7.6	38.7	53.1	52.2	54.0	54.0
1508D	4.8	17.2	15.9	17.4	20.4	22.8

*see Hurt, et al. [1992]

The total volatiles yield data are shown in Fig. 6.1 as a function of the oxygen content of the parent coal. The measured yields in the CDL and the CCL exceed the ASTM total volatiles yields for all five coals. The yields from the CDL-0 low rank coal experiments are 3-4% lower than the yields in the CCL-0 experiments, indicating that the increased temperature in the CCL resulted in additional mass release. However, for the Pittsburgh #8 hva bituminous coal (1451D) and the Pocahontas low volatile bituminous coal (1508D), the yield obtained in the CDL-0 experiments was nearly identical to the yield obtained in the CCL-0 experiments. The extent of mass release in the CCL-6 and CCL-12 experiments was 3 to 13% higher than in the CCL-0 experiment, with the most dramatic increase in yield with oxygen observed for the low rank coals. The increase in yield seen for the low rank coals is most likely due to the onset of heterogeneous char oxidation in the late stages of devolatilization. This hypothesis is consistent with the fact that lignite char reactivities are higher than bituminous coal char reactivities. The data for the low volatile coal (1508D) indicate that the presence of oxygen increases the extent of mass release at comparable residence times from 16% daf to 23% daf. The reactivity of high rank coals is much lower than the lignites, and hence chars from high rank coals shouldn't be expected to react with oxygen during the late stages of devolatilization. On the other hand, since the volatiles flux is quite low for such high rank coals, and oxygen may penetrate to the particle surface during devolatilization. This may allow enough residence time and high enough surface oxygen concentrations for char oxidation to occur before the completion of devolatilization.

Elemental Composition

The changes in elemental composition of coal chars during devolatilization in experiments conducted in the CDL are discussed in Chapter 5 in connection with a coalification diagram. The H/C vs. O/C coalification diagram also provides a useful visualization of the change in elemental composition of coal chars during the transition from devolatilization to char oxidation. Figure 6.2 shows the elemental compositions of chars from five coals examined in the CCL under the following conditions: (a) 0% post-flame oxygen (CCL-0), 47 ms; (b) 6% post-flame oxygen, 47 ms; and (c) 6% post-flame oxygen (CCL-6), 72 ms.

In general, the elemental compositions of the chars from the CCL-0 condition closely match those of the chars taken immediately after tar release in the CDL. However, chars taken from the CCL in the 6% post-flame oxygen condition at the same residence time (47 ms) contain substantially less hydrogen than chars from the CDL or CCL-0 condition (except for the Pittsburgh #8 char). Chars from the higher rank coals in the CCL require longer residence times to release the hydrogen, and reach the H/C ratio of the low rank coals at 72 ms in the CCL-6 condition. The oxygen content of the chars obtained at 72 ms in the CCL-6 condition is remarkably similar to the oxygen content of the chars from the CDL obtained at the longest residence times. This implies that in the early stages of char combustion, the hydrogen is attacked heterogeneously by oxygen, although this is difficult to distinguish from degassing reactions. Since the hydrogen in these chars exists as either attachments to aromatic

rings (Ar-H), attachments to aliphatic carbon (Ar-CH_3, Ar-CH_2-Ar), or phenols (Ar-OH), it is easy to see that the gas-phase oxygen likely reacts with hydrogen preferentially to carbon in the initial stages of char combustion.

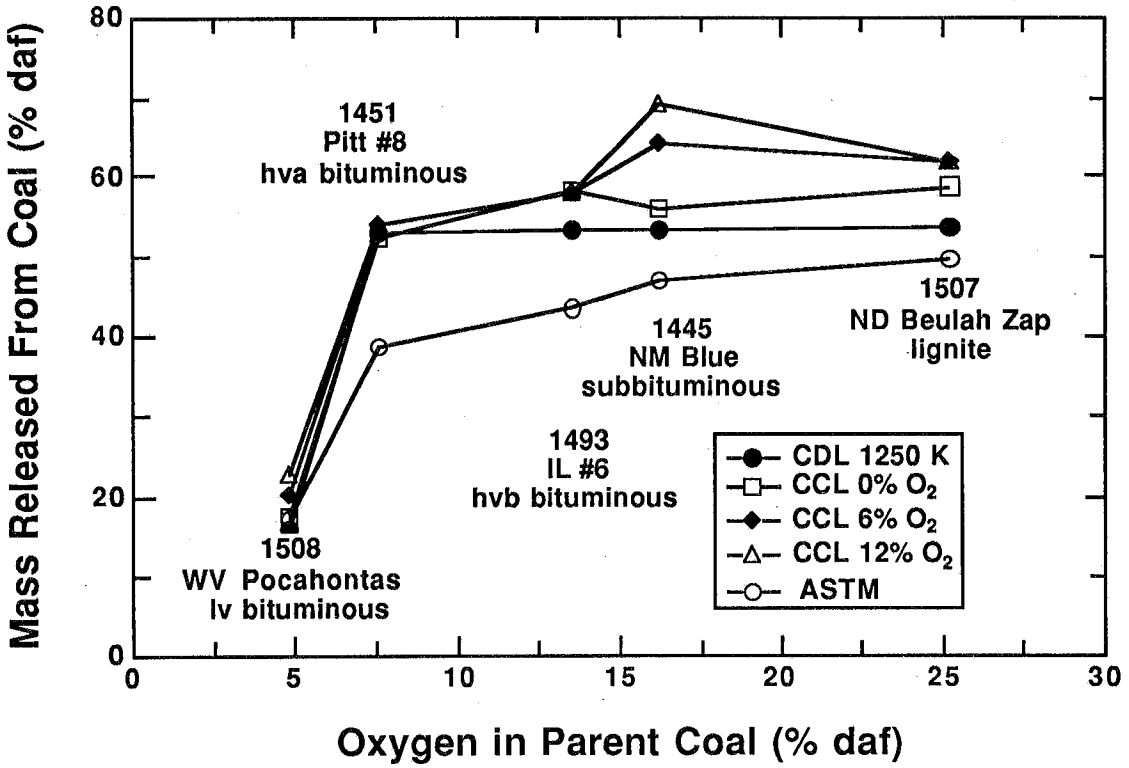

Figure 6.1 Comparison of mass release due to devolatilization in different experiments in the CDL and CCL for five PSOC-D coals. The ASTM total volatiles yields are shown for reference. The elemental oxygen level in the parent coal is used as an indicator of coal rank.

Chemical Structure of Coal Chars

Char samples from five coals collected at 47 ms residence time in the CCL with 0% post-flame oxygen were analyzed by ^{13}C NMR spectroscopy at the University of Utah in collaboration with Professor Ronald Pugmire and Dr. Mark Solum. These analyses are tabulated in the appendix. The chars taken from the CCL-0 condition are very similar in chemical structure to the chars taken immediately after tar release in the CDL experiments at 1250 K (residence times of approximately 70 to 100 ms). In the CDL, these chars have finished releasing tar, and are beginning the slower gas release phase. The chars in the CCL-0 condition at 47 ms have just completed tar release as well, and hence should be followed by a slower light gas release region. Examples of the similarity in chemical structure of chars from the 1250 K gas condition in the CDL and from the CCL-0 condition are shown in Figs. 6.3 to 6.5. The solid

lines in these figures represent the CDL-0 data at different residence times, while the dashed line represents data from the CCL-0 experiments.

The NMR analysis of the parent coals from the CDL was performed approximately two years earlier than the NMR analysis of the coals used in the CCL-0 experiments. These duplicate analyses are indicated by the solid circles in Figs. 6.3 to 6.5, and represent possible changes in composition of the parent coal as well as experimental errors in the NMR techniques. For the most part, the two sets of NMR analyses are in good agreement; the most notable exception is the cluster molecular weight of the parent Illinois #6 coal (~ 13 % daf oxygen). The 106-125 μm size fraction of this coal came to Sandia in two separate bottles from PETC, and the coal used in the CDL came from a different jar than that used in the CCL experiments. The elemental analyses of these two sets of Illinois #6 coals also indicate two different sets of coals, since the average compositions of the two sets of coal analyses differ by more than the experimental error. The carbon aromaticities and molecular weight of attachments to aromatic clusters for the two Illinois #6 coals agree much better than the cluster molecular weights.

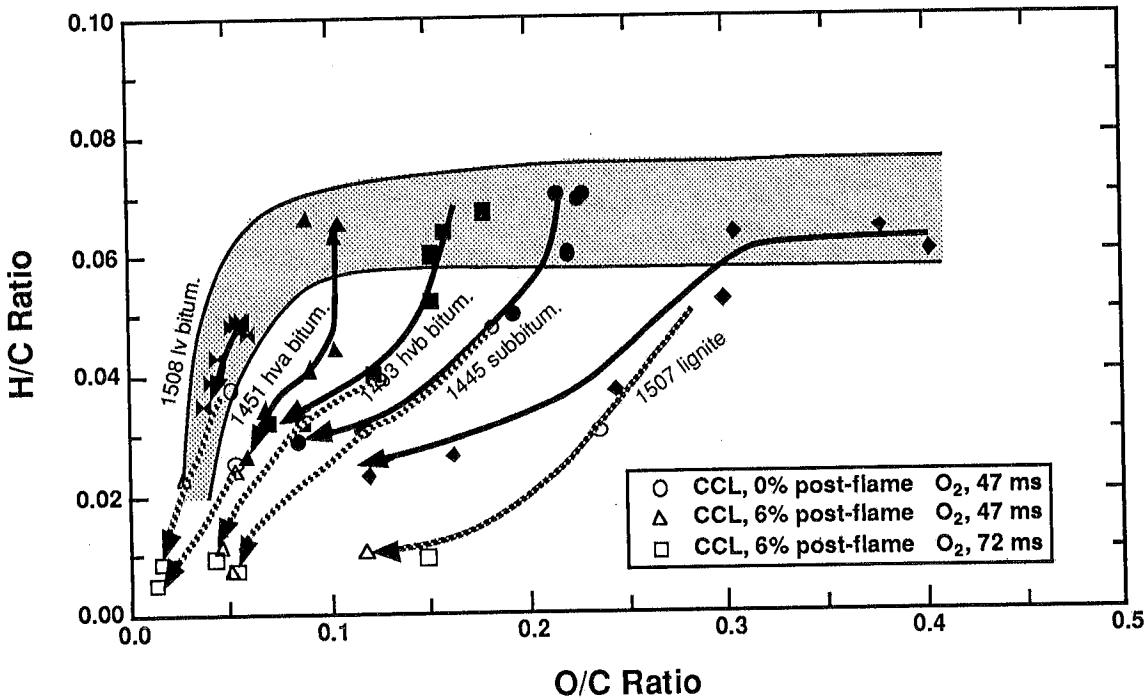

Figure 6.2 Coalification diagram showing the elemental compositions of parent coals and reacted chars from the CDL (solid lines and points) and the CCL (dashed lines and open points). The shaded area represents the typical range of compositions of unreacted coals.

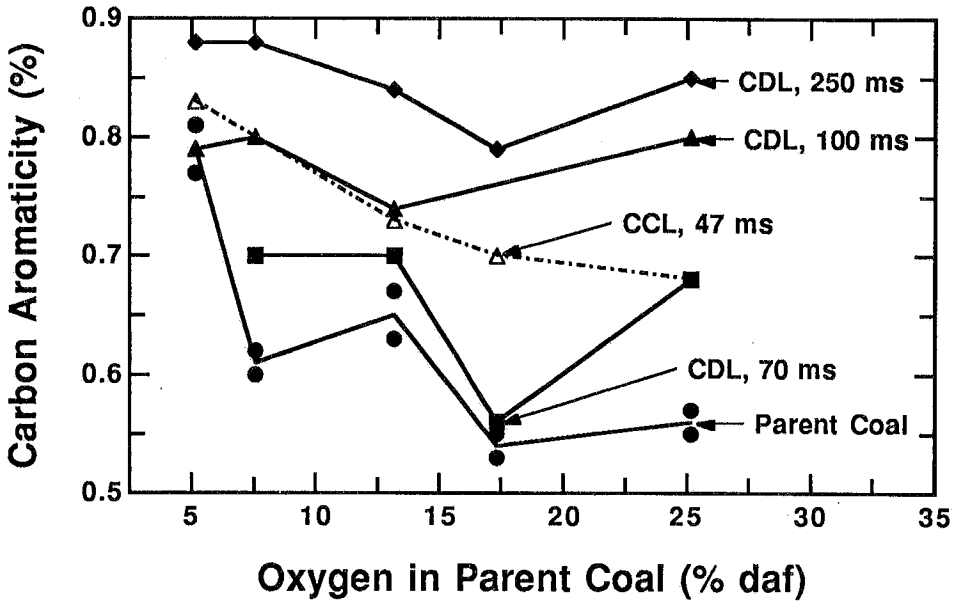

Figure 6.3 Comparison of carbon aromaticities in char samples from the CCL-0 condition and the 1250 K gas condition in the CDL.

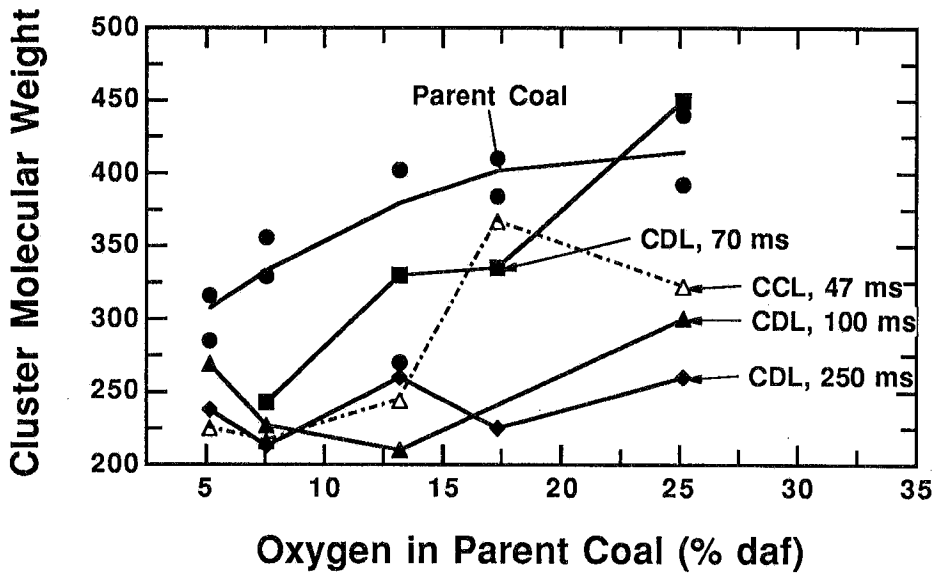

Figure 6.4 Comparison of cluster molecular weights in char samples from the CCL-0 condition and the 1250 K gas condition in the CDL.

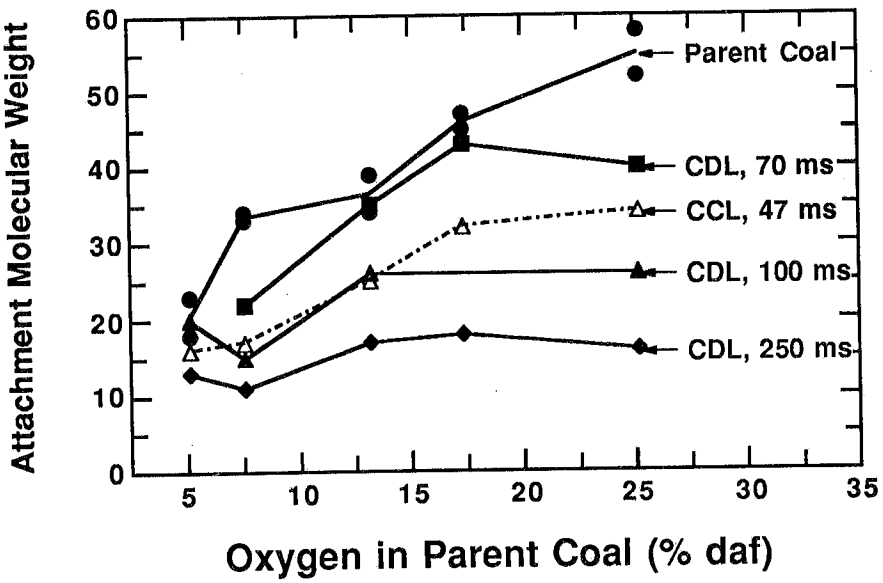

Figure 6.5 Comparison of molecular weights of attachments to aromatic clusters in char samples from the CCL-0 condition and the 1250 K gas condition in the CDL.

The carbon aromaticities (percentage of carbon in aromatic rings) in the CCL-0 chars from low rank coals (i.e., high oxygen content) are similar to the carbon aromaticities in chars collected at 70 ms in the 1250 K gas condition in the CDL. However, the carbon aromaticities in CCL-0 chars from the high rank coals are similar to the chars collected at 100 ms in the CDL. The molecular weights of clusters and attachments to clusters (Figs. 6.4 and 6.5) in the CCL-0 chars from the low rank coals lie halfway between the values observed in the chars collected at 70 and 100 ms in the CDL. In contrast, the molecular weights of clusters and attachments to clusters in CCL-0 chars from the high rank coals are most similar to the CDL chars collected at 100 ms.

Quantitative measures of chemical structure (e.g., carbon aromaticities, cluster molecular weights) for the CCL-0 chars always lie close to the values observed in the chars collected at 70 or 100 ms in the CDL, and do not approach the values observed at 250 ms in the CDL. The chemical structure data for the CCL-0 chars therefore indicate that tar release in the CCL is complete at 47 ms, but that further release of light pyrolysis gases is still underway in the early stages of char combustion. This is consistent with the observations of the elemental compositions of the CCL-0 chars discussed in the previous section of this chapter. Simultaneous char combustion and light gas evolution occur as the char ignites, and must both be considered in the determination of reactivities early in the char combustion process.

Swelling Behavior

The results of Lightman and Street [1968; Street, et al., 1969] indicate that particle swelling is reduced in the presence of oxygen. A possible physical explanation for this

phenomenon is that oxygen scavenges the radicals in the coal particle as the particle begins to soften, forming a rigid structure before the onset of devolatilization drives the oxygen from the particle surface. Differences in swelling behavior between experiments in the CDL and CCL for Pittsburgh #8 hva bituminous coal particles are observed that may be caused by the difference in the gas phase oxygen concentration in the two experiments. Experiments were therefore performed in the CDL to determine the effect of ambient gas phase oxygen concentration on the swelling behavior of a Pittsburgh #8 hva bituminous coal (PSOC-1451D). Oxygen was added in controlled amounts to both the flow reactor gas and the coal entrainment gas. Oxygen concentrations in the flow reactor were checked with an oxygen analyzer. Initial experiments were performed at low oxygen concentrations to reduce wear of flow reactor components and to limit the amount of char oxidation in the reactor. The apparent densities of the samples are an indicator of the amount of particle swelling, since the extent of mass release is virtually identical for all samples. For this coal, apparent density ratios of 0.2 correspond to 50% diameter change, while density ratios of 0.4 correspond to diameter changes of less than 10%.

The first set of samples were collected at the exit of the flow reactor (250 mm from the point of coal injection) in both the 1050 K and 1250 K gas conditions. Two general types of particles were encountered in the collected samples: (1) round, partially-transparent, balloon-like cenospheres; and (2) molten opaque particles with many blow holes. These two types of particles are illustrated in Fig. 6.6; the transparent nature of the particles is difficult to see in these photographs. The balloon-like cenospheres are much larger (110 to 180 μm) than the opaque particles (50 to 130 μm). Roughly 30-40% of the particles in a given sample were balloon-like cenospheres. The two types of particles were observed in electron micrographs and cross section photographs (see Figs. 5.31 and 5.32 in Chapter 5; see also Lightman and Street, 1968), although the electron micrographs do not reveal the transparent nature of the balloon-like cenospheres. Cross-section photographs show large internal voids (30-50 μm in diameter) in most of the particles. The balloon-like cenospheres are much lighter (lower apparent density) than the opaque particles, and accumulate at the top of the sample vials. Initial tap density measurements were performed on only a portion of the collected samples; the densities from these experiments were skewed because the balloon-like cenospheres were located at the top of the sample vial. This may be a source of error in previously reported experiments. Care was taken to use all of the sample from a given experiment during the tap density measurements reported here in order to avoid density classification.

Results of the sampling experiments conducted in the 1250 K gas condition in the CDL for PSOC-1451D (63-75 μm) are shown in Fig. 6.7. Samples were obtained at an axial distance of 250 mm, corresponding to residence times of 250 ms. Particle ignition was not observed in these experiments. The data indicate that the apparent density of the particles begins to rise at an ambient oxygen concentration of 3%. Optical microscopy of these samples showed, however, that the rise in apparent density is

a. Balloon-like cenospheres from the top of the sample vial

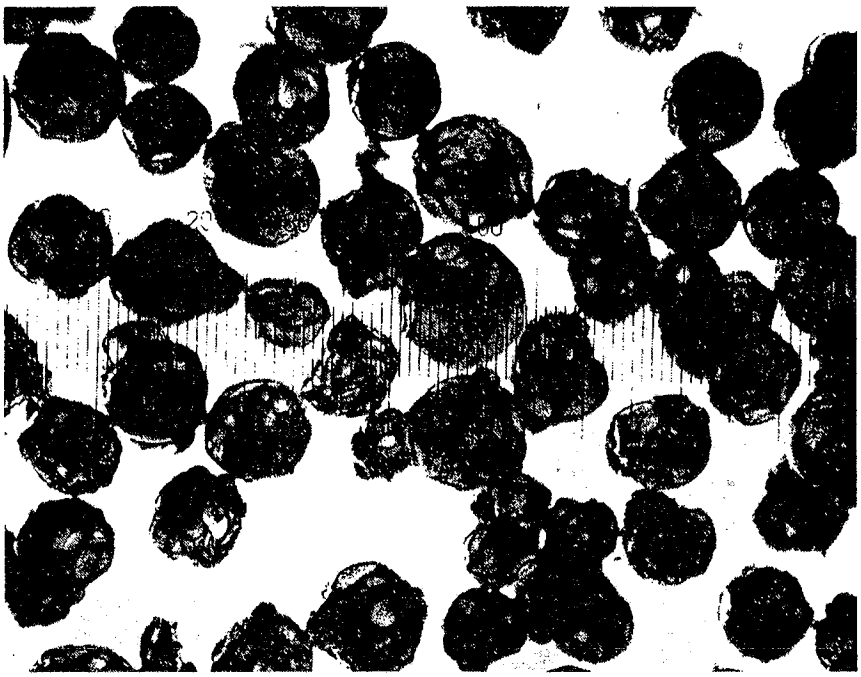

b. Opaque particles from the bottom of the sample vial

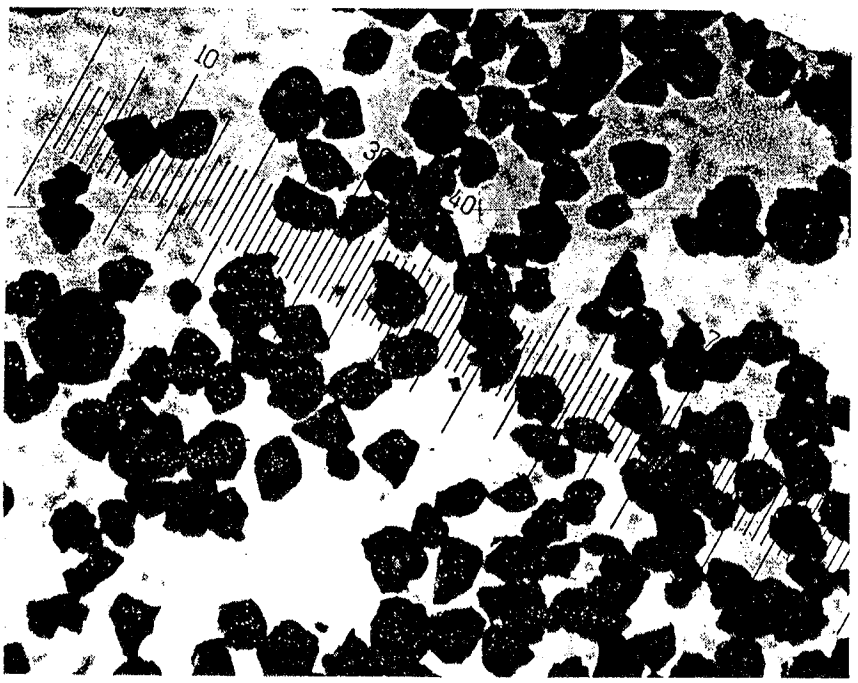

Figure 6.6 Photographs of char particles from PSOC-1451D (63-75 μm initial size fraction) collected at 250 ms in the 1250 K gas condition in 3% oxygen in the CDL. Ten divisions on the size scale are equivalent to 139 μm.

due to the partial oxidation and fragmentation of the balloon-like cenospheres. The apparent density of a broken shell fragment is much greater than that of an intact hollow sphere, since apparent density is the mass per external volume. The thin walls of balloon-like cenospheres burn more rapidly than the thick-walled cenospheres, and it is possible that the balloon-like cenospheres fragment due to oxidation prior to the first sampling location in most char combustion experiments. An examination of samples obtained in the char combustion experiments in the CCL revealed the absence of any transparent cenospheres; these types of particles were either not formed or were consumed upstream of the sampling location [Hurt, et al., 1992].

A second set of experiments was performed in the CDL to determine the effect of gas phase oxygen concentration on the degree of swelling during pyrolysis before the onset of char oxidation. The 75-106 μm size fraction of PSOC-1451D Pittsburgh #8 hva bituminous coal was used for these experiments, due to limited quantities of the 63-75 and 106-125 μm size fractions. As indicated in Chapter 5, the main region of mass release for the 1250 K gas condition occurs at residence times between 70 and 100 ms. Samples were therefore collected at residence times of 130 ms to ensure completion of devolatilization and to minimize residence time for oxidation of the balloon-like cenospheres. Oxygen concentrations of 0, 5, and 10 mole-% were employed in these experiments. Ignited particles were observed in the 10% oxygen experiments, with ignition of a few particles starting at 90 ms; no particle ignition was observed in the 5% oxygen experiments. Particle luminosity ceased at the probe tip due to the helium quench jets. Balloon-like cenospheres were observed in samples from all three oxygen conditions, since any ignited particles were quenched within 10-40 ms. The apparent density ratios of samples obtained in the CDL are all on the order of 0.15, as shown in Fig. 6.8. From these experiments, it is concluded that the ambient oxygen concentration does not affect the particle swelling behavior during pyrolysis at heating conditions encountered in the CDL (~10^4 K/s).

Pyrolysis experiments were conducted in the CCL at higher heating rates and temperatures by adjusting the flame stoichiometry to achieve post-flame oxygen levels in the 50 ppm range (referred to as 0% O_2). Mass release for this set of experiments are reported above in Table 6.2. The apparent density ratios (ρ/ρ_o) and the swelling ratios (d/d_o) obtained in the CDL and CCL for different coal types are given in Table 6.3. These data indicate that the oxygen concentration has little effect on the swelling behavior of coal particles sampled in the CCL-0 experiments (where heating rates are slightly higher than in the CDL, as indicated in the next section). Pittsburgh #8 coal particles swell by approximately 50% in the CDL experiments in oxygen concentrations ranging from 0 to 10%, and the apparent density ratios range from 0.15 to 0.20. These same particles swell by less than 10% in the CCL, even in the 0% post-flame oxygen condition. The differences in particle swelling behavior observed in the two reactors is therefore attributable to (a) differences in particle heating rate, or (b) the presence of combustion products (H_2O, CO_2, and radicals such as OH) from the flame in the CCL.

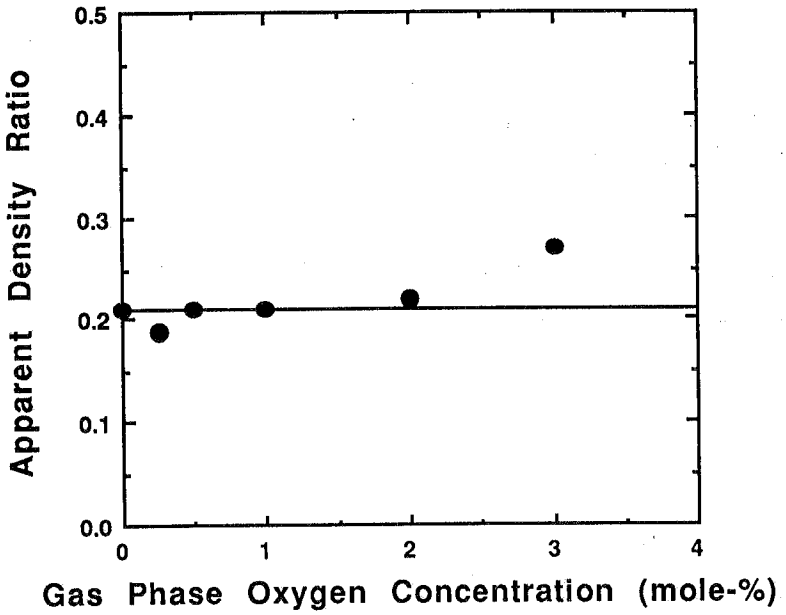

Figure 6.7 Apparent density ratios (ρ/ρ_o) for char particles from PSOC-1451D (63-75 μm size fraction) collected at 250 ms in the 1250 K gas condition in the CDL at different gas phase oxygen concentrations.

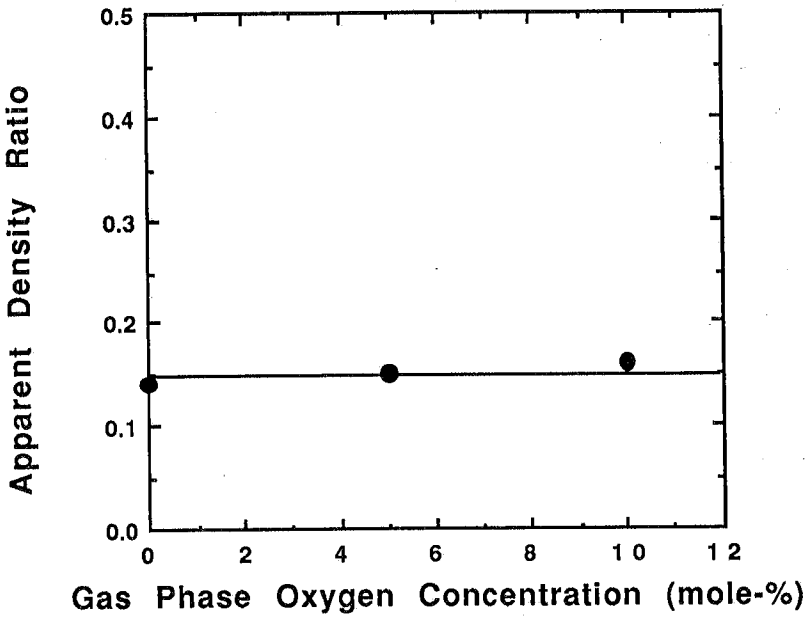

Figure 6.8 Apparent density ratios (ρ/ρ_o) for char particles from PSOC-1451D (75-106 μm size fraction) collected at 130 ms in the 1250 K gas condition in the CDL at different gas phase oxygen concentrations.

Table 6.3
Apparent Densities and Swelling Ratios for Chars Collected in the CCL at Three Different Gas Phase Oxygen Concentrations

a. Results of CCL, 0% Oxygen Experiments (47 ms residence time)

PSOC-	Coal	Size Fraction (μm)	Apparent Density (ρ/ρ_0)	Mass Remaining (m/m_0)	Diameter Change (d/d_0)
1507	Beulah Zap	75-106	0.64	0.48	0.90
1445	New Mexico Blue	106-125	0.32	0.40	1.08
1493	Illinois No. 6	106-125	0.35	0.48	1.11
1451	Pittsburgh No. 8	63-75	0.39	0.50	1.08
1508	WV Pocahontas	106-125	0.57	0.86	1.14

b. Results of CCL, 6% Oxygen Experiments (47 ms residence time)

PSOC-	Coal	Size Fraction (μm)	Apparent Density (ρ/ρ_0)	Mass Remaining (m/m_0)	Diameter Change (d/d_0)
1507	Beulah Zap	106-125	0.61	0.47	0.92
1445	New Mexico Blue	106-125	0.46	0.49	1.02
1493	Illinois No. 6	106-125	0.52	0.49	0.97
1451	Pittsburgh No. 8	106-125	0.38	0.50	1.10
1508	WV Pocahontas	106-125	0.46	0.83	1.22

c. Results of CCL, 12% Oxygen Experiments (47 ms residence time)

PSOC-	Coal	Size Fraction (μm)	Apparent Density (ρ/ρ_0)	Mass Remaining (m/m_0)	Diameter Change (d/d_0)
1507	Beulah Zap	106-125	0.63	0.47	0.91
1445	New Mexico Blue	106-125	0.39	0.49	1.08
1493	Illinois No. 6	106-125	0.47	0.49	1.01
1451	Pittsburgh No. 8	106-125	0.39	0.50	1.08
1508	WV Pocahontas	106-125	0.51	0.81	1.17

E. Heating Rates in the Char Combustion Laboratory

The most probable cause for the difference in particle swelling behavior in samples collected in the CDL and CCL is a difference in the particle heating rate. The particle heating rate in the CDL was carefully determined by measurements of particle size, temperature, and velocity, coupled with the use of a model of the transient heating process [Fletcher, 1989a and 1989b]. A similar detailed investigation of the particle heating rates in the CCL was not performed previous to this work, as it is not in general necessary for the determination of char oxidation rate parameters at measurements heights above this transient heating zone.

Inlet gas flow rates for the gas condition in the CCL flow reactor with 0% post-flame oxygen are listed in Table 6.4 and the corresponding gas temperatures as a function of height above the burner are listed in Table 6.5. The total volumetric gas flow rate into the reactor was 59.53 standard liters/min (slpm), corresponding to an initial gas velocity of 38.4 cm/s at the burner surface. The velocity constants c_1 and c_2 determined for this gas condition are 0.298 and 2.16 x 10^{-5}, respectively. The gas temperature between the burner surface and the first thermocouple measurement height (1.3 cm) is assumed to increase linearly, and hence the gas velocity in this region is assumed to also increase proportionally to temperature without any boundary layer effects. Gas velocities obtained using this method for the pre-flame region, along with velocities calculated from Eq. 2.1 for the post-flame region, are shown in Table 6.6.

The gas flow rate to the particle feeder is typically 5 standard cm^3/min (sccm) of N_2. This flow rate through a tube with an inside diameter of 0.102 cm results in an entrainment gas velocity entering the flow reactor of 72 cm/s. Particle velocities at the entrance to the flow reactor are calculated from the initial gas velocity using following expression for the gas-particle relative terminal velocity:

$$v_{term} = \frac{d^2 g (\rho_p - \rho_g)}{18 \mu_g} \tag{6.2}$$

where terms are defined in the nomenclature for this chapter.

With the gas temperature and velocity defined, as well as the initial particle velocity and temperature, the particle continuity, momentum and energy equations are solved as explained by Fletcher [1989a; see also Fletcher and Hardesty, 1989]. This work is limited to devolatilization in inert environments, where the particle temperature is not influenced by the combustion of volatiles near the particle surface. Properties of PSOC-1493D Illinois No. 6 hvb bituminous coal (106-125 μm) and initial reactor conditions used in these calculations are listed in Table 6.7. Particle heat capacities are taken as a function of particle temperature from the correlation of Merrick (1983) based on elemental composition of the parent coal. Additional calculations were

Table 6.4
Gas Flow Rates for Gas Condition 106 in the CCL

Species	Inlet Gas Flow Rates (standard liters/min)
CH_4	1.34
H_2	7.34
O_2	5.40
N_2(fuel stream)	3.34
N_2(oxidizer stream)	42.11
Total	59.53

Table 6.5
Centerline Gas Temperatures for Gas Condition 106 in the CCL

Height above burner (cm)	Thermocouple bead temperature (K)	Corrected gas temperature (K)
0.0	300	300
1.3	1543	1608
2.5	1521	1583
3.8	1508	1568
6.4	1487	1545
12.7	1443	1495
19.1	1401	1449
25.4	1357	1400
31.8	1312	1351
38.1	1271	1306

performed without the moisture in the coal. In order to obtain a direct comparison between laboratories, the adjustment to the characteristic particle heating time used to fit the measured particle temperatures in the CDL experiments ($\tau_p = 0.56\ \tau_{p,o}$) by Fletcher (1989) was also used as a parameter in the calculations of particle temperature in the CCL.

A typical particle temperature history for a 115 μm coal particle in Gas Condition 106 in the CCL (0% post-flame O_2) is shown in Fig. 6.9, along with the corresponding gas temperature and particle heating rate. The initial temperature rise between 0 and 18 ms is very slow, as moisture in the coal evaporates. This period is followed by a rapid rise in particle temperature due to the large difference in gas and particle temperature near the $CH_4/H_2/O_2/N_2$ diffusion flame. After the flame, the particle heating rate decreases as the particle reaches its asymptotic temperature. The slight dip in the particle heating rate profile between 35 and 80 ms is caused by the blowing effect of rapid volatiles release from the coal. In this region, the velocity of volatiles escaping

from the particle surface is large enough to impede conduction of heat from the surrounding gas.

Table 6.6
Gas Velocities for Gas Condition 106 in the CCL

Height above burner (cm)	Gas temperature (K)	Gas Velocity (cm/s)
0.00	300	38
0.25	557	71
0.50	815	104
0.75	1072	137
1.3	1608	176
2.5	1583	189
3.8	1568	199
6.4	1545	216
12.7	1495	247
19.1	1449	270
25.4	1400	287
31.8	1351	300
38.1	1306	310

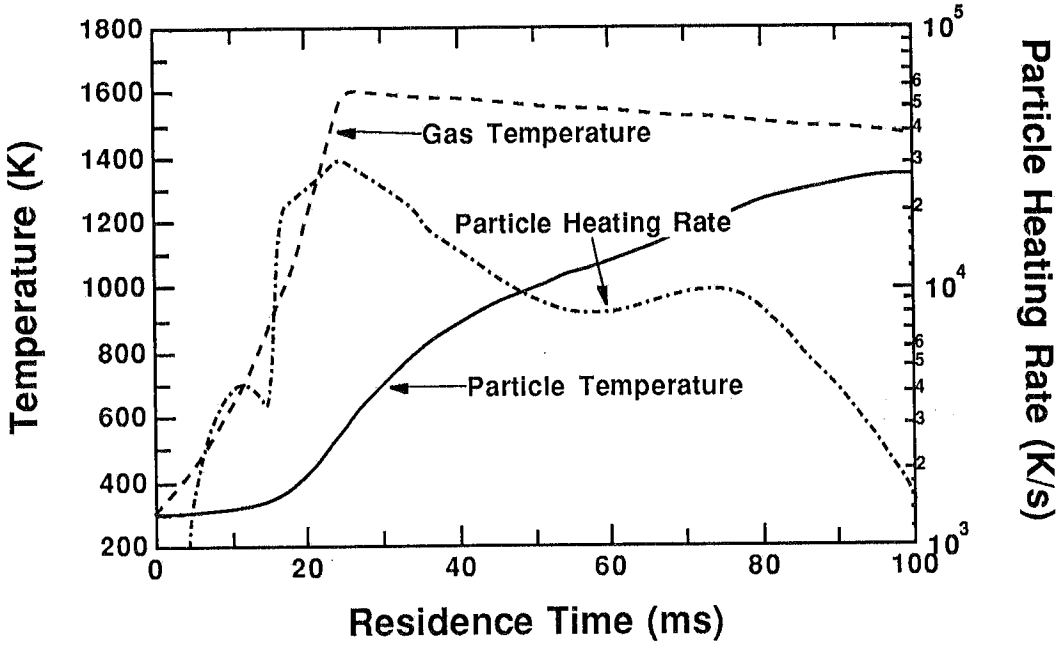

Figure 6.9 Particle and gas temperature histories for PSOC-1493D Illinois No. 6 hvb bituminous coal (106-125 μm size fraction) in gas condition 106 in the CCL. Calculations performed with 3.3% initial moisture without the Fletcher heating correction.

Table 6.7
Input Parameters for Calculation of
Coal Particle Temperature Histories in the CCL

Initial gas temperature (K)	300
Initial gas velocity (cm/s)	72
Initial particle density (g/cm^3)	1.2
Initial particle diameter (μm)	115
Swelling factor $(d_f-d_o)/d_o$	0.0
Heat of pyrolysis (cal/g)	-100
Initial moisture content (% of as rec'd coal)**	3.3
Initial ash content (% of dry coal)**	3.16
Total emissivity	0.7
Effective wall temperature (K)	500

Rate constants for 2-step model

A_1 (s^{-1})*	17,600
A_2 (s^{-1})*	1.46×10^{13}
E_1 (kcal/mol)*	17.6
E_2 (kcal/mol)*	60.0
Y_1**	0.39
Y_2**	1.0

Elemental Organic Composition of Parent Coal (% daf)**

Carbon	74.12
Hydrogen	4.96
Nitrogen	1.45
Oxygen	13.18
Sulfur	6.29

* Rate constants taken from Ubhayakar, et al. (1976)

** Coal properties and yield factors obtained by comparison with data for PSOC-1493D Illinois No. 6 hvb bituminous coal (106-125 μm size fraction) obtained in the Sandia CDL (Fletcher and Hardesty, 1989).

The particle temperature in the 0% O_2 environment eventually reaches a pseudo-equilibrium state with the local gas temperature; particle thermal radiative heat losses are balanced by convective heat transfer to the particle from the gas. Particle temperatures at residence times larger than 100 ms should therefore be 50 to 100 K lower than local gas temperatures in 0% O_2. If oxygen is present, the exothermic heat of char oxidation raises the particle temperature above the local gas temperature.

Particle heating rates in the CCL flow reactor were calculated for an Illinois No. 6 coal particle as a function of size, moisture content, and assumptions regarding the characteristic particle heating time. The peak particle heating rates for this set of calculations are summarized in Table 6.8, and compared with heating rates from the CDL in Fig 6.10. For the typical size fraction of coal used in char combustion experiments in the CCL (106-125 μm, or 115 μm average diameter), maximum particle heating rates are 4.5 x 10^4 K/s if the Fletcher heating correction is used and moisture is taken into account. For a size range more typical of an industrial boiler (55 μm), the maximum heating rate is just over twice that calculated for a 115 μm diameter particle. When moisture is excluded in the calculations, the calculated heating rate decreases slightly.

Table 6.8
Maximum Particle Heating Rates in the CCL
for an Illinois No. 6 hvb Bituminous Coal

Particle Size (μm)	% Moisture (as received)	Heating Rate (K/s)	
		with Fletcher heatup correction	without Fletcher heatup correction
115	0	4.0 x 10^4	2.9 x 10^4
"	3.3	4.5 x 10^4	3.2 x 10^4
55	0	8.9x 10^4	7.5 x 10^4
"	3.3	9.3 x 10^4	7.8 x 10^4

A maximum particle heating rate in the CDL of 2.2 x 10^4 K/s is calculated for the 115 μm size fraction (when moisture is included). This maximum heating rate is smaller than that in the CCL (for identical computational procedures) by a factor of 2 to 3. The maximum heating rates in the CCL for 55 μm particles is 2.3 times that in the CDL.

It is possible that flow reactor experiments in the CDL with helium as the carrier gas might increase the particle heating rate above that experienced in the CCL. If heating rates in the CDL using helium are, in fact, greater than in the CCL, this would be a good test of the hypothesis that the increased heating rate reduces the extent of particle swelling in softening coals.

The small difference of particle heating rates between the CDL with nitrogen gas and the CCL with 0% post-flame O_2 (a factor of two to three) seems like a narrow range to cause such a dramatic effect in particle swelling characteristics for a Pittsburgh No. 8 coal (50% diameter change in the CCL, 5% diameter change in the CDL, with accompanying changes in apparent density). This raises the possibility that the difference in swelling behavior may be caused by some other effect, such as differences in gas composition.

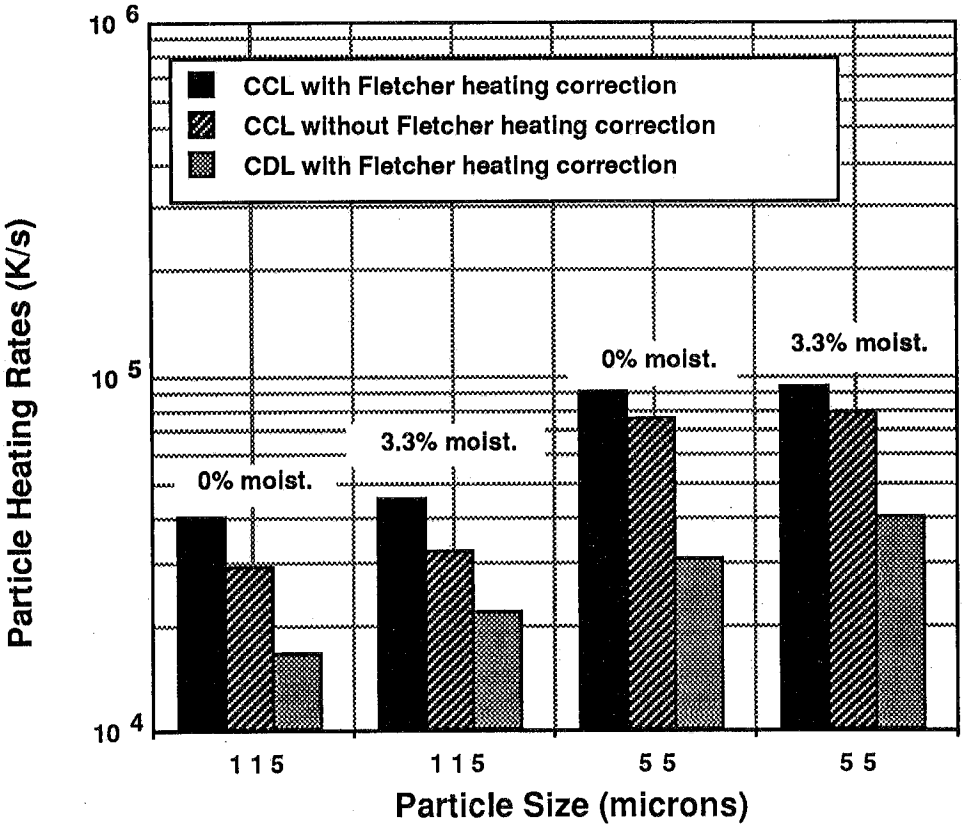

Figure 6.10 Comparison of calculated particle heating rates in the CDL flow reactor and in the CCL flow reactor in 0% O_2 for an Illinois No. 6 hvb bituminous coal as a function particle size and moisture content. Calculations in the CDL include a correction to the characteristic particle heating time, based on measured sizes, temperatures, and velocities of individual particles (Fletcher, 1989).

F. Conclusions

Based on the results of the experiments conducted in the CDL and the CCL as a function of gas phase oxygen concentration, the following conclusions are reached:

1. The degree of swelling during coal pyrolysis at rapid heating conditions ($> 10^4$ K/s) is not affected by the gas phase oxygen concentration. Changes in particle swelling caused by the presence of oxygen reported in other experiments may be due to partial oxidation of char samples subsequent to pyrolysis.

2. Pittsburgh #8 coal particles increased in diameter by 50% in the CDL experiments and by less than 10% in the CCL experiments. Differences in swelling behavior were caused by differences in particle heating rate and/or the

presence of post-flame combustion gases (e.g., CO_2, H_2O, or trace radical species).

3. An examination of samples obtained in the char combustion experiments in the CCL revealed the absence of any transparent cenospheres; these types of particles were either not formed or were consumed upstream of the sampling location.

4. Calculations of particle heating rates indicate that maximum particle heating rate in the CCL for the size fractions typically used (106-125 μm) is 4.5 x 10^4 K/s, which is a factor of two to three higher than the maximum heating rate experienced in the CDL experiments. The calculated difference between the particle heating rates at 0% O_2 in the two different laboratories may be responsible for the differences in the physical properties of the char particles. Because the heating rates were within a factor of two to three, however, other possible causes for the observed differences in swelling behavior should also be investigated.

Temperature Measurement of Burning Char Particles

A. Background

At the request of Phil Goldberg (Pittsburgh Energy Technology Center, PETC) and Don McCollor (University of North Dakota Energy and Mineral Research Center, UNDEMRC), temperatures of individual burning char particles were measured in a gas environment of roughly 10% oxygen and 1000 K in the CDL. The purpose of these experiments was to confirm the results obtained at similar conditions in a flow reactor at UNDEMRC. The reactivities determined from char combustion experiments at UNDEMRC are obtained from particle temperature measurements using three color pyrometry at wavelengths ranging from 0.8 to 1.0 μm. Two different samples were studied at UNDEMRC: (a) char from PSOC 1451 Pittsburgh #8 high volatile bituminous coal, 75-90 μm size fraction, and (b) char from PSOC 1507 Beulah Zap lignite, 75-90 μm size fraction. Roughly 400 mg of each char sample was received from UNDEMRC, with no details concerning how the char was formed. Photographs of the lignite char particles were taken through a microscope; these particles are non-spherical, with aspect ratios as high as 2. This means that major axis diameters were as large as 190 μm. The bituminous char particles appeared spherical, with diameters ranging from 70 to 100 μm.

B. Experimental Approach

In the CDL experiments, the flow reactor heaters were adjusted so that gas temperatures of 1000 K were achieved in the lower third of the quartz tower. A blend of nitrogen and air (total flow rate = 30 standard liters/min) was used to obtain the desired oxygen concentration in the flow reactor. Spherocarb particle temperatures were measured at z = 250 mm in 10% oxygen as a calibration reference; Spherocarb

particles are pure carbon spheres, and do not burn under these conditions. Table 6.9 shows the Spherocarb particle temperature measurements grouped into size bins of 10 μm. Note that the standard deviations in particle temperature for each size bin are less than 5 K under these conditions. The particle sizes also correspond to the expected sizes of Spherocarb particles (125-149 μm). The particle temperatures are roughly 50 K lower than the gas temperature due to radiative loss through the transparent flow reactor walls.

Table 6.9
Spherocarb Temperature Measurements in 10% O_2

COAL TYPE: Spherocarb, 3-30-88, UNDEMRC study
MAXIMUM GAS TEMPERATURE: 1000 K
SAMPLING HEIGHT: 250 mm

d_p (μm)	number	T_p (K)	σ_T (K)	v_p (m/s)	σ_v (m/s)	ε_p	σ_ε
105	0	0	0	0	0	0	0
115	1	948	0	0.87	0	0.925	0
125	7	948	4.8	0.91	0.03	0.852	0.034
135	17	951	3.1	0.93	0.03	0.781	0.052
145	11	947	4.7	0.94	0.03	0.755	0.049
155	10	945	4.7	0.97	0.03	0.727	0.084
165	4	942	4.7	1.00	0.02	0.693	0.060
175	3	943	3.9	0.98	0.02	0.631	0.058
185	0	0	0	0	0	0	0

NUMBER OF PARTICLES = 53

PARTICLES SCREENED BASED ON EMISSIVITIES FROM 0.00 TO 10.00

C. Results for Bituminous Coal Char

In a gas environment of 12% oxygen and 1000 K, UNDEMRC measurements of the bituminous char particles showed particle temperatures of 1680 K with a standard deviation of 33 K. In our study at 12% O_2 and 1000 K, the vast majority of these char particles did not ignite. Table 6.10 shows the results from the bituminous char particle experiments in the CDL. Note that these temperatures are very similar to the Spherocarb particle temperatures, indicating that the particles are not burning. It is estimated that only 1-5% of the bituminous char particles ignited, based on visual observations and the fraction of particle emission signals that were saturated when the oscilloscope was set for low voltage signals when the laser trigger was not used. Detailed temperature measurements of the few particles that ignited were not obtained, due to the limited quantity of char sample available. However, from the magnitude of the occasional emissions from ignited particles, it is estimated that these particles were burning at temperatures exceeding 1500 K (and possibly much higher).

This would support the bituminous char particle temperature of 1680 K measured at UNDEMRC under these conditions .

Table 6.10
Particle Temperature Measurements of PSOC-1451D Char in 12% O_2

COAL TYPE: UNDEMRC Pitt. #8 char, 12% O2
MAXIMUM GAS TEMPERATURE: 1000 K
SAMPLING HEIGHT: 200 mm

d_p (μm)	number	T_p (K)	σ_T (K)	v_p (m/s)	σ_v (m/s)	ε_p	σ_ε
35	0	0	0	0	0	0	0
45	0	0	0	0	0	0	0
55	1	1043	0	0.81	0	0.74	0
65	4	946	7.7	0.86	0.01	1.33	0.3
75	14	950	9.3	0.87	0.02	1.16	0.2
85	13	960	38.1	0.87	0.02	1.06	0.3
95	14	957	30.7	0.89	0.04	0.90	0.1
105	8	966	52.4	0.89	0.01	0.67	0.2
115	8	960	37.4	0.88	0.02	0.66	0.2
125	2	946	16.0	0.91	0.02	0.51	0.1
135	1	959	0	0.98	0	0.53	0.0
145	5	956	21.7	0.94	0.07	0.66	0.1
155	0	0	0	0.00	0	0	0
165	0	0	0	0.00	0	0	0
175	1	949	0	0.88	0	0.52	0
185	0	0	0	0	0	0	0

NUMBER OF PARTICLES = 71

PARTICLES SCREENED BASED ON EMISSIVITIES FROM 0.00 TO 10.00

The UNDEMRC experiment uses only particle emission as the triggering system to save oscilloscope traces for determination of particle temperatures. The pyrometer system used in that experiment has a lower temperature threshold of 1200-1300 K for individual 100 μm particles. Only ignited particles are therefore measured under these conditions. In a subsequent conversation with UNDEMRC personnel, it was revealed that the data rate for temperature measurement of these char particles was very slow, which would be consistent with the scenario of a large number of non-burning particles that were not detected in the UNDEMRC experiments.

D. Results for Lignite Char

The particle temperature reported by UNDEMRC for the lignite char was 1586 K with a standard deviation of 56 K for gas conditions of 10% O_2 and 1000 K. These lignite char particles were found to burn quite vigorously in our study in 10% O_2 at 1000 K. Bright streaks characteristic of burning char particles were observed to start at an axial distance of ~ 75 mm and extinguish at a distance of ~ 250 mm. Particle velocities in this gas condition were roughly 90 cm/s, which means that particle were ignited

extinguished in roughly 200 ms. The extinction of particle burning is due to depletion of carbonaceous material in the char particles. The gas concentration and temperature profiles in this region of the flow reactor do not change appreciably under these flow conditions. A small percentage of particles were seen to ignite in the exhaust duct after exiting the flow reactor; this is due to increased oxygen levels experienced before significant particle cooling. In 10% oxygen, though, very few (if any) ignited particles were observed at locations between z = 250 mm and the reactor exit (300 mm).

In order to reduce noise in the particle temperature data due to non-spherical particles and multiple particle emission, a particle emissivity is calculated from the measured particle size and two-color temperature using the emission intensity at the 2.2 μm wavelength. Only particles with similar emissivities are considered in the data analysis. This emissivity calculation reflects errors associated with the temperature and size measurements. With non-spherical particles such as the lignite char, the measured diameter of each individual particle can be different than the diameter corresponding to the particle surface area, and hence a fairly wide distribution of emissivities are calculated.

Lignite char particle temperature measurements were performed at z = 200 mm, although some of the char particles seemed to extinguish before this point. The experiments were therefore repeated at z = 185 mm, where particle extinction did not visually seem to occur. The emission from the burning particles was found to be almost as intense as the scattered light signal from the HeNe laser, and care was taken to adjust the level of trigger detection so that only emission signals triggered by the laser scattering were stored.

Particle temperature measurements during char combustion are generally grouped into size bins. However, this set of data exhibited large standard deviations in particle temperature for each size bin, and the data was therefore grouped into particle temperature bins (regardless of particle size). Table 6.11 shows the emissivity-classified temperature measurements for the lignite char in 10% O_2 at 1000 K, with particles grouped into temperature bins. A bimodal temperature distribution is observed, as shown in Fig. 6.11, with approximately 75% of the particles in the non-burning mode at 1000 K and 25% of the particles in the burning mode around 1600 K. The sizes of the particles at the two temperatures are the same, so that when particle temperatures are grouped into size bins (Table 6.12), the standard deviations in temperature for each size bin are 250 K. These size-classified temperature data are difficult to interpret without knowledge of the bimodal temperature distribution.

The lignite char was also studied in a gas environment of 5% O_2 at 1000 K. The char streaks under these conditions were less intense, and extended past the reactor exit. No extinction of burning char particles was observed under these conditions. Table 6.13 shows the measured temperature distribution of the emissivity-classified lignite char particles in this 5% O_2 environment, grouped into particle temperature bins. There are still significant numbers of slowly burning or non-burning particles, but 75% of the particles measured are burning at close to 1350 K, as shown in

Table 6.11
Particle Temperature Measurements of PSOC-1507D Char in 10% O_2

COAL TYPE: UNDEMRC Lignite Char, 10% O2, 4-1-88, Laser Trigger
MAXIMUM GAS TEMPERATURE: 1000 K
SAMPLING HEIGHT: 185 mm

T_p (K)	number	avg. T_p (K)	σ_T (K)	v_p (m/s)	σ_v (m/s)	ε_p	σ_ε
925	3	934	11.9	0.98	0.02	0.54	0.1
975	13	979	13.6	0.97	0.07	0.52	0.1
1025	9	1016	12.9	0.94	0.05	0.50	0.2
1075	5	1079	12.9	0.95	0.07	0.48	0.1
1125	1	1138	0.0	0.90	0	0.71	0.0
1175	3	1164	13.7	0.95	0.05	0.51	0.1
1225	1	1226	0	0.90	0	0.75	0.0
1275	0	0	0	0.00	0	0.00	0.0
1325	1	1332	0	0.84	0	0.39	0
1375	1	1382	0	1.00	0	0.52	0
1425	0	0	0	0.00	0	0.00	0
1475	0	0	0	0	0	0	0
1525	2	1523	17.4	0.99	0.01	0.58	0.1
1575	4	1588	9.2	0.87	0.02	0.58	0.1
1625	2	1605	4.0	0.87	0.01	0.65	0.1
1675	2	1677	20.5	0.90	0.06	0.54	0.1

NUMBER OF PARTICLES = 47

PARTICLES SCREENED BASED ON EMISSIVITIES FROM 0.30 TO 0.80

Table 6.12
Particle Temperature Measurements of PSOC-1507D Char in 10% O_2

COAL TYPE: UNDEMRC Lignite Char, 10% O2, 4-1-88, Laser Trigger
MAXIMUM GAS TEMPERATURE: 1000 K
SAMPLING HEIGHT: 185 mm

d_p (μm)	number	T_p (K)	σ_T (K)	v_p (m/s)	σ_v (m/s)	ε_p	σ_ε
55	2	963	59	1.00	0.01	0.51	0.2
65	2	1068	44	0.97	0.08	0.52	0.3
75	4	1278	280	0.95	0.05	0.54	0.1
85	7	1134	237	0.96	0.06	0.48	0.1
95	6	1135	250	0.93	0.10	0.59	0.1
105	9	1224	241	0.93	0.06	0.56	0.1
115	7	1132	212	0.93	0.04	0.63	0.1
125	3	979	34	0.92	0.06	0.43	0.1
135	5	1356	267	0.93	0.07	0.48	0.1
145	0	0	0	0.00	0	0.00	0.0
155	2	1015	9	0.94	0	0.36	0

NUMBER OF PARTICLES = 47

PARTICLES SCREENED BASED ON EMISSIVITIES FROM 0.30 TO 0.80

Table 6.13
Particle Temperature Measurements of PSOC-1507D Char in 5% O_2

COAL TYPE: UNDEMRC Lignite Char, 5% O2, 4-1-88, Laser Trigger
MAXIMUM GAS TEMPERATURE: 1000 K
SAMPLING HEIGHT: 185 mm

T_p (K)	number	avg. T_p (K)	σ_T (K)	v_p (m/s)	σ_v (m/s)	ε_p	σ_ε
975	4	984	10	1.05	0.07	0.51	0.1
1025	3	1013	6	0.98	0.05	0.57	0.2
1075	9	1083	9	0.93	0.02	0.68	0.1
1125	6	1122	10	0.92	0.01	0.65	0.1
1175	3	1180	17	0.91	0.01	0.63	0.2
1225	4	1228	14	0.88	0.08	0.59	0.2
1275	3	1277	14	0.90	0.04	0.49	0.2
1325	19	1335	12	0.87	0.08	0.56	0.1
1375	22	1368	11	0.86	0.09	0.60	0.1
1425	1	1413	0	0.84	0.00	0.61	0.0

NUMBER OF PARTICLES = 74

PARTICLES SCREENED BASED ON EMISSIVITIES FROM 0.30 TO 0.90

Table 6.14
Particle Temperature Measurements in 5% O_2

COAL TYPE: UNDEMRC Lignite Char, 5% O2, 4-1-88, Laser Trigger
MAXIMUM GAS TEMPERATURE: 1000 K
SAMPLING HEIGHT: 185 mm

d_p (μm)	number	T_p (K)	σ_T (K)	v_p (m/s)	σ_v (m/s)	ε_p	σ_ε
55	1	1382	0	0.85	0.00	0.72	0.0
65	2	1385	13	0.90	0.00	0.68	0.1
75	5	1274	81	0.87	0.02	0.71	0.2
85	6	1235	136	0.91	0.07	0.65	0.1
95	20	1221	139	0.90	0.12	0.65	0.1
105	16	1249	127	0.92	0.05	0.60	0.1
115	10	1269	137	0.89	0.03	0.57	0.1
125	4	1239	117	0.90	0.02	0.47	0.1
135	4	1254	155	0.92	0.05	0.48	0.1
145	5	1282	134	0.84	0.16	0.40	0.1

NUMBER OF PARTICLES = 74

PARTICLES SCREENED BASED ON EMISSIVITIES FROM 0.30 TO 0.90

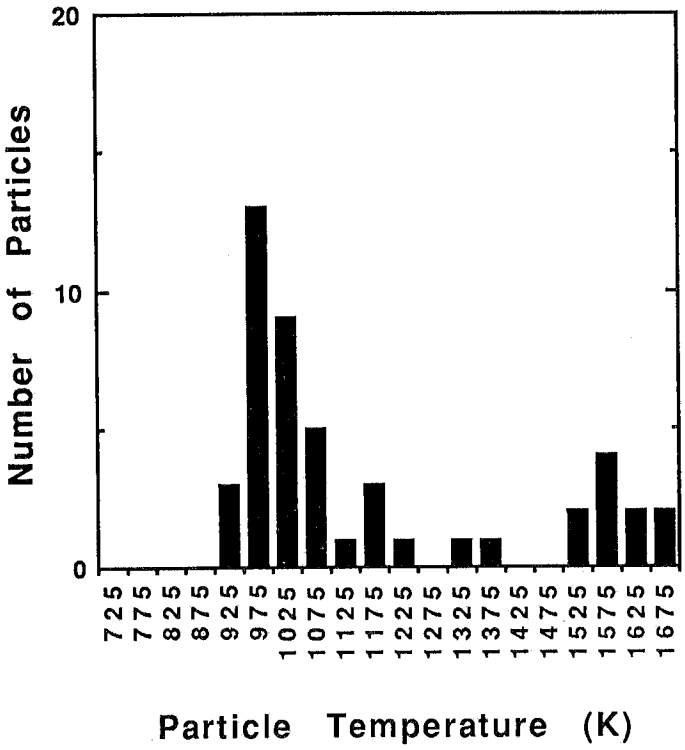

Figure 6.11 Particle temperature distribution for lignite char burning in 10% O_2 at a gas temperature of 1000 K in the CDL. Measurements taken at 185 mm from the particle injector.

Fig. 6.12. The size-classified temperature data in Table 6.14, grouped into particle size bins, show standard deviations of 125 K for each bin, which can be attributed to the presence of non-reacting particles.

E. Discussion

The particle to particle variation in mode of burning is not surprising, since coal is known to be heterogeneous in nature. Different particles exhibit variations in organic composition, maceral structure, shape, mineral content. Char particle ignition in this lightly loaded system is a function of gas temperature, oxygen level, and particle composition. Gas temperatures of 1000 K must be close to the ignition limit for these char particles, since a fraction of the particles do not burn. In experiments at higher gas temperatures, such as in the SNLL char combustion facility, non-burning particles are not observed until char combustion is nearly complete. For example, Fig. 6.13 shows a typical set of measured particle temperature data from the CCL for PSOC-1507D Zap lignite [Hurt, et al., 1992]. Gas temperatures in theis experiment are approximately 1500 K, so the small fraction of particles in the 1500 K temperature bin represents non-burning particles.

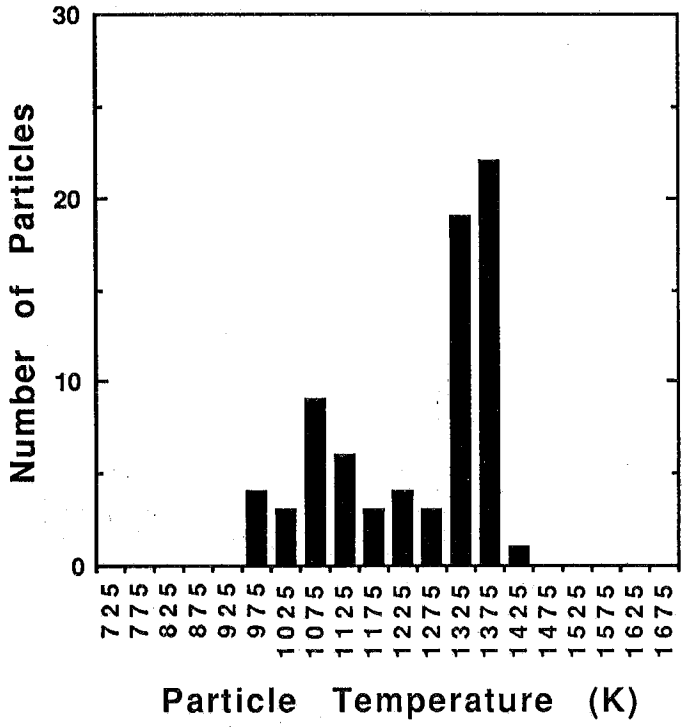

Figure 6.12 Particle temperature distribution for lignite char burning in 5% O_2 at a gas temperature of 1000 K in the CDL. Measurements taken at 185 mm from the particle injector.

The presence of non-burning particles makes determination of reactivities very difficult. Reactivities obtained from mass measurements or gas phase CO_2 measurements assume that all of the particles behave uniformly. Such reactivities are empirical in nature, and include the ratio of burning particles. Reactivities based on conditionally-averaged particle temperature measurements (where only the burning particles are observed) may only be applied to systems where 100% of the particles burn. Combined measurements of particle mass and temperature are also difficult to interpret if some fraction of the particles do not ignite.

F. Conclusions

The size and temperatures of burning char particles were measured in the CDL in N_2-O_2 atmospheres at 1000 K containing up to 12% O_2. Temperatures of burning bituminous char particles were estimated to exceed 1500 K (compared to 1686 K measured at UNDEMRC), but less than 5% of the particles ignited under these conditions, and detailed statistical measurements were not possible. It is difficult to compare the temperatures measured in this experiment with those measured at UNDEMRC, since it not clear how to conditionally average the data from ignited and non-reacting particles. Lignite char particle temperatures measured in the CDL in 10% O_2 were approximately 1600 K, which is the in the same range as measured at

UNDEMRC, since it not clear how to conditionally average the data from ignited and non-reacting particles. Lignite char particle temperatures measured in the CDL in 10% O_2 were approximately 1600 K, which is the in the same range as measured at UNDEMRC (1586 K). However, data from the lignite char experiments in the CDL also indicate the presence of significant numbers of non-burning particles (25 to 75%). Extents of burnout in solid samples taken from experiments where significant numbers of char particles have not ignited are impossible to interpret unless the precise percentage of non-burning particles is known.

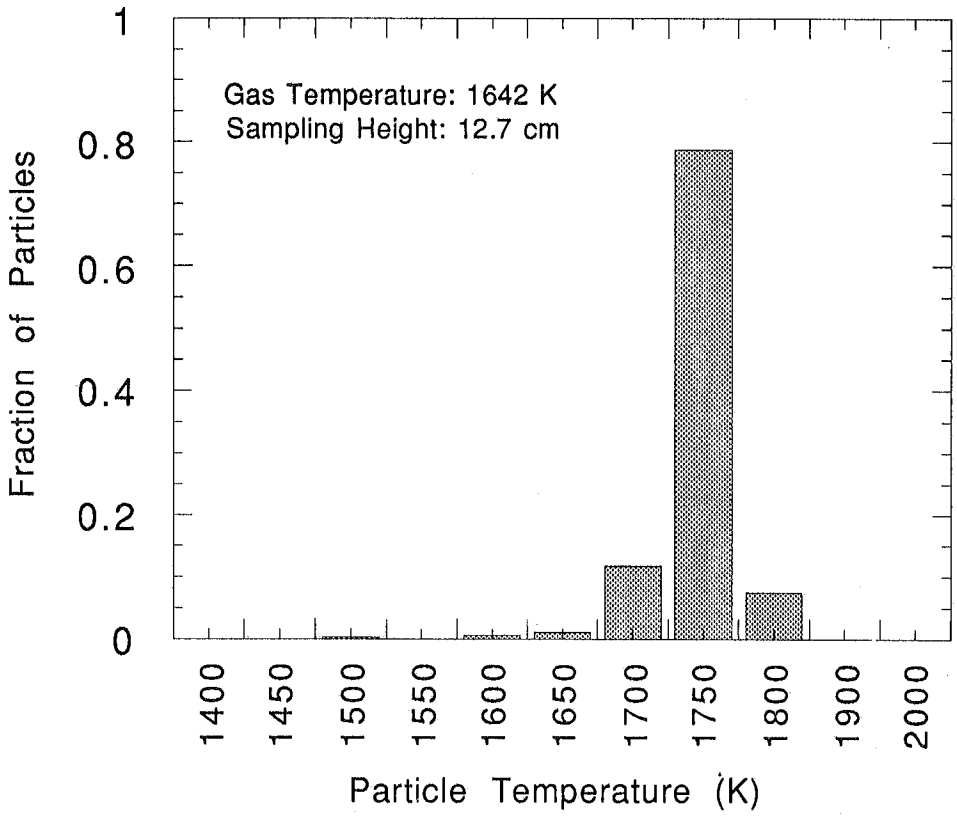

Figure 6.13 The distribution of temperatures for char particles of Beulah Zap lignite (PSOC-1507D) burning in 6 mole-% oxygen in the CCL flow reactor. [Figure taken from Hurt, et al., 1992]

Nomenclature for Chapter 6

Symbol	Definition
d	diameter
g	gravitational constant
m	mass (per particle)
T_p	particle temperature
v	velocity
z	axial distance
ρ	density
μ	viscosity

Subscripts

g	gas
o	initial
p	particle
$term$	terminal

References for Chapter 6

Blair, D. W., J. O. L. Wendt, and W. Bartok, *Sixteenth Symp. (Int.) on Comb.*, The Combustion Institute, 475 (1976).

Fletcher, T. H., *Comb. Sci. & Tech.*, **63**, 89 (1989a).

Fletcher, T., H., *Comb. & Flame*, **78**, 223 (1989b).

Fletcher, T. H. and D. R. Hardesty, "Coal Combustion Science: Task 1, Coal Devolatilization," DOE/PETC Quarterly Progress Report for January to March, 1989, edited by D,. R. Hardesty, Sandia Report No. SAND89-8241, available NTIS (1989).

Hurt, R. H., R. E. Mitchell, and D. R. Hardesty, "Compilation of Sandia Coal Char Combustion Data and Kinetic Analyses," Milestone Report for DOE/PETC Contract FWP 0709 (in press, 1992).

Kimber, G. M., and M. D. Gray, *Comb. Flame*, **11**, 360 (1967).

Kobayashi, H., J. B. Howard, and A. F. Sarofim, *Sixteenth Symp. (Int.) on Comb.*, The Combustion Institute, 411 (1976).

Lightman, P. and P. J. Street, *Fuel*, **47**, 7 (1968).

Melia, P. F. and C. T. Bowman, *Combust. Sci. Tech.*, **31**, 195 (1983).

Morgan, M. E., and J. S. A. Dekker, "Characterisation of Coals for Use in Pulverised Coal Combustion," IFRF Doc. No. K 70/a/5 (October, 1987).

Pohl, J. H., and A. F. Sarofim, *Sixteenth Symp. (Int.) on Comb.*, The Combustion Institute, p. 491 (1976).

Pohl, J. H., S. H. Kobayashi, and A. F. Sarofim, "The Effects of Temperature and Time on the Swelling Characteristics of Pulverized Coal Particles," presented at the Western States Section/The Combustion Institute, Boulder, Colorado (1978).

Serio, M. A., D. G. Hamblen, J. R. Markham, and P. R. Solomon, *Energy & Fuels*, **1**, 38 (1987).

Street, P. J., R. P. Weight, and P. Lightman, *Fuel*, **48**, 343 (1969).

Tamhankar, S. S., J. T. Sears, and C. Wen, *Fuel*, **63**, 1230 (1984).

Tsai, C. and A. W. Scaroni, *Fuel*, **66**, 200 (1987).

Ubhayakar, S. K., D. N. Stickler, C. W. von Rosenberg, and R. E. Gannon, *16th Symp. (Int.) on Comb.*, The Combustion Institute, Pittsburgh, PA, 427 (1976).

Wornat, M. J., A. F. Sarofim, and J. P. Longwell, *Energy & Fuels*, **1**, 431 (1987).

7. SUMMARY AND CONCLUSIONS

The motivation for the development of the Sandia Coal Devolatilization Laboratory was to provide a means for determining devolatilization rates based on direct measurements of the size, temperature, and velocity of individual particles during devolatilization. After that task was accomplished, attention was focused on studying the chemical and physical processes that occur to coal particles during devolatilization in experiments where the particle temperature was well characterized. This comprehensive document presents all of the coal devolatilization data obtained at Sandia, and discusses the results. The quantitative information contained in the appendix represents a significant contribution, since these data may now be used to refine modern devolatilization models. The data for different coals are discussed in the main body of the report with regard to a number of subtopics (e.g., elemental mass release, chemical structure, etc.) relevant to coal devolatilization. The presentation of the data and discussion of the results are included in the main body of the document by topic. Conclusions from the different areas of research are summarized below.

Experiments in 100% N_2

A. Particle Temperature Histories

The large differences in reported devolatilization rates are attributed to the difficulty in determining accurate particle time-temperature profiles during devolatilization under rapid heating conditions. This difficulty arises because a major portion of volatiles are released during particle heating. Particle temperature histories are acutely sensitive to the local gas temperature and to the diameter, heat capacity, and apparent density of the particles.

In order to avoid the difficulties associated with inferred particle temperatures, an optically accessible entrained flow reactor and infrared sizing-pyrometer system was developed and used to measure simultaneously the size, temperature, and velocity of individual particles in the flow reactor at different residence times. This is the first time that individual coal particle temperatures have been measured during devolatilization. Comparison of measured sizes and temperatures of pure carbon spheres with those of pyrolizing coal particles shows that the temperature measurement is not influenced significantly by the tar cloud surrounding each particle. Results indicate that gas and particle temperatures and velocities in the flow reactor are significantly influenced by local cooling near the point of coal injection, which may be a cause for the large discrepancy in reported devolatilization rates measured in conventional drop tube reactors.

Temperatures as low as 850 K were measured for 100 μm diameter particles, which is low enough for particle temperature measurements during the middle to late stages of devolatilization at rapid heating rates. Spherocarb and coal particle temperatures, measured as a function of particle size, were compared with calculated temperatures as a function of residence time. Measured particle temperatures were found to be

higher than calculated based on the centerline gas temperatures, emphasizing the need for the particle temperature measurements. Measured coal particle temperatures and velocities are fit using the general form of the particle energy equation in order to extrapolate to particle temperatures lower than 850 K.

B. Extent of Mass Release

Extents of mass release were determined from char samples using Si, Al, Ti, and total ash content as tracers. Tracers were chosen for each coal to minimize scatter in the mass release data, since the ICP and ashing procedures did not seem to give uniform results as a function of coal type. The total volatiles yields for four of the coals in the 1250 K gas condition (lignite, subbituminous, hvb and hva bituminous) were ~ 53% on a daf basis, while the total yield for the low volatile bituminous coals in this gas condition was 16% daf. The measured yields were in excess of the ASTM volatiles yields by factors ranging from 1.08 for the lignite to 1.37 for the hva bituminous coal, while the ASTM volatiles yield for the low volatile bituminous coal was similar to the measured yield.

C. Coal Devolatilization Rates

Char particles were collected from the flow reactor using a helium quench probe with an on-line aerodynamic separation of char particles from the devolatilized tars and gases. Char samples were analyzed for elemental inorganic composition, and several elements were used as tracers to determine the extent of mass release during devolatilization. The statistical uncertainty in the mass release data is reduced by using the average of four independent tracers. The measured mass of volatiles released in the flow reactor has been compared with several commonly used rate models.

The data show evidence that the volatiles release is very rapid, and agrees quite well with the 1-step Arrhenius expression for tar release reported by Solomon, et al. [1986] for coals experiencing similar heating rates. Three simple rate models, with constants taken from other experiments, have also been compared with these temperature-resolved experimental data. Only the 2-step model with coefficients recommended by Ubhayakar et al. [1976] gives pyrolysis time scales comparable with this set of data. A more sophisticated model based on the chemical structure of the coal (the CPD model) used these data as a basis to determine rate coefficients. Evidence for rank-dependent kinetics is observed when the CPD model is compared with the time-dependent mass release data from five different coals at two temperature conditions.

The particle temperature measurements are viewed as critical to the determination of pulverized coal pyrolysis rates under rapid heating conditions. Kinetic coefficients derived from this experiment should be more universally applicable than previous data where particle temperature measurements were not performed. The facts that the minimum particle temperature measurement threshold is 850 K, and that

devolatilization commences at lower temperatures than 850 K, do not impede the use of these data. On the contrary, if the kinetic rates were slower, as proposed by other investigators, 850 K would be the temperature at which devolatilization begins. The data presented here, however, indicate that approximately 50% of the mass release during devolatilization occurs by the time a particle temperature of 850 K is achieved, and hence kinetic rates obtained from these data are higher than initially expected. These data therefore serve as an excellent basis for determining the kinetics of devolatilization, even though temperature measurements over the entire extent of mass release are not available. *When this project started, the range of devolatilization rates at any temperature was five orders of magnitude. As a result of these experiments, the current uncertainty in devolatilization rates at rapid heating rates is thought to be less than a factor of five.*

D. Physical Structure of Char Particles

Char samples collected in the CDL and in the CCL were analyzed for apparent density, and an effective diameter was calculated from the apparent density and the extent of mass release. Maximum particle swelling occurred in the chars from Pittsburgh #8 coal collected in the CDL, with a 50% diameter increase observed. The low rank coals did not swell significantly. The low rank coal chars exhibited a great increase in internal surface area compared with the high rank coals chars. Chars from a softening coal (Pittsburgh #8) were examined with SEM in order to show the different stages of swelling, including the opening of fissures, the generation of internal voids, and the rounding of surface features due to softening.

E. Elemental Mass Release

Elemental release rates from five different coals during devolatilization were measured. Low rank coals release oxygen earlier than high rank coals. In general, oxygen and hydrogen release occur at similar rates, while carbon and nitrogen release rates are correlated for all coals. The carbon release rate is proportional to the total mass release rate in the high rank coals, but is slower than the total mass release for low rank coals due to the large quantity of oxygen that is released early in the devolatilization process.

When coals devolatilize, the elemental release profiles do not follow the coalification band. Oxygen and hydrogen are released during devolatilization at similar rates, and hence the low rank coal char profiles bypass the bend in the coalification band. The fully-devolatilized coal chars all lie in a small region of the coalification chart compared to the diversity of the parent coals. However, the fully-devolatilized chars collected do exhibit slight differences, especially with respect to oxygen content, and none approach the composition of graphite.

F. Chemical Structure

Char Structure from NMR Analyses

Based on the NMR analyses of the chars formed during devolatilization of five coals of different rank at the 1250 K gas condition, the following conclusions are reached:

1) NMR data can be used to track lattice parameters associated with average cluster size and cross linking reactions. Under rapid heating conditions the NMR data demonstrate that the Zap lignite undergoes early cross linking behavior, while higher rank coals exhibit a slower overall rate of crosslinking.

2) Under rapid heating conditions (10^4 K/sec), the data exhibit: a) little evidence of cluster size growth in the macromolecular structure; b) crosslinking at the same time that aliphatic carbons are released; c) little evidence for graphitization under the temperature and residence time conditions of these experiments.

3) In the Illinois No. 6 coal, most of the mass release has occurred before significant changes in carbon aromaticity has occurred. In chars from Zap lignite, the changes in carbon aromaticity occur much earlier than for the bituminous coal.

4) The carbon skeletal structure of the final chars from coals of all ranks are quite similar, even though the structures of the initial coals are quite different.

Tar Structure from NMR Analyses

Based on the ^{1}H and ^{13}C NMR analysis of the tars collected from four coals of different rank in the 1250 K and 1050 K gas conditions, the following conclusions are reached:

1) The pyrolysis temperature has a major effect on the tar structure. The proton and carbon aromaticities of the tars from a given coal in the 1250 K gas condition are higher than for samples collected at comparable extents of mass release in the 1050 K gas condition.

2) The carbon aromaticities of the bituminous and subbituminous coal tars at 1250 K are higher than the values for the corresponding chars collected at the same residence time. On the other hand, the carbon aromaticities found in the Zap lignite tars are comparable to those observed in the chars.

3) The proton NMR data suggest that in the 1250 K gas condition, hydrogens associated with 2- and 3-ring aromatic compounds increase, while that of 1-ring compounds decrease for the Illinois No. 6 tars. Similar but less compelling evidence is noted for the lignite and subbituminous coal tars. These data may suggest the conversion of hydroaromatic species to condensed polynuclear aromatic species and/or ring polymerization.

4) The α-hydrogen content in the initial tars evolved increases as a function of coal rank. The α-hydrogen in the tars from the three non-lignitic coals decreases with residence time at the 1250 K condition but not at the 1050 K condition. This observation suggests that relatively stable CH and/or CH_2 bridges exist at the 1050 K gas condition in the higher rank coals. However, at 1250 K substantial bond rupture may be occurring.

5) The α-methyl groups are released early in tars from all four coals at 1250 K, but do not decrease significantly at 1050 K.

6) The γ-methyl groups in both tars are the most susceptible to cracking reactions in the gas phase, but the extent of release of the β- and γ-hydrogens is based on gas temperature conditions and residence time. The percentage of γ-methyl groups in the initial tar evolved decreases as coal rank increases.

The NMR data presented here for char and tar samples from the CDL have led to greater understanding of the pyrolysis process. These data are unique, not only because they are the first to be taken as a function of residence time at rapid heating rates, but because the temperature and reaction history is so well-characterized. The chemical percolation devolatilization (CPD) model [Grant, et al., 1989; Fletcher, et al, 1990; Fletcher, et al., 1991] directly uses these data on the chemical structure of parent coals as input parameters, and the data at later residence times are used to evaluate the model.

Tar Structure from Mass Spectrometry

Based on the Curie-point GC/MS and low-voltage MS analyses of the tar formed during devolatilization of Beulah Zap, New Mexico Blue, Illinois #6, Pittsburgh #8, and Pocahontas #3 coals, the following conclusions are reached:

1. The degree of aromaticity increases rapidly in tars from all five coals as a function of residence time at the 1250 K gas temperature. However, little increase in aromaticity in the tars is detected at the 1050 K gas temperature.

2. At a gas temperature of 1250 K, devolatilization is complete within 70 msec and secondary gas-phase reactions of tar vapors can be observed within 100 msec. At 1050 K, the devolatilization process appears to be more or less complete after 250 msec.

3. In order to study the complete devolatilization process and the possible onset of secondary reactions, further experiments should be conducted at an intermediate temperature, e.g., 1150 K.

These conclusions are consistent with the ^{1}H and ^{13}C NMR analyses performed previously on these same tars.

Results of Additional Experiments

A. Transition from Coal Devolatilization to Char Oxidation

Based on the results of the experiments conducted in the CDL and the CCL as a function of gas phase oxygen concentration, the following conclusions are reached:

1. The degree of swelling during coal pyrolysis at rapid heating conditions ($> 10^4$ K/s) is not affected by the gas phase oxygen concentration. Changes in particle swelling caused by the presence of oxygen reported in other experiments may be due to partial oxidation of char samples subsequent to pyrolysis.

2. Pittsburgh #8 coal particles increased in diameter by 50% in the CDL experiments and by less than 10% in the CCL experiments. Differences in swelling behavior were caused by differences in particle heating rate and/or the presence of post-flame combustion gases (e.g., CO_2, H_2O, or trace radical species).

3. An examination of samples obtained in the char combustion experiments in the CCL revealed the absence of any transparent cenospheres; these types of particles were either not formed or were consumed upstream of the sampling location.

4. Calculations of particle heating rates indicate that maximum particle heating rate in the CCL for the size fractions typically used (106-125 μm) is 4.5 x 10^4 K/s, which is a factor of two to three higher than the maximum heating rate experienced in the CDL experiments. The calculated difference between the particle heating rates at 0% O_2 in the two different laboratories may be responsible for the differences in the physical properties of the char particles. Because the heating rates were within a factor of two to three, however, other possible causes for the observed differences in swelling behavior should also be investigated.

B. Temperature Measurements of Burning Char Particles

The size and temperatures of burning char particles were measured in the CDL in N_2-O_2 atmospheres at 1000 K containing up to 12% O_2. Temperatures of burning bituminous char particles were estimated to exceed 1500 K (compared to 1686 K measured at UNDEMRC), but less than 5% of the particles ignited under these conditions, and detailed statistical measurements were not possible. It is difficult to compare the temperatures measured in this experiment with those measured at UNDEMRC, since it not clear how to conditionally average the data from ignited and

non-reacting particles. Lignite char particle temperatures measured in the CDL in 10% O_2 were approximately 1600 K, which is the in the same range as measured at UNDEMRC (1586 K). However, data from the lignite char experiments in the CDL also indicate the presence of significant numbers of non-burning particles (25 to 75%). Extents of burnout in solid samples taken from experiments where significant numbers of char particles have not ignited are impossible to interpret unless the precise percentage of non-burning particles is known.

References for Chapter 7

Fletcher, T. H., A. R. Kerstein, R. J. Pugmire, and D. M. Grant, "A Chemical Percolation Model for Devolatilization: 3. Chemical Structure as a Function of Coal Type," in press (1991). See also Fletcher, T. H. and D. R. Hardesty, "Coal Combustion Science: Task 1, Coal Devolatilization," DOE/PETC Quarterly Progress Report for October to December, 1990, edited by D. R. Hardesty, Sandia Report No. SAND91-8210, available NTIS (1991).

Fletcher, T. H., Kerstein, A. R., Pugmire, R. J., and Grant, D. M., *Energy & Fuels*, **4**, 54 (1990).

Grant, D. M., Pugmire, R. J., Fletcher, T. H., and Kerstein, A. R., *Energy & Fuels*, **3**, 175 (1989).

Solomon, P. R., Serio, M. A., Carangelo, R. M., and Markham, J. R., *Fuel*, **65**, 182 (1986).

Ubhayakar, S. K., D. N. Stickler, C. W. von Rosenberg, and R. E. Gannon, *16th Symp. (Int.) on Comb.*, The Combustion Institute, Pittsburgh, PA, 427 (1976).

8. ACKNOWLEDGEMENTS

Research at Sandia was supported by the U. S. Department of Energy's Pittsburgh Energy Technology Center's Direct Utilization AR&TD Program; James Hickerson was the project manager and Philip Goldberg was the project technical officer.

The NMR characterizations of char and tar were performed at the University of Utah and Brigham Young University by Dr. Mark Solum and Scott Critchfield, under the direction of Professors Ronald Pugmire and David Grant. The mass spectrometry was performed by Robert Lo at the University of Utah under the direction of Professor Henk Meuzelaar. The NMR and MS analyses of char and tar samples from Sandia represent an ongoing collaboration between Sandia and the University of Utah, and was supported through the Advanced Combustion Engineering Research Center at BYU and the Univ. of Utah, which is supported by the National Science Foundation, 23 industrial firms, and DOE/PETC. Additional support for the NMR work was provided through the Consortium for Fossil Fuel Liquefaction Science by DOE/PETC.

Special thanks are extended to Allen Salmi, William Kent, and Steve Smith who helped build the Coal Devolatilization Laboratory (CDL) at Sandia and obtain the experimental data. Ken Hencken and Dan Tichenor helped designed the optical system, and helped to debug the system. Scott Ferko helped with the experiments in the Char Combustion Laboratory (CCL). Larry Baxter helped perform most of the particle emissivity measurements and provided useful discussion in the early development of the CDL as a summer student from BYU, and later helped to develop a computer model to investigate the effects of rapid heating on the Nusselt number. Steve Hsu worked on part of his Ph. D. for one summer in collaboration with Jack Howard at MIT. William Replogle helped collect data for two summers in the CDL while studying at Chabot College and the Univ. of Calif. at Berkeley. David Ottesen provided helpful suggestions, and helped with the particle emissivity work. Reginald Mitchell provided many useful discussions and support. Don Hardesty helped arrange financial support, and gave many useful comments for the development of the laboratory and the publications that resulted from the research.

A special thanks is extended to Dr. Zak Hanna and his staff at Coors Analytical Laboratories Division, in Golden Colorado, who performed the proximate, ultimate, and ICP analyses of Sandia coal and char samples.

9. PUBLICATIONS AND PRESENTATIONS

Publications
(listed in chronological order)

Musarra, S. P., T. H. Fletcher, S. Niksa, and H. A. Dwyer, "Heat and Mass Transfer in the Vicinity of a Devolatilizing Coal Particle," *Combustion Science and Technology*, **45**, 289-307 (1986).

Holve, D. J., K. Gomi, and T. H. Fletcher, "Comparative Combustion Studies of Ultrafine Coal/Water Slurries and Pulverized Coal," *Combustion Science and Technology*, **52**, 269-291 (1987), Sandia Report SAND85-8706 (May 1985).

Niksa, S., A. R. Kerstein, and T. H. Fletcher, "Predicting Devolatilization at Typical Coal Combustion Conditions with the Distributed-Energy Chain Model," *Combustion and Flame*, **69**, 221-228 (1987).

Dudek, D. and T. H. Fletcher, "Numerical Calculation of the Drag Force Induced by Natural Convection on Spheres at Low Grashof Numbers," Sandia Report SAND87-8201 (February, 1987).

Fletcher, T. H., Baxter, L. L., and Ottesen, D. K., "Spectral Emissivities of Size-Graded Coal Particles: Implications for Pyrometry," *1987 International Conference on Coal Science*, ed. Moulijn, J. A., Nater, K. A. , and Chermin, H. A. G., Elsevier, New York, p. 945, 1987.

Smith, P. J. and T. H. Fletcher, "A Study of Two Chemical Reaction Models in Turbulent Coal Combustion," *Combustion Science and Technology*, **58**, 59-76 (1988).

Dudek, D. R., T. H. Fletcher, J. P. Longwell, and A. F. Sarofim, "Natural Convection Induced Drag Forces on Spheres at Low Grashof Numbers: Comparison of Theory with Experiment," *International Journal of Heat and Mass Transfer*, **31**:4, 863-873 (1988).

Baxter, L. L., Fletcher. T. H., and Ottesen, D. K., "Spectral Emittance of Coal Particles," *Energy and Fuels*, **2**, 423 (1988).

Grant, D. M., R. J. Pugmire, T. H. Fletcher, and A. R. Kerstein, "A Chemical Model of Coal Devolatilization Using Percolation Lattice Statistics," *Energy and Fuels*, **3**, 175 (1989).

Fletcher, T. H., "Time-Resolved Temperature Measurements of Individual Coal Particles During Devolatilization," *Combustion Science and Technology* **63**, 89 (1989).

Fletcher, T. H., "Time-Resolved Particle Temperature and Mass Loss Measurements of a Bituminous Coal During Devolatilization," *Combustion and Flame* **78**, 223 (1989).

Pugmire, R. J., T. H. Fletcher, D. M. Grant, and A. R. Kerstein, "A Chemical Model of Coal Devolatilization Using Percolation Lattice Statistics," *Proceedings of the 1989 International Conference on Coal Science*, Elsevier Press, London, England, vol. 1, p. 481 (October 23-27, 1989).

Fletcher, T. H., A. R. Kerstein, R. J. Pugmire, and D. M. Grant, "Chemical Percolation Model for Devolatilization: II. Temperature and Heating Rate Effects on Product Yields," *Energy and Fuels*, **4**, 54 (1990).

Fletcher, T. H., M. S. Solum, D. M. Grant, S. Critchfield, and R. J. Pugmire, "Solid-State ^{13}C and ^{1}H NMR Studies of the Evolution of the Chemical Structure of Coal Char and Tar During Devolatilization," *Twenty-Third Symposium (International) on Combustion*, The Combustion Institute, Pittsburgh, PA, p. 1231 (1990).

Pugmire, R. J., M. S. Solum, D. M. Grant, S. Critchfield, and T. H. Fletcher, "Structural Evolution of Matched Tar/Char Pairs in Rapid Pyrolysis Experiments," *Fuel*, **70**, 414 (1991).

Fletcher, T. H., A. R. Kerstein, R. J. Pugmire, and D. M. Grant, "A Chemical Percolation Model for Devolatilization: 3. Chemical Structure as a Function of Coal Type," submitted to *Energy and Fuels* (1991).

Solomon, P. R., T. H. Fletcher, and R. J. Pugmire, "Progress in Coal Pyrolysis," accepted for publication, *Fuel* (1992).

Presentations
(listed in chronological order)

Musarra, S. P., T. H. Fletcher, S. Niksa, and H. A. Dwyer, "Heat and Mass Transfer in the Vicinity of a Devolatilizing Coal Particle," presented at the 23rd ASME/AIChE National Heat Transfer Conference, Denver, Colorado, August 1985.

Fletcher, T. H., "Sensitivity of Combustion Calculations to Devolatilization Rate Expressions," presented at the 1985 Fall Meeting of the American Flame Research Committee, Sandia National Laboratories, Livermore, California, October 17-18, 1985.

Holve, D. J., J. Hoornstra, and T. H. Fletcher, "The Influence of Size Distribution Characteristics in Heterogeneous Combustion," presented at the 1985 Fall

Meeting of the American Flame Research Committee, Sandia National Laboratories, Livermore, California, October 17-18, 1985.

Smith, P. J. and T. H. Fletcher, "A Study of Two Chemical Reaction Models in Turbulent Coal Combustion," presented at the 1985 Fall Meeting of the Western States Section of the Combustion Institute, Davis, California, October 21-22, 1985.

Niksa, S., A. R. Kerstein, and T. H. Fletcher, "Predicting Devolatilization at Typical Coal Combustion Conditions with the Distributed-Energy Chain Model," American Chemical Society Division of Fuel Chemistry Preprints, **31**:3, 237, Anaheim, California (September, 1986)

Niksa, S., A. R. Kerstein, and T. H. Fletcher, "Predicting Devolatilization at Typical Coal Combustion Conditions with the Distributed-Energy Chain Model," presented at the 2nd ASME/JSME Thermal Engineering Joint Conference, Honolulu, Hawaii (March, 1987).

Baxter, L. L., D. K. Ottesen, and T. H. Fletcher, "Spectral Emission Characteristic of Coal Particles," presented at the Western States Section of the Combustion Institute 1987 Spring Meeting, Provo, Utah (April, 1987).

Fletcher , T. H., L. L. Baxter, and D. K. Ottesen, "Spectral Emission Characteristics of Size-Graded Coal Particles," ACS Div. Fuel Chem. Preprints, **32**:3, 42-50 (1987).

Fletcher, T. H., "Kinetics of Rapid Coal Devolatilization," presented at the 1987 PETC/METC AR&TD Contractors' Review Meeting, Morgantown, West Virginia (October 14-16, 1987).

Grant, D. M., R. J. Pugmire, T. H. Fletcher, and A. R. Kerstein, "A Chemical Model of Coal Devolatilization Using Percolation Lattice Statistics," presented at the Western States Section of the Combustion Institute 1988 Spring Meeting, Salt Lake City, Utah (March, 1988). Also in ACS Division of Fuel Chemistry preprints, Volume **33**:2, 322 (June, 1988).

Fletcher, T. H., "Time-Resolved Temperature Measurements of Individual Coal Particles During Devolatilization," presented at the Western States Section of the Combustion Institute 1988 Spring Meeting, Salt Lake City, Utah (March, 1988). Presented at the poster session of the 22nd Symposium (International) on Combustion, Seattle, Washington (August, 1988).

Fletcher, T. H., "Kinetics of Rapid Coal Devolatilization," presented at the 1988 PETC/METC AR&TD Contractors' Review Meeting, Pittsburgh, Pennsylvania (September 6-9, 1988).

Fletcher, T. H., "Time-Resolved Particle Temperature and Mass Loss Measurements of a Bituminous Coal During Devolatilization," presented at the Fall 1988 Meeting of the Western States Section of the Combustion Institute, Dana Point, California (October 17-18, 1988).

Fletcher, T. H., "Kinetics of Rapid Coal Devolatilization," invited seminar at the University of Utah (October 25, 1988). (no associated technical paper)

Solum, M. S., R. J. Pugmire, D. M. Grant, T. H. Fletcher, and P. Solomon, "Solid State ^{13}C NMR Studies of Coal Char Structure Evolution," presented at the 1989 Spring Meeting of the Western States Section of the Combustion Institute, Pullman, Washington (March 20-21, 1989).

Fletcher, T. H., A. R. Kerstein, R. J. Pugmire, and D. M. Grant, "Prediction of the Effects of Heating Rate and Temperature on Pulverized Coal Devolatilization," presented at the First Symposium on Advances in Coal Spectroscopy, Snowbird, Utah (June 14-16, 1989).

Fletcher, T. H., A. R. Kerstein, R. J. Pugmire, R. J., and D. M. Grant, "A Chemical Percolation Model for Devolatilization: II. Temperature and Heating Rate Effects," prepr.ACS Div. Fuel Chem. **34**:4, 1272 (1989).

Solum, M. S., R. J. Pugmire, D. M. Grant, T. H. Fletcher, and P. R. Solomon, "Solid State ^{13}C NMR Studies of Coal Char Structure Evolution," prepr. ACS Div. Fuel Chem., **34**:4, 1337 (1989).

Fletcher, T. H., A. R. Kerstein, R. J. Pugmire, and D. M. Grant, "A Chemical Percolation Model for Devolatilization: II. Temperature and Heating Rate Effects," presented at the WSS/CI Fall Meeting, Livermore, California (October, 1989).

Fletcher, T. H., "Kinetics of Rapid Coal Devolatilization," presented at the 1989 PETC/METC AR&TD Contractors' Review Meeting, Morgantown, West Virginia (October 3-5, 1989).

Mitchell, R. E. and T. H. Fletcher, "Particle-Sizing Pyrometry in Pulverized Coal-Seeded Flow Reactors," presented at the Annual Meeting of the American Institute of Chemical Engineers, San Francisco, CA (November, 1989). (no associated technical paper)

Lo, R., T. H. Fletcher, R. J. Pugmire, and H. Meuzelaar, "Curie-Point Desorption GC/MS and Low Voltage MS Studies of the Chemical Composition of Coal Tars During Rapid Devolatilization," presented at the 13th Annual Symposium of the Rocky Mountain Fuel Society, Salt Lake City, Utah (March, 1990).

Pugmire, R. J., T. H. Fletcher, M. S. Solum, S. Critchfield, and D. M. Grant, "Structural Evolution of Matched Tar/Char Pairs in Rapid Pyrolysis Experiments," presented at the poster session for the Twenty-Third Symposium (International) on Combustion, Orléans, France (July 22-27, 1990).

Lo, R., R. J. Pugmire, T. H. Fletcher, and H. L. C. Meuzelaar, "Mass Spectrometric Studies of the Chemical Composition of Coal Tars Produced in a Laminar Flow Reactor," prepr. ACS Div. of Fuel Chem., **35**:3, 697 (1990).

Pugmire, R. J., M. S. Solum, D. M. Grant, S. Critchfield, and T. H. Fletcher, "Structural Evolution of Matched Tar/Char Pairs in Rapid Pyrolysis Experiments," presented at the International Conference on Coal Structure and Reactivity, Queens College, Cambridge, UK (September 5-7, 1990).

Baxter, L. L., R. E. Mitchell, and T. H. Fletcher, "Experimental Determination of Mineral Matter Release During Coal Devolatilization," proceedings of the Seventh Annual International Pittsburgh Coal Conference, Pittsburgh, Pennsylvania, p. 62 (1990). Also Sandia Report No. SAND90-8667 (December, 1990).

Solomon, P. R., T. H. Fletcher, and R. J. Pugmire, "Progress in Coal Pyrolysis," proceedings of the Seventh Annual International Pittsburgh Coal Conference, Pittsburgh, Pennsylvania, p. 3 (1990).

Fletcher, T. H., "Rates and Mechanisms of Pulverized Coal Devolatilization at Rapid Heating Rates," presented at the DOE/PETC Advanced Research and Technology Development, Direct Utilization and Instrumentation and Diagnostics Contractors' Review Meeting, Pittsburgh, Pennsylvania (September 16-18, 1990).

Fletcher, T. H., D. M. Grant, and R. J. Pugmire, "Predicting Vapor Pressures of Tar and Metaplast During Coal Pyrolysis," prepr. ACS Div. of Fuel Chem., **36**:1, 250 (1991).

Fletcher, T. H., "Rates and Mechanisms of Pulverized Coal Devolatilization at Rapid Heating Conditions," presented at the Seventh Annual DOE/PETC Coal Preparation, Utilization, and Environmental Control Contractors Conference, Pittsburgh, Pennsylvania (1991).

Appendix A
Derivation of the Blowing Parameter

This appendix contains a formal derivation of the moisture evaporation equation at high rates of mass transfer. For a binary system (H_20 in N_2), the rate of mass transfer is defined as follows:

$$\mathbf{n}_A - \omega_A (\mathbf{n}_A + \mathbf{n}_B) = -\rho D_{AB} \vec{\nabla} \omega_A \tag{A.1}$$

or

$$\mathbf{n}_A = -\rho D_{AB} \vec{\nabla} \omega_A - \omega_A (\mathbf{n}_A + \mathbf{n}_B) \tag{A.2}$$

The sum ($\mathbf{n}_A + \mathbf{n}_B$) can be expressed as a total flux $\mathbf{n}_T$ to give:

$$\mathbf{n}_A = -\rho D_{AB} \vec{\nabla} \omega_A - \omega_A \mathbf{n}_T \tag{A.3}$$

In one-dimensional spherical coordinates, Eq. A.3 becomes:

$$n_A = -\rho D_{AB} \frac{\partial \omega_A}{\partial r} - \omega_A n_T \tag{A.4}$$

Multiplying both sides of Eq. A.4 by r^2 yields:

$$r^2 n_A = -\rho D_{AB} r^2 \frac{\partial \omega_A}{\partial r} - r^2 \omega_A n_T \tag{A.5}$$

The species continuity equation for a binary system is:

$$\frac{\partial \rho_A}{\partial t} = -\vec{\nabla} \cdot \mathbf{n}_A + \dot{r}_A \tag{A.6}$$

where $\dot{r}_A$ is the net production rate of species A in the gas phase, which is zero for the case of moisture evaporation. The process can also be assumed to be at steady state, with no unsteady accumulation of water vapor near the particle. Eq. A.6 then becomes:

$$\vec{\nabla} \cdot \mathbf{n}_A = 0 \tag{A.7}$$

or

$$\frac{1}{r^2}\frac{\partial}{\partial r}(r^2 n_A) = 0 \tag{A.8}$$

which reduces to:

$$r^2 n_A = c \tag{A.9}$$

where c is a constant. Equation A.5 can be differentiated with respect to r, resulting in the following:

$$\frac{1}{r^2}\frac{\partial}{\partial r}(r^2 n_A) = 0 = -\frac{\partial}{\partial r}\left(\rho D_{AB} r^2 \frac{\partial \omega_A}{\partial r}\right) + \frac{\partial}{\partial r}(r^2 \omega_A n_T) \tag{A.10}$$

Grouping terms, and assuming that ρD_{AB} does not vary with r,

$$\frac{\partial}{\partial r}\left(r^2 \frac{\partial \omega_A}{\partial r}\right) = \frac{\rho D_{AB}}{r^2 n_T}\frac{\partial}{\partial r}(\omega_A) \tag{A.11}$$

Equation A.12 is a second order partial differential equation:

$$(x^2 y')' = A y' \tag{A.12}$$

where

$$A = \frac{r^2 n_T}{\rho D_{AB}} \tag{A.13}$$

The solution to Eq. A.12 is:

$$y = c_1 e^{-A/x} + c_2 \tag{A.14}$$

where $y = \omega_A$ and $x = r$. As proof, take the appropriate derivatives and compare with Eq. A.12:

$$y' = \frac{A\, c_1\, e^{-A/x}}{x^2} \tag{A.15}$$

$$x^2\, y' = A\, c_1\, e^{-A/x} \tag{A.16}$$

$$(x^2\, y')' = \frac{A^2\, c_1\, e^{-A/x}}{x^2} = A\, y' \tag{A.17}$$

The boundary conditions for evaporation of a water droplet in an infinite medium become:

(a) at r = R:

$$\omega_A = \omega_{A,o} \quad (\text{at } x = R,\ y = y_o) \tag{A.18}$$

$$y_o = c_1\, e^{-A/R} + c_2 \tag{A.19}$$

(b) at r = ∞:

$$\omega_A = \omega_{A,\infty} \quad (\text{at } x = R,\ y = y_\infty) \tag{A.20}$$

$$y_\infty = c_1 + c_2 \tag{A.21}$$

Combining Eqs. A.19 and A.21,

$$c_2 = y_\infty - c_1 \tag{A.22}$$

and Eq. A.19 therefore becomes:

$$y_o = c_1\, e^{-A/R} - c_1 + y_\infty \tag{A.23}$$

so that

$$y_o - y_\infty = c_1 \left(e^{-A/R} - 1\right) \tag{A.24}$$

Solving for c_1,

$$c_1 = \frac{y_o - y_\infty}{(e^{-A/R} - 1)} \tag{A.25}$$

Using these boundary equations, Eq. A.3 becomes:

$$n_A|_{r=R} = -\rho D_{AB} \frac{A\, c_1\, e^{-A/R}}{R^2} + \omega_{A,o}\, n_T \tag{A.26}$$

$$n_A|_{r=R} = \frac{-\rho D_{AB}\, A\, (\omega_{A,o} - \omega_{A,\infty})\, e^{-A/R}}{R^2 (e^{-A/R} - 1)} + \omega_{A,o}\, n_T \tag{A.27}$$

Now let B = A/R. Equation A.27 becomes:

$$n_A|_{r=R} = \frac{-\rho D_{AB}\, (\omega_{A,o} - \omega_{A,\infty})}{R} \frac{B\, e^{-B}}{(e^{-B} - 1)} + \omega_{A,o}\, n_T \tag{A.28}$$

Multiplying the e^{-B} term by e^B/e^B,

$$n_A|_{r=R} = \frac{-\rho D_{AB}\, (\omega_{A,o} - \omega_{A,\infty})}{R} \frac{B}{(e^B - 1)} + \omega_{A,o}\, n_T \tag{A.29}$$

The mass transfer coefficient k_m is commonly correlated as:

$$Sh = \frac{k_m\, d_p}{\rho_g D_w} = 2 + 0.6\, Re^{0.5}\, Sc^{0.333} \tag{A.30}$$

where k_m is defined by the rate of mass transfer at low mass transfer rates:

$$n_A|_{r=R} = k_m (\omega_{A,o} - \omega_{A,\infty}) \tag{A.31}$$

At low particle Reynolds numbers typical of pulverized coal combustion, Sh = 2.0, and

$$k_m = \frac{2\, \rho D_{AB}}{d} = \frac{\rho D_{AB}}{R} \tag{A.32}$$

The mass transfer coefficient k_m defined in Eq. A.30-A.32 is therefore substituted into Eq. A.29:

$$n_A|_{r=R} = k_m(\omega_{A,o} - \omega_{A,\infty})\frac{B}{(e^B - 1)} + \omega_{A,o}\, n_T \qquad (A.33)$$

If water is the only reaction rate at the surface,

$$n_A|_{r=R} = n_T|_{r=R} = \frac{\dot{W}}{\pi d^2} \qquad (A.34)$$

After dropping the subscript A, Eq. A.33 becomes:

$$(1 - \omega_o)\, n_A|_{r=R} = k_m(\omega_o - \omega_\infty)\frac{B}{(e^B - 1)} \qquad (A.35)$$

or

$$n_A|_{r=R} = k_m \frac{(\omega_o - \omega_\infty)}{(1 - \omega_o)}\frac{B}{(e^B - 1)} \qquad (A.36)$$

The definition of B is therefore:

$$B = A/R = \frac{R\, n_T}{\rho D_{AB}} = \frac{\dot{W}}{2\pi d \rho D_{AB}} \qquad (A.37)$$

Nomenclature for Appendix A

Variable	Definition
d	particle diameter
D_{AB}	diffusivity of species A in species B
k_m	mass transfer coefficient
$\mathbf{n}_A$	mass flux vector of species A per unit area
n_A	mass flux of species A per unit area
r	radial distance
R	particle radius
$\dot{r}_A$	reaction rate of species A

Greek	
ρ	density
ω_A	mass fraction of species A

Subscripts	
A	species A
B	species B
o	initial condition
T	total
∞	free stream condition

APPENDIX B

MEASURED GAS TEMPERATURES, CORRECTED FOR RADIATION LOSSES

PSOC-1445D, 106-125 μm

1050 K*

z (mm)	T_g (K)
0.0	294
2.1	410
5.9	570
11.5	664
21.0	760
36.9	862
80.0	975
120.1	1004
150.1	1005
180.0	1000
220.1	989
250.2	977
280.1	972

1250 K

z (mm)	T_g (K)
0.0	294
1.6	455
2.1	474
3.1	522
4.0	565
5.5	636
6.9	682
8.4	720
10.5	761
12.6	794
16.3	843
21.6	898
26.1	936
35.1	979
39.8	1023
48.7	1064
59.0	1102
66.9	1126
76.3	1151
102.4	1188
118.5	1220
138.3	1234
159.7	1241
200.9	1241
217.1	1239
236.0	1234
252.1	1224
268.0	1216
285.0	1204

*The first data set for PSOC-1445D at 1050 K was in error, based on measured particle temperatures and velocities. The "duplicate set" is therefore used as the good set, and these data are from that "duplicate set."

PSOC-1451D, 106-125 μm,

1050 K

z (mm)	T_g (K)
0.0	294
4.0	453
6.0	505
8.0	543
10.0	573
12.0	597
14.0	618
16.0	636
18.0	654
20.0	669
24.0	699
28.0	725
32.0	750
36.0	774
40.0	796
45.0	822
50.0	847
55.0	872
60.0	893
65.0	910
70.0	929
80.0	959
90.0	980
100.0	996
120.0	1014
140.0	1021
160.0	1021
200.0	1015
220.0	1010
250.0	994

1250 K

z (mm)	T_g (K)
0.0	294
4.6	574
9.8	708
16.8	802
27.5	902
38.8	986
54.8	1085
75.0	1175
100.5	1234
123.4	1254
147.7	1256
171.4	1252
204.1	1241
236.4	1226
264.9	1208
287.7	1194

PSOC-1451D, 63-75 μm,

1050 K

z (mm)	T_g (K)
0.0	294
7.2	520
12.0	591
17.7	645
21.9	676
29.1	718
37.5	758
47.3	795
60.0	833
71.9	862
88.4	894
112.9	929
136.6	952
167.9	972
190.8	980
221.7	984
252.2	983
273.7	978
293.7	972

1250 K

z(mm)	T_g (K)
0.0	294
3.3	512
5.5	603
8.9	692
12.7	753
16.6	802
21.2	847
29.1	909
37.4	960
50.4	1018
65.0	1066
82.1	1108
101.2	1142
124.9	1171
147.2	1188
173.5	1200
192.5	1203
223.7	1201
253.9	1191
281.2	1178
297.0	1166

(repeat experiments)

1050 K

z (mm)	T_g (K)
0.0	294
2.1	410
5.9	570
11.5	664
21.0	760
36.9	862
80.0	975
120.1	1004
150.1	1005
180.0	1000
220.1	989
250.2	977
280.1	972

PSOC-1493D, 106-125 μm

1050 K

z(mm)	Tg (K)
3.0	438
6.1	547
11.5	651
21.0	749
29.8	809
43.8	876
60.5	928
82.7	970
100.1	990
120.0	1005
150.0	1015
180.0	1017
200.0	1016
220.0	1013
250.2	1003
280.0	992

1250 K

z (mm)	Tg (K)
0.8	414
2.4	476
4.1	567
6.8	680
10.1	762
16.7	870
24.8	965
34.7	1045
45.0	1108
61.2	1169
82.9	1216
125.8	1247
140.0	1249
178.4	1240
221.0	1220
250.0	1202
280.0	1182

(repeat experiments at 1250 K)

z (mm)	T_g (K)	z (mm)	T_g (K)
0.0	292	21.4	936
1.8	418	26.5	984
2.8	516	33.2	1033
3.4	576	44.4	1086
4.2	631	70.0	1151
5.2	674	100.1	1181
7.1	727	150.0	1192
9.5	772	180.3	1188
12.8	832	250.1	1165
16.5	884	280.5	1152

PSOC-1507D, 75-106 μm

1050 K

z(mm)	Tg (K)
0	293.97
3.7	468
5.8	526
9.6	592
12.9	629
17.5	668
23.8	711
29.8	744
38.0	781
49.8	823
63.5	861
78.9	894
96.6	924
116.1	948
138.8	969
160.5	982
185.3	993
195.5	995
221.4	997
250.6	994
271.4	989
296.6	979

1250 K

z(mm)	Tg (K)
0.0	294
3.3	551
9.7	732
14.7	800
21.8	870
29.5	926
39.3	980
50.0	1026
67.9	1083
88.0	1129
112.7	1169
134.5	1193
161.3	1210
179.2	1215
215.8	1217
243.8	1211
271.4	1201
297.4	1186

PSOC-1507D, 75-106 μm
(repeat experiments)

1050 K

z(mm)	Tg (K)
0.0	294
2.1	410
5.9	570
11.5	664
21.0	760
36.9	862
80.0	975
120.1	1004
150.1	1005
180.0	1000
220.1	989
250.2	977
280.1	972

1250 K

z(mm)	Tg (K)
0.0	292
1.8	418
2.8	516
3.4	576
4.2	631
5.2	674
7.1	727
9.5	772
12.8	832
16.5	884
21.4	936
26.5	984
33.2	1033
44.4	1086
70.0	1151
100.1	1181
150.0	1192
180.3	1188
250.1	1165
280.5	1152

PSOC-1508D, 106-125 μm,

1050 K

z(mm)	Tg (K)
0.0	294
1.2	375
2.2	393
4.4	479
5.9	541
8.3	599
11.8	653
17.9	720
24.6	776
32.0	823
43.0	873
60.9	928
83.9	969
112.7	998
143.7	1013
188.7	1018
221.2	1013
250.7	1003
280.7	992

1250 K

z(mm)	Tg (K)
0.0	292
2.1	479
3.0	547
4.7	645
7.5	733
10.5	797
15.1	865
23.0	945
27.7	983
37.4	1043
47.5	1086
67.3	1146
97.9	1191
141.7	1214
180.0	1214
201.0	1208
225.0	1198
251.0	1185
280.0	1167

APPENDIX C

Summary of Sizing-Pyrometry Data

PSOC-1445D, 106-125 μm, 1250 K

z (mm)	t (ms)	v_p (cm/s)	T_p (K)	σ_T (K)
50	58	102	982	59
60	67	105	1000	65
100	103	118	1044	28
180	172	113	1118	14
250	238	98	1107	10

PSOC-1445D, 106-125 μm, 1050 K

z (mm)	t (ms)	v_p (cm/s)	T_p (K)	σ_T (K)
80	88	115	889	50
120	123	111	941	42
180	180	100	974	25
250	253	87	953	25

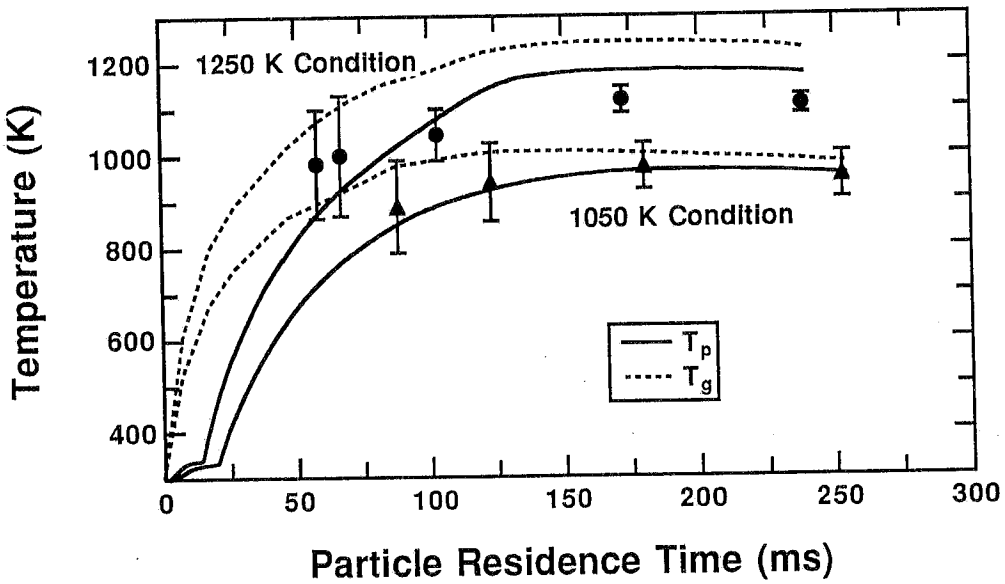

Figure C.1 Calculated (solid curves) and measured (data points) particle temperature histories for the 106-125 μm size fraction of PSOC-1445D New Mexico Blue #1 subbituminous coal in the CDL. Error bars represent two standard deviations in the measured particle temperature.

PSOC-1451D, 106-125 μm, 1250 K

z (mm)	t (ms)	v_p (cm/s)	T_p (K)	σ_T (K)
60	69	103	976	48
80	89	107	1048	30
120	127	105	1164	16
200	204	99	1146	16
240	254	99	1155	17

PSOC-1451D, 106-125 μm, 1050 K

z (mm)	t (ms)	v_p (cm/s)	T_p (K)	σ_T (K)
70	93	82	*	*
90	118	83	911	19
120	154	81	949	11
200	258	73	1023	6
250	336	57	1001	9

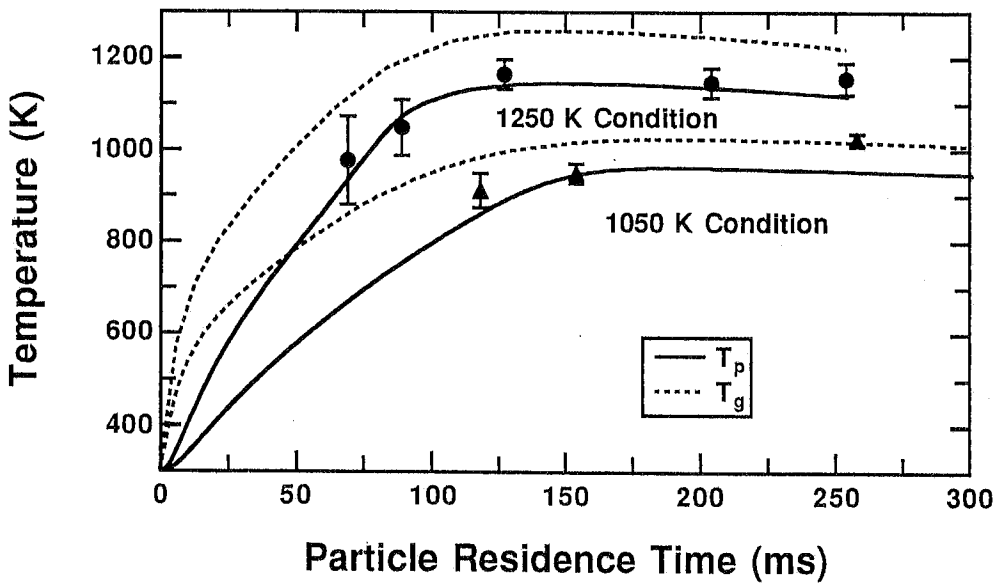

Figure C.2 Calculated (solid curves) and measured (data points) particle temperature histories for the 106-125 μm size fraction of PSOC-1451D Pittsburgh #8 hva bituminous coal in the CDL. Error bars represent two standard deviations in the measured particle temperature.

PSOC-1451D, 63-75 μm, 1250 K

z (mm)	t (ms)	v_p (cm/s)	T_p (K)	σ_T (K)
50	60	95	1017	25
80	90	102	1105	33
120	130	103	1095	19
180	190	98	1164	18
250	255	86	1128	34

PSOC-1451D, 63-75 μm, 1050 K

z (mm)	t (ms)	v_p (cm/s)	T_p (K)	σ_T (K)
80	95	100	909	50
120	136	98	876	21
180	200	88	944	56
250	288	72	922	20

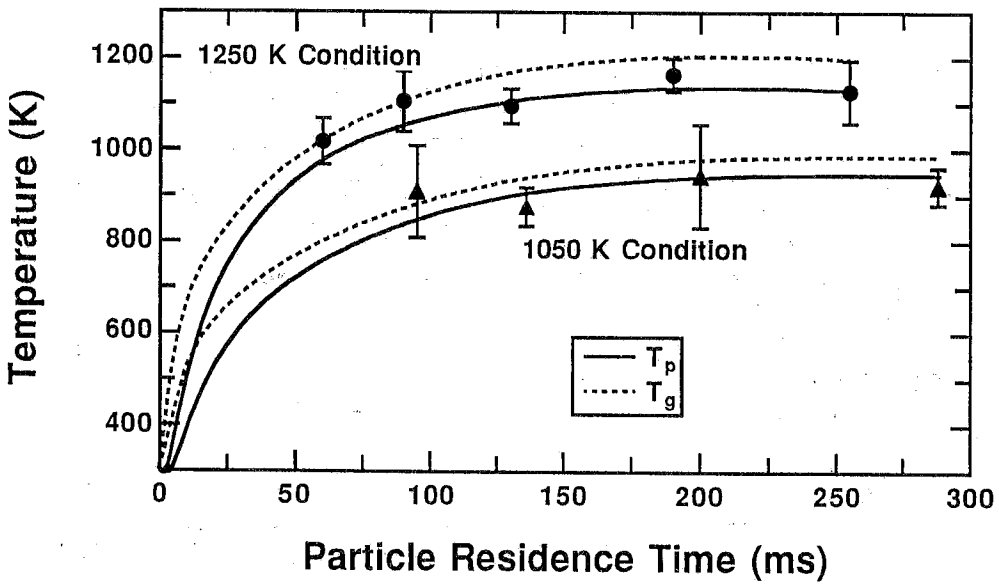

Figure C.3 Calculated (solid curves) and measured (data points) particle temperature histories for the 63-75 μm size fraction of PSOC-1451D Pittsburgh #8 hva bituminous coal in the CDL. Error bars represent two standard deviations in the measured particle temperature.

PSOC-1493D, 106-125 μm, 1250 K

z (mm)	t (ms)	v_p (cm/s)	T_p (K)	σ_T (K)
60	58	142	*	*
80	73	126	1091	71
120	104	129	1150	55
180	154	107	1153	25
250	224	87	1135	18

PSOC-1493D, 106-125 μm, 1050 K

z (mm)	t (ms)	v_p (cm/s)	T_p (K)	σ_T (K)
80	91	107	892	48
120	128	107	908	36
180	186	100	922	25
250	266	77	917	14

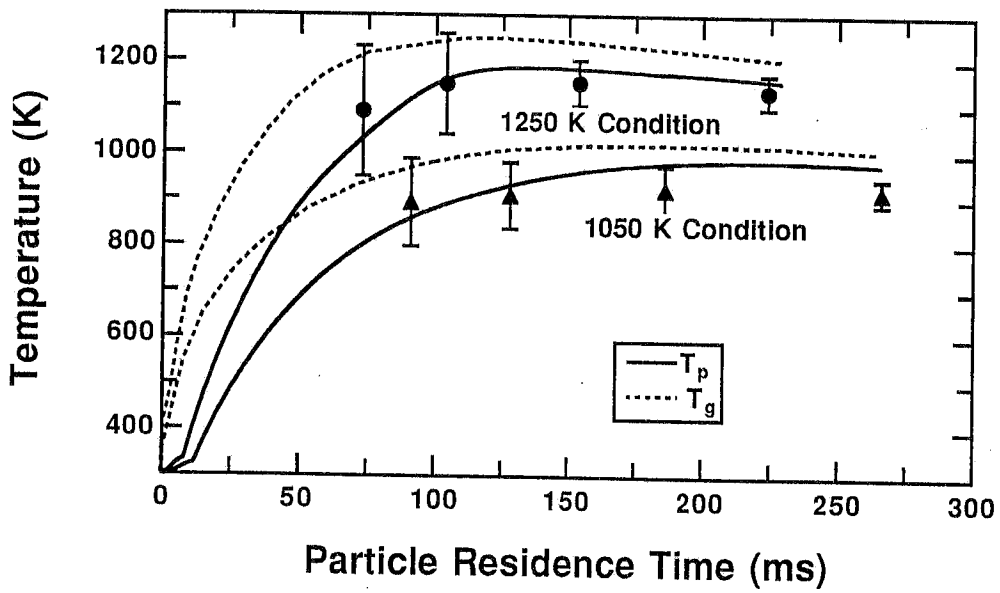

Figure C.4 Calculated (solid curves) and measured (data points) particle temperature histories for the 106-125 μm size fraction of PSOC-1493D Illinois #6 hvb bituminous coal in the CDL. Error bars represent two standard deviations in the measured particle temperature.

PSOC-1507D, 75-106 μm, 1250 K

z (mm)	t (ms)	v_p (cm/s)	T_p (K)	σ_T (K)
30	36	98	*	*
50	55	106	*	*
80	82	116	1076	44
120	116	119	1136	41
180	168	114	1182	32
250	233	101	1182	23

PSOC-1507D, 75-106 μm, 1050 K

z (mm)	t (ms)	v_p (cm/s)	T_p (K)	σ_T (K)
60	70	102	*	*
80	89	100	*	*
120	129	101	953	36
180	193	89	974	21
250	278	74	962	19

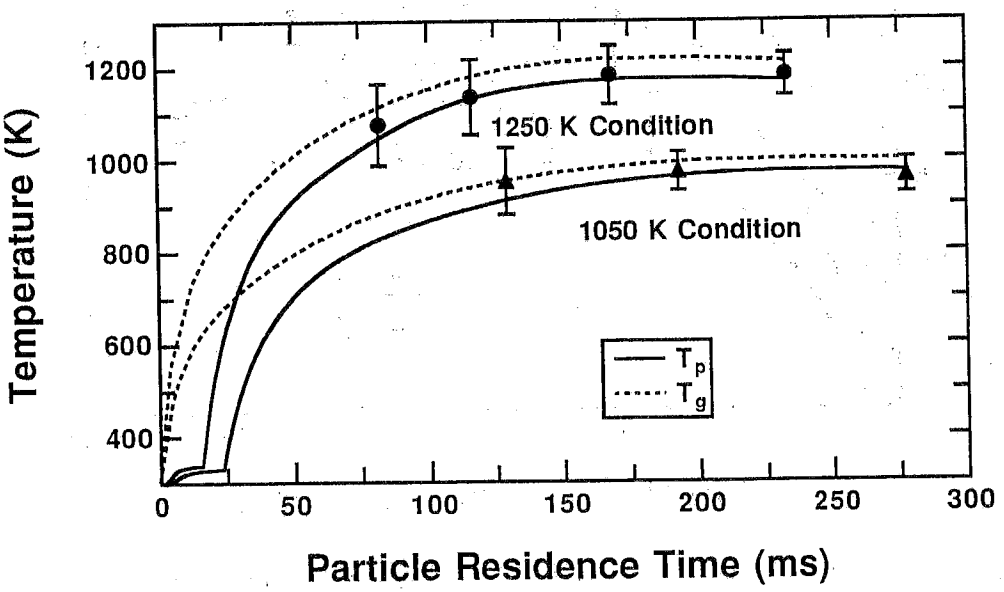

Figure C.5 Calculated (solid curves) and measured (data points) particle temperature histories for the 75-106 μm size fraction of PSOC-1507D North Dakota Beulah Zap lignite in the CDL. Error bars represent two standard deviations in the measured particle temperature.

PSOC-1508D, 106-125 μm, 1250 K

z (mm)	t (ms)	v_p (cm/s)	T_p (K)	σ_T (K)
60	66	113	953	35
80	83	119	1008	50
120	116	122	1053	43
180	168	109	1103	32
250	239	90	1099	23

PSOC-1508D, 106-125 μm, 1050 K

z (mm)	t (ms)	v_p (cm/s)	T_p (K)	σ_T (K)
60	70	101	*	*
80	89	103	919	50
120	127	110	926	31
180	185	98	972	34
250	269	74	989	30

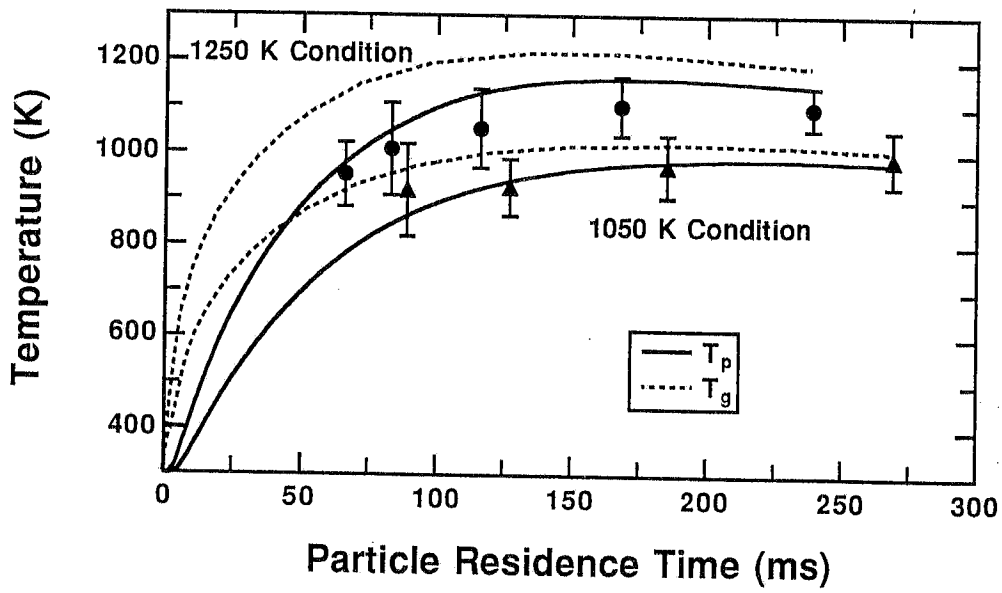

Figure C.6 Calculated (solid curves) and measured (data points) particle temperature histories for the 106-125 μm size fraction of PSOC-1508D West Virginia Pocahontas #3 lv bituminous coal in the CDL. Error bars represent two standard deviations in the measured particle temperature.

APPENDIX D

Data Summary:

PSOC-1445D

New Mexico Blue #1

subbituminous coal

SAMPLE HISTORY

PENN STATE NUMBER	PSOC-1445
COLLECTED BY	PENNSYLVANIA STATE UNIVERSITY
COLLECTION DATE	4/2/85
COLLECTOR'S NUMBER	
REPORTED RANK	SUBBITUMINOUS
SAMPLE TYPE	CHANNEL WHOLE SEAM
OTHER SAMPLE INFORMATION	REPRESENTS BOTH UPPER & LOWER BLUE
SAMPLE RESERVE	900
SEAM NAME	BLUE #1
ALTERNATE SEAM NAME	
TOTAL SEAM THICKNESS	0 FT. 51 IN.
THICKNESS OF SEAM SAMPLED	0 FT. 51 IN.
PORTION RECOVERED IN CORE	
DIAMETER OF CORE	

SAMPLE LOCATION

COUNTRY	U.S.A.
STATE	NEW MEXICO
COUNTY	MCKINLEY
TOWNSHIP	
NEAREST TOWN	WINDOW ROCK
COAL PROVINCE	ROCKY MOUNTAIN
COAL REGION	SAN JUAN RIVER
COAL FIELD	

SEAM NAME	BLUE #1	COUNTRY	U.S.A.
APPARENT RANK	HIGH VOLATILE C BITUMINOUS (HVCB)	STATE	NEW MEXICO

GEOLOGIC INFORMATION

SYSTEM (AGE)	CRETACEOUS
SERIES	
GROUP	MESAVERDE
FORMATION	GALLUP SANDSTONE
OVERBURDEN LITHOLOGY	SHALE
FLOOR LITHOLOGY	SHALE

SEAM STRATA INFORMATION

THICKNESS	LITHOTYPE

SEAM NAME	BLUE #1	COUNTRY	U.S.A.
APPARENT RANK	HIGH VOLATILE C BITUMINOUS (HVCB)	STATE	NEW MEXICO

CHEMICAL DATA 1

PROXIMATE ANALYSIS	AS REC'D	DRY	DAF	DMMF (PAFF)	DMMF (PARR-G)	DMMF (DIR MM)
% MOISTURE	12.22					
% ASH	4.04	4.60				
% VOLATILE MATTER	40.33	45.95	48.17	47.86	47.87	
% FIXED CARBON	43.41	49.45	51.83	52.14	52.13	

CALORIFIC VALUE (GROSS BTU/LB)	DRY	AS REC'D MOIST.	EQUIL MOIST.
MM-FREE, DIRECT MM-CONTAINING	13179	11569	11435
MM-FREE (PARR)	13888	12107	11961
MM-FREE (MOD.P)	13906	12096	11950
BEST MM FREE		12096	11950
NET CV, DMMF BTU/LB	11379		
ASH-FREE	13814		

MOTT-SPOONER DIFFERENCE = 565.

ASSOCIATED ANALYSES	DRY	MMF
% EQUILIBRIUM MOISTURE	13.23	13.98
% TOTAL SULFUR	0.72	

RANK CALCULATIONS

APPARENT RANK (AS REC'D MOIST)	HIGH VOLATILE C BITUMINOUS (HVCB)
ASTM RANK (EQUIL. MOIST.)	HIGH VOLATILE C BITUMINOUS (HVCB)
REFLECTANCE RANK CATEGORY	HIGH VOLATILE C BITUMINOUS (HVCB)
INTERNATIONAL RANK	
AS REC'D MOIST.	
EQUIL. MOIST	
REPORTED RANK	SUBBITUMINOUS

SEAM NAME	BLUE #1	COUNTRY	U.S.A.
APPARENT RANK	HIGH VOLATILE C BITUMINOUS (HVCB)	STATE	NEW MEXICO

CHEMICAL DATA 2

ULTIMATE ANALYSIS	AS REC'D	DRY	DAF	DMMF(PARR) (5.36 % MM)
% ASH	4.04	4.60		
% CARBON	62.78	71.52	74.97	75.57
% HYDROGEN	*4.72	5.38	5.64	5.68
% NITROGEN	1.18	1.34	1.40	1.42
% SULFUR	0.63	0.72	0.75	
% CHLORINE	0.03	0.03	0.03	0.03
% OXYGEN (DIFF)	*14.40	16.41	17.20	17.30

SULFUR FORMS	% PYRITIC	% SULFATIC	% ORGANIC	% TOTAL
DRY	0.16	0.01	0.55	0.72
DAF	0.17	0.01	0.58	0.75

OPTICAL

ELEMENTAL ANALYSIS	DRY	DMMF (MOD.P) (5.29 % MM)	DMMF(DIR.) (% MM)
% CARBON	71.42	75.41	
% HYDROGEN	5.35	5.65	
% NITROGEN	1.34	1.42	
% ORGANIC SULFUR	0.55	0.58	
% OXYGEN (DIFF)	16.05	16.91	
% CHLORINE	0.03	0.03	
% MINERAL MATTER (INCLUDES 0.30 % FES2)	5.29		

ATOM RATIOS (DMMF)	PARR	MOD.PAR	DIRECT
ATOMIC H/C	0.904	0.900	
ATOMIC O/C	0.172	0.178	

MISC. CHEMICAL DATA	DRY	OF DMMF COAL	OF DMMF OXYGEN
% O AS COOH			
% O AS OH			
% S AS SO4, IN ASH			
% CARBONATE AS CO2	0.35		
% CHLORINE	0.06		

INFRA-RED ANALYSIS

(*)- EXCLUDES MOISTURE

SEAM NAME	BLUE #1	COUNTRY	U.S.A.
APPARENT RANK	HIGH VOLATILE C BITUMINOUS (HVCB)	STATE	NEW MEXICO

CHEMICAL DATA 3

% MOISTURE IN COAL = 9.25
% HIGH TEMPERATURE ASH = 3.62 AT 750 DEGREES C

TRACE ELEMENT ANALYSIS	PPM HTA	PPM TOTAL COAL
AG		
B		
BA	2880	104
BE	53	2
BI		
CE		
CO		
CR	85	3
CU	140	5
GA		
GE		
LA		
LI		
MN	1060	38
MO		
NI	100	4
NB		
PB		
RB	25	1
SC		
SN		
SR	930	34
TH		
U		
V	140	5
Y		
YB		
ZN	570	21
ZR	290	10

MAJOR ELEMENT ANALYSIS	OXIDE % OF HTA	ELEMENT % OF TOTAL DRY COAL
SI02	48.60	0.82
AL203	23.50	0.45
TI02	1.12	0.02
FE203	9.90	0.25
MG0	1.19	0.03
CA0	6.03	0.16
NA20	0.24	0.01
K20	0.50	0.02
P205	0.17	0.00
S03	6.00	0.09

VOLATILES	PPM TOTAL COAL
AS	
BR	
CD	
CL	
F	
HG	
SB	
SE	

SEAM NAME	BLUE #1	COUNTRY	U.S.A.
APPARENT RANK	HIGH VOLATILE C BITUMINOUS (HVCB)	STATE	NEW MEXICO

MINERALOGICAL DATA

TOTAL MINERAL MATTER

% MM-PARR	5.36
% MM-MODIFIED PARR	5.29
% MM-KMC	
% MM-DIRECT	
% MM-BEST AVAILABLE	5.29
VOL % MM-PARR	2.66

MINERAL COMPOSITION

NONE

SEAM NAME	BLUE #1	COUNTRY	U.S.A.
APPARENT RANK	HIGH VOLATILE C BITUMINOUS (HVCB)	STATE	NEW MEXICO

PETROGRAPHIC DATA

MACERAL COMPOSITION WHITE ANALYSIS ONLY

	DRY VOLUME %	DMMF VOLUME %
HUMINITE	80.9	83.1
INERTINITE	12.8	13.2
LIPTINITE	3.6	3.7
MINERAL MATTER (CALC.)	2.7	
TEXTINITE	0.0	0.0
ULMINITE	77.9	80.0
ATTRINITE		
DENSINITE		
HUMODETRINITE(ANAL)	0.4	0.4
GELINITE	1.3	1.3
CORPOHUMINITE	1.4	1.4
SPORINITE		
CUTINITE		
EXINTITE(ANAL.)	2.4	2.5
RESINITE	1.2	1.2
SUBERINITE	0.0	0.0
EXUDATINITE	0.0	0.0
FLUORINITE	0.0	0.0
BITUMINITE	0.0	0.0
ALGINITE	0.0	0.0
LIPTODETRINITE	0.0	0.0
FUSINITE	2.4	2.5
SEMI-FUSINITE	6.5	6.7
MACRINITE	3.8	3.9
MICRINITE	0.0	0.0
SCLEROTINITE	0.1	0.1
INERTODETRINITE	0.0	0.0
MINERAL MATTER(ANAL.)		
HUMINITE(ANAL.)		
INERTINITE(ANAL.)		
LIPTINITE(ANAL.)		

REFLECTANCE DATA (% IN OIL)	HIGH	LOW	RANGE	MEAN MAX	STAND.DEV.
ULMINITE	0.69	0.45	0.24	0.57	0.05

SEAM NAME	BLUE #1	COUNTRY	U.S.A.
APPARENT RANK	HIGH VOLATILE C BITUMINOUS (HVCB)	STATE	NEW MEXICO

PETROGRAPHIC DATA

CONTINUED

% VITRINOID REFLECTANCE	HALF-TYPE	VOLUME PERCENT	% VITRINOID REFLECTANCE	V-TYPE	VOLUME PERCENT
0.40-0.44	VHT 0.425	0.00			
0.45-0.49	VHT 0.475	8.00	0.50-0.59	V4	8.00
0.50-0.54	VHT 0.525	33.00			
0.55-0.59	VHT 0.575	34.00	0.50-0.59	V5	67.00
0.60-0.64	VHT 0.625	24.00			
0.65-0.69	VHT 0.675	1.00	0.60-0.69	V6	25.00

PHYSICAL PROPERTIES

HARDGROVE GRINDABILITY	38.8
VICKER'S MICROHARDNESS	
FREE SWELLING INDEX	0.0
GRAY KING COKE TYPE	

ASH FUSION ANALYSIS (DEGREES F)	REDUCING	OXIDIZING
INITIAL DEFORMATION TEMPERATURE	2305	2535
SOFTENING TEMPERATURE	2395	2580
HEMISPHERE TEMPERATURE	2525	2630
FLUID TEMPERATURE	2680	2655

ANALYSIS LOG

ANALYSIS	DATE	PERFORMED BY
A.R. MOIST	6/4/85	WARNER LABORATORIES
EQUIL. MOIST.	6/4/85	WARNER LABORATORIES
PROXIMATE	6/4/85	WARNER LABORATORIES
ULTIMATE	6/4/85	WARNER LABORATORIES
SULFUR FORMS	6/4/85	WARNER LABORATORIES
FSI	8/15/85	COAL PETROGRAPHY LABORATORIES-PSU
PLASTOMETER		
DIRECT MM		
GRAY-KING		

PSOC-1445D
New Mexico Blue #1
Subbituminous Coal
106-125 μm Size Fraction,
1250 K Gas Condition in the CDL (100% N_2)

A. Char Sample Analyses

Sampling Height (mm)	0	20	40	70	100	150	250
Residence Time (ms)	0	26	48	77	103	146	238
Mass Release (% daf)*	0.0	1.5	0.0	26.8	32.8	51.6	53.6
90% conf. interval (±)	0.0	3.6	0.0	10.0	3.5	0.4	2.3

Moisture (mass %)	9.31	1.33	0.99	0.52	1.22	0.52	0.83
C (mass %, daf)	75.60	76.42	75.73	76.71	78.82	85.26	87.74
H	5.26	5.36	5.26	4.63	3.96	2.66	2.58
O	17.33	16.50	17.20	16.90	15.31	9.97	7.37
N	1.32	1.33	1.30	1.41	1.50	1.72	1.71
S	0.49	0.39	0.50	0.35	0.40	0.38	0.59
Ash (mass %, dry)	3.48	3.07	3.04	4.03	5.00	6.99	6.93
SiO2	1.68	1.47	1.52	2.37	2.42	3.33	3.44
K2O	0.05	0.05	0.05	0.05	0.06	0.05	0.05
TiO2	0.05	0.05	0.05	0.07	0.08	0.09	0.10
Fe2O3	0.28	0.26	0.26	0.38	0.44	0.52	0.53
Al2O3	0.84	0.74	0.75	1.19	1.20	1.68	1.74
CaO	0.14	0.11	0.14	0.68	0.40	0.68	0.43
Na2O	0.01	0.01	0.02	0.02	0.03	0.03	0.02
MgO	0.01	0.01	0.01	0.22	0.01	0.16	0.09
Ash2	3.19	3.08	3.06	4.04	5.41	7.30	6.37

*Mass release based on Si, Ti, Al, and ash as tracers.

B. Mass Balance Data†

m/m_o (as rec'd)	0.86	0.87	0.67	0.56	0.41	0.40
tar/m_o (as rec'd)	0.02	0.00	0.05	0.15	0.08	0.06
m/m_o (normalized)	1.00	1.01	0.79	0.65	0.48	0.47
tar/m_o (normalized)	0.02	0.00	0.05	0.16	0.09	0.07
estimated V(daf)	0	-2	25	40	60	61
estimated tar(daf)	2	0	6	19	10	8
tar estimated from tar/char ratio and tracer analysis	0	0	7	16	9	7

†Shown for reference only; tracers were used to determine extent of mass release.

PSOC-1445D (cont.)
New Mexico Blue #1
Subbituminous Coal
106-125 μm Size Fraction,
1250 K Gas Condition in the CDL (100% N_2)

C. Tap Densities and Apparent Densities of Char Samples

Sampling Height (mm)	0	20	40	70	100	150	250
Residence Time (ms)	0	26	48	77	103	146	238
Mass Release (% dry)	0.00	0.00	0.00	25.80	31.70	49.80	51.70
m/m_o(dry)	1.00	1.00	1.00	0.74	0.68	0.50	0.48
m/m_o(wet)	1.00	0.92	0.92	0.68	0.63	0.46	0.44
Aparent Density (ρ/ρ_o)*	1.00	0.90	0.90	0.50	0.37	0.31	0.32
Diameter Ratio	1.00	1.01	1.01	1.10	1.19	1.14	1.12

*Apparent densities measured using volumetric technique (tap densities)

D. Mercury Porosimetry and BET Analyses of Char Samples

Sampling Height (mm)	0	20	40	70	100	150	250
Residence Time (ms)	0	26	48	77	103	146	238
Mass Release (% daf)*	0.0	1.5	0.0	26.8	32.8	51.6	53.6

BET Surface Area (m^2/g)	6.75	4.06	4.90	9.40	10.74	251.3	335.3
Standard Deviation	0.12	0.16	0.16	0.99	0.21	4.8	6.8
Langmuir Surface Area	n.a.	n.a.	n.a.	n.a.	n.a.	335.3	443.1
Standard Deviation	n.a.	n.a.	n.a.	n.a.	n.a.	3.7	3.8
Cumulative Pore Area (m^2/g)	88.5	91.0	89.2	148.3	128.5	135.5	125.7
Median Pore Diameter (μm)							
By Volume	36.21	36.04	35.83	28.94	32.39	30.91	35.09
By area	0.0042	0.0044	0.0045	0.0052	0.0042	0.0046	0.0047
By 4V/A	0.0436	0.0480	0.0507	0.0745	0.1056	0.1100	0.1014
Density, g/cc							
Bulk	0.573	0.521	0.512	0.273	0.223	0.208	0.221
Skeletal	1.281	1.212	1.214	1.107	0.909	0.920	0.742
Porosity (%)	55.3	57.0	57.8	75.4	75.5	77.4	70.3

PSOC-1445D (cont.)
New Mexico Blue #1
Subbituminous Coal
106-125 μm Size Fraction,
1250 K Gas Condition in the CDL (100% N_2)

E. NMR Analyses of Char Samples

Sampling Distance (mm)	0	70	250
Residence Time (ms)	0	77	238
Mass Release (% daf)	0.0	26.8	53.6
Aromatic carbon, $f_a = f_a' + f_a^C$	0.59	0.67	0.84
Carbonyl, f_a^C	0.06	0.08	0.05
Aromatic carbon, carbonyl subtracted, f_a'	0.53	0.56	0.79
Protonated aromatic carbon, f_a^H	0.19	0.22	0.36
Non-protonated aromatic C, $f_a^N = f_a^P + f_a^S + f_a^B$	0.34	0.34	0.43
Aromatic carbon with O attachment, f_a^P	0.07	0.07	0.05
Aromatic carbon with alkyl attachment, f_a^S	0.12	0.13	0.17
Aromatic bridgehead and inner carbon, f_a^B	0.15	0.14	0.21
Aliphatic carbon, f_{al}	0.41	0.33	0.16
Aliphatic CH and CH_2, f_{al}^H	0.30	0.25	0.12
Aliphatic CH_3 and non-protonated carbon, f_{al}^*	0.11	0.08	0.04
Aliphatics with oxygen attachment, f_{al}^O	0.07	0.10	0.08
Proton spin-relaxation time, $T_{1\rho}^{Har}$ (ms)	4.7	2.1	7.3
Total carbons per cluster	26	21	16
Aromatic carbons per cluster, C	14	12	13
Aliphatic carbons per cluster	12	9	3
Total attachments per cluster, $\sigma+1$	5.0	4.3	3.6
Bridges and loops per cluster, B_C	2.1	2.6	3.0
Side chains per cluster	2.9	1.7	0.6
Fraction of intact bridges per cluster, p	0.42	0.60	0.82
Average cluster molecular weight	410	335	225
Side chain molecular weight	47	43	18

PSOC-1445D (cont.)
New Mexico Blue #1
Subbituminous Coal
106-125 μm Size Fraction,
1250 K Gas Condition in the CDL (100% N_2)

F. NMR Analyses of Tar Samples

Sampling Height (mm)	0	20	40	70	100	150	250
Residence Time (ms)	0	26	48	77	103	146	238
Mass Release (% daf)	0.0	1.5	0.0	26.8	32.8	51.6	53.6

α-H	n.a.	n.a.	n.a.	30	n.a.	n.a.	16
α-CH_3	n.a.	n.a.	n.a.	8	n.a.	n.a.	2
β– and γ–H	n.a.	n.a.	n.a.	20	n.a.	n.a.	3
γ-CH_3	n.a.	n.a.	n.a.	4	n.a.	n.a.	2
Aromatic H	23*	n.a.	n.a.	42	n.a.	n.a.	74
1-Ring	n.a.	n.a.	n.a.	8	n.a.	n.a.	6
2-Ring	n.a.	n.a.	n.a.	12	n.a.	n.a.	19
3-Ring	n.a.	n.a.	n.a.	22	n.a.	n.a.	49
Aromatic C	53**	n.a.	n.a.	72	n.a.	n.a.	98

*Estimated from the C/H ratio and the carbon aromaticity f_a' of the parent coal
**Estimated as the carbon aromaticity of the parent coal

PSOC-1445D
New Mexico Blue #1
Subbituminous Coal
106-125 μm Size Fraction,
1050 K Gas Condition in the CDL (100% N_2)
Duplicate Experiment**

A. Char Sample Analyses

Sampling Height (mm)	0	50	80	120	150	180	250
Residence Time (ms)	0	59	88	123	150	180	253
Mass Release (% daf)*	0.0	0.0	6.1	30.8	22.0**	39.0	46.9
90% conf. interval (±)	0.0	0.0	3.3	8.2	6.1	4.6	3.8

Moisture (mass %)	5.51	3.46	3.56	3.33	2.44	3.07	4.07
C (mass %, daf)	77.29	73.16	79.55	79.39	79.02	79.42	83.01
H	5.56	4.92	5.11	4.63	4.98	4.13	3.75
O	15.11	20.00	13.20	13.75	13.87	14.15	10.85
N	1.35	1.30	1.45	1.53	1.47	1.59	1.74
S	0.69	0.62	0.68	0.70	0.66	0.71	0.65
Ash (mass %, dry)	3.68	3.61	3.96	5.55	4.94	6.08	6.66
SiO2	1.60	1.60	1.74	2.39	2.08	2.65	3.02
K2O	0.03	0.00	0.00	0.01	0.00	0.01	0.01
TiO2	0.05	0.05	0.05	0.06	0.06	0.07	0.08
Fe2O3	0.29	0.32	0.32	0.36	0.35	0.39	0.49
Al2O3	0.82	0.80	0.87	1.21	1.05	1.35	1.57
CaO	0.16	0.23	0.15	0.26	0.48	0.36	0.34
Na2O	0.01	0.00	0.01	0.02	0.01	0.06	0.01
MgO	0.01	0.03	0.01	0.15	0.10	0.04	0.05
Ash2	4.13	3.45	4.11	5.28	4.36	5.35	6.93

*Mass release based on Si, Ti, Al, and ash as tracers.

**The first data set for PSOC-1445D at 1050 K was in error, based on measured particle temperatures and velocities. The "duplicate set" was therefore used as the good data set.

B. Mass Balance Data†

m/m_o (as rec'd)	0.84	0.76	0.61	0.64	0.46	0.42
tar/m_o (as rec'd)	0.01	0.02	0.08	0.05	0.11	0.14
m/m_o (normalized)	1.00	0.90	0.72	0.76	0.55	0.50
tar/m_o (normalized)	0.01	0.02	0.09	0.05	0.13	0.16
estimated V(daf)	0	11	31	26	49	55
estimated tar(daf)	2	3	10	6	14	18
tar estimated from tar/char ratio and tracer analysis	0	1	10	5	11	15

†Shown for reference only; tracers were used to determine extent of mass release.

PSOC-1445D (cont.)
New Mexico Blue #1
Subbituminous Coal
106-125 μm Size Fraction,
1050 K Gas Condition in the CDL (100% N_2)
Duplicate Experiment

C. Tap Densities and Apparent Densities of Char Samples

Sampling Height (mm)	0	50	80	120	150	180	250
Residence Time (ms)	0	59	88	123	150	180	253
Mass Release (% dry)	0.00	0.00	5.90	29.70	21.20	37.60	45.20
m/m_o(dry)	1.00	1.00	0.94	0.70	0.79	0.62	0.55
m/m_o(wet)	1.00	0.98	0.92	0.69	0.76	0.61	0.54
Aparent Density (ρ/ρ_o)*	1.00	0.90	0.65	0.45	0.56	0.42	0.39
Diameter Ratio	1.00	1.03	1.12	1.15	1.11	1.13	1.11

*Apparent densities measured using volumetric technique (tap densities)

D. Mercury Porosimetry and BET Analyses of Char Samples**

Sampling Height (mm)	0	50	80	120	150	180	250
Residence Time (ms)	0	59	88	123	150	180	253
Mass Release (% daf)*	0.0	1.5	0.0	26.8	32.8	51.6	53.6

BET Surface Area (m^2/g)	11.82	25.34	17.37	6.63	11.82	25.27	14.74
Standard Deviation	0.48	1.46	1.49	0.70	0.37	2.65	0.93
Cumulative Pore Area (m^2/g)	73.5	96.10	74.18	93.11	110.2	95.47	141.3
Median Pore Diameter (μm)							
By Volume	36.57	37.09	35.64	35.28	32.46	33.41	25.36
By area	0.0044	0.0044	0.0049	0.0053	0.0046	0.0050	0.0043
By 4V/A	0.0496	0.0420	0.0547	0.1012	0.1176	0.1469	0.0950
Density, g/cc							
Bulk	0.606	0.570	0.575	0.324	0.239	0.212	0.237
Skeletal	1.354	1.343	1.379	1.365	1.056	0.829	1.162
Porosity (%)	55.2	57.5	58.3	76.3	77.4	74.4	79.6

**These mercury porosimetry and BET surface area data are from the first data set at the same sample heights; the residence times in this table, however, correspond to the second data set.

PSOC-1445D (cont.)
New Mexico Blue #1
Subbituminous Coal
106-125 μm Size Fraction,
1050 K Gas Condition in the CDL (100% N_2)
Duplicate Experiment

E. NMR Analyses of Char Samples

Sampling Distance (mm)	0	50	80	120	150	180	250
Residence Time (ms)	0	59	88	123	150	180	253
Mass Release (% daf)	0.0	0.0	6.1	30.8	22.0	39.0	46.9
Aromatic carbon, $f_a = f_a' + f_a^C$	0.59	0.58	0.59	0.64	0.65	0.65	0.74
Carbonyl, f_a^C	0.06	0.05	0.05	0.06	0.07	0.06	0.10
Aromatic carbon, carbonyl subtracted, f_a'	0.53	0.53	0.54	0.58	0.58	0.59	0.64
Protonated aromatic carbon, f_a^H	0.19	0.16	0.17	0.20	0.20	0.20	0.23
Non-protonated aromatic C, $f_a^N = f_a^P + f_a^S + f_a^B$	0.34	0.37	0.37	0.38	0.38	0.39	0.41
Aromatic carbon with O attachment, f_a^P	0.07	0.07	0.06	0.06	0.08	0.08	0.07
Aromatic carbon with alkyl attachment, f_a^S	0.12	0.13	0.14	0.13	0.13	0.14	0.15
Aromatic bridgehead and inner carbon, f_a^B	0.15	0.17	0.17	0.19	0.17	0.17	0.19
Aliphatic carbon, f_{al}	0.41	0.42	0.41	0.36	0.35	0.35	0.26
Aliphatic CH and CH_2, f_{al}^H	0.30	0.30	0.30	0.26	0.23	0.25	0.20
Aliphatic CH_3 and non-protonated carbon, f_{al}^*	0.11	0.12	0.11	0.10	0.12	0.10	0.06
Aliphatics with oxygen attachment, f_{al}^O	0.07	0.07	0.08	0.10	0.08	0.08	0.12
Proton spin-relaxation time, $T_{1\rho}^{Har}$ (ms)	4.7	4.7	3.5	3.1	3.7	3.2	2.5
Total carbons per cluster	26	30	28	28	24	24	22
Aromatic carbons per cluster, C	14	16	15	16	14	14	14
Aliphatic carbons per cluster	12	14	13	12	10	10	8
Total attachments per cluster, $\sigma+1$	5.0	6.0	5.6	5.3	5.1	5.2	4.8
Bridges and loops per cluster, B_C	2.0	2.0	2.5	2.5	2.2	2.9	3.5
Side chains per cluster	3.0	4.0	3.1	2.8	2.9	2.3	1.3
Fraction of intact bridges per cluster, p	0.42	0.40	0.45	0.47	0.43	0.55	0.73
Average cluster molecular weight	410	496	419	417	367	359	316
Side chain molecular weight	47	49	42	41	38	36	30

PSOC-1445D (cont.)
New Mexico Blue #1
Subbituminous Coal
106-125 μm Size Fraction,
1050 K Gas Condition in the CDL (100% N_2)
Duplicate Experiment

F. NMR Analyses of Tar Samples

Sampling Height (mm)	0	50	80	120	150	180	250
Residence Time (ms)	0	59	88	123	150	180	253
Mass Release (% daf)	0.0	0.0	6.1	30.8	22.0	39.0	46.9

α-H	n.a.	n.a.	n.a.	32	33	31	36
α-CH_3	n.a.	n.a.	n.a.	11	10	12	10
β– and γ–H	n.a.	n.a.	n.a.	31	22	24	16
γ-CH_3	n.a.	n.a.	n.a.	10	8	10	4
Aromatic H	23*	n.a.	n.a.	26	31	33	43
1-Ring	n.a.	n.a.	n.a.	8	8	12	8
2-Ring	n.a.	n.a.	n.a.	8	7	8	11
3-Ring	n.a.	n.a.	n.a.	10	16	15	25
Aromatic C	53**	n.a.	n.a.	59	56	66	74

*Estimated from the C/H ratio and the carbon aromaticity f_a' of the parent coal
**Estimated as the carbon aromaticity of the parent coal

APPENDIX E

Data Summary:

PSOC-1451D

Pittsburgh #8

hva bituminous coal

SAMPLE HISTORY

PENN STATE NUMBER	PSOC-1451
COLLECTED BY	PENNSYLVANIA STATE UNIVERSITY
COLLECTION DATE	5/1/85
COLLECTOR'S NUMBER	
REPORTED RANK	HIGH VOLATILE A BITUMINOUS (HVAB)
SAMPLE TYPE	CHANNEL WHOLE SEAM
OTHER SAMPLE INFORMATION	
SAMPLE RESERVE	
SEAM NAME	PITTSBURGH
ALTERNATE SEAM NAME	#8
TOTAL SEAM THICKNESS	6 FT. 5 IN.
THICKNESS OF SEAM SAMPLED	6 FT. 5 IN.
PORTION RECOVERED IN CORE	
DIAMETER OF CORE	

SAMPLE LOCATION

COUNTRY	U.S.A.
STATE	PENNSYLVANIA
COUNTY	WASHINGTON
TOWNSHIP	NORTH STRABANE
NEAREST TOWN	LINDEN
COAL PROVINCE	EASTERN
COAL REGION	APPALACHIAN
COAL FIELD	MAIN BITUMINOUS

SEAM NAME PITTSBURGH
APPARENT RANK HIGH VOLATILE A BITUMINOUS (HVAB)

COUNTRY U.S.A.
STATE PENNSYLVANIA

GEOLOGIC INFORMATION

SYSTEM (AGE)	PENNSYLVANIAN
SERIES	
GROUP	MONOGAHELA
FORMATION	
OVERBURDEN LITHOLOGY	SHALE
FLOOR LITHOLOGY	SHALE

SEAM STRATA INFORMATION

THICKNESS	LITHOTYPE

SEAM NAME PITTSBURGH COUNTRY U.S.A.
APPARENT RANK HIGH VOLATILE A BITUMINOUS (HVAB) STATE PENNSYLVANIA

CHEMICAL DATA 1

PROXIMATE ANALYSIS	AS REC'D	DRY	DAF	DMMF (PAFF)	DMMF (PARR-G)	DMMF (DIR MM)
% MOISTURE	2.54					
% ASH	13.32	13.67				
% VOLATILE MATTER	33.56	34.43	39.88	38.81	38.21	
% FIXED CARBON	50.58	51.90	60.12	61.19	61.79	

CALORIFIC VALUE (GROSS BTU/LB)	DRY	AS REC'D MOIST.	EQUIL MOIST.
MM-FREE, DIRECT MM-CONTAINING	12855	12528	12541
MM-FREE (PARR)	15135	14682	14699
MM-FREE (MOD.P)	15227	14736	14754
BEST MM FREE		14736	14754
NET CV, DMMF BTU/LB	14713		
ASH-FREE	14891		

MOTT-SPOONER DIFFERENCE =

ASSOCIATED ANALYSES	DRY	MMF
% EQUILIBRIUM MOISTURE	2.44	2.89
% TOTAL SULFUR	1.36	

RANK CALCULATIONS

APPARENT RANK (AS REC'D MOIST)	HIGH VOLATILE A BITUMINOUS (HVAB)
ASTM RANK (EQUIL. MOIST.)	HIGH VOLATILE A BITUMINOUS (HVAB)
REFLECTANCE RANK CATEGORY	HIGH VOLATILE A BITUMINOUS (HVAB)
INTERNATIONAL RANK	
AS REC'D MOIST.	
EQUIL. MOIST	
REPORTED RANK	HIGH VOLATILE A BITUMINOUS (HVAB)

SEAM NAME PITTSBURGH COUNTRY U.S.A.
APPARENT RANK HIGH VOLATILE A BITUMINOUS (HVAB) STATE PENNSYLVANIA

CHEMICAL DATA 2

ULTIMATE ANALYSIS	AS REC'D	DRY	DAF	DMMF(PARR) (15.51 % MM)
% ASH	13.32	13.67		
% CARBON	70.05	71.88	83.26	85.08
% HYDROGEN	*455	4.67	5.41	5.53
% NITROGEN	1.33	1.36	1.58	1.61
% SULFUR	1.33	1.36	1.58	
% CHLORINE	0.07	0.08	0.09	0.09
% OXYGEN (DIFF)	*6.81	6.99	8.10	7.71

SULFUR FORMS	% PYRITIC	% SULFATIC	% ORGANIC	% TOTAL
DRY	0.82	0.01	0.53	1.36
DAF	0.95	0.01	0.61	1.58
OPTICAL				

ELEMENTAL ANALYSIS	DRY	DMMF (MOD.P) (15.87 % MM)	DMMF(DIR.) (% MM)
% CARBON	71.64	85.16	
% HYDROGEN	4.64	5.52	
% NITROGEN	1.36	1.61	
% ORGANIC SULFUR	0.53	0.63	
% OXYGEN (DIFF)	5.95	7.00	
% CHLORINE	0.08	0.09	
% MINERAL MATTER (INCLUDES 1.53 % FES2)	15.87		

ATOM RATIOS (DMMF)	PARR	MOD.PAR	DIRECT
ATOMIC H/C	0.780	0.778	
ATOMIC O/C	0.068	0.073	

MISC. CHEMICAL DATA	DRY	OF DMMF COAL	OF DMMF OXYGEN
% O AS COOH			
% O AS OH			
% S AS SO4, IN ASH			
% CARBONATE AS CO2	0.87		
% CHLORINE	0.15		

INFRA-RED ANALYSIS

(*)- EXCLUDES MOISTURE

SEAM NAME PITTSBURGH COUNTRY U.S.A.
APPARENT RANK HIGH VOLATILE A BITUMINOUS (HVAB) STATE
PENNSYLVANIA

CHEMICAL DATA 3

% MOISTURE IN COAL = 1.52
% HIGH TEMPERATURE ASH = 13.20 AT 750 DEGREES C

TRACE ELEMENT ANALYSIS	PPM HTA	PPM TOTAL COAL
AG		
B		
BA	540	71
BE	7	1
BI		
CE		
CO		
CR	150	20
CU	80	11
GA		
GE		
LA		
LI		
MN	140	18
MO		
NI	65	9
NB		
PB		
RB	100	13
SC		
SN		
SR	590	78
TH		
U		
V	200	26
Y		
YB		
ZN	85	11
ZR	240	32

MAJOR ELEMENT ANALYSIS	OXIDE % OF HTA	ELEMENT % OF TOTAL DRY COAL
SI02	54.40	3.36
AL203	24.50	1.71
TI02	1.14	0.09
FE203	9.16	0.85
MG0	0.85	0.07
CA0	2.97	0.28
NA20	0.61	0.06
K20	2.02	0.22
P205	0.34	0.02
S03	2.30	0.12

VOLATILES	PPM TOTAL COAL
AS	
BR	
CD	
CL	
F	
HG	
SB	
SE	

SEAM NAME PITTSBURGH COUNTRY U.S.A.
APPARENT RANK HIGH VOLATILE A BITUMINOUS (HVAB) STATE PENNSYLVANIA

MINERALOGICAL DATA

TOTAL MINERAL MATTER

% MM-PARR	15.51
% MM-MODIFIED PARR	15.87
% MM-KMC	
% MM-DIRECT	
% MM-BEST AVAILABLE	15.87
VOL % MM-PARR	8.13

MINERAL COMPOSITION

NONE

SEAM NAME PITTSBURGH COUNTRY U.S.A.
APPARENT RANK HIGH VOLATILE A BITUMINOUS (HVAB) STATE PENNSYLVANIA

PETROGRAPHIC DATA

MACERAL COMPOSITION WHITE ANLAYSIS ONLY

	DRY VOLUME %	DMMF VOLUME %	DRY WEIGHT %
VITRINITE (CALC.)	80.1	87.2	73.7
INERTINITE (CALC.)	8.7	9.5	8.0
LIPTINITE (CALC.)	3.0	3.3	2.8
MINERAL MATTER (CALC.)	8.1		15.5
VITRINOIDS			
VITRINITE	80.1	87.2	73.7
PSEUDOVITRINITE	0.0	0.0	0.0
FUSINITE	1.8	2.0	1.7
SEMI-FUSINITE	4.2	4.6	3.9
MACRINITE	0.7	0.8	0.7
MICRINITE	1.9	2.1	1.8
SCLEROTINITE	0.0	0.0	0.0
SPORINITE			
CUTINITE			
EXINITE(ANAL.)	3.0	3.3	2.8
RESINITE	0.0	0.0	0.0
SUBERINITE			
EXUDATINITE			
FLOURINITE			
BITUMINITE			
ALGINITE	0.0	0.0	0.0
LIPTODETRINITE			
MINERAL MATTER (ANAL.)			
INERTINITE(ANAL.)			
LIPTINITE(ANAL.)			

REFLECTANCE DATA (% IN OIL)	HIGH	LOW	RANGE	MEAN MAX	STAND.DEV.
VITRINITE	0.89	0.62	0.27	0.77	0.06
PSEUDOVITRINITE					
VITRINOIDS					

SEAM NAME PITTSBURGH COUNTRY U.S.A.
APPARENT RANK HIGH VOLATILE A BITUMINOUS (HVAB) STATE
PENNSYLVANIA

PETROGRAPHIC DATA

CONTINUED

% VITRINOID REFLECTANCE	HALF-TYPE	VOLUME PERCENT	% VITRINOID REFLECTANCE	V-TYPE	VOLUME PERCENT
0.60-0.64	VHT 0.625	3.00			
0.65-0.69	VHT 0.675	9.00	0.60-0.69	V6	12.00
0.70-0.74	VHT 0.725	18.00			
0.75-0.79	VHT 0.775	37.00	0.70-0.79	V7	55.00
0.80-0.84	VHT 0.825	25.00			
0.85-0.89	VHT 0.875	8.00	0.80-0.89	V8	33.00

PHYSICAL PROPERTIES

HARDGROVE GRINDABILITY	38.9
VICKER'S MICROHARDNESS	
FREE SWELLING INDEX	7.5
GRAY KING COKE TYPE	

ASH FUSION ANALYSIS (DEGREES F)	REDUCING	OXIDIZING
INITIAL DEFORMATION TEMPERATURE	2435	2570
SOFTENING TEMPERATURE	2585	2640
HEMISPHERE TEMPERATURE	2670	2690
FLUID TEMPERATURE	2685	2700

ANALYSIS LOG

ANALYSIS	DATE	PERFORMED BY
A.R. MOIST	2/14/86	WARNER LABORATORIES
EQUIL. MOIST.	6/4/85	WARNER LABORATORIES
PROXIMATE	2/14/86	WARNER LABORATORIES
ULTIMATE	2/14/86	WARNER LABORATORIES
SULFUR FORMS	6/4/85	WARNER LABORATORIES
FSI	8/15/85	COAL PETROGRAPHY LABORATORIES-PSU
PLASTOMETER	5/29/85	COAL PETROGRAPHY LABORATORIES-PSU
DIRECT MM		
GRAY-KING		

PSOC-1451D
Pittsburgh #8 hva Bituminous Coal
106-125 μm Size Fraction,
1250 K Gas Condition in the CDL (100% N_2)

A. Char Sample Analyses

Sampling Height (mm)	0	20	40	70	100	150	250
Residence Time (ms)	0	26	49	79	108	155	254
Mass Release (% daf)*	0.0	2.3	0.0	30.8	40.3	39.0	45.5
90% conf. interval (±)	0.0	2.1	0.0	10.6	1.2	3.7	2.9

Moisture (mass %)	1.51	1.07	0.69	0.76	1.06	1.20	1.18
C (mass %, daf)	81.92	82.94	82.37	82.12	82.44	85.96	88.79
H	6.45	5.50	5.50	4.80	3.89	2.97	2.99
O	8.72	8.72	9.33	9.90	9.52	7.38	5.24
N	1.65	1.61	1.41	1.60	1.71	1.53	1.74
S	1.26	1.23	1.38	1.59	2.42	2.16	1.24
Ash (mass %, dry)	11.20	10.50	9.80	17.10	17.80	16.30	18.20
SiO2	5.20	5.30	5.10	6.20	8.10	8.20	9.20
K2O	0.18	0.18	0.17	0.30	0.34	0.31	0.34
TiO2	0.12	0.12	0.11	0.17	0.18	0.19	0.19
Fe2O3	0.66	0.67	0.72	1.50	1.60	1.40	1.40
Al2O3	2.60	2.70	2.50	3.60	4.00	3.90	4.30
CaO	0.29	0.29	0.29	0.55	0.57	0.47	0.51
Na2O	0.06	0.07	0.07	0.11	0.13	0.10	0.12
MgO	n.a.	n.a.	n.a.	n.a.	n.a.	n.a.	n.a.
Ash2	n.a.	n.a.	n.a.	n.a.	n.a.	n.a.	n.a.

*Mass release based on Si, Ti, Al, and ash as tracers.

B. Mass Balance Data†

m/m_0 (as rec'd)		0.89	0.89	0.45	0.52	n.a.	0.43
tar/m_0 (as rec'd)		-0.01	0.12	0.24	0.23	n.a.	0.00
m/m_0 (normalized)		1.00	1.00	0.51	0.59	n.a.	0.49
tar/m_0 (normalized)		-0.01	0.13	0.27	0.26	n.a.	0.00
estimated V(daf)		0	0	56	47	n.a.	58
estimated tar(daf)		-2	15	31	30	n.a.	0
tar estimated from tar/char ratio and tracer analysis		0	0	17	25	n.a.	0

†Shown for reference only; tracers were used to determine extent of mass release.

PSOC-1451D (cont.)
Pittsburgh #8 hva Bituminous Coal
106-125 μm Size Fraction,
1250 K Gas Condition in the CDL (100% N_2)

C. Tap Densities and Apparent Densities of Char Samples

Sampling Height (mm)	0	20	40	70	100	150	250
Residence Time (ms)	0	26	49	79	108	155	254
Mass Release (% dry)	0.00	2.00	0.00	27.30	35.80	34.60	40.40
m/m_o(dry)	1.00	0.98	1.00	0.73	0.64	0.65	0.60
m/m_o(wet)	1.00	0.98	0.99	0.72	0.64	0.65	0.59
Aparent Density (ρ/ρ_o)*	1.00	0.94	0.77	0.51	0.37	0.26	0.27
Diameter Ratio	1.00	1.01	1.09	1.12	1.20	1.35	1.31

*Apparent densities measured using volumetric technique (tap densities)

D. Mercury Porosimetry and BET Analyses of Char Samples**

Sampling Height (mm)	0.0	45	70	100	130	210
Residence Time (ms)						
Mass Release (% daf)*						

BET Surface Area (m^2/g)	4.16	1.22	1.40	2.49	2.38	5.86
Cumulative Pore Area (m^2/g)	59.01	71.28	52.11	73.28	144.35	103.04
Median Pore Diameter (μm)						
By Volume	28.32	33.05	37.11	36.55	36.39	34.79
By area	0.0046	0.0052	0.0047	0.0048	0.0050	0.0044
By 4V/A	0.0544	0.0774	0.1861	0.2509	0.1852	0.2367
Density, g/cc						
Bulk	0.673	0.458	0.316	0.189	0.134	0.146
Skeletal	1.462	1.241	1.352	1.397	1.269	1.321
Porosity (%)	54.0	63.1	76.6	86.5	89.5	89.0

**These mercury porosimetry and BET surface area data are from an early set of experiments (with Steve Hsu) at the indicated sample heights. The gas condition was similar to those determined from the later experiments, but residence times and particle temperatures are not available for these early data.

PSOC-1451D (cont.)
Pittsburgh #8 hva Bituminous Coal
106-125 μm Size Fraction,
1250 K Gas Condition in the CDL (100% N_2)

E. NMR Analyses of Char Samples

(Not available)

F. NMR Analyses of Tar Samples

(Not available)

PSOC-1451D
Pittsburgh #8 hva Bituminous Coal
106-125 μm Size Fraction,
1050 K Gas Condition in the CDL (100% N_2)

A. Char Sample Analyses

Sampling Height (mm)	0	40	85	130	180	250
Residence Time (ms)	0	54	112	167	231	337
Mass Release (% daf)*	0.0	0.0	1.1	19.0	37.7	43.8
90% conf. interval (±)	0.0	0.0	2.5	7.4	4.3	1.6

Moisture (mass %)	1.51	1.35	0.23	0.24	0.55	0.22
C (mass %, daf)	81.92	82.96	82.22	82.67	81.75	82.49
H	6.45	5.53	5.49	5.14	4.94	4.09
O	8.72	8.91	9.43	9.79	10.14	10.26
N	1.65	1.49	1.70	1.26	1.82	1.87
S	1.26	1.12	1.16	1.15	1.36	1.29
Ash (mass %, dry)	9.50	8.30	9.10	10.50	14.70	15.90
SiO2	4.90	4.40	5.10	6.00	7.00	8.00
K2O	0.16	0.16	0.14	0.25	0.31	0.35
TiO2	0.11	0.10	0.10	0.14	0.16	0.17
Fe2O3	0.59	0.51	0.59	0.56	0.91	1.10
Al2O3	2.30	2.20	2.30	2.80	3.70	3.90
CaO	0.29	0.21	0.26	0.21	0.45	0.47
Na2O	0.06	0.06	0.06	0.05	0.10	0.12
MgO	n.a.	n.a.	n.a.	n.a.	n.a.	n.a.
Ash2	n.a.	n.a.	n.a.	n.a.	n.a.	n.a.

*Mass release based on Si, Ti, Al, and ash as tracers.

B. Mass Balance Data†

m/m_o (as rec'd)	0.75	1.03	0.60	0.49	0.38
tar/m_o (as rec'd)	0.01	0.01	0.05	0.12	0.15
m/m_o (normalized)	1.00	1.37	0.80	0.66	0.50
tar/m_o (normalized)	0.02	0.01	0.06	0.16	0.20
estimated V(daf)	0	-42	22	39	56
estimated tar(daf)	2	1	7	18	23
tar estimated from tar/char ratio and tracer analysis	0	0	6	17	18

†Shown for reference only; tracers were used to determine extent of mass release.

PSOC-1451D (cont.)
Pittsburgh #8 hva Bituminous Coal
106-125 μm Size Fraction,
1050 K Gas Condition in the CDL (100% N_2)

C. Tap Densities and Apparent Densities of Char Samples

(Not available)

D. Mercury Porosimetry and BET Analyses of Char Samples**

Sampling Height (mm)	0.0	50	90	140	200	250
Residence Time (ms)	n.a.	n.a.	n.a.	n.a.	n.a.	n.a.
Mass Release (% daf)*	n.a.	n.a.	n.a.	n.a.	n.a.	n.a.

BET Surface Area (m^2/g)	4.16	1.88	1.86	1.61	3.11	4.01
Cumulative Pore Area (m^2/g)	59.01	60.74	59.17	75.29	104.7	125.44
Median Pore Diameter (μm)						
By Volume	28.32	29.97	34.90	41.76	37.42	40.35
By area	0.0046	0.0047	0.0055	0.0048	0.0047	0.0047
By 4V/A	0.0544	0.0612	0.1091	0.1409	0.2117	0.2060
Density, g/cc						
Bulk	0.673	0.594	0.424	0.280	0.155	0.137
Skeletal	1.462	1.327	1.346	1.092	1.075	1.184
Porosity (%)	54.0	55.2	68.5	74.3	84.7	88.4

**These mercury porosimetry and BET surface area data are from an early set of experiments (with Steve Hsu) at the indicated sample heights. The gas condition was similar to those determined from the later experiments, but residence times and particle temperatures are not available for these early data.

E. NMR Analyses of Char Samples

(Not available)

F. NMR Analyses of Tar Samples

(Not available)

PSOC-1451D
Pittsburgh #8 hva Bituminous Coal
63-75 μm Size Fraction,
1250 K Gas Condition in the CDL (100% N_2)

A. Char Sample Analyses

Sampling Height (mm)	0	20	40	70	100	150	250
Residence Time (ms)	0	27	52	86	119	173	288
Mass Release (% daf)*	0.0	0.0	1.5	40.3	42.4	51.3	53.1
90% conf. interval (±)	0.0	0.0	3.6	3.2	13.5	2.8	5.2

Moisture (mass %)	1.44	0.80	0.83	1.11	1.33	1.14	1.64
C (mass %, daf)	84.23	83.26	83.43	84.73	85.98	88.19	89.77
H	5.54	5.39	5.28	3.74	3.51	3.02	2.33
O	7.56	8.81	8.69	8.83	7.80	6.10	5.30
N	1.65	1.62	1.60	1.79	1.85	1.87	1.77
S	1.01	0.92	1.00	0.91	0.86	0.81	0.84
Ash (mass %, dry)	3.73	3.66	3.97	6.13	4.94	7.84	8.75
SiO2	1.90	1.90	1.90	3.30	3.70	3.80	3.70
K2O	0.07	0.08	0.03	0.05	0.15	0.15	0.20
TiO2	0.06	0.06	0.06	0.10	0.11	0.12	0.12
Fe2O3	0.31	0.32	0.29	0.52	0.56	0.61	0.57
Al2O3	1.20	1.10	1.20	1.90	2.20	2.30	2.40
CaO	0.11	0.11	0.10	0.19	0.20	0.21	0.20
Na2O	0.01	0.02	0.01	0.01	0.02	0.01	0.03
MgO	0.03	0.03	0.03	0.05	0.06	0.06	0.06
Ash2	n.a.	n.a.	n.a.	n.a.	n.a.	n.a.	n.a.

*Mass release based on Si, Ti, Al, and ash as tracers.

B. Mass Balance Data†

m/m_o (as rec'd)	0.75	0.73	0.59	0.53	0.47	0.46
tar/m_o (as rec'd)	0.00	0.01	0.01	0.00	0.01	0.00
m/m_o (normalized)	1.00	0.97	0.78	0.71	0.63	0.62
tar/m_o (normalized)	0.00	0.01	0.02	0.00	0.02	0.00
estimated V(daf)	0	4	34	46	58	61
estimated tar(daf)	0	1	3	0	3	0
tar estimated from tar/char ratio and tracer analysis	0	6	1	0	2	0

†Shown for reference only; tracers were used to determine extent of mass release.

PSOC-1451D (cont.)
Pittsburgh #8 hva Bituminous Coal
63-75 μm Size Fraction,
1250 K Gas Condition in the CDL (100% N_2)

C. Tap Densities and Apparent Densities of Char Samples

Sampling Height (mm)	0	20	40	70	100	150	250
Residence Time (ms)	0	27	52	86	119	173	288
Mass Release (% dry)	0.00	0.00	1.50	38.80	40.80	49.40	51.10
m/m_o(dry)	1.00	1.00	0.99	0.61	0.59	0.51	0.49
m/m_o(wet)	1.00	0.99	0.98	0.61	0.59	0.50	0.49
Aparent Density (ρ/ρ_o)*	1.00	0.77	0.52	0.21	0.18	0.20	0.19
Diameter Ratio	1.00	1.09	1.23	1.43	1.49	1.36	1.37

*Apparent densities measured using volumetric technique (tap densities)

D. Mercury Porosimetry and BET Analyses of Char Samples**

(not available)

PSOC-1451D (cont.)
Pittsburgh #8 hva Bituminous Coal
63-75 μm Size Fraction,
1250 K Gas Condition in the CDL (100% N_2)

E. NMR Analyses of Char Samples

Residence Time (ms)	0	86	119	288
Sampling Distance (mm)	0	70	100	250
Mass Release (% daf)	0	40.3	42.4	53.1
Aromatic carbon, $f_a = f_a' + f_a^C$	.63	.75	.84	.90
Carbonyl, f_a^C	.03	.05	.04	.02
Aromatic carbon, carbonyl subtracted, f_a'	.60	.70	.80	.88
Protonated aromatic carbon, f_a^H	.22	.27	.32	.39
Non-protonated aromatic C, $f_a^N = f_a^P + f_a^S + f_a^B$	.38	.43	.48	.49
Aromatic carbon with O attachment, f_a^P	.05	.07	.06	.04
Aromatic carbon with alkyl attachment, f_a^S	.15	.18	.21	.19
Aromatic bridgehead and inner carbon, f_a^B	.18	.18	.21	.26
Aliphatic carbon, f_{al}	.37	.22	.16	.10
Aliphatic CH and CH_2, f_{al}^H	.26	.16	.11	.07
Aliphatic CH_3 and non-protonated carbon, f_{al}^*	.11	.09	.05	.03
Aliphatics with oxygen attachment, f_{al}^O	.08	.10	.05	.06
Proton spin-relaxation time, $T_{1\rho}^{Har}$ (ms)	5.1	3.2	5.5	13.8
Total carbons per cluster	25	17	16	16
Aromatic carbons per cluster, C	15	12	13	14
Aliphatic carbons per cluster	10	5	3	2
Total attachments per cluster, $\sigma+1$	5.0	4.3	4.4	3.7
Bridges and loops per cluster, B_C	2.3	2.8	3.6	3.2
Side chains per cluster	2.7	1.5	0.8	0.5
Fraction of intact bridges per cluster, p	.45	.64	.81	.87
Average cluster molecular weight	356	243	227	213
Side chain molecular weight	34	22	15	11

PSOC-1451D (cont.)
Pittsburgh #8 hva Bituminous Coal
63-75 μm Size Fraction,
1250 K Gas Condition in the CDL (100% N_2)

F. NMR Analyses of Tar Samples

Sampling Height (mm)	0	20	40	70	100	150	250
Residence Time (ms)	0	27	52	86	119	173	288
Mass Release (% daf)	0.0	0.0	1.5	40.3	42.4	51.3	53.1

α-H	n.a.	n.a.	n.a.	32	29	n.a.	21
α-CH_3	n.a.	n.a.	n.a.	7	5	n.a.	3
β– and γ–H	n.a.	n.a.	n.a.	9	4	n.a.	6
γ-CH_3	n.a.	n.a.	n.a.	1	0.3	n.a.	2
Aromatic H	28*	n.a.	n.a.	53	63	n.a.	69
1-Ring	n.a.	n.a.	n.a.	n.a.	n.a.	n.a.	n.a.
2-Ring	n.a.	n.a.	n.a.	n.a.	n.a.	n.a.	n.a.
3-Ring	n.a.	n.a.	n.a.	n.a.	n.a.	n.a.	n.a.
Aromatic C	60**	n.a.	n.a.	n.a.	n.a.	n.a.	n.a.

*Estimated from the C/H ratio and the carbon aromaticity f_a' of the parent coal
**Estimated as the carbon aromaticity of the parent coal

PSOC-1451D
Pittsburgh #8 hva Bituminous Coal
63-75 μm Size Fraction,
1050 K Gas Condition in the CDL (100% N_2)

A. Char Sample Analyses

Sampling Height (mm)	0	50	80	120	150	180	250
Residence Time (ms)	0	63	95	136	167	200	287
Mass Release (% daf)*	0.0	0.0	12.5	25.1	33.7	33.2	55.5
90% conf. interval (±)	0.0	0.0	5.8	7.3	6.7	10.0	8.0

Moisture (mass %)	1.44	0.69	0.76	0.72	0.66	0.71	0.96
C (mass %, daf)	84.23	84.32	84.36	83.28	84.66	83.37	86.29
H	5.54	5.40	5.44	4.82	4.43	3.98	3.79
O	7.56	8.06	7.92	9.14	8.20	9.61	7.03
N	1.65	1.64	1.64	1.70	1.78	1.82	1.89
S	1.01	0.58	0.64	1.07	0.94	1.22	1.00
Ash (mass %, dry)	3.73	3.45	4.48	5.43	5.73	4.82	8.60
SiO2	1.90	1.50	2.10	2.40	2.70	2.70	3.50
K2O	0.07	0.13	0.10	0.09	0.12	0.09	0.17
TiO2	0.06	0.05	0.07	0.08	0.09	0.09	0.13
Fe2O3	0.31	0.35	0.34	0.42	0.43	0.47	0.57
Al2O3	1.10	1.10	1.30	1.50	1.80	1.90	2.80
CaO	0.11	0.11	0.12	0.17	0.18	0.19	0.23
Na2O	0.01	0.01	0.01	0.01	0.06	0.03	0.03
MgO	0.03	0.03	0.03	0.04	0.05	0.05	0.06
Ash2							

*Mass release based on Si, Ti, Al, and ash as tracers.

B. Mass Balance Data†

m/m_0 (as rec'd)	0.84	0.85	0.49	0.54	0.54	0.43
tar/m_0 (as rec'd)	0.03	0.04	0.11	0.21	0.23	0.22
m/m_0 (normalized)	1.00	1.01	0.58	0.65	0.65	0.51
tar/m_0 (normalized)	0.04	0.04	0.13	0.25	0.27	0.27
estimated V(daf)	0	-1	44	37	37	52
estimated tar(daf)	4	5	14	26	29	28
tar estimated from tar/char ratio and tracer analysis	0	-48	8	24	26	30

†Shown for reference only; tracers were used to determine extent of mass release.

PSOC-1451D (cont.)
Pittsburgh #8 hva Bituminous Coal
63-75 μm Size Fraction,
1050 K Gas Condition in the CDL (100% N_2)

C. Tap Densities and Apparent Densities of Char Samples

Sampling Height (mm)	0	50	80	120	150	180	250
Residence Time (ms)	0	63	95	136	167	200	287
Mass Release (% dry)	0.00	0.00	12.10	24.10	32.50	31.90	53.40
m/m_o(dry)	1.00	1.00	0.88	0.76	0.68	0.68	0.47
m/m_o(wet)	1.00	0.99	0.87	0.75	0.67	0.68	0.46
Aparent Density (ρ/ρ_o)*	1.00	0.80	0.44	0.39	0.19	0.16	0.18
Diameter Ratio	1.00	1.07	1.26	1.25	1.52	1.62	1.37

*Apparent densities measured using volumetric technique (tap densities)

D. Mercury Porosimetry and BET Analyses of Char Samples**

Sampling Height (mm)	0	30	60	90	120	150
Residence Time (ms)	n.a.	n.a.	n.a.	n.a.	n.a.	n.a.
Mass Release (% daf)*	n.a.	n.a.	n.a.	n.a.	n.a.	n.a.

BET Surface Area (m^2/g)	4.49	2.67	8.16	7.52	14.26	16.98
Cumulative Pore Area (m^2/g)	87.79	65.73	74.65	62.67	102.06	88.24
Median Pore Diameter (μm)						
By Volume	16.87	18.91	20.50	21.21	25.35	23.65
By area	0.0039	0.0049	0.0050	0.0052	0.0050	0.0052
By 4V/A	0.0396	0.0589	0.1113	0.2051	0.2267	0.2911
Density, g/cc						
Bulk	0.617	0.563	0.344	0.245	0.148	0.137
Skeletal	1.330	1.237	1.206	1.158	1.049	1.154
Porosity (%)	53.7	54.5	71.5	78.8	85.9	88.1

**These mercury porosimetry and BET surface area data are from an early set of experiments (with Steve Hsu) at the indicated sample heights. The gas condition was similar to those determined from the later experiments, but residence times and particle temperatures are not available for these early data.

PSOC-1451D (cont.)
Pittsburgh #8 hva Bituminous Coal
63-75 μm Size Fraction,
1050 K Gas Condition in the CDL (100% N_2)

E. NMR Analyses of Char Samples

(Not available)

F. NMR Analyses of Tar Samples

Sampling Height (mm)	0	50	80	120	150	180	250
Residence Time (ms)	0	63	95	136	167	200	287
Mass Release (% daf)	0.0	0.0	12.5	25.1	33.7	33.2	55.5

α-H	n.a.	n.a.	n.a.	n.a.	n.a.	38	34
α-CH_3	n.a.	n.a.	n.a.	n.a.	n.a.	9	9
β– and γ–H	n.a.	n.a.	n.a.	n.a.	n.a.	18	13
γ-CH_3	n.a.	n.a.	n.a.	n.a.	n.a.	4	3
Aromatic H	28*	n.a.	n.a.	n.a.	n.a.	38	47
1-Ring	n.a.	n.a.	n.a.	n.a.	n.a.	n.a.	n.a.
2-Ring	n.a.	n.a.	n.a.	n.a.	n.a.	n.a.	n.a.
3-Ring	n.a.	n.a.	n.a.	n.a.	n.a.	n.a.	n.a.
Aromatic C	60**	n.a.	n.a.	n.a.	n.a.	n.a.	n.a.

*Estimated from the C/H ratio and the carbon aromaticity f_a' of the parent coal
**Estimated as the carbon aromaticity of the parent coal

PSOC-1451D
Pittsburgh #8 hva Bituminous Coal
63-75 μm Size Fraction,
1050 K Gas Condition in the CDL (100% N_2)
(Duplicate Experiments)

A. Char Sample Analyses

Sampling Height (mm)	0	180	250
Residence Time (ms)	0	200	287
Mass Release (% daf)*	0.0	34.2	50.7
90% conf. interval (±)	0.0	7.0	4.1

Moisture (mass %)	2.72	2.21	1.75
C (mass %, daf)	84.93	84.94	85.33
H	5.45	4.69	3.89
O	7.03	7.62	8.03
N	1.68	1.87	1.89
S	0.92	0.89	0.85
Ash (mass %, dry)	3.92	6.64	8.44
SiO2	2.07	3.03	4.08
K2O	0.06	0.09	0.12
TiO2	0.06	0.08	0.11
Fe2O3	0.29	0.43	0.57
Al2O3	1.13	1.64	2.18
CaO	0.15	0.21	0.27
Na2O	0.03	0.03	0.04
MgO	0.02	0.03	0.06
Ash2			

*Mass release based on Si, Ti, Al, and ash as tracers.

B. Mass Balance Data†

m/m_0 (as rec'd)	0.60	0.51
tar/m_0 (as rec'd)	0.20	0.25
m/m_0 (normalized)	0.71	0.61
tar/m_0 (normalized)	0.24	0.30
estimated V(daf)	31	42
estimated tar(daf)	25	32
tar estimated from tar/char ratio and tracer analysis	28	39

†Shown for reference only; tracers were used to determine extent of mass release.

PSOC-1451D (cont.)
Pittsburgh #8 hva Bituminous Coal
106-125 μm Size Fraction,
1050 K Gas Condition in the CDL (100% N_2)
(Duplicate Experiments)

C. Tap Densities and Apparent Densities of Char Samples

Sampling Height (mm)	0	180	250
Residence Time (ms)	0	200	287
Mass Release (% dry)	0.00	32.90	48.70
m/m_o(dry)	1.00	0.67	0.51
m/m_o(wet)	1.00	0.67	0.51
Aparent Density $(\rho/\rho_o)^*$	1.00	0.30	0.32
Diameter Ratio	1.00	1.31	1.17

*Apparent densities measured using volumetric technique (tap densities)

D. Mercury Porosimetry and BET Analyses of Char Samples

(not available)

E. NMR Analyses of Char Samples

(not available)

F. NMR Analyses of Tar Samples

(not available)

PSOC-1451D
Pittsburgh #8 hva Bituminous Coal
106-125 μm Size Fraction,
1350 K High Velocity Gas Condition in the CDL (100% N_2)**

A. Char Sample Analyses

Sampling Height (mm)	0	20	40	70	100	150	250
Residence Time (ms)	0	0	0	0	0	0	0
Mass Release (% daf)*	0.0*	0.0	0.0	18.5	48.6	56.6	52.2
90% conf. interval (±)	0.0*	0.0	0.0	6.7	17.5	25.9	21.9

Moisture (mass %)	1.40	0.66	0.66	0.61	0.67	1.21	1.06
C (mass %, daf)	83.01	83.94	84.51	84.10	85.07	87.63	91.29
H	5.42	5.49	5.47	5.28	4.42	3.33	2.77
O	8.77	7.75	7.26	7.73	7.79	5.73	3.03
N	1.63	1.84	1.78	1.85	1.78	2.11	2.03
S	1.18	0.97	0.98	1.04	0.94	1.20	0.87
Ash (mass %, dry)	18.05	9.48	9.20	10.42	12.54	23.44	12.16
SiO2	9.13	5.57	4.83	6.90	12.05	8.83	12.30
K2O	0.44	0.32	0.15	0.29	0.44	0.68	0.55
TiO2	0.18	0.12	0.11	0.15	0.22	0.18	0.26
Fe2O3	0.90	0.67	0.52	0.72	1.41	2.49	1.40
Al2O3	4.21	2.64	2.42	3.28	5.50	10.70	6.24
CaO	1.15	0.85	0.56	1.15	1.83	1.08	1.46
Na2O	0.10	0.06	0.06	0.08	0.14	0.25	0.12
MgO	0.29	0.14	0.18	0.27	0.41	0.09	0.30
Ash2	n.a.	n.a.	n.a.	n.a.	n.a.	n.a.	n.a.

*Mass release based on Si, Ti, Al, and ash as tracers. The raw coal analyses associated with this set of pyrolysis chars was obviously in error, and hence the sample taken at 20 mm was used here as the normalization standard to determine the extent of mass release.

**The increased velocity in this condition caused flow instabilities in the reactor, and the particles did not flow in a straight line. This caused uncertainties in the determination of the particle history and made particle temperature measurement impossible due to the low probability of a particle entering the optical diagnostic volume. No other analyses were performed on this set of coal samples.

PSOC-1451D
Pittsburgh #8 hva Bituminous Coal
63-75 μm Size Fraction,
850 K Gas Condition in the CDL (100% N_2)
(Early experiments performed with Steve Hsu)

A. Char Sample Analyses

(not available)

B. Tap Densities and Apparent Densities of Char Samples

(not available)

C. Mercury Porosimetry and BET Analyses of Char Samples

Sampling Height (mm)	0	80	160	240	280
Residence Time (ms)	n.a.	n.a.	n.a.	n.a.	n.a.
Mass Release (% daf)	n.a.	n.a.	n.a.	n.a.	n.a.

BET Surface Area (m^2/g)	4.49	0.97	0.40	0.39*	0.24*
Cumulative Pore Area (m^2/g)	87.79	78.37	102.05	118.05	78.71
Median Pore Diameter (μm)					
By Volume	16.87	18.09	24.22	23.89	22.79
By area	0.0039	0.0047	0.0050	0.0045	0.0046
By 4V/A	0.0396	0.0525	0.1441	0.0937	0.1336
Density, g/cc					
Bulk	0.617	0.559	0.218	0.277	0.289
Skeletal	1.330	1.316	1.100	1.176	1.195
Porosity (%)	53.7	57.5	80.2	76.5	75.9

*These mercury porosimetry and BET surface area data are from an early set of experiments (with Steve Hsu) at the indicated sample heights. The gas condition was similar to those determined from the later experiments, but residence times and particle temperatures are not available for these early data. The 850 K gas condition characterized by measurements of gas temperature, but particle temperatures were below the detection limit of the particle sizing-pyrometer system. No other analyses of these samples were performed.

PSOC-1451D
Pittsburgh #8 hva Bituminous Coal
106-125 μm Size Fraction,
850 K Gas Condition in the CDL (100% N_2)
(Early experiments performed with Steve Hsu)

A. Char Sample Analyses

(not available)

B. Tap Densities and Apparent Densities of Char Samples

(not available)

C. Mercury Porosimetry and BET Analyses of Char Samples

Sampling Height (mm)	0.0	50	100	150	200	250	290
Residence Time (ms)	n.a.	n.a.	n.a.	n.a.	n.a.	n.a.	n.a.
Mass Release (% daf)	n.a.	n.a.	n.a.	n.a.	n.a.	n.a.	n.a.
BET Surface Area (m^2/g)	4.16	2.56	1.87	1.63	1.37	1.07	1.81
Cumulative Pore Area (m^2/g)	59.01	52.53	61.56	69.10	83.51	10.14	13.77
Median Pore Diameter (μm)							
By Volume	28.32	29.06	30.69	33.45	35.17	47.65	48.15
By area	0.0046	0.0047	0.0049	0.0056	0.0050	0.0037	0.0042
By 4V/A	0.0544	0.0641	0.0621	0.0759	0.1022	0.8887	0.6826
Density, g/cc							
Bulk	0.673	0.637	0.596	0.479	0.342	0.262	0.250
Skeletal	1.462	1.375	1.386	1.286	1.268	0.637	0.608
Porosity (%)	54.0	53.6	57.0	62.8	73.0	59.0	58.8

*These mercury porosimetry and BET surface area data are from an early set of experiments (with Steve Hsu) at the indicated sample heights. The gas condition was similar to those determined from the later experiments, but residence times and particle temperatures are not available for these early data. The 850 K gas condition characterized by measurements of gas temperature, but particle temperatures were below the detection limit of the particle sizing-pyrometer system. No other analyses of these samples were performed.

APPENDIX F

Data Summary:

PSOC-1493D

Illinois #6

hvb bituminous coal

SAMPLE HISTORY

PENN STATE NUMBER	PSOC-1493
COLLECTED BY	PENNSYLVANIA STATE UNIVERSITY
COLLECTION DATE	9/1/85
COLLECTOR'S NUMBER	
REPORTED RANK	HIGH VOLATILE B BITMUMINOUS (HVBB)
SAMPLE TYPE	CHANNEL WHOLE SEAM
OTHER SAMPLE INFORMATION	
SAMPLE RESERVE	900
SEAM NAME	ILLINOIS #6
ALTERNATE SEAM NAME	HERRIN
TOTAL SEAM THICKNESS	5 FT. 6 IN.
THICKNESS OF SEAM SAMPLED	5 FT. 6 IN.
PORTION RECOVERED IN CORE	
DIAMETER OF CORE	

SAMPLE LOCATION

COUNTRY	U.S.A.
STATE	ILLINOIS
COUNTY	PERRY
TOWNSHIP	SIX MILE PRAIRIE
NEAREST TOWN	CUTLER
COAL PROVINCE	INTERIOR
COAL REGION	EASTERN
COAL FIELD	

SEAM NAME	ILLINOIS #6	COUNTRY	U.S.A.
APPARENT RANK	HIGH VOLATILE C BITUMINOUS (HVCB)	STATE	ILLINOIS

GEOLOGIC INFORMATION

SYSTEM (AGE)	PENNSYLVANIAN
SERIES	
GROUP	
FORMATION	CARBONDALE
OVERBURDEN LITHOLOGY	SHALE
FLOOR LITHOLOGY	CLAY

SEAM STRATA INFORMATION

THICKNESS	LITHOTYPE

SEAM NAME	ILLINOIS #6	COUNTRY	U.S.A.
APPARENT RANK	HIGH VOLATILE C BITUMINOUS (HVCB)	STATE	ILLINOIS

CHEMICAL DATA 1

PROXIMATE ANALYSIS	AS REC'D	DRY	DAF	DMMF (PAFF)	DMMF (PARR-G)	DMMF (DIR MM)
% MOISTURE	9.43					
% ASH	13.74	15.17				
% VOLATILE MATTER	34.34	37.91	44.69	42.91	42.93	
% FIXED CARBON	42.50	46.92	55.31	57.09	57.07	

CALORIFIC VALUE (GROSS BTU/LB)	DRY	AS REC'D MOIST.	EQUIL MOIST.
MM-FREE, DIRECT			
MM-CONTAINING	11963	10835	10637
MM-FREE (PARR)	14484	12832	12550
MM-FREE (MOD.P)	14485	12707	12430
BEST MM FREE		12707	12430
NET CV, DMMF BTU/LB	14011		
ASH-FREE	14102		

MOTT-SPOONER DIFFERENCE =

ASSOCIATED ANALYSES	DRY	MMF
% EQUILIBRIUM MOISTURE	11.08	13.70
% TOTAL SULFUR	4.98	

RANK CALCULATIONS

APPARENT RANK (AS REC'D MOIST)	HIGH VOLATILE C BITUMINOUS (HVCB)
ASTM RANK (EQUIL. MOIST.)	HIGH VOLATILE C BITUMINOUS (HVCB)
REFLECTANCE RANK CATEGORY	HIGH VOLATILE C BITUMINOUS (HVCB)
INTERNATIONAL RANK	
AS REC'D MOIST.	
EQUIL. MOIST	
REPORTED RANK	HIGH VOLATILE B BITUMINOUS (HVBB)

SEAM NAME ILLINOIS #6 COUNTRY U.S.A.
APPARENT RANK HIGH VOLATILE C BITUMINOUS (HVCB) STATE ILLINOIS

CHEMICAL DATA 2

ULTIMATE ANALYSIS	AS REC'D	DRY	DAF	DMMF(PARR) (19.12 % MM)
% ASH	13.74	15.17		
% CARBON	59.98	66.23	78.07	81.89
% HYDROGEN	*3.78	4.17	4.92	5.16
% NITROGEN	1.15	1.27	1.50	1.57
% SULFUR	4.51	4.98	5.87	
% CHLORINE	0.03	0.03	0.04	0.04
% OXYGEN (DIFF)	*7.38	8.15	9.61	11.35

SULFUR FORMS	% PYRITIC	% SULFATIC	% ORGANIC	% TOTAL
DRY	2.61	0.04	2.33	4.98
DAF	3.08	0.05	2.75	5.87
OPTICAL				

ELEMENTAL ANALYSIS	DRY	DMMF (MOD.P) (18.38 % MM)	DMMF(DIR.) (% MM)
% CARBON	66.07	80.96	
% HYDROGEN	4.44	5.44	
% NITROGEN	1.27	1.57	
% ORGANIC SULFUR	2.33	2.85	
% OXYGEN (DIFF)	7.50	9.16	
% CHLORINE	0.03	0.04	
% MINERAL MATTER (INCLUDES 4.88 % FES2)	18.38		

ATOM RATIOS (DMMF)	PARR	MOD.PAR	DIRECT
ATOMIC H/C	0.756	0.807	
ATOMIC O/C	0.104	0.104	

MISC. CHEMICAL DATA	DRY	OF DMMF COAL	OF DMMF OXYGEN
% O AS COOH			
% O AS OH			
% S AS SO4, IN ASH			
% CARBONATE AS CO2	0.57		
% CHLORINE	0.06		

INFRA-RED ANALYSIS

(*)- EXCLUDES MOISTURE

SEAM NAME ILLINOIS #6
APPARENT RANK HIGH VOLATILE C BITUMINOUS (HVCB)
COUNTRY U.S.A.
STATE ILLINOIS

CHEMICAL DATA 3

% MOISTURE IN COAL = 2.37
% HIGH TEMPERATURE ASH = 14.30 AT 750 DEGREES C

TRACE ELEMENT ANALYSIS	PPM HTA	PPM TOTAL COAL
AG		
B		
BA	540	77
BE	9	1
BI		
CE		
CO		
CR	130	19
CU	120	17
GA		
GE		
LA		
LI		
MN	430	61
MO		
NI	60	9
NB		
PB		
RB	100	14
SC		
SN		
SR	170	24
TH		
U		
V	220	31
Y		
YB		
ZN	440	63
ZR	150	21

MAJOR ELEMENT ANALYSIS	OXIDE % OF HTA	ELEMENT % OF TOTAL DRY COAL
SI02	41.20	2.75
AL203	15.70	1.19
TI02	0.76	0.07
FE203	23.90	2.39
MG0	0.90	0.08
CA0	7.39	0.76
NA20	0.40	0.04
K20	1.70	0.20
P205	0.26	0.02
S03	7.90	0.45

VOLATILES	PPM TOTAL COAL
AS	
BR	
CD	
CL	
F	
HG	
SB	
SE	

SEAM NAME ILLINOIS #6
APPARENT RANK HIGH VOLATILE C BITUMINOUS (HVCB)

COUNTRY U.S.A.
STATE ILLINOIS

MINERALOGICAL DATA

TOTAL MINERAL MATTER

% MM-PARR	19.12
% MM-MODIFIED PARR	18.38
% MM-KMC	
% MM-DIRECT	
% MM-BEST AVAILABLE	18.38
VOL % MM-PARR	10.23

MINERAL COMPOSITION

NONE

SEAM NAME	ILLINOIS #6	COUNTRY	U.S.A.
APPARENT RANK	HIGH VOLATILE C BITUMINOUS (HVCB)	STATE	ILLINOIS

PETROGRAPHIC DATA

MACERAL COMPOSITION WHITE ANALYSIS ONLY

	DRY VOLUME %	DMMF VOLUME %	DRY WEIGHT %
VITRINITE (CALC.)	77.6	86.4	69.9
INERTINITE (CALC.)	11.0	12.2	9.9
LIPTINITE (CALC.)	1.3	1.4	1.1
MINERAL MATTER (CALC.)	10.2		19.1
VITRINOIDS			
VITRINITE	77.6	86.4	69.9
PSEUDOVITRINITE	0.0	0.0	0.0
FUSINITE	3.2	3.6	2.9
SEMI-FUSINITE	4.8	5.4	4.4
MACRINITE	0.4	0.5	0.4
MICRINITE	2.4	2.7	2.2
SCLEROTINITE	0.0	0.0	0.0
SPORINITE			
CUTINITE			
EXINITE (ANAL.)	1.1	1.2	1.0
RESINITE	0.2	0.2	0.2
SUBERINITE			
EXUDATINITE			
FLUORINITE			
BITUMINITE			
ALGINITE	0.0	0.0	0.0
LIPTODETRINITE			
MINERAL MATTER (ANAL.)			
INERTINITE (ANAL.)			
LIPTODETRINITE (ANAL.)			

REFLECTANCE DATA (%, IN OIL)	HIGH	LOW	RANGE	MEAN MAX	STAND.DEV.
VITRINITE	0.68	0.42	0.26	0.53	0.06
PSEUDOVITRINITE					
VITRINOIDS					

SEAM NAME ILLINOIS #6 COUNTRY U.S.A.
APPARENT RANK HIGH VOLATILE C BITUMINOUS (HVCB) STATE ILLINOIS

PETROGRAPHIC DATA

CONTINUED

% VITRINOID REFLECTANCE	HALF-TYPE	VOLUME PERCENT	% VITRINOID REFLECTANCE	V-TYPE	VOLUME PERCENT
0.40-0.44	VHT 0.425	7.00			
0.45-0.49	VHT 0.475	32.00	0.50-0.59	V4	39.00
0.50-0.54	VHT 0.525	26.00			
0.55-0.59	VHT 0.575	19.00	0.50-0.59	V5	45.00
0.60-0.64	VHT 0.625	12.00			
0.65-0.69	VHT 0.675	4.00	0.60-0.69	V6	16.00

PHYSICAL PROPERTIES

HARDGROVE GRINDABILITY	47.0
VICKER'S MICROHARDNESS	
FREE SWELLING INDEX	3.0
GRAY KING COKE TYPE	

ASH FUSION ANALYSIS (DEGREES F)	REDUCING	OXIDIZING
INITIAL DEFORMATION TEMPERATURE	1965	2330
SOFTENING TEMPERATURE	2035	2395
HEMISPHERE TEMPERATURE	2125	2515
FLUID TEMPERATURE	2205	2550

ANALYSIS LOG

ANALYSIS	DATE	PERFORMED BY
A.R. MOIST	12/13/85	WARNER LABORATORIES
EQUIL. MOIST.	12/13/85	WARNER LABORATORIES
PROXIMATE	12/13/85	WARNER LABORATORIES
ULTIMATE	12/13/85	WARNER LABORATORIES
SULFUR FORMS	12/51385	WARNER LABORATORIES
FSI	12/5/85	COAL PETROGRAPHY LABORATORIES-PSU
PLASTOMETER	12/2/85	COAL PETROGRAPHY LABORATORIES-PSU
DIRECT MM		
GRAY-KING		

PSOC-1493D
Illinois #6 hvb Bituminous Coal
106-125 μm Size Fraction,
1250 K Gas Condition in the CDL (100% N_2)

A. Char Sample Analyses

Sampling Height (mm)	0	20	40	70	100	150	250
Residence Time (ms)	0	24	43	65	89	128	224
Mass Release (% daf)*	0.0	0.4	19.0	39.2	47.2	51.4	52.0
90% conf. interval (±)	0.0	0.6	3.8	8.6	3.0	4.4	5.3

Moisture (mass %)	3.28	0.74	0.58	0.64	0.84	1.03	0.90
C (mass %, daf)	74.12	74.69	77.04	73.19	75.89	78.18	83.94
H	4.96	4.80	4.66	3.82	3.06	2.49	2.71
O	13.18	11.81	11.70	11.13	9.37	6.77	5.84
N	1.45	1.53	1.53	1.50	1.60	1.66	1.67
S	6.29	7.16	5.06	10.36	10.07	10.90	5.84
Ash (mass %, dry)	11.30	13.60	13.61	21.71	23.12	23.36	22.31
SiO2	4.77	4.79	5.84	7.66	8.28	8.96	8.92
Al2O3	1.78	1.79	2.16	2.83	3.13	3.36	3.47
Fe2O3	3.58	4.91	3.91	8.93	8.46	7.68	6.94
TiO2	0.10	0.10	0.12	0.14	0.17	0.17	0.18
Ash2	13.22	15.16	12.61	22.91	24.37	22.85	20.52

*Mass release based on Si, Ti, and Al as tracers (not ash).

B. Mass Balance Data†

m/m_o (as rec'd)	1.00	0.76	0.61	0.53	0.50	0.49
tar/m_o (as rec'd)	0.01	0.06	0.14	0.17	0.17	0.13
m/m_o (normalized)	1.00	0.76	0.61	0.53	0.50	0.49
tar/m_o (normalized)	0.01	0.06	0.14	0.17	0.17	0.13
estimated V(daf)	0	28	45	55	58	60
estimated tar(daf)	1	7	16	20	19	16
tar estimated from tar/char ratio and tracer analysis	0	5	14	18	17	14

†Shown for reference only; tracers were used to determine extent of mass release.

PSOC-1493D (cont.)
Illinois #6 hvb Bituminous Coal
106-125 μm Size Fraction,
1250 K Gas Condition in the CDL (100% N_2)

C. Tap Densities and Apparent Densities of Char Samples

Sampling Height (mm)	0	20	40	70	100	150	250
Residence Time (ms)	0	24	43	65	89	128	224
Mass Release (% dry)	0.00	0.30	16.80	34.80	41.90	45.50	46.10
m/m_o(dry)	1.00	1.00	0.83	0.65	0.58	0.55	0.54
m/m_o(wet)	1.00	0.97	0.81	0.63	0.57	0.53	0.53
Aparent Density $(\rho/\rho_o)^*$	1.00	0.56	0.36	0.38	0.34	0.31	0.36
Diameter Ratio	1.00	1.20	1.31	1.19	1.19	1.20	1.13

*Apparent densities measured using volumetric technique (tap densities)

D. Mercury Porosimetry and BET Analyses of Char Samples

(not available)

PSOC-1493D (cont.)
Illinois #6 hvb Bituminous Coal
106-125 μm Size Fraction,
1250 K Gas Condition in the CDL (100% N_2)

E. NMR Analyses of Char Samples

Residence Time (ms)	0	43	65	89	128	223
Sampling Distance (mm)	0	40	70	100	150	250
Mass Release (% daf)	0	22	38	47	51	51
Aromatic carbon, $f_a = f_a' + f_a^C$	.71	.72	.74	.79	.81	.86
Carbonyl, f_a^C	.04	.05	.04	.05	.03	.02
Aromatic carbon, carbonyl subtracted, f_a'	.67	.67	.70	.74	.78	.84
Protonated aromatic carbon, f_a^H	.27	.29	.27	.34	.33	.32
Non-protonated aromatic C, $f_a^N = f_a^P + f_a^S + f_a^B$	.40	.38	.43	.40	.45	.52
Aromatic carbon with O attachment, f_a^P	.08	.09	.07	.07	.05	.05
Aromatic carbon with alkyl attachment, f_a^S	.17	.19	.16	.19	.18	.22
Aromatic bridgehead and inner carbon, f_a^B	.15	.10	.20	.14	.22	.25
Aliphatic carbon, f_{al}	.29	.28	.26	.21	.19	.14
Aliphatic CH and CH_2, f_{al}^H	.18	.19	.17	.15	.14	.10
Aliphatic CH_3 and non-protonated carbon, f_{al}^*	.11	.09	.09	.06	.05	.04
Aliphatics with oxygen attachment, f_{al}^O	.07	.07	.05	.08	.07	.07
Proton spin-relaxation time, $T_{1\rho}^{Har}$ (ms)	4.0	2.6	2.7	4.4	6.1	8.3
Total carbons per cluster	16	14	19	13	17	18
Aromatic carbons per cluster, C	11	10	14	10	14	15
Aliphatic carbons per cluster	4.8	4.2	5.2	2.8	3.4	2.5
Total attachments per cluster, $\sigma+1$	4.1	4.2	4.6	3.5	4.1	4.8
Bridges and loops per cluster, B_C	2.3	2.8	2.8	2.7	3.2	4.1
Side chains per cluster	1.8	1.4	1.8	0.8	0.9	0.7
Fraction of intact bridges per cluster, p	.56	.68	.61	.77	.78	.85
Average cluster molecular weight	270	230	330	210	280	260
Side chain molecular weight	34	26	35	26	27	17

PSOC-1493D (cont.)
Illinois #6 hvb Bituminous Coal
106-125 μm Size Fraction,
1250 K Gas Condition in the CDL (100% N_2)

F. NMR Analyses of Tar Samples

Sampling Height (mm)	0	43	65	89	128	223
Residence Time (ms)	0	40	70	100	150	250
Mass Release (% daf)	0	22	38	47	51	51

α-H	n.a.	35	33	26	24	19
α-CH_3	n.a.	14	9	7	4	4
β– and γ–H	n.a.	19	14	7	4	4
γ-CH_3	n.a.	7	4	1	1	1
Aromatic H	34*	39	50	62	72	75
1-Ring	n.a.	13	19	16	23	10
2-Ring	n.a.	8	19	19	20	25
3-Ring	n.a.	14	9	21	24	35
Aromatic C†	67**	n.a.	n.a.	n.a.	n.a.	n.a.

*Estimated from the C/H ratio and the carbon aromaticity f_a' of the parent coal
**Estimated as the carbon aromaticity of the parent coal
†See duplicate experiments in next table.

PSOC-1493D
Illinois #6 hvb Bituminous Coal
106-125 μm Size Fraction,
1250 K Gas Condition in the CDL (100% N_2)
(Duplicate Experiments)

A. Char Sample Analyses

Sampling Height (mm)	0	40	70	180	250
Residence Time (ms)	0	43	65	154	224
Mass Release (% daf)*	0.0	24.9	37.1	49.9	49.2
90% conf. interval (±)	0.0	6.5	4.3	3.9	3.9

Moisture (mass %)	3.26	1.94	2.59	2.82	2.51
C (mass %, daf)	74.81	75.49	78.15	83.26	85.59
H	5.13	4.58	3.81	2.69	2.79
O	12.93	11.83	10.96	5.50	4.96
N	1.38	1.46	1.73	1.87	1.68
S	5.74	6.64	5.35	6.68	4.99
Ash (mass %, dry)	11.30	18.30	17.20	22.20	20.80
SiO2	4.78	6.46	7.35	8.93	8.71
Al2O3	1.96	2.47	2.82	3.40	3.34
Fe2O3	4.47	6.03	5.46	6.64	5.69
TiO2	0.10	0.13	0.15	0.18	0.18
Ash2	13.42	13.06	17.02	25.74	22.47

*Mass release based on Si, Ti, and Al as tracers (not ash).

B. Mass Balance Data†

m/m_0 (as rec'd)	0.79	0.54	0.49	0.46
tar/m_0 (as rec'd)	0.08	0.13	0.12	0.11
m/m_0 (normalized)	1.00	0.68	0.62	0.59
tar/m_0 (normalized)	0.11	0.16	0.15	0.14
estimated V(daf)	0	37	45	48
estimated tar(daf)	12	19	18	17
tar estimated from tar/char ratio and tracer analysis	0	19	20	17

†Shown for reference only; tracers were used to determine extent of mass release.

PSOC-1493D (cont.)
Illinois #6 hvb Bituminous Coal
106-125 μm Size Fraction,
1250 K Gas Condition in the CDL (100% N_2)
(Duplicate Experiments)

C. Tap Densities and Apparent Densities of Char Samples

Sampling Height (mm)	0	40	70	180	250
Residence Time (ms)	0	43	65	154	224
Mass Release (% dry)	0.00	22.10	32.90	44.30	43.70
m/m_o(dry)	1.00	0.78	0.67	0.56	0.56
m/m_o(wet)	1.00	0.77	0.67	0.55	0.56
Aparent Density $(\rho/\rho_o)^*$	1.00	0.40	0.42	0.41	0.42
Diameter Ratio	1.00	1.24	1.17	1.11	1.10

*Apparent densities measured using volumetric technique (tap densities)

D. Mercury Porosimetry and BET Analyses of Char Samples

(not available)

E. NMR Analyses of Char Samples

(not available)

PSOC-1493D (cont.)
Illinois #6 hvb Bituminous Coal
106-125 μm Size Fraction,
1250 K Gas Condition in the CDL (100% N_2)
(Duplicate Experiments)

F. NMR Analyses of Tar Samples

Sampling Height (mm)	0	40	70	180	250
Residence Time (ms)	0	43	65	154	224
Mass Release (% daf)	0.0	24.9	37.1	49.9	49.2

α-H	n.a.	n.a.	n.a.	n.a.	n.a.
α-CH_3	n.a.	n.a.	n.a.	n.a.	n.a.
β– and γ–H	n.a.	20	10	n.a.	1
γ-CH_3	n.a.	6.3	3	0.4	0.2
Aromatic H	33	36	53	n.a.	79
1-Ring	n.a.	16	19	n.a.	11
2-Ring	n.a.	11	14	n.a.	27
3-Ring	n.a.	9	27	n.a.	41
Aromatic C	67	74	84	96	96

*Estimated from the C/H ratio and the carbon aromaticity f_a' of the parent coal
**Estimated as the carbon aromaticity of the parent coal

PSOC-1493D
Illinois #6 hvb Bituminous Coal
106-125 μm Size Fraction,
1050 K Gas Condition in the CDL (100% N_2)

A. Char Sample Analyses

Sampling Height (mm)	0	50	80	120	150	180	250
Residence Time (ms)	0	61	91	127	156	186	266
Mass Release (% daf)*	0.0	1.8	27.9	29.3	36.7	38.3	43.5
90% conf. interval (±)	0.0	4.2	8.4	6.5	6.6	7.5	9.6

Moisture (mass %)	3.28	0.94	1.01	0.53	0.71	1.00	0.71
C (mass %, daf)	74.12	73.98	75.34	75.49	74.36	73.45	75.22
H	4.96	4.76	4.99	4.35	4.01	3.67	3.28
O	13.18	13.07	12.18	12.16	11.72	11.95	10.53
N	1.45	1.38	1.42	1.59	1.54	1.43	1.42
S	6.29	6.80	6.07	6.41	8.37	9.49	9.55
Ash (mass %, dry)	11.30	12.06	16.24	16.58	18.37	19.36	22.05
SiO2	4.77	4.58	6.62	6.54	7.18	7.21	7.67
Al2O3	1.78	1.68	2.36	2.37	2.61	2.63	2.80
Fe2O3	3.58	4.03	5.00	5.23	5.78	6.30	7.69
TiO2	0.10	0.09	0.12	0.13	0.14	0.14	0.15
Ash2	13.22	10.86	15.52	16.12	20.18	20.46	24.39

*Mass release based on Si, Ti, Al, and ash as tracers.

B. Mass Balance Data†

m/m_0 (as rec'd)	0.79	0.76	0.71	0.56	0.59	0.56
tar/m_0 (as rec'd)	0.01	0.03	0.09	0.10	0.15	0.17
m/m_0 (normalized)	1.00	0.96	0.91	0.71	0.74	0.71
tar/m_0 (normalized)	0.01	0.04	0.11	0.13	0.19	0.21
estimated V(daf)	0	4	11	34	30	34
estimated tar(daf)	1	5	13	16	23	25
tar estimated from tar/char ratio and tracer analysis	0	32	36	17	29	32

†Shown for reference only; tracers were used to determine extent of mass release.

PSOC-1493D (cont.)
Illinois #6 hvb Bituminous Coal
106-125 μm Size Fraction,
1050 K Gas Condition in the CDL (100% N_2)

C. Tap Densities and Apparent Densities of Char Samples

Sampling Height (mm)	0	50	80	120	150	180	250
Residence Time (ms)	0	61	91	127	156	186	266
Mass Release (% dry)	0.00	1.60	24.70	26.00	32.60	34.00	38.60
m/m_o(dry)	1.00	0.98	0.75	0.74	0.67	0.66	0.61
m/m_o(wet)	1.00	0.96	0.74	0.72	0.66	0.64	0.60
Aparent Density $(\rho/\rho_o)^*$	1.00	0.81	0.48	0.44	0.44	0.52	0.58
Diameter Ratio	1.00	1.06	1.15	1.18	1.14	1.07	1.01

*Apparent densities measured using volumetric technique (tap densities)

D. Mercury Porosimetry and BET Analyses of Char Samples

(not available)

E. NMR Analyses of Char Samples

(not available)

PSOC-1493D (cont.)
Illinois #6 hvb Bituminous Coal
106-125 μm Size Fraction,
1050 K Gas Condition in the CDL (100% N_2)

F. NMR Analyses of Tar Samples

Sampling Height (mm)	0	50	80	120	150	180	250
Residence Time (ms)	0	61	91	127	156	186	266
Mass Release (% daf)	0.0	1.8	27.9	29.3	36.7	38.3	43.5

α-H	n.a.	n.a.	35	34	42	35	39
α-CH_3	n.a.	n.a.	8	9	8	9	11
β– and γ–H	n.a.	n.a.	25	18	16	16	15
γ-CH_3	n.a.	n.a.	8	8	5	3	4
Aromatic H	34*	n.a.	32	41	42	45	42
1-Ring	n.a.	n.a.	10	10	11	8	15
2-Ring	n.a.	n.a.	10	10	11	8	14
3-Ring	n.a.	n.a.	8	15	13	14	7
Aromatic C	67**	n.a.	n.a.	64	70	80	81

*Estimated from the C/H ratio and the carbon aromaticity f_a' of the parent coal
**Estimated as the carbon aromaticity of the parent coal

APPENDIX G

Data Summary:

PSOC-1507D

North Dakota

Beulah Zap lignite

ZAP

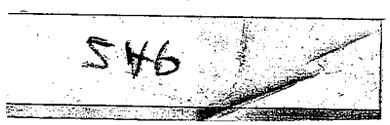
546

SAMPLE HISTORY

PENN STATE NUMBER	PSOC-1507
COLLECTED BY	PENNSYLVANIA STATE UNIVERSITY
COLLECTION DATE	7/2/85
COLLECTOR'S NUMBER	
REPORTED RANK	LIGNITE
SAMPLE TYPE	CHANNEL WHOLE SEAM
OTHER SAMPLE INFORMATION	UPPER & LOWER BEULAH SEAM COMBINED
SAMPLE RESERVE	300
SEAM NAME	BEULAH
ALTERNATE SEAM NAME	ZAP
TOTAL SEAM THICKNESS	12 FT. 1 IN.
THICKNESS OF SEAM SAMPLED	12 FT. 1 IN.
PORTION RECOVERED IN CORE	
DIAMETER OF CORE	

SAMPLE LOCATION

COUNTRY	U.S.A.
STATE	NORTH DAKOTA
COUNTY	MERCER
TOWNSHIP	
NEAREST TOWN	ZAP
COAL PROVINCE	NORTHERN GREAT PLAINS
COAL REGION	FORT UNION
COAL FIELD	

SEAM NAME	BEULAH	COUNTRY	U.S.A.
APPARENT RANK	LIGNITE A (LIGA)	STATE	NORTH DAKOTA

GEOLOGIC INFORMATION

SYSTEM (AGE)	TERTIARY
SERIES	PALEOCENE
GROUP	
FORMATION	FORT UNION
OVERBURDEN LITHOLOGY	
FLOOR LITHOLOGY	BLACK SHALE

SEAM STRATA INFORMATION

THICKNESS	LITHOTYPE

SEAM NAME BEULAH
APPARENT RANK LIGNITE A (LIGA)

COUNTRY U.S.A.
STATE NORTH DAKOTA

CHEMICAL DATA 1

PROXIMATE ANALYSIS	AS REC'D	DRY	DAF	DMMF (PAFF)	DMMF (PARR-G)	DMMF (DIR MM)
% MOISTURE	33.57					
% ASH	8.30	12.49				
% VOLATILE MATTER	27.08	40.77	46.59	45.73	45.29	
% FIXED CARBON	31.06	46.75	53.42	54.27	55.71	

CALORIFIC VALUE (GROSS BTU/LB)	DRY	AS REC'D MOIST.	EQUIL MOIST.
MM-FREE, DIRECT	10627	7060	6792
MM-CONTAINING	12313	7747	7423
MM-FREE (PARR)	12375	7734	7412
MM-FREE (MOD.P)		7734	7412
BEST MM FREE	11899		
NET CV, DMMF BTU/LB	12144		
ASH-FREE			

MOTT-SPOONER DIFFERENCE =

ASSOCIATED ANALYSES	DRY	MMF
% EQUILIBRIUM MOISTURE	36.09	42.10
% TOTAL SULFUR	1.43	

RANK CALCULATIONS

APPARENT RANK (AS REC'D MOIST)	LIGNITE A (LIGA)
ASTM RANK (EQUIL. MOIST.)	LIGNITE A (LIGA)
REFLECTANCE RANK CATEGORY	
INTERNATIONAL RANK	
AS REC'D MOIST.	
EQUIL. MOIST	
REPORTED RANK	LIGNITE

SEAM NAME BEULAH
APPARENT RANK LIGNITE A (LIGA)
COUNTRY U.S.A.
STATE NORTH DAKOTA

CHEMICAL DATA 2

ULTIMATE ANALYSIS	AS REC'D	DRY	DAF	DMMF(PARR) (14.28 % MM)
% ASH	8.30	12.49		
% CARBON	41.59	62.61	71.55	73.04
% HYDROGEN	*2.93	4.41	5.04	5.14
% NITROGEN	0.55	0.83	0.95	0.97
% SULFUR	0.95	1.43	1.63	
% CHLORINE	0.01	0.02	0.02	0.02
% OXYGEN (DIFF)	*12.09	18.21	20.81	20.83

SULFUR FORMS	% PYRITIC	% SULFATIC	% ORGANIC	% TOTAL
DRY	0.02	0.01	1.40	1.43
DAF	0.02	0.01	1.60	1.63
OPTICAL				

ELEMENTAL ANALYSIS	DRY	DMMF (MOD.P) (14.13 % MM)	DMMF(DIR.) (% MM)
% CARBON	62.44	72.71	
% HYDROGEN	4.25	4.95	
% NITROGEN	0.83	0.97	
% ORGANIC SULFUR	1.40	1.63	
% OXYGEN (DIFF)	16.95	19.73	
% CHLORINE	0.02	0.02	
% MINERAL MATTER (INCLUDES 0.04 % FES2)	14.13		

ATOM RATIOS (DMMF)	PARR	MOD.PAR	DIRECT
ATOMIC H/C	0.846	0.817	
ATOMIC O/C	0.214	0.237	

MISC. CHEMICAL DATA	DRY	OF DMMF COAL	OF DMMF OXYGEN
% O AS COOH			
% O AS OH			
% S AS SO4, IN ASH			
% CARBONATE AS CO2			
% CHLORINE	0.04		

INFRA-RED ANALYSIS

(*)- EXCLUDES MOISTURE

SEAM NAME BEULAH
APPARENT RANK LIGNITE A (LIGA)

COUNTRY U.S.A.
STATE NORTH DAKOTA

CHEMICAL DATA 3

% MOISTURE IN COAL = 21.00
% HIGH TEMPERATURE ASH = 8.68 AT 750 DEGREES C

TRACE ELEMENT ANALYSIS	PPM HTA	PPM TOTAL COAL
AG		
B		
BA	6570	570
BE	7	1
BI		
CE		
CO		
CR	65	6
CU	100	9
GA		
GE		
LA		
LI		
MN	1400	122
MO		
NI	45	4
NB		
PB		
RB	40	3
SC		
SN		
SR	4900	425
TH		
U		
V	85	7
Y		
YB		
ZN	40	3
ZR	190	16

MAJOR ELEMENT ANALYSIS	OXIDE % OF HTA	ELEMENT % OF TOTAL DRY COAL
SI02	19.70	0.80
AL203	9.34	0.43
TI02	0.37	0.02
FE203	12.90	0.78
MG0	5.33	0.28
CA0	23.20	1.44
NA20	5.87	0.38
K20	0.69	0.05
P205	0.34	0.01
S03	20.00	0.69

VOLATILES	PPM TOTAL COAL
AS	
BR	
CD	
CL	
F	
HG	
SB	
SE	

SEAM NAME	BEULAH	COUNTRY	U.S.A.
APPARENT RANK	LIGNITE A (LIGA)	STATE	NORTH DAKOTA

MINERALOGICAL DATA

TOTAL MINERAL MATTER

% MM-PARR	14.28
% MM-MODIFIED PARR	14.13
% MM-KMC	
% MM-DIRECT	
% MM-BEST AVAILABLE	14.13
VOL % MM-PARR	7.43

MINERAL COMPOSITION

NONE

SEAM NAME	BEULAH	COUNTRY	U.S.A.
APPARENT RANK	LIGNITE A (LIGA)	STATE	NORTH DAKOTA

PETROGRAPHIC DATA

PETROGRAPHIC DATA NOT AVILABLE

PHYSICAL PROPERTIES

HARDGROVE GRINDABILITY	
VICKER'S MICROHARDNESS	
FREE SWELLING INDEX	0.0
GRAY KING COKE TYPE	

ASH FUSION ANALYSIS (DEGREES F)	REDUCING	OXIDIZING
INITIAL DEFORMATION TEMPERATURE	2330	2320
SOFTENING TEMPERATURE	2350	2340
HEMISPHERE TEMPERATURE	2360	2370
FLUID TEMPERATURE	2370	2420

ANALYSIS LOG

ANALYSIS	DATE	PERFORMED BY
A.R. MOIST		
EQUIL. MOIST.		
PROXIMATE		
ULTIMATE		
SULFUR FORMS		
FSI	4/29/86	COAL PETROGRAPHY LABORATORIES-PSU
PLASTOMETER		
DIRECT MM		
GRAY-KING		

PSOC-1507D
North Dakota Beulah Zap lignite
75-106 μm Size Fraction,
1250 K Gas Condition in the CDL (100% N_2)

A. Char Sample Analyses

Sampling Height (mm)	0	20	40	70	100	180	250
Residence Time (ms)	0	25	46	74	99	168	233
Mass Release (% daf)*	0.0	9.5	17.0	17.6	30.4	49.4	53.7
90% conf. interval (±)	n.a.	n.a.	n.a.	n.a.	n.a.	n.a.	n.a.

Moisture (mass %)	18.04	2.76	1.81	2.44	2.39	2.01	2.45
C (mass %, daf)	66.56	69.19	64.36	70.91	74.92	79.00	83.04
H	4.26	4.37	3.86	3.70	2.78	2.07	1.87
O	25.16	21.12	25.93	21.29	18.36	12.84	9.94
N	1.12	1.21	1.24	1.34	1.45	1.54	1.48
S	2.89	4.12	4.61	2.77	2.50	4.56	3.67
Ash (mass %, dry)	18.70	20.27	21.70	21.83	24.85	31.25	33.21
SiO2	2.50	2.04	2.47	3.01	4.42	4.64	4.77
K2O	0.42	0.48	0.05	0.25	0.25	0.21	0.20
TiO2	0.03	0.02	0.05	0.04	0.08	0.05	0.07
Fe2O3	8.10	7.81	4.37	8.98	4.66	6.60	6.74
Al2O3	2.50	2.08	1.06	3.00	1.92	1.88	2.00
CaO	7.66	8.09	2.90	11.90	2.99	6.73	5.21
Na2O	1.51	1.49	0.80	1.91	1.06	1.10	1.18
MgO	0.76	0.70	0.24	0.75	1.00	0.18	0.88
Ash2	18.71	18.65	19.44	22.84	25.52	29.66	31.12

*Mass release based on ash content only, due to large scatter in the ICP inorganic analyses of these lignite samples.

B. Mass Balance Data†

m/m_o (as rec'd)	0.75	0.73	0.59	0.53	0.47	0.46
tar/m_o (as rec'd)	0.00	0.01	0.01	0.00	0.01	0.00
m/m_o (normalized)	1.00	0.97	0.78	0.71	0.63	0.62
tar/m_o (normalized)	0.00	0.01	0.02	0.00	0.02	0.00
estimated V(daf)	0	4	34	46	58	61
estimated tar(daf)	0	1	3	0	3	0
tar estimated from tar/char ratio and tracer analysis	0	6	1	0	2	0

†Shown for reference only; tracers were used to determine extent of mass release.

PSOC-1507D (cont.)
North Dakota Beulah Zap lignite
75-106 μm Size Fraction,
1250 K Gas Condition in the CDL (100% N_2)

C. Tap Densities and Apparent Densities of Char Samples

Sampling Height (mm)	0	20	40	70	100	180	250
Residence Time (ms)	0	25	46	74	99	168	233
Mass Release (% dry)	0.00	7.70	13.80	14.30	24.70	40.20	43.70
m/m_o(dry)	1.00	0.92	0.86	0.86	0.75	0.60	0.56
m/m_o(wet)	1.00	0.78	0.72	0.72	0.63	0.50	0.47
Aparent Density $(\rho/\rho_o)^*$	1.00	1.00	0.95	0.83	0.75	0.77	0.77
Diameter Ratio	1.00	0.92	0.91	0.95	0.94	0.87	0.85

*Apparent densities measured using volumetric technique (tap densities)

D. Mercury Porosimetry and BET Analyses of Char Samples

Sampling Height (mm)	0	20	40	70	100	180	250
Residence Time (ms)	0	25	46	74	99	168	233
Mass Release (% daf)	0.0	9.5	17.0	17.6	30.4	49.4	53.7

BET Surface Area (m^2/g)	5.93	4.57	4.25	5.68	29.11	215	225
Standard Deviation	0.18	0.22	0.05	0.19	0.48	5.2	5.3
Langmuir Surface Area	n.a.	n.a.	n.a.	n.a.	n.a.	284	297
Standard Deviation	n.a.	n.a.	n.a.	n.a.	n.a.	1.1	1.3
Cumulative Pore Area (m^2/g)	34.1	41.3	30.1	59.3	37.9	45.4	47.4
Median Pore Diameter (μm)							
By Volume	24.19	25.6	25.52	24.15	22.17	23.06	22.19
By area	0.0046	0.0048	0.0041	0.0053	0.0048	0.0056	0.0052
By 4V/A	0.1047	0.0967	0.1333	0.0894	0.1396	0.13	0.1229
Density, g/cc							
Bulk	0.652	0.61	0.6	0.512	0.514	0.476	0.485
Skeletal	1.561	1.559	1.509	1.597	1.607	1.605	1.652
Porosity (%)	58.2	60.9	60.3	67.9	68	70.3	70.6

PSOC-1507D (cont.)
North Dakota Beulah Zap lignite
75-106 μm Size Fraction,
1250 K Gas Condition in the CDL (100% N_2)

E. NMR Analyses of Char Samples

						Error Estimate
Residence Time (ms)	0	0	74	99	233	± 5
Sampling Distance (mm)	0	0	70	100	250	
Mass Release (% daf)	0	0	18	30	54	± 3
Aromatic carbon, $f_a = f_a' + f_a^C$	.65	.65	.75	.84	.89	± .03
Carbonyl, f_a^C	.08	.08	.07	.04	.04	± .02
Aromatic carbon, carbonyl subtracted, f_a'	.57	.57	.68	.80	.85	± .04
Protonated aromatic carbon, f_a^H	.19	.20	.21	.30	.31	± .03
Non-protonated aromatic C, $f_a^N = f_a^P + f_a^S + f_a^B$	.38	.37	.47	.50	.54	± .03
Aromatic carbon with O attachment, f_a^P	.07	.08	.08	.07	.07	± .02
Aromatic carbon with alkyl attachment, f_a^S	.14	.14	.14	.18	.21	± .03
Aromatic bridgehead and inner carbon, f_a^B	.17	.15	.25	.25	.26	± .04
Aliphatic carbon, f_{al}	.35	.35	.25	.16	.11	± .02
Aliphatic CH and CH_2, f_{al}^H	.24	.26	.16	.12	.08	± .02
Aliphatic CH_3 and non-protonated carbon, f_{al}^*	.11	.09	.09	.04	.03	± .03
Aliphatics with oxygen attachment, f_{al}^O	.11	.10	.09	.10	.06	± .02
Proton spin-relaxation time, $T_{1\rho}^{Har}$ (ms)	7.6	7.5	3.3	3.6	6.2	± 2
Total carbons per cluster	23	21	25	18	17	± 3
Aromatic carbons per cluster, C	14	13	18	15	15	± 3
Aliphatic carbons per cluster	8.5	8.0	6.6	3.0	1.9	± 2
Total attachments per cluster, $\sigma+1$	5.2	5.0	5.8	4.7	4.9	± 1
Bridges and loops per cluster, B_C	2.4	3.0	3.4	4.0	4.4	± 1
Side chains per cluster	2.8	2.0	2.4	0.7	0.5	± 1
Fraction of intact bridges per cluster, p	.48	.59	.59	.84	.89	± .05
Average cluster molecular weight	440	410	450	300	260	± 30
Side chain molecular weight	52	51	40	26	16	± 5

PSOC-1507D (cont.)
North Dakota Beulah Zap lignite
75-106 μm Size Fraction,
1250 K Gas Condition in the CDL (100% N_2)

F. NMR Analyses of Tar Samples

Sampling Height (mm)	0	20	40	70	100	180	250
Residence Time (ms)	0	25	46	74	99	168	233
Mass Release (% daf)	0.0	9.5	17.0	17.6	30.4	49.4	53.7

α-H	n.a.	n.a.	n.a.	20	25	21	21
α-CH_3	n.a.	n.a.	n.a.	7	4	4	3
β– and γ–H	n.a.	n.a.	n.a.	11	8	6	6
γ-CH_3	n.a.	n.a.	n.a.	2	1	1	2
Aromatic H	25*	n.a.	n.a.	60	61	67	70
1-Ring	n.a.	n.a.	n.a.	10	16	16	14
2-Ring	n.a.	n.a.	n.a.	13	19	23	23
3-Ring	n.a.	n.a.	n.a.	21	19	25	25
Aromatic C	57**	n.a.	n.a.	81	88	89	89

*Estimated from the C/H ratio and the carbon aromaticity f_a' of the parent coal
**Estimated as the carbon aromaticity of the parent coal

PSOC-1507D
North Dakota Beulah Zap lignite
75-106 μm Size Fraction,
1250 K Gas Condition in the CDL (100% N_2)
(Duplicate Experiments)

A. Char Sample Analyses

Sampling Height (mm)	0	100	150	250
Residence Time (ms)	0	100	135	233
Mass Release (% daf)*	0.0	30.2	36.6	44.0
90% conf. interval (±)	0.0	8.7	6.8	2.7

Moisture (mass %)	10.87	5.85	5.04	5.35
C (mass %, daf)	67.99	76.27	76.93	79.61
H	4.24	2.67	2.48	2.06
O	24.83	17.59	16.16	13.94
N	0.99	1.29	1.24	1.28
S	1.95	2.19	3.17	3.11
Ash (mass %, dry)	18.40	27.10	28.40	29.90
SiO2	3.24	3.92	4.25	4.92
K2O	0.11	0.14	0.15	0.17
TiO2	0.06	0.07	0.08	0.09
Fe2O3	2.74	6.04	6.61	5.40
Al2O3	1.25	1.66	1.78	1.93
CaO	5.65	6.49	6.28	7.98
Na2O	0.38	1.42	1.08	1.16
MgO	0.65	1.00	1.02	1.34
Ash2	20.15	33.49	32.08	24.02

*mass release based on ash content only, due to large scatter in the ICP inorganic analyses of these lignite samples.

B. Mass Balance Data†

m/m_o (as rec'd)	0.51	0.55	0.56
tar/m_o (as rec'd)	0.02	0.01	0.02
m/m_o (normalized)	0.69	0.73	0.75
tar/m_o (normalized)	0.03	0.02	0.02
estimated V(daf)	44	38	35
estimated tar(daf)	4	3	3
tar estimated from tar/char ratio and tracer analysis	18	5	6

†Shown for reference only; tracers were used to determine extent of mass release.

PSOC-1507D (cont.)
North Dakota Beulah Zap lignite
75-106 μm Size Fraction,
1250 K Gas Condition in the CDL (100% N_2)
(Duplicate Experiments)

C. Tap Densities and Apparent Densities of Char Samples

Sampling Height (mm)	0	100	150	250
Residence Time (ms)	0	100	135	233
Mass Release (% dry)	0.00	32.10	35.20	38.50
m/m_o(dry)	1.00	0.68	0.65	0.62
m/m_o(wet)	1.00	0.64	0.61	0.58
Aparent Density $(\rho/\rho_o)^*$	1.00	0.60	0.62	0.60
Diameter Ratio	1.00	1.02	0.99	0.99

*Apparent densities measured using volumetric technique (tap densities)

D. Mercury Porosimetry and BET Analyses of Char Samples

(not available)

E. NMR Analyses of Char Samples

(not available)

F. NMR Analyses of Tar Samples

(not available)

PSOC-1507D
North Dakota Beulah Zap lignite
75-106 μm Size Fraction,
1050 K Gas Condition in the CDL (100% N_2)

A. Char Sample Analyses

Sampling Height (mm)	0	50	80	100	150	180	250
Residence Time (ms)	0	60	90	109	160	193	278
Mass Release (% daf)*	0.0	0.0	0.0	21.5	47.3	30.4	52.5
90% conf. interval (±)	n.a.	n.a.	n.a.	n.a.	n.a.	n.a.	n.a.

Moisture (mass %)	18.04	4.24	2.44	1.46	0.99	1.86	1.94
C (mass %, daf)	66.56	64.41	64.83	68.70	67.26	69.43	74.60
H	4.26	4.07	3.97	3.41	2.63	2.69	2.77
O	25.16	24.75	24.82	21.70	22.88	21.32	17.62
N	1.12	1.13	1.10	1.20	1.32	1.37	1.36
S	2.89	5.64	5.28	5.00	5.92	5.19	3.65
Ash (mass %, dry)	18.70	18.78	18.43	22.67	30.38	24.85	32.61
SiO2	2.50	1.65	2.09	2.36	3.13	2.34	4.31
K2O	0.42	0.26	1.03	0.49	0.29	0.11	0.28
TiO2	0.03	0.03	0.04	0.03	0.02	0.04	0.04
Fe2O3	8.10	4.48	5.78	9.51	6.99	2.35	5.75
Al2O3	2.50	0.70	0.88	2.56	1.31	0.97	1.72
CaO	7.66	2.74	3.36	10.10	6.29	2.02	5.19
Na2O	1.51	0.55	0.56	1.82	0.99	0.39	1.21
MgO	0.76	0.07	0.11	1.10	0.48	0.16	0.78
Ash2	18.71	16.53	20.75	20.89	24.45	24.32	27.02

*mass release based on ash content only, due to large scatter in the ICP inorganic analyses of these lignite samples.

B. Mass Balance Data†

m/m_0 (as rec'd)	0.58	0.44	0.55	0.59	0.52	0.52
tar/m_0 (as rec'd)	0.00	0.01	0.00	0.06	0.04	0.02
m/m_0 (normalized)	0.77	0.59	0.74	0.78	0.70	0.69
tar/m_0 (normalized)	0.00	0.01	0.00	0.08	0.05	0.03
estimated V(daf)	36	65	41	34	48	48
estimated tar(daf)	0	2	0	13	7	5
tar estimated from tar/char ratio and tracer analysis	0	0	0	18	5	6

†Shown for reference only; tracers were used to determine extent of mass release.

PSOC-1507D (cont.)
North Dakota Beulah Zap lignite
75-106 μm Size Fraction,
1050 K Gas Condition in the CDL (100% N_2)

C. Tap Densities and Apparent Densities of Char Samples

Sampling Height (mm)	0	50	80	100	150	180	250
Residence Time (ms)	0	60	90	109	160	193	278
Mass Release (% dry)	0.00	0.00	0.00	17.50	38.40	24.70	42.70
m/m_o(dry)	1.00	1.00	1.00	0.83	0.62	0.75	0.57
m/m_o(wet)	1.00	0.86	0.84	0.69	0.51	0.63	0.48
Aparent Density $(\rho/\rho_o)^*$	1.00	1.04	0.96	0.89	0.83	0.82	0.84
Diameter Ratio	1.00	0.94	0.96	0.92	0.85	0.92	0.83

*Apparent densities measured using volumetric technique (tap densities)

D. Mercury Porosimetry and BET Analyses of Char Samples

(not available)

E. NMR Analyses of Char Samples

(not available)

PSOC-1507D (cont.)
North Dakota Beulah Zap lignite
75-106 μm Size Fraction,
1050 K Gas Condition in the CDL (100% N_2)

F. NMR Analyses of Tar Samples

Sampling Height (mm)	0	50	80	100	150	180	250
Residence Time (ms)	0	60	90	109	160	193	278
Mass Release (% daf)	0.0	0.0	0.0	21.5	47.3	30.4	52.5

α-H	n.a.	n.a.	n.a.	n.a.	21	20	23
α-CH_3	n.a.	n.a.	n.a.	n.a.	8	10	8
β– and γ–H	n.a.	n.a.	n.a.	n.a.	37	33	26
γ-CH_3	n.a.	n.a.	n.a.	n.a.	6	6	5
Aromatic H	25*	n.a.	n.a.	n.a.	33	34	42
1-Ring	n.a.	n.a.	n.a.	n.a.	9	12	8
2-Ring	n.a.	n.a.	n.a.	n.a.	7	8	10
3-Ring	n.a.	n.a.	n.a.	n.a.	8	8	15
Aromatic C	57**	n.a.	n.a.	n.a.	64	65	70

*Estimated from the C/H ratio and the carbon aromaticity f_a' of the parent coal
**Estimated as the carbon aromaticity of the parent coal

PSOC-1507D
North Dakota Beulah Zap lignite
75-106 μm Size Fraction,
1050 K Gas Condition in the CDL (100% N_2)
(Duplicate Experiments)

A. Char Sample Analyses

Sampling Height (mm)	0	150	180	250
Residence Time (ms)	0	160	193	278
Mass Release (% daf)*	0.0	29.0	37.8	30.5
90% conf. interval (±)				

Moisture (mass %)	10.87	6.29	5.48	5.96
C (mass %, daf)	67.99	72.79	71.39	73.32
H	4.24	3.15	2.98	3.17
O	24.83	19.58	19.79	19.11
N	0.99	1.16	1.11	1.21
S	1.95	3.32	4.73	3.19
Ash (mass %, dry)	18.40	24.10	26.60	24.50
SiO2	3.24	3.29	3.57	3.79
K2O	0.11	0.11	0.12	0.13
TiO2	0.06	0.06	0.07	0.07
Fe2O3	2.74	4.84	6.68	4.72
Al2O3	1.25	1.35	1.44	1.61
CaO	5.65	6.51	5.87	6.63
Na2O	0.38	0.54	0.23	0.69
MgO	0.65	0.90	0.72	1.11
Ash2	20.15	22.62	26.62	26.71

*mass release based on ash content only, due to large scatter in the ICP inorganic analyses of these lignite samples.

B. Mass Balance Data†

m/m_o (as rec'd)	0.51	0.55	0.56
tar/m_o (as rec'd)	0.02	0.01	0.02
m/m_o (normalized)	0.69	0.73	0.75
tar/m_o (normalized)	0.03	0.02	0.02
estimated V(daf)	45	39	35
estimated tar(daf)	4	3	3
tar estimated from tar/char ratio and tracer analysis	2	3	3

†Shown for reference only; tracers were used to determine extent of mass release.

PSOC-1507D (cont.)
North Dakota Beulah Zap lignite
75-106 μm Size Fraction,
1050 K Gas Condition in the CDL (100% N_2)
(Duplicate Experiments)

C. Tap Densities and Apparent Densities of Char Samples

Sampling Height (mm)	0	150	180	250
Residence Time (ms)	0	160	193	278
Mass Release (% dry)	0.00	23.70	30.80	24.90
m/m_o(dry)	1.00	0.76	0.69	0.75
m/m_o(wet)	1.00	0.73	0.65	0.71
Aparent Density (ρ/ρ_o)*	1.00	0.82	0.81	0.80
Diameter Ratio	1.00	0.96	0.93	0.96

*Apparent densities measured using volumetric technique (tap densities)

D. Mercury Porosimetry and BET Analyses of Char Samples

(not available)

E. NMR Analyses of Char Samples

(not available)

F. NMR Analyses of Tar Samples

(not available)

APPENDIX H

Data Summary:

PSOC-1508D

West Virginia Pocahontas #3

lvb bituminous

SAMPLE HISTORY

PENN STATE NUMBER	PSOC-1508
COLLECTED BY	PENNSYLVANIA STATE UNIVERSITY
COLLECTION DATE	11/5/85
COLLECTOR'S NUMBER	
REPORTED RANK	LOW VOLATILE BITUMINOUS (LVB)
SAMPLE TYPE	CHANNEL WHOLE SEAM
OTHER SAMPLE INFORMATION	
SAMPLE RESERVE	
SEAM NAME	POCAHONTAS #3
ALTERNATE SEAM NAME	
TOTAL SEAM THICKNESS	4 FT. 11 IN.
THICKNESS OF SEAM SAMPLED	4 FT. 11 IN.
PORTION RECOVERED IN CORE	
DIAMETER OF CORE	

SAMPLE LOCATION

COUNTRY	U.S.A.
STATE	WEST VIRGINIA
COUNTY	MCDOWELL
TOWNSHIP	
NEAREST TOWN	WELCH
COAL PROVINCE	EASTERN
COAL REGION	APPALACHIAN
COAL FIELD	SOUTHERN

SEAM NAME	POCAHONTAS #3	COUNTRY	U.S.A.
APPARENT RANK	LOW VOLATILE BITUMINOUS (LVB)	STATE	WEST VIRGINIA

GEOLOGIC INFORMATION

SYSTEM (AGE)	PENNSYLVANIAN
SERIES	
GROUP	POTTSVILLE
FORMATION	POCAHONTAS
OVERBURDEN LITHOLOGY	SILTY SHALE
FLOOR LITHOLOGY	SILTY SHALE

SEAM STRATA INFORMATION

THICKNESS	LITHOTYPE

SEAM NAME	POCAHONTAS #3	COUNTRY	U.S.A.
APPARENT RANK	LOW VOLATILE BITUMINOUS (LVB)	STATE	WEST VIRGINIA

CHEMICAL DATA 1

PROXIMATE ANALYSIS	AS REC'D	DRY	DAF	DMMF (PAFF)	DMMF (PARR-G)	DMMF (DIR MM)
% MOISTURE	1.14					
% ASH	7.36	7.44				
% VOLATILE MATTER	15.52	15.70	16.96	16.21	15.96	
% FIXED CARBON	75.98	76.86	83.04	83.79	84.04	

CALORIFIC VALUE (GROSS BTU/LB)	DRY	AS REC'D MOIST.	EQUIL MOIST.
MM-FREE, DIRECT	14542	14376	14145
MM-CONTAINING	15838	15642	15368
MM-FREE (PARR)	15885	15658	15383
MM-FREE (MOD.P)		15685	15383
BEST MM FREE	15474		
NET CV, DMMF BTU/LB	15711		
ASH-FREE			

MOTT-SPOONER DIFFERENCE =

ASSOCIATED ANALYSES	DRY	MMF
% EQUILIBRIUM MOISTURE	2.73	2.98
% TOTAL SULFUR	0.64	

RANK CALCULATIONS

APPARENT RANK (AS REC'D MOIST)	LOW VOLATILE BITUMINOUS (LVB)
ASTM RANK (EQUIL. MOIST.)	LOW VOLATILE BITUMINOUS (LVB)
REFLECTANCE RANK CATEGORY	LOW VOLATILE BITUMINOUS (LVB)
INTERNATIONAL RANK	
AS REC'D MOIST.	
EQUIL. MOIST	LOW VOLATILE BITUMINOUS (LVB)
REPORTED RANK	

SEAM NAME POCAHONTAS #3
APPARENT RANK LOW VOLATILE BITUMINOUE (LVB)

COUNTRY U.S.A.
STATE WEST VIRGINIA

CHEMICAL DATA 2

ULTIMATE ANALYSIS	AS REC'D	DRY	DAF	DMMF(PARR) (8.39 % MM)
% ASH	7.36	7.44		
% CARBON	83.70	84.67	91.48	92.42
% HYDROGEN	*4.00	4.05	4.38	4.42
% NITROGEN	1.01	1.02	1.10	1.11
% SULFUR	0.63	0.64	0.69	
% CHLORINE	0.05	0.05	0.06	0.06
% OXYGEN (DIFF)	*2.10	2.13	2.30	1.99

SULFUR FORMS	% PYRITIC	% SULFATIC	% ORGANIC	% TOTAL
DRY	0.14	0.00	0.50	0.64
DAF	0.15	0.00	0.54	0.69
OPTICAL				

ELEMENTAL ANALYSIS	DRY	DMMF (MOD.P) (8.50 % MM)	DMMF(DIR.) (% MM)
% CARBON	84.50	92.35	
% HYDROGEN	3.95	4.32	
% NITROGEN	1.02	1.11	
% ORGANIC SULFUR	0.50	0.55	
% OXYGEN (DIFF)	1.53	1.62	
% CHLORINE	0.05	0.06	
% MINERAL MATTER (INCLUDES 0.26 % FES2)	8.50		

ATOM RATIOS (DMMF)	PARR	MOD.PAR	DIRECT
ATOMIC H/C	0.575	0.562	
ATOMIC O/C	0.016	0.014	

MISC. CHEMICAL DATA	DRY	OF DMMF COAL	OF DMMF OXYGEN
% O AS COOH			
% O AS OH			
% S AS SO4, IN ASH			
% CARBONATE AS CO2	0.62		
% CHLORINE	0.11		

INFRA-RED ANALYSIS

(*)- EXCLUDES MOISTURE

SEAM NAME POCAHONTAS #3
APPARENT RANK LOW VOLATILE BITUMINOUS (LVB)
COUNTRY U.S.A.
STATE WEST VIRGINIA

CHEMICAL DATA 3

% MOISTURE IN COAL = 0.22
% HIGH TEMPERATURE ASH = 7.63 AT 750 DEGREES C

TRACE ELEMENT ANALYSIS	PPM HTA	PPM TOTAL COAL
AG		
B		
BA	1800	137
BE	29	2
BI		
CE		
CO		
CR	170	13
CU	230	18
GA		
GE		
LA		
LI		
MN	340	26
MO		
NI	160	12
NB		
PB		
RB	25	2
SC		
SN		
SR	1350	103
TH		
U		
V	210	16
Y		
YB		
ZN	50	4
ZR	400	31

MAJOR ELEMENT ANALYSIS	OXIDE % OF HTA	ELEMENT % OF TOTAL DRY COAL
SI02	46.50	1.66
AL203	24.40	0.99
TI02	1.76	0.08
FE203	8.29	0.44
MG0	1.31	0.06
CA0	7.38	0.40
NA20	1.12	0.06
K20	0.53	0.03
P205	0.32	0.01
S03	8.40	0.26

VOLATILES	PPM TOTAL COAL
AS	
BR	
CD	
CL	
F	
HG	
SB	
SE	

SEAM NAME	POCAHONTAS #3	COUNTRY	U.S.A.
APPARENT RANK	LOW VOLATILE BITUMINOUS (LVB)	STATE	WEST VIRGINIA

MINERALOGICAL DATA

TOTAL MINERAL MATTER

% MM-PARR	8.39
% MM-MODIFIED PARR	8.50
% MM-KMC	
% MM-DIRECT	
% MM-BEST AVAILABLE	8.50
VOL % MM-PARR	4.23

MINERAL COMPOSITION

NONE

SEAM NAME	POCAHONTAS #3	COUNTRY	U.S.A.
APPARENT RANK	LOW VOLATILE BITUMINOUS (LVB)	STATE	WEST VIRGINIA

PETROGRAPHIC DATA

MACERAL COMPOSITION WHITE ANALYSIS ONLY

	DRY VOLUME %	DMMF VOLUME %	DRY WEIGHT %
VITRINITE (CALC.)	74.9	78.2	71.7
INERTINITE (CALC.)	20.9	21.8	20.0
LIPTINITE (CALC.)		0.0	0.0
MINERAL MATTER (CALC.)	4.2		8.4
VITRINOIDS			
VITRINITE	72.2	75.4	69.1
PSEUDOVITRINITE	2.7	2.8	2.6
FUSINITE	5.5	5.7	5.2
SEMI-FUSINITE	11.1	11.6	10.6
MACRINITE	1.0	1.0	0.9
MICRINITE	3.4	3.5	3.2
SCLEROTINITE	0.0	0.0	0.0
SPORINITE	0.0	0.0	0.0
CUTINITE	0.0	0.0	0.0
EXINITE (ANAL.)			
RESINITE	0.0	0.0	0.0
SUBERINITE			
EXUDATINITE			
FLUORINITE			
BITUMINITE			
ALGINITE	0.0	0.0	0.0
LIPTODETRINITE			
MINERAL MATTER (ANAL.)			
INERTINITE (ANAL.)			
LIPTINITE (ANAL.)			

REFLECTANCE DATA	HIGH	LOW	RANGE	MEAN MAX	STAND.DEV.
(%, IN OIL)					
VITRINITE	1.97	1.71	0.26	1.85	0.05
PSEUDOVITRINITE					
VITRINOIDS					

SEAM NAME POCAHONTAS #3 COUNTRY U.S.A.
APPARENT RANK LOW VOLATILE BITUMINOUS (LVB) STATE WEST VIRGINIA

PETROGRAPHIC DATA

CONTINUED

% VITRINOID REFLECTANCE	HALF-TYPE	VOLUME PERCENT	% VITRINOID REFLECTANCE	V-TYPE	VOLUME PERCENT
1.70-1.74	VHT 1.725	3.00			
1.75-1.79	VHT 1.775	13.00	1.70-1.79	V17	16.00
1.80-1.84	VHT 1.825	32.00			
1.85-1.89	VHT 1.875	37.00	1.80-1.99	V18	69.00
1.90-1.94	VHT 1.925	13.00			
1.95-1.99	VHT 1.975	2.00	1.90-1.99	V19	15.00

PHYSICAL PROPERTIES

HARDGROVE GRINDABILITY	
VICKER'S MICROHARDNESS	
FREE SWELLING INDEX	6.5
GRAY KING COKE TYPE	

GIESELER PLASTICITY DATA

MAXIMUM FLUIDITY	10
MAXIMUM FLUIDITY TEMPERATURE	486
INITIAL SOFTENING TEMPERATURE	460
SOLIDIFICATION TEMPERATURE	504
FLUID TEMPERATURE RANGE	44
PLASTOMETER TYPE	GEISELER - PSU

ASH FUSION ANALYSIS (DEGREES F)	REDUCING	OXIDIZING
INITIAL DEFORMATION TEMPERATURE	2290	2380
SOFTENING TEMPERATURE	2375	2455
HEMISPHERE TEMPERATURE	2470	2495
FLUID TEMPERATURE	2530	2570

SEAM NAME	POCAHONTAS #3	COUNTRY	U.S.A.
APPARENT RANK	LOW VOLATILE BITUMINOUS (LVB)	STATE	WEST VIRGINIA

ANALYSIS LOG

ANALYSIS	DATE	PERFORMED BY
A.R. MOIST	12/23/85	WARNER LABORATORIES
EQUIL. MOIST.	12/23/85	WARNER LABORATORIES
PROXIMATE	12/23/85	WARNER LABORATORIES
ULTIMATE	12/23/85	WARNER LABORATORIES
SULFUR FORMS	12/23/85	WARNER LABORATORIES
FSI	12/5/85	COAL PETROGRAPHY LABORATORIES-PSU
PLASTOMETER	12/7/85	COAL PETROGRAPHY LBAORATORIES-
PSUDIRECT MM		
GRAY-KING		

PSOC-1508D
West Virginia Pocahontas #3 lvb Bituminous Coal
106-125 μm Size Fraction,
1250 K Gas Condition in the CDL (100% N_2)

A. Char Sample Analyses

Sampling Height (mm)	0	20	40	70	100	150	250
Residence Time (ms)	0	25	47	74	100	142	239
Mass Release (% daf)*	0.0	0.0	0.0	8.0	6.1	12.7	16.1
90% conf. interval (±)	n.a.	n.a.	n.a.	n.a.	n.a.	n.a.	n.a.

Moisture (mass %)	0.70	0.60	0.59	0.65	0.73	0.97	1.12
C (mass %, daf)	88.83	89.10	89.45	89.03	90.51	91.22	91.89
H	4.37	4.38	4.27	4.15	3.92	3.55	3.21
O	5.14	4.94	4.69	5.31	4.05	3.75	3.45
N	1.06	1.03	1.03	0.99	1.00	0.97	0.99
S	0.60	0.55	0.56	0.53	0.52	0.50	0.47
Ash (mass %, dry)	16.72	15.95	15.80	15.51	15.43	18.42	17.97
SiO2	8.48	8.04	8.10	7.11	8.13	9.73	8.76
K2O	0.07	0.07	0.07	0.06	0.07	0.08	0.09
TiO2	0.31	0.28	0.28	0.27	0.28	0.08	0.30
Fe2O3	0.95	0.87	0.88	0.86	0.89	1.06	0.95
Al2O3	3.83	3.59	3.73	3.59	3.71	4.40	3.97
CaO	1.29	2.36	0.68	0.89	1.78	1.16	1.81
Na2O	0.12	0.14	0.14	0.15	0.16	0.16	0.16
MgO	0.30	0.39	0.11	0.17	0.32	0.16	0.26
Ash2	16.72	15.59	16.49	14.32	15.08	18.77	18.14

*The ASTM ashing temperature was not adequate to fully oxidize all of the char samples for this low volatile coal, which is very non-reactive. The extent of mass release determined from mineral tracers was therefore suspect. The extent of mass release shown here was determined from a mass balance (±5% daf for this low volatile coal).

B. Mass Balance Data

m/m_o (as rec'd)	0.91	0.94	0.87	0.88	0.83	0.81
tar/m_o (as rec'd)	0.00	0.01	0.06	0.05	0.07	0.05
m/m_o (normalized)	0.98	1.01	0.93	0.95	0.89	0.87
tar/m_o (normalized)	0.00	0.01	0.06	0.05	0.07	0.05
estimated V(daf)	2	-1	8	6	13	16
estimated tar(daf)	1	1	8	6	8	6
tar estimated from tar/char ratio and tracer analysis	0	0	8	6	8	6

PSOC-1508D (cont.)
West Virginia Pocahontas #3 lvb Bituminous Coal
106-125 μm Size Fraction,
1250 K Gas Condition in the CDL (100% N_2)

C. Tap Densities and Apparent Densities of Char Samples

Sampling Height (mm)	0	20	40	70	100	150	250
Residence Time (ms)	0	25	47	74	100	142	239
Mass Release (% dry)	0	0	0	6.3	5.1	13.6	13.4
m/m_o(dry)	1	1.00	1.00	0.94	0.95	0.86	0.87
m/m_o(wet)	1	1.00	1.00	0.94	0.95	0.87	0.87
Aparent Density (ρ/ρ_o)*	1	0.88	0.71	0.51	0.63	0.38	0.48
Diameter Ratio	1	1.04	1.12	1.22	1.15	1.32	1.22

*Apparent densities measured using volumetric technique (tap densities)

D. Mercury Porosimetry and BET Analyses of Char Samples

(not available)

PSOC-1508D (cont.)
West Virginia Pocahontas #3 lvb Bituminous Coal
106-125 μm Size Fraction,
1250 K Gas Condition in the CDL (100% N_2)

E. NMR Analyses of Char Samples

Sampling Distance (mm)	0	100	250
Residence Time (ms)	0	100	239
Mass Release (% daf)	0.0	6.1	16.1
Aromatic carbon, $f_a = f_a' + f_a^C$	.78	.81	.88
Carbonyl, f_a^C	.01	.02	.00
Aromatic carbon, carbonyl subtracted, f_a'	.77	.79	.88
Protonated aromatic carbon, f_a^H	.32	.36	.44
Non-protonated aromatic C, $f_a^N = f_a^P + f_a^S + f_a^B$	.45	.43	.44
Aromatic carbon with O attachment, f_a^P	.02	.03	.02
Aromatic carbon with alkyl attachment, f_a^S	.15	.14	.14
Aromatic bridgehead and inner carbon, f_a^B	.28	.26	.28
Aliphatic carbon, f_{al}	.22	.19	.12
Aliphatic CH and CH_2, f_{al}^H	.15	.13	.08
Aliphatic CH_3 and non-protonated carbon, f_{al}^*	.07	.06	.04
Aliphatics with oxygen attachment, f_{al}^O	.07	.06	.04
Proton spin-relaxation time, $T_{1\rho}^{Har}$ (ms)	4.3	5.2	9.3
Total carbons per cluster	23	20	18
Aromatic carbons per cluster, C	18	16	16
Aliphatic carbons per cluster	5	6	2
Total attachments per cluster, $\sigma+1$	4.0	3.5	2.9
Bridges and loops per cluster, B_C	2.3	2.3	2.2
Side chains per cluster	1.7	1.2	0.7
Fraction of intact bridges per cluster, p	.59	.65	.75
Average cluster molecular weight	316	269	238
Side chain molecular weight	23	20	13

F. NMR Analyses of Tar Samples

(not available, due to small amount of tars from this low volatile coal)

PSOC-1508D
West Virginia Pocahontas #3 lvb Bituminous Coal
106-125 μm Size Fraction,
1050 K Gas Condition in the CDL (100% N_2)

A. Char Sample Analyses

Sampling Height (mm)	0	50	80	120	150	180	250
Residence Time (ms)	0	60	89	127	155	185	269
Mass Release (% daf)*	0.0	0.0	0.0	0.0	3.0	5.3	6.6
90% conf. interval (±)	n.a.	n.a.	n.a.	n.a.	n.a.	n.a.	n.a.

Moisture (mass %)	0.70	0.51	0.56	0.69	0.65	0.72	0.60
C (mass %, daf)	88.83	88.56	87.66	88.78	90.06	90.29	89.24
H	4.37	4.39	4.30	4.34	4.34	4.31	4.12
O	5.14	5.41	6.49	5.32	4.06	3.76	5.04
N	1.06	1.04	0.98	0.98	1.01	1.06	1.01
S	0.60	0.60	0.58	0.57	0.53	0.58	0.59
Ash (mass %, dry)	16.72	17.67	15.76	16.05	15.07	14.73	18.88
SiO2	8.48	9.25	7.94	7.96	7.63	7.54	9.94
K2O	0.07	0.08	0.08	0.07	0.04	0.06	0.09
TiO2	0.31	0.31	0.28	0.28	0.27	0.26	0.34
Fe2O3	0.95	0.99	0.81	0.86	0.82	0.82	1.04
Al2O3	3.83	3.94	3.61	3.59	3.55	3.56	4.29
CaO	1.29	1.20	0.74	0.91	0.77	0.67	1.15
Na2O	0.12	0.14	0.13	0.13	0.13	0.12	0.14
MgO	0.30	0.17	0.12	0.13	0.14	0.14	0.16
Ash2	16.72	19.08	15.72	16.12	15.95	12.90	17.41

*The ASTM ashing temperature was not adequate to fully oxidize all of the char samples for this low volatile coal, which is very non-reactive. The extent of mass release determined from mineral tracers was therefore suspect. The extent of mass release shown here was determined from a mass balance (±5% daf for this low volatile coal).

B. Mass Balance Data

m/m_o (as rec'd)	0.95	0.92	0.96	0.91	0.89	0.88
tar/m_o (as rec'd)	0.01	0.01	0.01	0.02	0.04	0.04
m/m_o (normalized)	1.02	0.98	1.03	0.98	0.96	0.95
tar/m_o (normalized)	0.01	0.01	0.01	0.02	0.04	0.05
estimated V(daf)	-3	2	-4	3	5	7
estimated tar(daf)	2	1	1	3	5	6
tar estimated from tar/char ratio and tracer analysis	0	0	0	3	5	6

PSOC-1508D (cont.)
West Virginia Pocahontas #3 lvb Bituminous Coal
106-125 μm Size Fraction,
1050 K Gas Condition in the CDL (100% N_2)

C. Tap Densities and Apparent Densities of Char Samples

Sampling Height (mm)	0	50	80	120	150	180	250
Residence Time (ms)	0	60	89	127	155	185	269
Mass Release (% dry)	0	0	1.6	0	2.50	4.40	5.50
m/m_o(dry)	1.00	1.00	0.98	1.00	0.98	0.96	0.95
m/m_o(wet)	1.00	1.00	0.98	1.00	0.97	0.96	0.94
Aparent Density (ρ/ρ_o)*	1.00	1.00	0.84	0.57	0.40	0.33	0.48
Diameter Ratio	1.00	1.00	1.05	1.21	1.35	1.42	1.25

*Apparent densities measured using volumetric technique (tap densities)

D. Mercury Porosimetry and BET Analyses of Char Samples

(not available)

PSOC-1508D (cont.)
West Virginia Pocahontas #3 lvb Bituminous Coal
106-125 μm Size Fraction,
1050 K Gas Condition in the CDL (100% N_2)

E. NMR Analyses of Char Samples

Sampling Distance (mm)	0	120	250
Residence Time (ms)	0	127	269
Mass Release (% daf)	0.0	0.0	6.6
Aromatic carbon, $f_a = f_a' + f_a^C$	0.78	0.77	0.80
Carbonyl, f_a^C	0.01	0.01	0.01
Aromatic carbon, carbonyl subtracted, f_a'	0.77	0.76	0.79
Protonated aromatic carbon, f_a^H	0.32	0.31	0.36
Non-protonated aromatic C, $f_a^N = f_a^P + f_a^S + f_a^B$	0.45	0.45	0.43
Aromatic carbon with O attachment, f_a^P	0.02	0.03	0.04
Aromatic carbon with alkyl attachment, f_a^S	0.15	0.17	0.15
Aromatic bridgehead and inner carbon, f_a^B	0.28	0.25	0.24
Aliphatic carbon, f_{al}	0.22	0.23	0.20
Aliphatic CH and CH_2, f_{al}^H	0.15	0.15	0.14
Aliphatic CH_3 and non-protonated carbon, f_{al}^*	0.07	0.08	0.06
Aliphatics with oxygen attachment, f_{al}^O	0.07	0.07	0.07
Proton spin-relaxation time, $T_{1\rho}^{Har}$ (ms)	4.3	3.8	2.9
Total carbons per cluster	23	22	19
Aromatic carbons per cluster, C	18	16	15
Aliphatic carbons per cluster	5	6	4
Total attachments per cluster, $\sigma+1$	4.0	4.2	3.6
Bridges and loops per cluster, B_C	2.3	2.5	2.5
Side chains per cluster	1.7	1.7	1.1
Fraction of intact bridges per cluster, p	0.59	0.60	0.68
Average cluster molecular weight	316	285	256
Side chain molecular weight	23	20	19

F. NMR Analyses of Tar Samples

(not available, due to small amount of tars from this low volatile coal)

APPENDIX I

Char Sample Analyses from Devolatilization Experiments in the Char Combustion Laboratory with 0% post-flame O2

Results of Devolatilization Experiments in the CCL
0% Post-Flame O_2
(Sampling height = 6.4 cm above the burner, or 47 ms)

A. Char Sample Analyses

PSOC-	1445D (Blue #1)[1]		1451D (Pittsburgh #8)[1]		1493D (Illinois #6)[1]		1507D (Beulah Zap)[2]		1508D (Pocahontas #3)[3]	
	coal	char	coal	char	coal	char	coal	char	coal	char
Mass Release (% daf)	0.0	56.2	0.0	52.2	0.0	58.3	0.0	58.6	0.0	17.4
Moisture (mass %)	0.87	0.87	0.94	0.45	0.59	0.35	1.65	1.18	0.29	0.31
C (mass %, daf)	74.90	79.41	82.55	90.47	71.22	80.98	61.21	71.39	88.50	90.20
H	5.53	3.78	5.53	2.30	4.92	3.19	4.20	2.16	4.41	3.41
O	17.58	14.55	9.19	4.78	14.42	10.12	29.08	16.82	5.41	4.61
N	1.34	1.63	1.74	1.77	1.43	1.65	0.89	1.16	1.09	1.15
S	0.65	0.63	0.99	0.68	8.01	4.06	4.62	8.47	0.59	0.63
Ash (mass %, dry)	2.96	6.49	3.73	8.18	10.70	20.00	17.40	33.70	16.10	20.25
SiO_2	1.44	3.19	1.94	4.04	3.59	8.28	2.34	5.52	8.37	10.75
Al_2O_3	0.72	1.54	1.06	2.15	1.36	3.07	0.90	1.96	3.78	4.55
Fe_2O_3	0.24	0.51	0.30	0.60	4.08	5.81	3.10	6.93	0.90	1.17
TiO_2	0.037	0.083	0.060	0.110	0.081	0.168	0.036	0.073	0.243	0.294
MgO	0.051	0.084	0.030	0.067	0.083	0.185	0.554	0.949	0.229	0.297
Na_2O	0.011	0.028	0.020	0.040	0.049	0.059	0.570	0.993	0.176	0.221
CaO	0.164	0.358	0.120	0.199	0.541	0.804	5.01	7.30	1.18	1.64
K_2O	0.005	0.007	0.042	0.095	0.117	0.267	0.040	0.112	0.045	0.067

[1]Mass release based on Si, Ti, and Al as tracers.
[2]Mass release based on ash as a tracer, due to large variance in elemental ash composition.
[3]Mass release based on mass balance, due to large variance in inorganic analyses.

Results of Devolatilization Experiments in the CCL
0% Post-Flame O_2
(Sampling height = 6.4 cm above the burner, or 47 ms)

B. Tap Densities and Apparent Densities of Char Samples

PSOC-	1445D (Blue #1)		1451D (Pittsburgh #8)		1493D (Illinois #6)		1507D (Beulah Zap)		1508D (Pocahontas #3)	
	coal	char	coal	char	coal	char	coal	char	coal	char
Mass Release (% daf)	0.0	56.2	0.0	52.2	0.0	58.3	0.0	58.6	0.0	17.4
m/m_o(wet)	0.0	0.45	0.0	0.50	0.0	0.48	0.0	0.51	0.0	0.85
Aparent Density $(\rho/\rho_o)^*$	1.0	0.328	1.0	0.392	1.0	0.350	1.0	0.713	1.0	0.574
Diameter Ratio	1.0	1.11	1.0	1.08	1.0	1.11	1.0	0.90	1.0	1.14
BET Surface Area $(m^2/g)^{**}$	7.8	2.8	1.7	3.5	9.4	4.3	1.9	165	1.7	4.4

*Apparent densities measured using volumetric technique (tap densities)
**Internal surface areas measured using nitrogen adsorption, performed by Coors Analytical Laboratories.

Results of Devolatilization Experiments in the CCL
0% Post-Flame O_2
(Sampling height = 6.4 cm above the burner, or 47 ms)

C. NMR Analyses of Char Samples

PSOC-	1445D (Blue #1)		1451D (Pittsburgh #8)		1493D (Illinois #6)		1507D (Beulah Zap)		1508D (Pocahontas #3)	
	coal	char	coal	char	coal	char	coal	char	coal	char
Mass Release (% daf)	0.0	56.2	0.0	52.2	0.0	58.3	0.0	58.6	0.0	17.4
Arom. C, $f_a = f_a' + f_a^C$	0.60	0.75	0.65	0.86	0.66	0.77	0.64	0.80	0.81	0.85
Carbonyl, f_a^C	0.05	0.05	0.03	0.06	0.03	0.04	0.09	0.12	0.00	0.02
Arom. C w/o carbonyl, f_a'	0.55	0.70	0.62	0.80	0.63	0.73	0.55	0.68	0.81	0.83
Protonated arom. C, f_a^H	0.19	0.26	0.23	0.38	0.21	0.32	0.20	0.24	0.33	0.40
Non-protonated arom. C	0.36	0.44	0.39	0.42	0.42	0.41	0.35	0.44	0.48	0.43
Arom. C w/ O attach.	0.08	0.06	0.05	0.06	0.07	0.05	0.08	0.07	0.03	0.04
Arom. C w/ alkyl attach.	0.13	0.14	0.16	0.14	0.16	0.18	0.14	0.18	0.17	0.15
Arom. bridgehead C, f_a^B	0.15	0.24	0.18	0.22	0.19	0.18	0.13	0.19	0.28	0.24
Aliph. C, f_{al}	0.40	0.25	0.35	0.14	0.34	0.23	0.36	0.20	0.19	0.15
Aliph. CH & CH_2	0.29	0.17	0.24	0.11	0.24	0.17	0.27	0.14	0.13	0.11
Aliph. CH_3 & non-pro. C	0.11	0.08	0.11	0.03	0.10	0.06	0.09	0.06	0.06	0.04
Aliphatics w/ O attach.	0.07	0.09	0.07	0.06	0.08	0.11	0.11	0.11	0.02	0.06
Total C per clust.	24	24	23	16	24	16	20	19	21	17
Arom. C per clust., C	13	17	14	13	15	12	11	13	17	14
Aliph. carbons per clust.	11	7	9	3	9	4	9	6	4	3
Total attach. per clust., $\sigma+1$	5.0	4.9	4.8	3.2	5.5	3.8	4.4	4.8	4.2	3.2
Bridges & loops/clust., B_C	2.4	2.9	2.3	2.7	2.9	2.8	2.6	3.6	2.9	2.2
Side chains per cluster	2.6	2.0	2.5	0.5	2.6	1.0	1.8	1.2	1.3	1.0
Intact bridges/clust., p	0.48	0.60	0.48	0.85	0.52	0.74	0.59	0.76	0.70	0.68
Average clust. mol. wt.	384	367	329	216	402	244	392	322	285	225
Side chain molecular weight	45	32	33	17	39	25	58	34	18	16

INITIAL DISTRIBUTION

Ms. Kay Downey (2)
MS 58-M217
U.S. DOE/PETC
P.O. Box 10940
Pittsburgh, PA 15236-0940

Mr. James M. Ekmann
Director, Coal Combustion Division
U.S. DOE/PETC
P.O. Box 10940, MS 84-307
Pittsburgh, PA 15241

Mr. Charles Garrett
Office of Technical Coordination
U.S. DOE/GTN
FE 14, Room B-107
Washington, DC 20545

Mr. Philip M. Goldberg (2)
Coal Utilization Division
U.S. DOE/PETC, 922-H
P.O. Box 10940
Pittsburgh, PA 15236-0940

Mr. James Hickerson
Coal Utilization Division
U.S.DOE/PETC, 922-H
P.O. Box 10940
Pittsburgh, PA 15236-0940

Mr. James Jovanovich
PM-01, MS922-206
U.S. DOE/PETC, 922-H
P.O. Box 10940
Pittsburgh, PA 15236-0940

Professor Robert Essenhigh
Mechanical Engineering Department
Ohio State University
206 West 18th Avenue
Columbus, OH 43210

Professor Thomas H. Fletcher
Chemical Engineering Department
Brigham Young University
350 CB
Provo, UT 84602

Dr. Michael L. Jones
Energy and Mineral Research Center
University of North Dakota
Box 8213, University Station
Grand Forks, ND 58202
Attn: Dr. Steve Benson

Professor John P. Longwell
Chemical Engineering Department
Massachusetts Institute of Technology
Room 66554
Cambridge, MA 02139

Professor Reginald E. Mitchell
High Temperature Gasdynamics Lab.
Stanford University
Mechanical Engineering Department
Palo Alto, CA 94305

Professor Ronald Pugmire
Vice President for Research
University of Utah
210 Park Building
Salt Lake City, UT 84112

Professor Daniel E. Rosner
Director, High Temperature Chem. Engr. Lab.
Yale University
P.O. Box 2159
New Haven, CT 06520-8167

Professor Adel Sarofim
Department of Chemical Engineering
Massachusetts Institute of Technology
66-466
Cambridge, MA 02139

Professor Terry Wall
Department of Chemical & Materials Engr.
The University of Newcastle
Newcastle, NSW 2308
AUSTRALIA

Professor Jost Wendt
Department of Chemical Engineering
University of Arizona
Tuscon, AZ 85721

Dr. Seymour B. Alpert
P.O. Box 10412
Electric Power Research Institute
3412 Hillview Avenue
Palo Alto, CA 94308

Dr. Arthur Boni, President
PSI Technology Company
20 New England Business Center
Andover, MA 01810
Attn: Dr. Joseph Helble Dr. Connie Senior
Dr. Srivats Srinivasachar

Mr. Richard W. Borio
Combustion Engineering Inc.
1000 Prospect Hill Road, P.O. Box 500
Windsor, CT 06095
Attn: Mr. Michael Hargrove

Dr. James Freihaut
United Technologies Research Center
Combustion Sciences
Silver Lane, MS 30
East Hartford, CT 06108

Mr. Peter Torslev Jensen
ELSAM
Fuel Department
DK-7000 Fredericia
DENMARK

Dr. Flynt Kennedy, Vice President
Research & Development
Consolidation Coal Co.
4000 Brownsville Road
Library, PA 15129
Attn: Dr. Anthony Fonseca

Dr. John S. Maulbetsch
Exploratory Research
EPRI
3412 Hillview Avenue
Palo Alto, CA 94303

Dr. Arun K. Mehta
P.O. Box 10412
Electric Power Research Institute
3412 Hillview Avenue
Palo Alto, CA 94308

Mr. Eric H. Reichl
P.O. Box 472
Princeton, NJ 08542

Professor Philip Smith
Department of Chemical Engineering
University of Utah
2250 Merrill Engineering Bldg.
Salt Lake City, UT 84112

Mr. Ian W. Smith, Manager
Coal Utilization Program
CSIRO
51 Delhi Road, P.O. Box 136
North Ryde, NSW, 2113
AUSTRALIA

Mr. Stanley Vecci, Director
Energy Systems Lab/Research Development Division
Babcock & Wilcox
1562 Beeson Street
Alliance, OH 44602
Attn: Mr. Thomas Morris
Mr. Larry Rodgers
Dr. Hamid Sarv
Mr. James Warchol
Mr. Ralph Bailey
Mr. George Farthing

Dr. Harold W. Wahle, Manager
Heat Transfer & Fluid Mech.
Babcock & Wilcox
1562 Beeson St.
Alliance, OH 44601
Attn: Dr. Woodrow Fiveland
Mr. John Berthold

6200 B. W. Marshall
ATTN: 6211 A.P. Sylvester
6211 G.A. Carlson
6212 H.R. Stephens

8000 J. C. Crawford
ATTN: 8100 M.E. John
8101 T.M. Dyer
8113 J.C. Swearengen
8700 R.C. Wayne
8713 J.M. Hruby
8713 D.K. Ottesen
8714 N.Y.C. Yang

8300 W. J. McLean
ATTN: 8301 J.S. Binkley
8301 W. Bauer
8341 W. Wolfer
8342 R. Stulen
8347 K. Wilson
8351 D.W. Sweeney
8353 G.A. Fisk
8354 R.P. Lucht
8362 R.W. Carling

8361 L. L. Baxter

8361 D. R. Hardesty (15)

8361 R. H. Hurt

8361 M. J. Wornat

8535 Publications Division

8535 Publications Division for OSTI (10)

8524 Central Technical Files (3)

3141 Technical Library Processes (3)